Green Plug – Switched Filter Compensator Devices for Nonlinear Loads and Renewable Energy Systems

by

Albe Mousa A. Bloul

Submitted in partial fulfillment of the
requirements for the degree of Doctor of Philosophy

at

Dalhousie University
Halifax, Nova Scotia

August 2024

I dedicate this thesis to my parents (Mousa and Alshallah),

my wife (Aesha), my children (Mousa, Yakeen, Takwa, Takiaddin, Tsneem, and Mohammad), and all my family.

Table of Contents

List of Tables

List of Figures

Abstract

This research investigates and validates several AC switched filter capacitive compensation schemes for boosting power quality, reducing AC-side harmonics, improving the power factor, and decreasing inrush currents and transient over-voltages by utilizing fuzzy logic type-2 controllers along with a multi-regulation multi-loop proportional-integral-derivative (PID) controller. The study also discusses flexible alternating current transmission systems (FACTS) for voltage stabilization and efficient energy utilization, in addition to new strategies and control approaches to interface renewable energy sources, analyze its usage, and stabilize the voltage. FACTS-based filters can be utilized in industrial drivers using DC and AC motors powered by alternative/renewable sources such as tidal, wind, wave, photovoltaic (PV), fuel cell, micro gas turbines, and hybrid renewable energy sources.

The research approach adopted in this thesis validates both single- and three-phase systems for regulating modulated switched filter duty cycle ratios and proves their compatibility with either DC or AC green plugs. Further, the control systems are fine-tuned to save energy and enhance power quality. By using a modified version of a capacitor filter compensation (MFCC-SFC), the energy efficiency is improved. The three-loop dynamic error-driven fuzzy logic controller (FLC) employs a switched or modulated capacitor filter to improve the effectiveness of electric vehicle (EV) and vehicle-to-house (V2H) battery charging stations.

The main objectives of the thesis are to develop models using MATLAB/Simulink-2023b software to validate new power electronic switching filter compensator topologies for power generation, electric vehicles, and battery charging in order to improve power quality, reduce total harmonic distortion, reduce AC- and DC-side inrush currents, and provide AC- and DC-side voltage stabilization. The research covers renewable integrated AC/DC systems with the FACTS-based filter capacitor compensation family of extended power electronic devices and converters, including MFCC-SFC, MF, and HSFC schemes; smart grid AC/DC renewable energy schemes with modified dynamic control strategies for electric vehicles; vehicle-to-home (V2H)/vehicle-to-grid (V2G) battery local and utility stations; and hybrid renewable energy and micro grid renewable/alternative energy utilization.

In addition, this thesis investigates a number of AC plugs and DC switched filter compensation schemes for nonlinear, inrush current-type load efficient operation, power factor correction, and power quality enhancement. The AC-DC interface schemes for AC and DC EV-drives, V2H/V2G battery chargers, and hybrid renewable energy utilization systems with flexible control strategies are validated using digital simulation in a MATLAB/Simulink/SimPowerSystems-2023b environment, exhibiting significant improvements in power quality and energy delivery reliability. The use of renewable energy requires innovative integrated network solutions that ensure optimal efficiency of the system.

The thesis results validate the full effectiveness of the modulated filter and DC green plugs. The same switched filters are then utilized and validated in a MATLAB software simulation environment in AC/DC, using V2G battery-charging schemes. The multi-use, flexible, modulated AC green plugs and switched filters presented and validated in this thesis can be extended to energy storage/smart utility systems and DC micro grids using PV, fuel cell, wind, and tidal/wave renewable energy systems.

List of Abbreviations and Symbols Used

AC	Alternating Current
ACC	Average Current Control
ANN	Artificial Neural Network
APFs	Active Power Filters
ASD	Adjustable Speed Drives
APC	Active Power Compensator
APFC	Active Power Factor Correction
BEV	Battery-Electric Vehicle
BLDC	Brushless DC motor
BTAF	Bank-Tuned Arm Filter
BMS	Battery Management System
BPEV	Battery-Powered Electric Vehicle
CCM	Continuons Conduction Mode
CFLs	Compact Fluorescent Lamps
CO2	Carbon Oxide
CSI	Current-Source-Inverter
DCM	Discontinuous Conduction Mode
DC	Direct Current
DG	Distributed Generation
DHPC	Dynamic Hybrid Power Compensator
DVRs	Dynamic Voltage Restorers
DVS	Dynamic Voltage Stabilization
EMF	Electro-Motive Force
EMI	Electromagnetic Interference
ESS	Energy Storage System
EV	Electric Vehicles
FACTS	Flexible Alternating Current Transmission Systems
FC	Fuel Cell
FCS	Fast Charging Stations
FLC	Fuzzy logic control
FFT	Fast Fourier Transformation
GEVs	Green Electric Vehicles
GP	General Purpose
GPFC	Green Power Filter Compensators
GSC	Grid Side Converter
GTOs	Gate Turn-Offs
HAPF	Hybrid Active Power Filters
HCC	Hysteresis Current Control
HEVs	Hybrid Electrical Vehicles
HFC	Hybrid Filter Compensator
HSFC	Hybrid Switched Filter Compensator
IGBT	Insulated-Gate Bipolar Transistor
IM	Induction Motor
LED	Light Emitting Diodes
MDIBC	Multi-Device Interleaved DC-DC Boost Converter
MFCC	Modulated Filter Capacitor Compensator
MF-HFC	Modified Filter-Hybrid Filter Compensator

MOPSO	Multi-Objective Particle Swarm Optimization
MPC	Model Predictive Control
MPFC	Modulated Power Filter Compensator
MPP	Maximum Power Point
MPPT	Maximum Power Point Tracking
NP-SFC	Neutral Point Switching Filter Compensation
OC	Open Circuit
PF	Power Factor
PFC	Power Factor Correction
PHEV	Plug-In Hybrid Electric Vehicle
PI	Proportional and Integral Controller
PID	Proportional–Integral–Derivative Controller
PIEVs	Plug-In Electric Vehicles
PFC	Power Factor Correction
PLC	Programmable Logic Controllers
PQ	Power Quality
PSO	Particle Swarm Optimization
PU	Per Unit
PV	Photovoltaic
PWM	Pulse Width Modulation
RMS	Root Mean Square
SAPF	Shunt Active Power Filter
SC	Short Circuit
SFC	Switched Filter Compensator
SMC	Sliding Mode Controller
SPWM	Sinusoidal Pulse Width Modulation
SOC	State Of Charge
SSC	Stator Side Converter
SSPFC	Single-Stage Power Factor Correction
SSSC	Static Synchronous Series Compensator
TCRs	Thyristor-Controlled Reactors
THDi	Total Harmonic Distortion of the Current
THDv	Total Harmonic Distortion of the Voltage
TSCs	Thyristor-Switched Capacitors
STATCOM	Static Synchronous Compensator
THD	Total Harmonic Distortion
V2H	Vehicle-to-Home
V2G	Vehicle-to-Grid
VSC	Voltage Source Converter
VSI	Voltage Source Inverter
WBGSs	Wide Band Gap Semiconductors
WECS	Wind Energy Conversion System
WMPID	Weighted Modified Proportional Integral Derivative

Acknowledgements

I would like to express my sincere gratitude to everyone who helped and supported me throughout my Ph.D. studies. It has been a very difficult yet memorable journey. Without the encouraging words and heartfelt support from supervisors, family, friends, and colleagues, I would not have been able to persevere and continue my research to its successful conclusion.

First of all, I would like to thank God for his guidance throughout these past few years. He never left me lost, confused, or overwhelmed when I needed him most.

As well, I would like to express my sincere thanks, gratitude, and appreciation to my supervisor, Professor Dr. Jason Gu, and my co-supervisors, Professor Dr. Adel M. Sharaf and Dr. Hamed Aly, for their continuing guidance, inspiration, constant encouragement, fruitful comments, and advice, throughout the course of this research work. I would also like to thank the examining committee: Dr. Issam Hammad as an external committee member. Additionally, I am immensely grateful to the external examiner, Prof. Dr. Dayan Ban, professor of Electrical and Computer Engineering at the University of Waterloo, Canada, for his valuable time and for agreeing to evaluate my thesis and join the defence. My deepest thanks go as well to the staff and administrators in the Electrical and Computer Engineering Department and Dalhousie University for their support, inspiration, and encouragement.

The loss of my late professor, Dr. El-Hawary, was a very heavy moment during my Ph.D. journey. His unexpected death hit me quite hard, both mentally and emotionally. His valuable guidance will forever be missed, as will the unwavering support he provided me at the beginning steps of the journey. Without his encouraging words to guide me in my Ph.D. studies, I would not be where I am today.

Many people supported me during the completion of this thesis with helpful assistance, references, and criticism. This thesis would have never been possible without them. I would like to send a huge thanks to everyone but would also like to mention a few names: Thank you to the Department Head, Dr. Jean-Francios Bousquet, my former Grad Advisor, and to Dr. Hamed Aly, for showing endless guidance during my transition to the new supervision.

Finally, I would like to acknowledge my family and friends: My wife, and my children, especially my eldest son, Mousa, for his support of our family and for giving me the space for my research time and patience as I completed my degree. I also thank my parents, who, though thousands of miles away, have never stopped sending their love and their prayers.

Chapter 1: Introduction

1.1 Background and Problem Statment

The quality of electric power systems is crucial due to the increasing use of renewable energy resources. Any minor voltage or frequency variation can disrupt operations and lead to financial losses. Flexible alternating current transmission systems (FACTS) are a hardware/software combination used in transmission substations to improve reliability and capacity. FACTS is a power electronic-based system that provides control of one or more AC transmission system parameters to enhance controllability and increase power transfer capability [1].

Modern electrical distribution/utilization systems face increasing nonlinear loads, such as uninterruptible power supplies, rectifier equipment, communication networks, motors, adjustable speed drives (ASD), and energy-efficient lighting These loads cause disturbances in voltage and current waveforms, necessitating the installation of equipment capable of delivering high-quality voltage and current. A modulated/switched tuned arm filter is utilized to reduce harmonic currents and simplify filter topology [2].

Passive filters are considered active alternatives to reduce current harmonics and enhance power factor correction. However, they cannot follow dynamic changes of nonlinear loads. Passive filters offer advantages such as good terminal voltage regulation, voltage variation reduction, and voltage balance improvement in three phases [3].

Enhancement of power quality and improvement of the power factor have been proposed in various configurations in the literature on filters. Fuzzy logic control (FLC) is most suitable for controlling pulse width modulation to overcome the negative effects of system nonlinearities and dynamic load variations [4]. A low-cost SFC C-type scheme has been implemented and extended to improve power quality and efficient utilization in smart utilization grid applications [5]. The proposed MFCC-based single-phase filter uses a tri-loop dynamic error-driven FLC to control the SFC, resulting in power factor enhancement and power quality improvement, fully limiting the transient over-voltage and inrush current conditions [6].

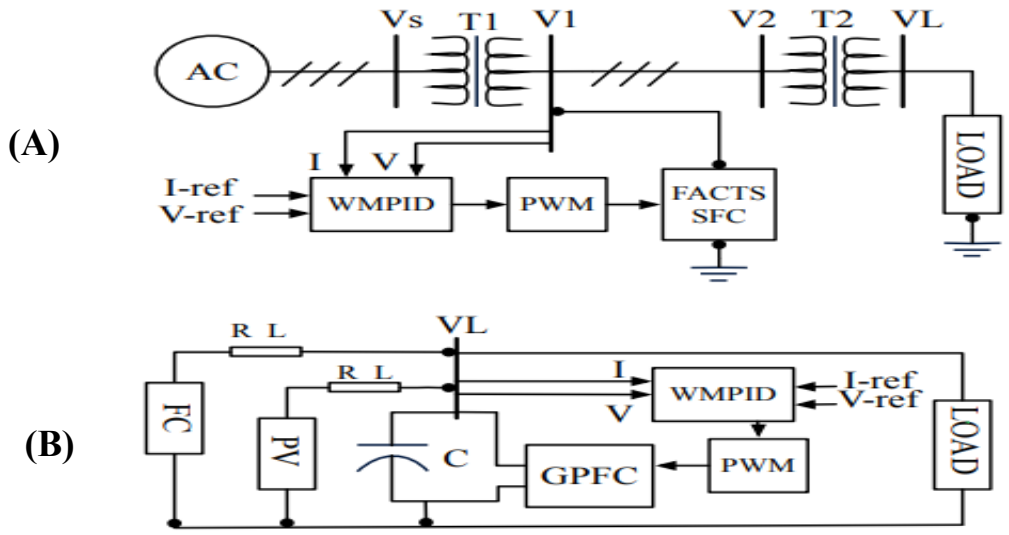

Figure 1.1 (A) AC-Side FACTS-Based SFC Scheme. (B) DC-Side GPFC Scheme.

The increasing complexity of power system loads, along with the emergence of the global smart grid, has led to a growing need for high-quality, low-priced, stable, and secure power. FACTS controllers and related devices are playing a significant role in power systems, with some already operational [7]. FACTS-based power quality and voltage stability boosters have been introduced in various scenarios, such as a novel Modulated Power Filter Compensator (MPFC) scheme for hybrid renewable energy schemes and an active power compensator (APC) scheme [8]. Other FACTS devices, such as hybrid switched filter compensators and active power filters (APFs), are being used to improve the power factor, reduce line current harmonics, and enhance power quality for AC smart grids, battery-charging systems, and integrated renewable AC/DC systems [9].

As the demand for greater power capacity increases, electric utilities must find ways to satisfy these growing demands. Programs that reward conservation, efficient appliances, and smart electronics can contribute to reductions in electricity consumption. FACTS technology can provide enhanced performance by using currently installed transmission lines, with GTO thyristor devices offering cost savings and improved power handling abilities. By incorporating electronic switching

from voltage source converters, FACTS technologies can serve as a new controllable reactive power source [10].

Green energies are used to generate the electricity people have in their homes and businesses.

- Solar – Wind – Geothermal – Hydropower - Biomass / Biogas
- Green energy is energy that can be produced using a method, and from a source, that causes no harm to the natural environment.

Examples of renewable energy sources include wind power, solar power, bioenergy (organic matter burned as a fuel) and hydroelectric, including tidal energy as shown in figure 1.2.

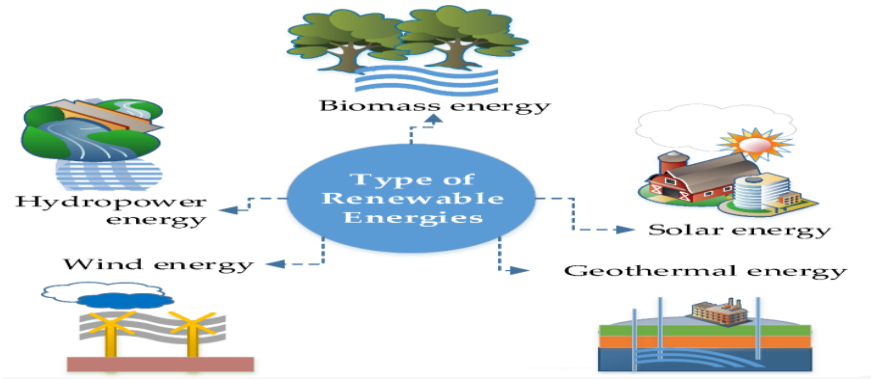

Figure 1.2 Renewable energy sources

Variation-source inverters (VSIs) are being widely used as reactive power controllers instead of traditional VAR compensation devices like thyristor-controlled reactors (TCRs) and thyristor-switched capacitors (TSCs) [11]. However, FACTS devices' dynamic models are nonlinear and highly complex, making state-based models applied to FACTS devices accurate enough to convey the hardware system but simple enough to implement in a power system simulation [12]. Furthermore, FACTS topologies that have been modified offer other advantages, such as power flow control, electromechanical oscillations damping, loading capability boosting in lines, mitigation of cascading blackouts, mitigation of overloads and short-circuit currents, and enhancing of system security by increasing transient stability limits. Additional benefits of this technology involve the provision of secure tie-line connections within neighboring utilities and regions, which serves to reduce overall generation power/energy reserve requirements and leads to better flexibility when siting new generation and upgrading lines. There is also a reduction in

reactive power flows, which enables the lines to hold more active power, thereby reducing the occurrence of loop flows and boosting utilization of more cost-effective generation [13].

Power systems require both transient and dynamic stability to ensure reliability and security in case of short-circuit faults or major disturbances. The deregulation and restructuring of the power industry has led to a focus on maximizing power systems within a competitive environment, with FACTS technology playing a central role in improving system transient stability margin [14]. Design approaches for off-line FACTS-based device controllers have been the main focus, but these techniques are not very flexible when power system operating conditions and configurations vary [15]. FACTS controllers can, however, control variables like phase angle and voltage magnitude for specific bus/line impedances [16]. Currently, five different control-related FACTS devices are being used by power utilities, with some limitations.

FACTS technology is categorized as a converter for flexible control systems and solid-state power electronic devices, acting like conventional power system controllers. FACTS control systems and devices can regulate nodal voltage magnitude, line/angle reactance, and active/reactive power transfer [17]. Replacing mechanical switches with semiconductor switches offers a faster response time and fewer restrictions on control actions, but FACTS technologies are typically more expensive than mechanical technologies. The two main classes of FACTS devices are older devices based on thyristor valves and more recent devices employing voltage source converters (VSC) [18].

In general, FACTS devices are categorized according to their connection with power systems, such as shunt, series, or shunt-series. Shunt devices provide dynamic voltage support and reactive power compensation for lines and loads, while series devices offer variable susceptance and smooth control across a broad spectrum [19]. To maintain harmonic and voltage stability for weak AC buses, shunt and series reactive power VAR compensation can boost a power network's maximum transfer capacity [20].

Moreover, FACTS technologies decrease costs for utilities by extending the life of current systems and delaying the need for replacement or new transmission systems. They feature flexible controllers and module converters that can satisfy transmission line or substation performance needs. Utilities can optimize their existing equipment using FACTS devices, reducing instability issues and increasing operational flexibility [1]. They can also incorporate renewable energy sources, such as PV solar energy systems, wave and tidal generators, small/micro hydro generation,

and water pumping stations. Emerging energy-efficient plug-in locomotion and other EV technologies have been driven by a rising awareness of lowering hydrocarbon emissions. A new generation of EV solutions includes "green" electric vehicles (EVs), which can be fueled by Lithium-ion rechargeable batteries with an AC/DC vehicle-to-home (V2H) interface and vehicle-to-garage (V2G) charging stations [21].

EV propulsion can be applied to different types of electric motors, such as permanent magnet synchronous motors, permanent magnet brushless DC motors, and induction motors [22]. The use of EVs is predicted to lower annual CO2 emissions by around 3.1 million tons, comprising a 2.4% reduction for total emissions in the transport sector. EVs require battery-charging stations that feature renewable energy use and V2H/V2G smart grid integration schemes. Research into novel decoupled stable V2H models using EV batteries for mass backup energy storage for power systems is urgently needed, as EVs could be utilized for power systems when not in use [23]. Researchers in [24] presented a review of FACTS/D-FACTS strategies and their various applications for electric utilities that utilize RESs as power electronic converters. The FACTS-based solutions are accompanied by several control techniques that aim to resolve issues around EV-charging, battery storage, renewable energy sources and the use of sensitive/nonlinear loads.

Foad et al. [25] presented a shunt filter compensator FACTS DVS/green plug filter to dynamically modulate AC bus admittance to stabilize energy transfer. The filter improved system security, voltage regulation, and power quality at key AC buses, while limiting inrush currents, transient overvoltage, and switching recovery voltage excursions [25]. Plug-In Electric Vehicles (PIEVs) aim to decrease green-house gas emissions in compliance with the Kyoto Accord. In this emerging technology, isolated high-frequency AC-DC converters have been used to move power to traction battery packs from energy mains. The battery packs store the energy needed by EV motors for propulsion. In the present work, a traditional passive EMI filter, which has been embedded in the main high-frequency planar transformer in the DC/DC converter, is presented. It is an effective and efficient approach to EVs and can be applied as an affordable EMI filtering solution in PIEVs. Furthermore, the modified planar transformer layout offers a viable alternative for EV applications that use high switching frequency converters [26].

The authors in [27] provided an elegant solution for dealing with high-switching frequency converters for EVs. They proposed a planar transformer layout that suppresses CM EMI noise and

eliminates oscillatory currents by eliminating the low-impedance differential path. Dynamic controlled FACTS devices are introduced to boost power factor and power quality, eliminating line current harmonics. A Hybrid Filter Compensator (HFC) is a FACTS-based device that is moderated using a quad-loop multi-zonal dynamic controller. In low-impact V2H battery-charging in EVs, Lithium-ion batteries are quickly and efficiently charged using a single-phase source that employs a dynamic error-driven multi-loop controller [1]. This approach effectively controls the FACTS NP-SFC filter compensator and the boost-type DC chopper, which can then be used to moderate power transfers between Lithium-ion cell batteries and AC sources.

Additionally, a novel low-impact, low-cost V2H battery-charging approach is designed in this thesis for electric vehicles (EVs), controlled using a dynamic multi-regulator technique. The V2H charger and filter compensator utilize a new type of error-driver control method to obtain stability of DC bus voltage and reduced inrush current and transient conditions during periods of battery-charging. The weighted dynamic PID controller has a fast error-squared compensation loop as well as stabilization, and the boost DC chopper is used to charge the Lithium-ion battery. This results in enhanced power usage and efficiency with a decrease in both inrush current and transient voltage conditions [23].

As well, a novel EV-DC hybrid fuel cell battery-driven strategy is presented, which can be stabilized by utilizing a FACTS-based Green Filter Compensator (GFC) for stabilizing the DC bus voltage under conditions of load and source excursions [28]. The Green Plug Filter Compensator (GPFC)- and Battery-Powered Electric Vehicle (BPEV)-coordinated control strategy uses a FACTS-based GPFC to stabilize DC bus voltage under minimal inrush current conditions and for load excursions where load demand exceeds the capacity of Nickel-Metal-Hybrid cell batteries. A type-B dual-DC/DC converter is utilized to match and control power transfer between the cell battery and motor load [29].

Furthermore, the present study introduces switched smart filter-compensated devices that employ GPFCs in single-phase induction motors. The GPFCs achieve various desired aims, such as optimal energy efficiency, reducing feeder loss, stabilizing voltage, enhancing the power factor, and creating minimal current ripples. All of this is accomplished with negligible effects on either reliability or electric grid security [30]. The power management compensator uses Multi-Objective Particle Swarm Optimization (MOPSO) to obtain highly efficient coordinated operation in two

separate energy sources [31]. The MOPSO search technique can be applied to power generation on island and hydrogen mode, using a micro-hydro water turbine and fuel cell power source to conserve energy, reduce loss, stabilize voltage, improve power quality, and correct the power factor in systems characterized by hybrid multi-source energy usage [32].

The energy management control strategy particle swarm optimization (PSO) method proposed here ensures the best available control gain settings for minimizing global dynamic errors dynamically [33]. The primary goals of controllers include voltage stabilization, dynamic matching of loads, and "green" and efficient energy generation and usage. The integrated hybrid green energy system along with key subsystems can be simulated digitally with MATLAB/Simulink/2023 SimPower software, after which they can be tested on efficient energy usage and power quality of the interface in a variety of load excursions and operational environments.

Finally, the study presents a hybrid wind/PV renewable green energy utilization scheme for a village/island micro-grid. The system uses an error-driven multi-regulator/multi-loop coordinated controller, ensuring optimal power quality, common AC/DC bus stabilization, and optimal energy usage across different load excursions and operational environments. The system employs a wind-driven PMDC generator, a PV array source, an AC-DC inverter, a modulated power filter compensator, and DC/DC converters. The error-driven controller scheme uses green renewable energy and has been validated for various wind speeds and sudden DC load excursions. Dynamic error-driven regulators are also introduced to stabilize common AC/DC bus interfaces, thus minimizing current ripple and maximizing energy usage [34]. FLC is chosen for its advantages, including simplicity of control, low cost, and the ability to design without knowing the exact mathematical model of the process. Also to choose type of filters will be Based on cost, simplicity, admittance, adequacy and effective operation usually two types of filters are used extensity including tuned arm filter and C- type filter.

Linear loads are electrical loads that have a linear relationship between the current and voltage applied to them. Examples of linear loads include resistors, incandescent light bulbs, transformers, capacitors and motors operating at a constant speed.

- Linear loads Advantages:
  1. Generally, more efficient than non-linear loads, as they do not produce harmonics that can cause power losses and increase the size of power system components.

2. Simple to analyze and design circuits for, as their behavior is probable and follows Ohm's law.

- Linear loads Disadvantages:
  1. May not be able to endure large changes in voltage or current without suffering damage.
  2. May not be suitable for applications that require a large range of output power, as their power output is directly proportional to the applied voltage.

Non-linear loads are electrical loads that do not have a linear relationship between the current and voltage applied to them. Examples of non-linear loads include rectifiers, Induction motor, DC ARC motor, inverters and welding equipment.

- Non-linear loads Advantages:
  1. May be more suitable for certain types of applications, such as those that require a variable output power.
  2. Can operate over a wide range of output power levels, as their power output is not directly proportional to the applied voltage.

- Non-linear loads Disadvantages:
  1. Can source power quality problems, such as voltage distortion and harmonics, due to their complex relationship between voltage and current.
  2. May be less efficient than linear loads, as they can produce harmonics that can cause power losses and increase the size of power system components.
  3. They are more difficult to analyze and design circuits for, as their behavior is more complex and may not follow Ohm's law.
  4. May require special power conditioning equipment to operate properly.

1.2 Thesis Objectives

The main objective of this work is to design and validate a number of modulated/switched power filters (MPFs/SPFs) for nonlinear and inrush current motorized loads to:

- Improve energy utilization.

- Improve the power factor at both sources and load buses.
- Reduce the harmonics content on the host AC system.
- Improve the power quality and Total Harmonic Distortion (THD) of voltage and current.

The PID and fuzzy logic based multi-loop global error-weighted signal is utilized to control the duty cycle ratio of the modulated switched filters using AC and DC green plugs. These control schemes are optimized for energy efficient operation and power quality enhancement.

1.3 Thesis Contributions

The main contributions in this work are described as follows:

1. Optimizing the selection of the switched/Modulated power filter and AC green plugs to enhance system energy utilization power factor and power quality.
2. Selection and tuning of modified power PID and FLC type – 2 parameters to ensure fast response and effective control stabilization with minimal inrush current and transit over voltage, created by switching transit, due to systems inductance added capacitor.
3. Proposed a modulated filter capacitor compensator (MFCC) with different novel PID controllers to control IGBT switches for closing and opening situations in order to improve energy operation towards a more efficient system and high-power quality. Also, the contribution of the MFCC-SFC is to change the apparent impedance of the system at point of interface to reduce number of harmonics and transit.
4. Reduced the harmonic content using a modulated single-phase and three-phase AC-DC green plug switched power filter with fuzzy logic and an optimal PID controller.
5. Proposed two efficient fast-charging schemes for V2H/V2G schemes for battery charging to ensure efficient energy utilization and decoupled AC-DC operation as well as reduced impact on the host and systems. These schemes help improve power quality, reduce DC inrush current, limit transient over-voltages, and modify weighted Voltage, Current and Power, (V.I.P.) controllers for battery charging.

1.4 Thesis Methodology

In this work, the MATLAB/Simulink-2023b simulator program is used for an integrated AC and DC digital simulation. A fuzzy logic system is used for overall system control along with a modified PID optimized controller under varying load conditions as well as an efficient green plug filter. State Of Charge (SOC) battery charging conditions, AC and DC system for open- and short-circuit conditions, and inclusion of super capacitor models are all applied and tested. In addition, the effect of pulse-modulated complementary switching using novel multi-loop controllers is validated for a number of motorized inrush and nonlinear loads.

1.5 Thesis Outline

The thesis consists of seven chapters, as follows:

Chapter 1 introduces the main themes of the thesis. It also provides the thesis objectives, methodology, and contributions, as well as a brief summary of related work in the literature.

Chapter 2 explains a proposed robust fuzzy logic controller for a green plug switched filter for nonlinear loads and an energy-saving green plug device for a single-phase system.

Chapter 3 focuses on a proposed energy-efficient green plug filter compensation scheme for hybrid nonlinear loads in a three-phase system.

Chapter 4 introduces a low-impact V2H battery-charging station scheme using AC green plug switched filters and a fuzzy logic type-2 controller.

Chapter 5 describes a novel AC green plug switched filter scheme for low-impact efficient V2G battery-charging stations and a modified PID controller.

Chapter 6 proposes an Efficient Shunt-Modulated AC Green Plug – Switched Filter Compensation Scheme for Nonlinear Loads.

Chapter 7 provides the conclusion for the thesis and suggests future research directions.

Chapter 2: A Single-Phase Switched Filter Green Plug and an Energy-Saving Green Plug Device for Nonlinear Loads

2.1 Single-Phase Switched Filter Green Plug Scheme for Nonlinear Loads

2.1-1 Abstract

The chapter presents a robust switched tuned arm filter and capacitor compensation (SFC) scheme for single-phase voltage stabilization and efficient energy utilization. The novel modulated filter-capacitor compensator (MFCC)-SFC is controlled and improves the power factor at the source. It also enhances power quality by reducing current harmonic contents. The FACTS-based MF-SFC device is a member of the family of green plug/filter/compensation schemes used for efficient energy utilization, power quality enhancement, and voltage/inrush current/soft starting control using a novel tri-loop dynamic error-driven fuzzy logic controller (FLC). MATLAB/Simulink models are used to validate the new FACTS-based green plug-SFC scheme with a simple fuzzy dynamic gain controller for effective power quality to reduce transient inrush currents and voltage fluctuations at the load bus. This is done using a dynamic pulsing scheme of the MFCC, allowing the filter to cope with dynamic and varying conditions in the nonlinear load.

2.1-2 Introduction

A Fuzzy Logic Controller (FLC) was chosen as a controller for this work because it has several advantages compared to other controllers. The main FLC advantages are simplicity of control, low cost, and the possibility to design without knowing the exact mathematical model of the process [26], [35], [36], [37]. Power quality problems involve any variation in frequency, current, or voltage that may lead to an equipment malfunction or failure [38]. In a modern electrical distribution/utilization system, there has been a continuous increase of nonlinear loads, such as uninterruptible power supplies, rectifier equipment used in domestic appliances, communication networks, motors, adjustable speed drives (ASD), and energy-efficient lighting [39], [29], [40], [41]. All these loads cause disturbances in the voltage and current waveforms [26]. The generating authority must install equipment capable of delivering high-quality voltage and current [42].

Modulated/switched tuned arm filters can be utilized to reduce harmonic currents, lower costs, and simplify filter topology [39], [29]. The main purpose of filters is to reduce the number of harmonics in order to improve power quality. Passive filters are considered active alternatives to reduce current harmonics and

enhance the power factor correction. The disadvantage of passive filters is that they are unable to follow the dynamic changes of nonlinear loads [43], while the advantages of passive filters are good terminal voltage regulation, voltage variation reduction, and voltage balance improvement in three phases [44].

Enhancement of power quality and improvement of the power factor have been proposed in many configurations within the literature on filters [35], [36], [40], [41]. Fuzzy system control is most suited for controlling pulse-width modulation to overcome the negative effects of system nonlinearities and dynamic load variations and variable-uncertainties [45]. A low-cost SFC C-type scheme has been implemented and extended in this chapter to improve the power quality and efficient utilization in smart utilization grid application. The proposed MNFC-based single-phase filter utilizes a tri-loop dynamic error-driven FLC to control the SFC. The proposed scheme has been implemented and succeeds in power factor enhancement and power quality improvement, fully limiting any transient overvoltage and inrush current conditions. The scheme can be extended to three-phase systems [27].

2.1-3 Single-Phase AC System

As mentioned in the Introduction, this thesis explores the further development of a single-phase switched/modulated power filter. Figure 2.1 shows a single-phase AC utilization system feeding an arc-type load. The proposed dynamic error-driven tri-loop FLC controller (Figures 2.3 and 2.4) is used to reduce the switching transients and current inrush excursions as well as excursions in the low-voltage utilization system for efficient power/energy utilization and power quality enhancement. The AC single-phase system includes the following components:

A. Single-phase AC power supply.

B. Novel modulated filter-capacitor compensator (MFCC) scheme.

C. Nonlinear load.

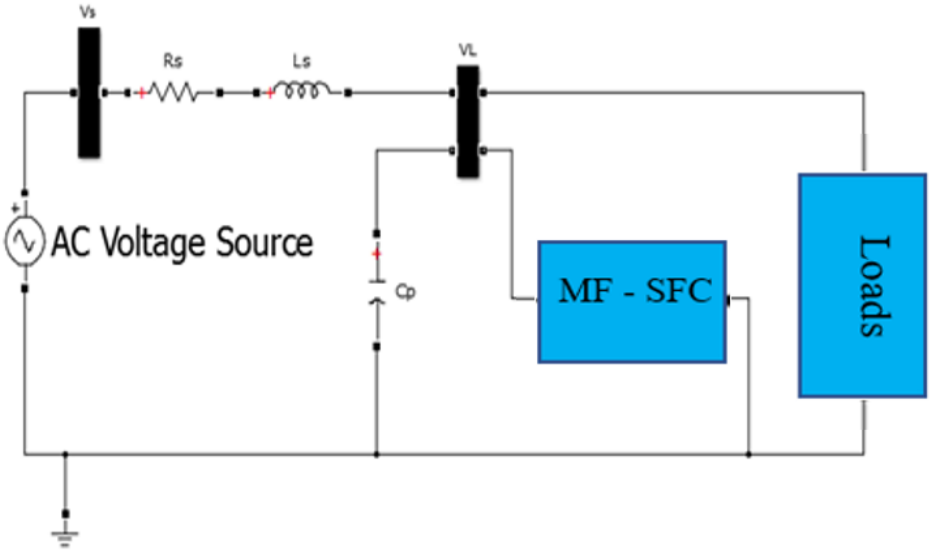

Figure 2.1 Single-Phase Electric Utilization System

In rules-based linguistic-controlled databases, rules are processed in the fuzzy defuzzification unit to influence the result, which is then sent to mark out the next step until arriving at the final result. In Figure 2.3, E(k) indicates the error signal; e(k-1) refers to the change of error in a sampling period; M1, M2, and M3 denote gain values; Du(k) represents a clarification of a previous value of unit output; and D(k-1) with D(k) are obtained when the input of the system is given. These variables are produced according to the rules-based unit rule table.

As shown in the figure, a basic structure of fuzzy controller membership functions has been used. Although the selection indicates completely arbitrary functions of a membership triangle, trapezoid, sinusoid, Cauchy, bell, sigmoid, and Gaussian types [46], FLC is typically used in the input variables, where P: positive, Z:zero, PB: positive big, PS: positive small, NB: negative big, NS: negative big, control error (e), and duration of a sampling error change (Δe) form [47]. Given these variables of the rule base unit, a rule table is created, as, shown in Table 2.1.

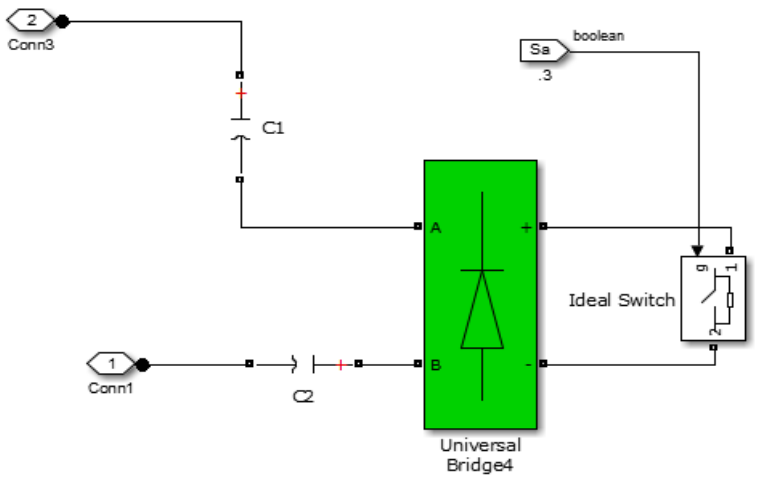

Figure 2.2 MFCC Switched Green Plug – Filter Compensator (SFC) Scheme

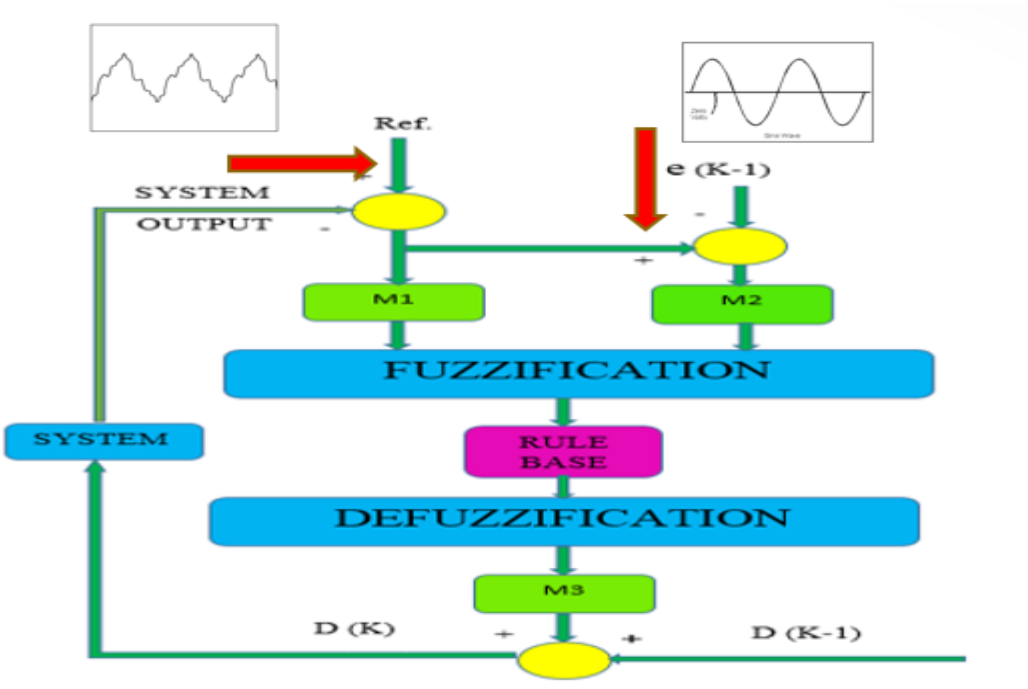

Figure 2.3 Basic Block Structure of Fuzzy Logic Control

Table 2.1: Rules-Assigned Matrix

		Δe				
		NB	NS	Z	PS	P
e	PB	Z	PS	PS	PB	PB
	PS	NS	Z	PS	PS	PB
	Z	NS	NS	Z	PS	PS
	NS	NB	NB	NS	Z	PS
	NB	NB	NS	NS	NS	Z

2.1-4 Controller Design:

The membership functions are the basic elements of an FLC, and triangular membership functions are used in the present study [47]. The input comes from the membership values of space necessary for the weight coefficients of each rule, which are determined based on minimums [45], [48]. After determining the weight coefficients of the required unit of blurring, the rules for multiplying these values are sent to the processed parts. The FLC uses the exact method of de-fuzzification unit values to obtain the central areas. FLC systems design proceeds according to the logic block error feedback and input directly, but referencing is also possible for performing data processing. FLC will determine whether the limits of membership functions can be determined, as shown in Figure 2.4.

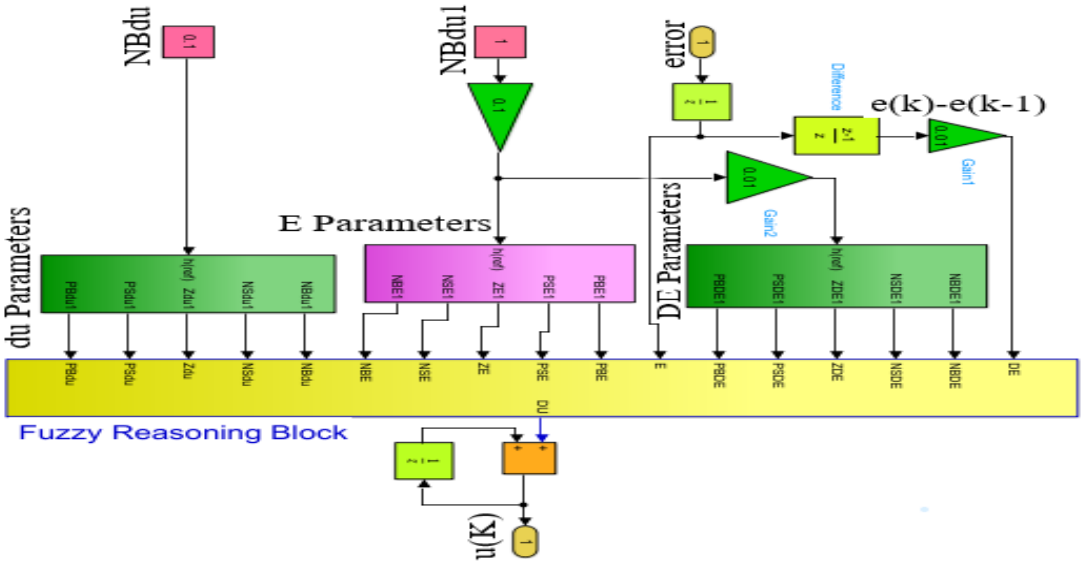

Figure 2.4 Fuzzy Logic Controller Structure

2.1-5 Digital Simulation Results

The digital simulation results using the MATLAB/Simulink/Sim-Power software environment for the proposed MFCC-based SFC scheme with nonlinear load are illustrated in Figures 2.5 to 2.8.

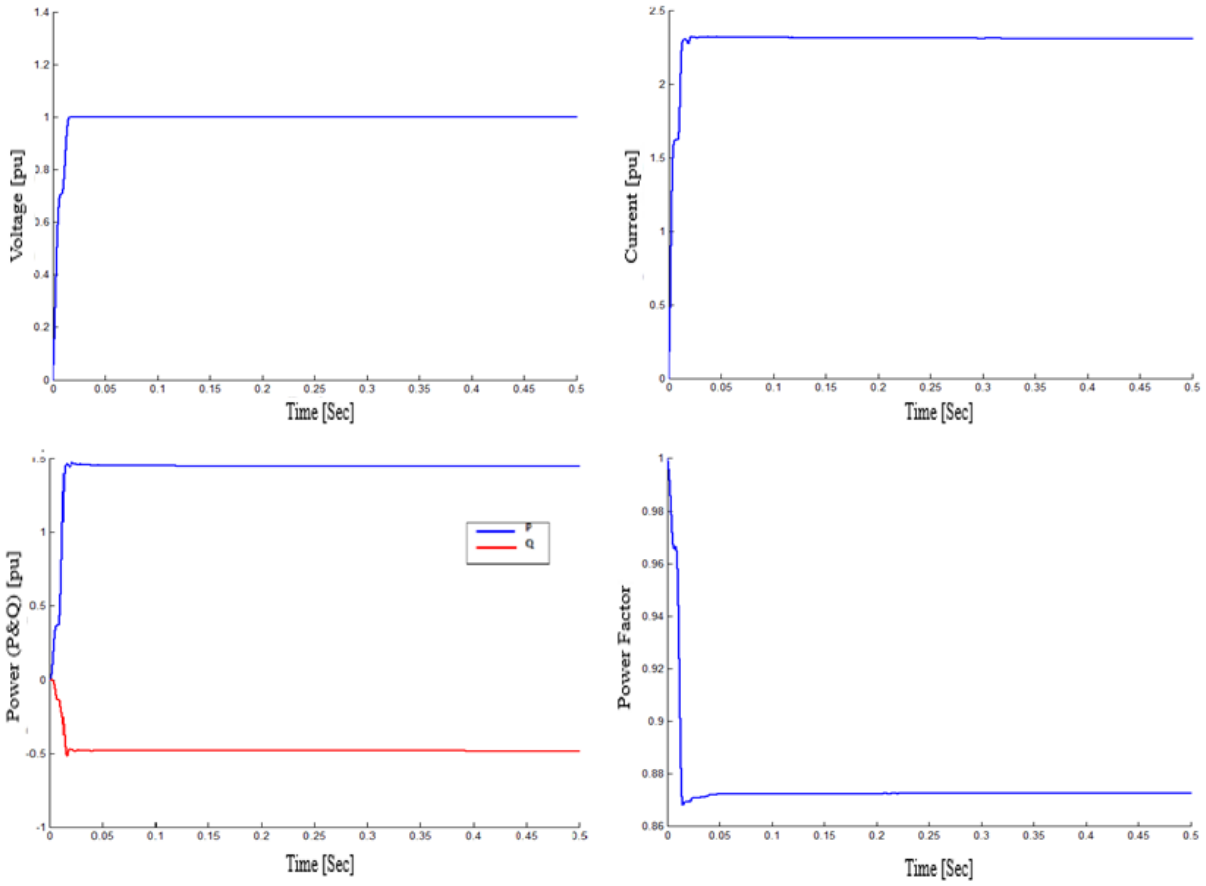

Figure 2.5 RMS V, I, P, Q, and PF Values at AC Source Bus Vs under Nonlinear Load Variations with MFCC-SFC Device

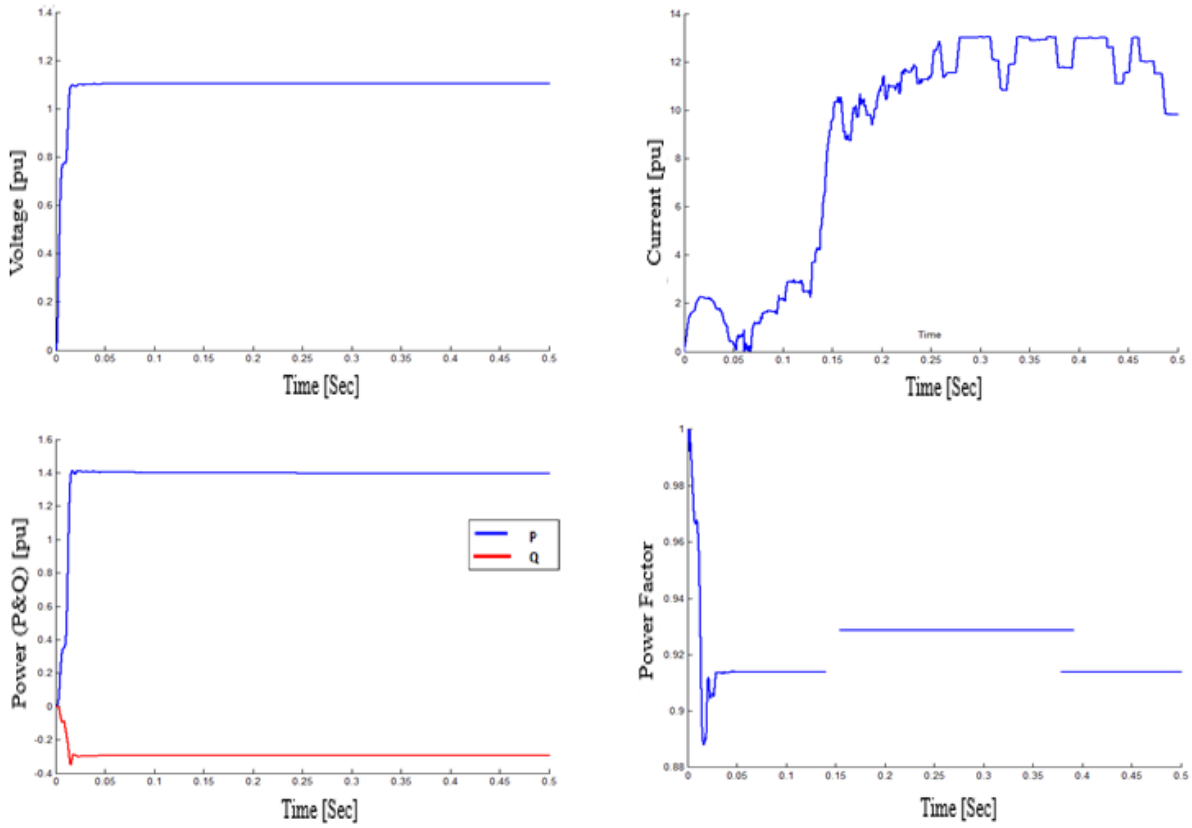

Figure 2.6 RMS V, I, P, Q, and PF Values at Load bus Vs under Nonlinear Load Variations with MFCC-SFC Device

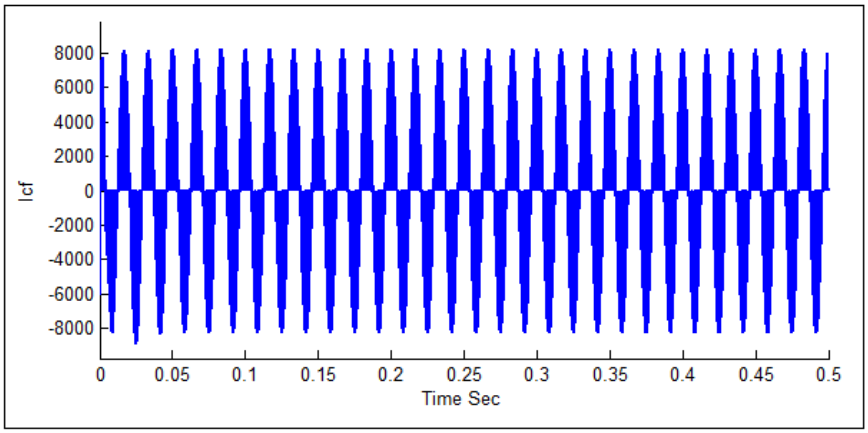

Figure 2.7 RMS Currents for Filter and Capacitors under Nonlinear Load Variations with MFCC-SFC Device

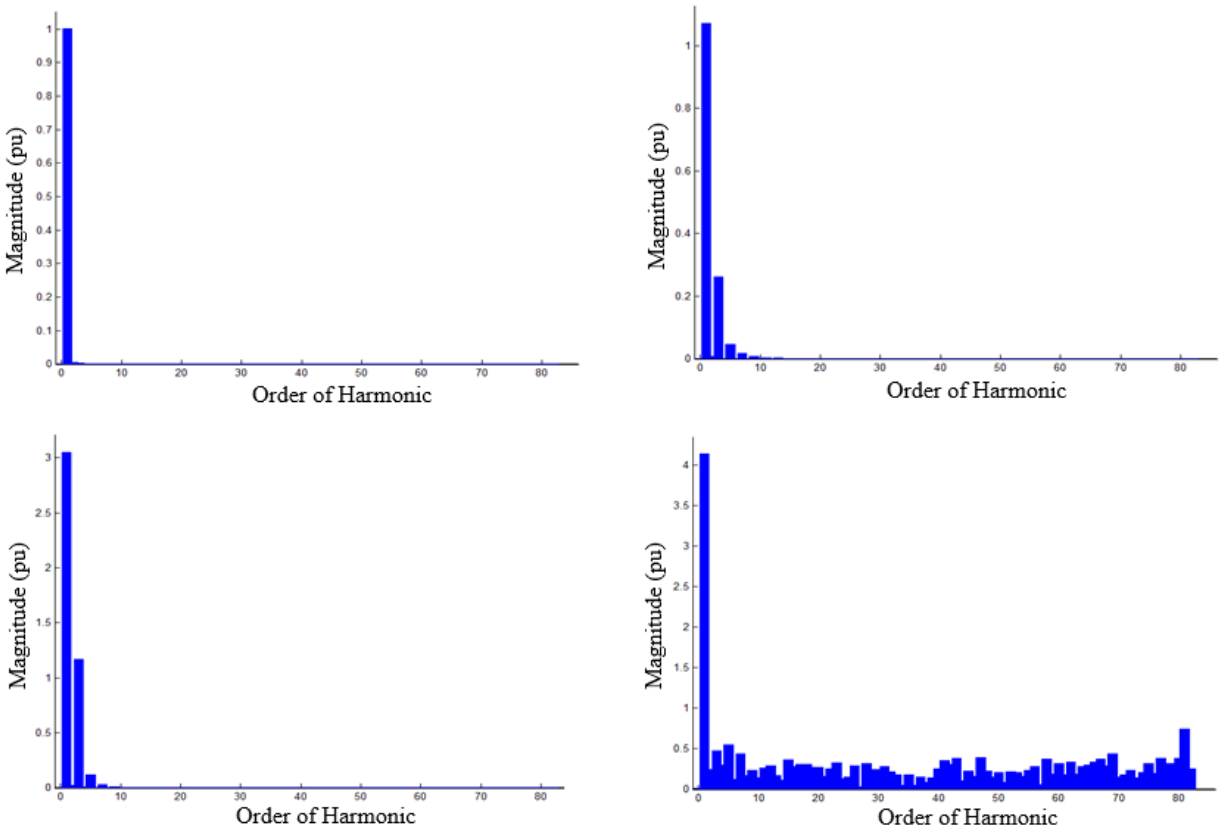

Figure 2.8 Fourier FFT Frequency Spectra of V and I Waveforms at Both Source and Load Buses

2.1-6 Conclusions and Summary

The results given in this chapter validated a novel simple FACTS-based filter compensation and green plug scheme and equipped with a dynamic gain-adjusting fuzzy logic controller for an MFCC-based SFC. The SFC was controlled by a dynamic tri-loop error-driven FLC controller. The MATLAB/Simulink model validation and dynamic simulation of the green-plug SFC scheme validated the effectiveness of the FACTS device for enhanced power quality, voltage stabilization, and source power factor correction. The SFC-green plug-based filter compensator scheme is very useful in nonlinear loads and smart grid distributed/dispersed renewable generation interface schemes for efficient electric utilization and power quality/power factor/harmonic reduction task.

Its tuned arm switched/SPWM switched capacitor/filter/green plug/soft-starting scheme for voltage stabilization/reduced inrush currents and power factor improvement at source to reduce harmonics enhance power quality. Moreover, it can be extended to three-phase nonlinear loads and utilized for voltage dynamic stabilization with hybrid smart grid-renewable energy PV/wind/fuel cell hybrid schemes to reduce transient voltages, soft-starting inrush currents, and quasi-dynamic slow-acting voltage fluctuations at the load bus. Different green plug – SFC filter topology variations and other dynamic ANN/NFIS/GA/PSO-based variable structure and gain-scheduling control techniques can also be implemented in complex hybrid renewable energy generation.

2.2 Energy-Saving Green Plug Device for Nonlinear Loads

2.2-1 Abstract

This section presents a low-cost FACTS-based flexible fuzzy logic-based modulated/switched tuned arm filter and green plug compensation scheme for single-phase nonlinear loads, ensuring both voltage stabilization and efficient energy utilization. The novel Green Plug – Switched Filter Compensator (GP-SFC)-modulated LC-Filter PWM switched capacitive compensation device is controlled using a fuzzy logic regulator to enhance power quality, improve the power factor at source, and reduce switching transients and inrush current conditions as well harmonic contents in the source current. The FACTS-based SFC-GP device is a member of the family of green plug/filter/compensation schemes used for efficient energy utilization, power quality enhancement, and voltage/inrush current/soft-starting control, utilizing a dynamic error-driven fuzzy logic controller. The controller is validated in a MATLAB/Simulink software environment for enhanced power quality, improved power factor, and reduced inrush currents. This is achieved using modulated PWM switching of the filter-capacitive compensation scheme to cope with dynamic type nonlinear and inrush cyclical loads.

2.2-2 Introduction

Fuzzy logic control is utilized as the preferred PWM dynamic switching/regulation scheme for the SFC-GP FACTS device used to enhance power quality and energy utilization for single-phase nonlinear loads. It has key advantages compared to other classical PID controllers. The

advantages of FLC are simplicity, low cost, and flexibility in case of uncertain load with unknown mathematical model or process dynamics [39], [49], [44], [9]. Power quality problems are defined as any variation in frequency, current, or voltage that may lead to an equipment malfunction or failure [4]. In a modern electrical distribution/utilization system, there has been a continuous increase of nonlinear loads, such as uninterruptible power supplies, rectifier equipment used in domestic appliances, communication networks, motors, adjustable speed drives, etc. [36], [50], [29], [35].

Power quality-related problems are becoming a major concern nowadays. The widespread use of electronic equipment, such as programmable logic controllers (PLC), information technology equipment, power electronics like adjustable speed drives (ASD), and energy-efficient LED-lighting, has led to severe nonlinearity and varying ranges of electric loads. Power quality is the main victim of load disturbances in the voltage and current waveform [39].

Whatever the power factor is, however, the generating authority must install machines capable of delivering a particular voltage and current. Even though most voltage and current products aim to improve efficiency, reactive compensation using the capacitors is utilized to improve the power factor and reduce harmonic content in nonlinear-load current [35]. A modulated/switched tuned arm filter is employed here not only to reduce harmonic currents but also to reduce cost and simplify the filter topology [36], [50]. Filters aim to reduce the harmonics in order to improve power quality. Passive filters are usually considered as active alternatives to reduce current harmonic and enhance the power factor correction. One major disadvantage of passive filters is that they are not able to follow the dynamic behavior changes of nonlinear loads [40]. On the other hand, the advantages of passive filters are their terminal voltage regulations, voltage variation reduction, and voltage balance improvement in three phases [38].

The limitations of fixed structure/fixed parameter and detuned passive filters causing series/parallel resonance between system, capacitors, and existing AC supply impedance is fully documented. A low-cost passive filter can be utilized with simple switching devices to enhance dynamics, bandwidth, and operation with slow dynamic cyclical and inrush type nonlinear loads. Effective control using PWM-switched power LC-filters can improve the effectiveness of passive filter compensation [29], [40].

The enhancement of power quality and improvement of the power factor have been proposed in the literature [42], [49], [44]. Fuzzy system control (FLC) is most suited for control of the pulse width modulation to overcome the negative effects of system nonlinearities and dynamic load variations and variable-uncertainties [41]. A low-cost GP-SFC, C-type scheme has been implemented and extended to improve the power quality and efficient utilization in smart utilization grid application. The proposed MNFC-based single-phase filter utilizes multi-loop dynamic error-driven fuzzy logic-FLC to control the SFC-GP FACTS device. The proposed scheme has implemented and succeeded in power factor enhancement and power quality improvement, fully limiting transient overvoltage and inrush current conditions. The scheme can be extended to three-phase systems [51].

2.2-3 Overall Design of AC Single-Phase System

A single-phase AC utilization system driving an arc-type load is shown in Figure 2.9 (A). By analyzing the figure, we can divide the AC single-phase system into three components, namely single-phase power source, modulated green plug filter, and nonlinear load. The load in the system is the source of nonlinearity and generates harmonics in the power line. Such transients and input current excursions generated by the load need to be compensated. In this thesis, we have designed a green plug filter to perform this compensation task.

The proposed green plug filter is placed in parallel with the load, as shown in Figure 2.9 (A). The inner construction of the green plug filter is shown in Figure 2.9 (B). In order to optimally control the operation of the filter, we have deployed a two-input fuzzy logic controller, which is inherently a nonlinear controller that is robust to disturbances. The block diagram of the fuzzy logic controller is shown in Figure 2.3, with its inner construction depicted in Figure 2.4. The fuzzy logic-controlled green plug filter will ensure that the energy is utilized efficiently, and the power quality is also improved [26].

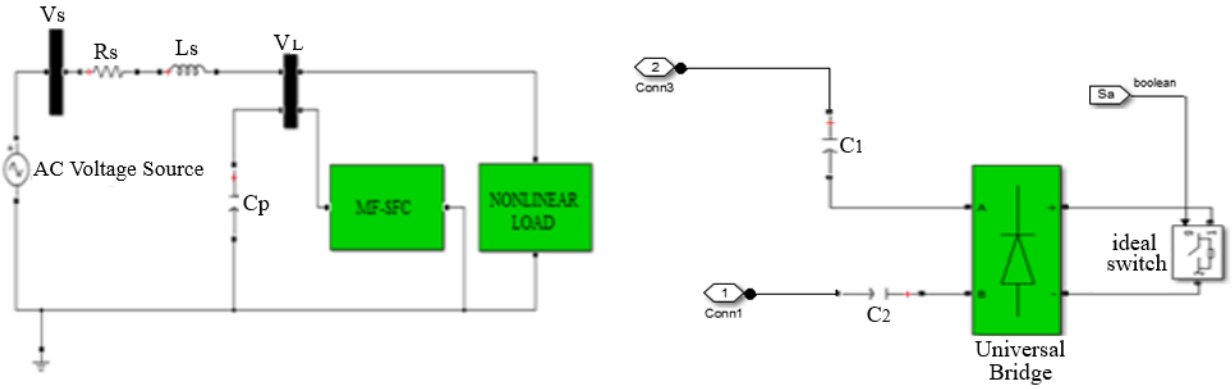

Figure 2.9 (A) Components of a Single-Phase Utility System. (B) Structure of a Green Plug Switched Filter.

2.2.4 Digital Simulation Results

In order to check the effectiveness of the proposed green plug filter, we conducted simulations in a MATLAB/Simulink environment with several types of nonlinear loads. The results of the simulation are shown in Figures 2.10 through 2.13. The simulation results include the waveforms for voltage, current, active power, reactive power, and the frequency spectrum for each load type. It can be seen that the green plug switched filter is effective in improving the power quality and reducing the inrush currents due to several types of loads present in the industrial environment.

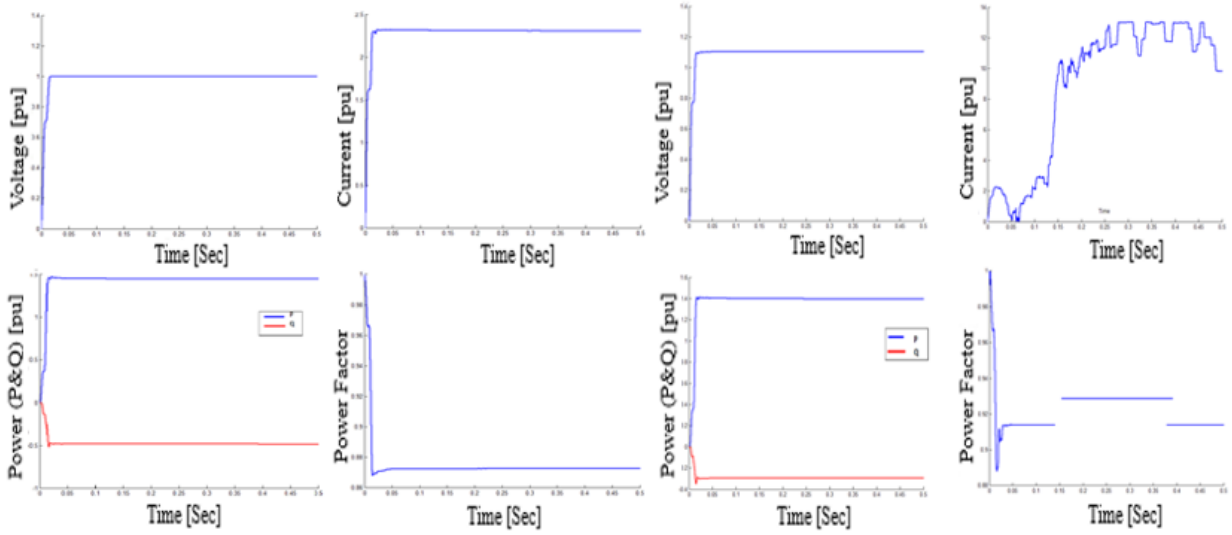

A B

Figure 2.10 (A) Nonlinear Load-RMS V, I, P, Q, and PF at AC Source Bus
(B) Nonlinear Load-RMS V, I, P, Q, and PF at AC Load Bus

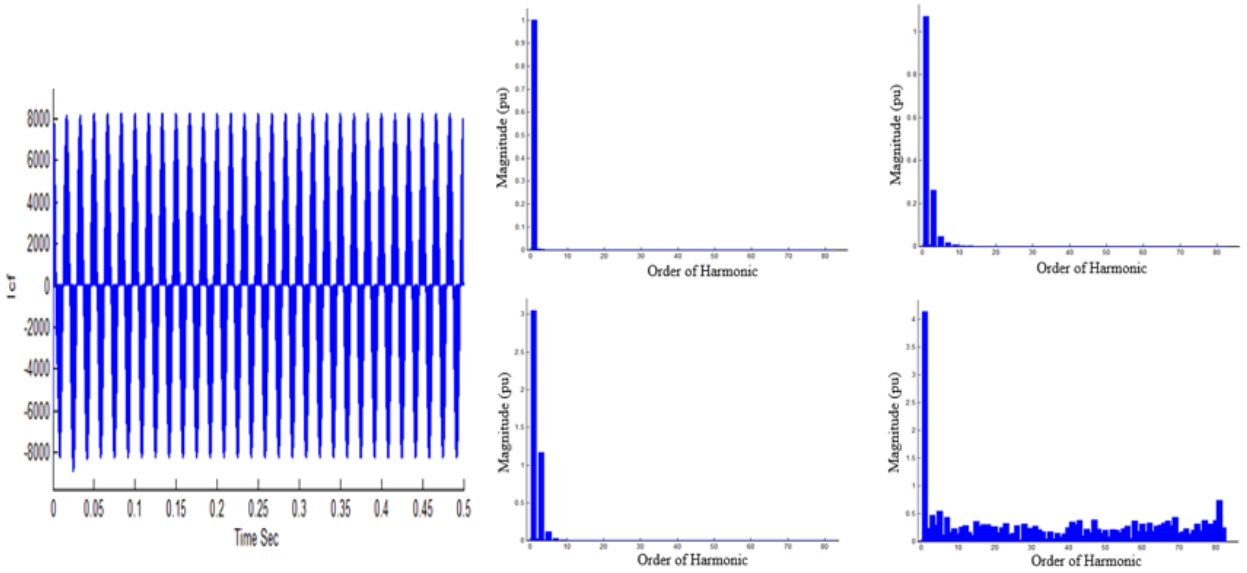

A B

Figure 2.11 (A) Nonlinear Load-Capacitor Variation.
(B) Nonlinear Load-FFT Frequency Filter Current Spectra of V and I Waveforms at Both Source and Load Sides.

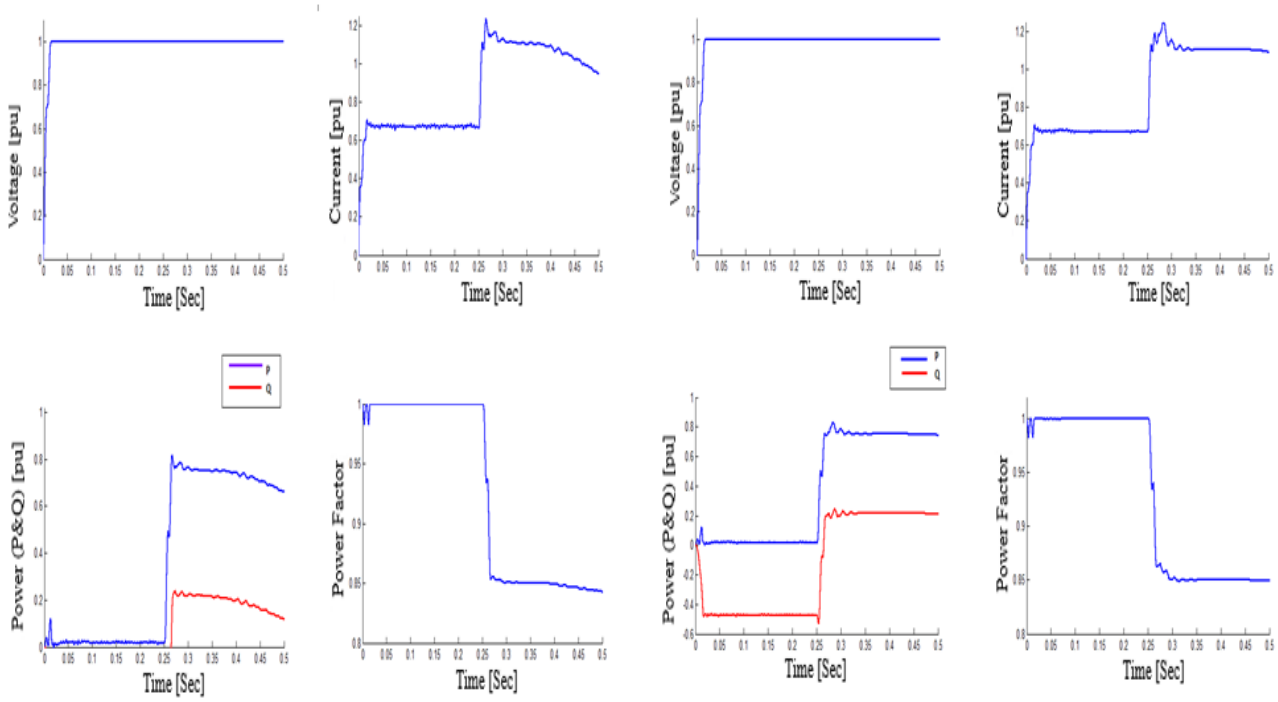

A B

Figure 2.12 (A) Induction Motor Cyclic Load (Full Load) RMS V, I, P, Q, and PF Values at AC Source Bus
(B) Induction Motor Cyclic Load (Full Load) RMS V, I, P, Q, and PF Values at AC Load Bus

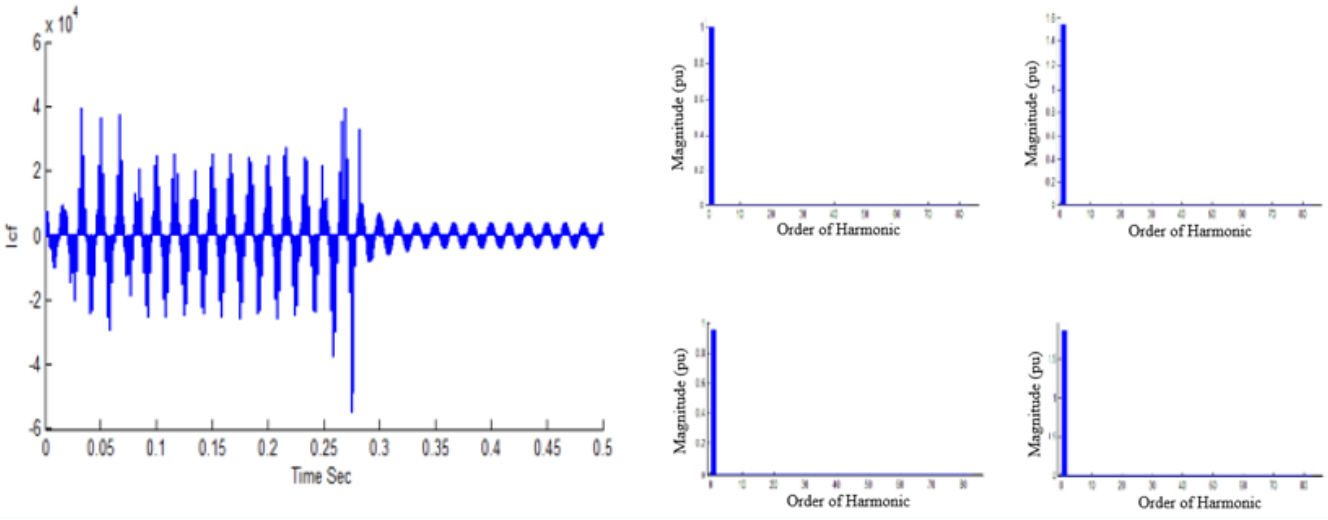

A B

Figure 2.13 (A) Induction Motor Cyclic Load (Full Load) Capacitor Filter Current Variation.
(B) Induction Motor Cyclic Load (Full Load) FT Frequency Spectra of V and I Waveforms at Both Source and Load Sides.

2.2-5 Conclusion and Summary

This part of the thesis presented a FACTS-based green plug switched filter compensation (SFC-GP) scheme controlled by a dynamic multi-loop, error-driven FLC. The SFC-GP was validated in a MATLAB/Simulink software environment using a fast-acting dynamic FLC. In the simulations, the SFC-GP device was controlled by a dynamic tri-loop error-driven FLC controller. The SFC-GP device with FLC is a scheme validated for enhanced power quality, voltage stabilization, and efficient utilization. The SFC-GP FACTS device employs a PWM-SFC scheme that was demonstrated to be highly suited to ensuring nonlinear inrush, dynamic, cyclical, and motorized loads, efficient electric utilization, enhanced power quality and power factor, and harmonic reduction. It can also be applied as a starting scheme for voltage stabilization/reduced inrush currents and power factor.

Moreover, it can be extended to three-phase nonlinear loads and utilized for voltage dynamic stabilization with hybrid smart grid-renewable energy interface schemes using PV/wind/fuel to reduce transient voltages, ensure soft starting, and limit inrush currents and flicker control. Both the SFC-GP device topology and the control strategies can be modified to suit specific applications and control duties using fixed topologies as well as modified optimized structures of soft-computing ANN/NFIS/GA/PSO regulators with optimal gain scheduling and modified weightings.

Chapter 3: A Three-Phase Switched Filter Green Plug Scheme for Nonlinear Loads

3.1 Abstract

This chapter presents a switched modulated filter compensation/modulated filter capacitive compensator (SFC/MFCC) scheme to improve electrical energy utilization, enhance power quality, and reduce excursions on distribution/utilization hybrid linear and nonlinear/inrush type motorized loads on AC electric utility systems. The dual pulse width modulated (PWM)-switched SFC/MFCC functions as a harmonic tuned arm filter plus reactive compensation device for hybrid linear/nonlinear motorized loads. This is achieved by complementary modulation of switching PWM action, controlled by a multi-loop fuzzy logic controller (FLC). The pulse modulation is determined in each control time-step by the aggregate sum of deviation errors in voltage and dynamic current/power changes. The novel FMCC-SFC filter can be extended to other interface applications of nonlinear DC-AC grid systems and customized to voltage dynamic stabilization and voltage regulation tasks on AC grid systems.

3.2 Introduction

Over the past two decades, problems with power quality have become increasingly significant in electrical power transmission and distribution systems. This issue has been exacerbated by the growing adoption of renewable energy sources, such as distributed generation, in modern electrical networks. Such changes have brought about a notable transformation in the operation of electrical systems [52], [53].

However, the introduction of Flexible AC Transmission System (FACTS) devices is starting to mitigate these issues. FACTS are power electronics-based devices that are designed to control and manage the flow of power on electrical grids. They are also proving to be the best method currently available to improve power quality. FACTS-based devices can be dynamically adjusted to regulate voltage levels, control power flows, and stabilize system parameters. This

makes them valuable tools for power frequency and improving the overall quality of electricity distribution [54], [55].

The aim in using FACTS components is to increase transfer capacity and ease the integration of renewable energy sources. The goal is to create a technique that, considering variables like voltage stability, power flow regulation, and transient stability, optimally positions FACTS devices along the transmission line [56], [57]. Also, FACTS uses FLC as the PWM dynamic switching/regulation scheme to improve power quality and energy consumption for three-phase system loads. In contrast to other traditional PID controllers, it provides significant advantages. The benefits of FLC include ease of use, affordability, and adaptability in the occurrence of an uncertain load with an unknown mathematical model or process dynamics. With regard to problems relating to power quality [58], the most important power electronics, such as adjustable speed drives (ASD), energy-efficient light emitting diodes (LED), and programmable logic controllers (PLC), have resulted in severe nonlinearity and a wide variety of electric load disturbances [59].

To overcome these and other related issues, and irrespective of the power factor, the generating authority must install equipment capable of delivering a specific voltage and current. Reactive compensation using capacitors increases the power factor and lowers harmonic content in nonlinear load currents. A modulated switched tuned arm filter (MFCC) is used to reduce harmonic currents, cut costs, and simplify filter design, as filters are primarily designed to reduce harmonic content to enhance power quality. The primary purpose of passive filters is to improve power factor correction by reducing current harmonics. On the other hand, passive filters have the drawback of being unable to adapt to the dynamic behavior changes of nonlinear loads [49].

Harmonics reduce feeder active and reactive power and also increase the response on the electrical system to open- and short-circuit operations and load changing due to faults and load-switching. Fixed, switched, and modulated capacitor banks have been widely used in modern electrical systems to overcome these issues [56], [57], as harmonics and dynamic switching excursions can result in electric equipment failure, malfunction, fire, and shock hazard, in addition to poor power factor. inefficient utilization of electric energy, and severely distorted voltage and current waveforms. To improve efficiency, capacitors may be employed, which also improves the power factor of the mains [60], [61], [62], [63], [59].

While fixed power filters and capacitor banks have their place in improving power quality by reducing harmonics and reactive power in electrical systems, they do have limitations when dealing with dynamic loads and potential resonance issues. Advanced solutions like active power filters and tuned passive filters offer a more effective means to handling these challenges, especially in industrial utilization networks [64], [49]. In the following sections, a new low-cost flexible alternating current transmission system FACTS-DVS/GP device is validated using MATLAB-Simulink software and a new FLC for voltage stabilization and efficient energy secure delivery to the load. The new FACTS-DVS/GP is developed and utilizes switches to implement dynamic error-driven control strategies for improved response.

3.3 Literature Review

Betala et al. [62] looked at power factor issues at fast EV charging stations that were due to the switching of supplies in power electronics. The proposed system improving the power factor by utilizing an Active Power Factor Correction (APFC). This approach is based on a fuzzy logic fractional order controller that optimizes the input power factor and decreases harmonics distortion. The APFC has the potential to be applied more broadly in, for instance, three-phase systems to enhance power consumption benefits and the power factor. Raja et al. highlighted the significance of power quality concerns for engineers and power companies, emphasizing the role of devices like Dynamic Voltage Restorers (DVRs) to mitigate disruptions and enhance power stability in distribution networks, demonstrated through MATLAB/Simulink simulations [62].

The authors in [64] focused on the benefits of the CHB-DVR system for improving power quality on the distribution side, emphasizing its ability to mitigate voltage fluctuations, harmonics, and outages, and highlighting its potential for enhancing power stability and efficiency in industrial and commercial settings while suggesting future research directions including advanced control strategies and the integration of storage systems for increased reliability [63]. KYW Hong tested a “plug-and-play” AI-based framework for extracting real-time filter parameters as digital power control. The framework functions without any hardware modifications or extra sensors, instead using an LSTM network and a predefined control law. The model, which obtained reasonably accurate results for different filter orders, was also tested on a buck DC/DC converter set at various filter configurations [59].

Xu et al.'s study [65] introduced an energy storage control strategy for AC/DC hybrid systems after DC fault-blocking, enhancing safe operation through a double-layer control approach. The technique was evaluated using a DC power transfer influence factor, and validated via simulations on a power grid model, demonstrating improved system stability and suppression of power oscillations. The authors also introduced an energy storage control strategy using DC power transfer factor evaluation in an AC-DC hybrid system after a DC fault, demonstrating improved AC system stability through energy storage's quick impact mitigation on AC lines and a double-layer control approach. The method was validated using CEPRI36V7 power grid model simulations [65].

S. Benisha et al. [66] proposed a cost-effective approach using power factor correction (PFC) and a Cuk converter. Their stated aim was to improve power quality in low voltage applications integrated with a brushless DC motor (BLDC) drive and voltage source inverter (VSI) for reduced switching losses. The effectiveness of their novel strategy was evaluated across different modes and conditions through MATLAB/ Simulink simulations. A Cuk converter-driven BLDC motor is designed to achieve unity power factor, utilizing various operating modes in continuous and discontinuous conduction modes (CCM and DCM), with experimental validation favoring the DICM mode for improved power factor correction in low-power equipment [66]. In another study, Busacca et al. [67] investigated experimentally the harmonic content and efficiency in a Cascaded H. Bridges Multilevel Inverter, using several different modulation methods. The author explored the effects of frequency switching on both harmonic distortion and efficiency for a three-phase, five-level CHBMI prototype. The author also looked at different PWM techniques and modulation indices, discovering the differential sensitivity found in PD-, SCAMOD-, and CD-based schemes about harmonic distortion/efficiency and frequency switching [67].

Miao and colleagues [68] presented a method deriving line outage distribution factors for N-2 double branch power flow transfer that enables rapid and accurate calculation of active power flow transfer after dual branch breaks. Their novel creation was validated through IEEE 39 bus system simulations, offering practicality for N-2 contingency assessment and power generation plan verification. The study also addressed cascading faults' impact on power grid safety by developing a formula for calculating the N-2 power flow transfer distribution factor from N-1 outage factors. This approach enabled quick active power flow assessment after dual line breaks.

The authors then analyzed the coupling effects and proposed a grid disconnection judgment method, with accurate simulation results suggesting applicability for N-2 contingency assessment and power system planning. Their future work aims to focus on refining accuracy by considering grid loss and reactive power flow effects [68].

Vinodhini et al. addressed power quality challenges in [69]. Their work introduced an FLC-based boost converter for power factor correction that aimed to enhance power factor, reduce harmonics, and regulate output. The voltage in the power systems was demonstrated through MATLAB/Simulink simulations, with controller robustness validated against traditional controllers. In an industrial combined power system, the proposed boost converter with an FLC improved the power factor, reduced harmonic distortion, and provided regulated output voltage for enhanced overall system performance. As such, it presented a viable and economical solution for industrial applications, with the potential for further stability enhancement using advanced techniques like neural networks [69].

Patil and colleague [70] assessed AC-DC converter topologies for EV battery charging, focusing on boost converter-based power factor correction options such as traditional boost, interleaved boost, and bridgeless totem pole boost converters. Their aim was to achieve high efficiency, good power factor, and compliance with IEEE standards by simulations using MATLAB/Simulink for universal AC input voltage and 400 V DC output. Power factor correction solutions using boost converters for EV battery chargers were presented and performance was compared through circuit simulations. The simulation results showed that interleaved boost PFC has lower harmonic distortion and higher efficiency, outperforming other boost PFC topologies for EV battery-charging applications at 1 kW output power and 100 kHz switching frequency [70].

Vadivu et al. [71] investigated three-level full bridge power factor correction (PFC) converter power quality parameters using several different control strategies. These include Sliding Mode Controller (SMC) and Average Current Control (ACC). The tests were conducted through simulations on MATLAB/Simulink. The authors found that ACC demonstrated superior power quality results, achieving a power factor of 0.993 and total harmonic distortion (THD) of 0.12% while maintaining stability under varying line and load conditions. A Single-Stage Power Factor Correction (SSPFC) converter was also designed with cascaded control loops using SMC and ACC, resulting in enhanced power quality in terms of THD and input power factor. ACC outperformed

SMC, giving a power factor of 0.9977 and reduced THD of 0.04%, even under variations in input voltage and load conditions. The results thus met IEEE-519 standards [71].

Sarker et al. [72] studied an interleaved, bi-phase, boost PFC topology, aiming to decrease harmonics and enhance power quality during the process of EV charging. The authors proposed a 6-kw interleaved bi-phase boost PFC converter-based EV charging system to satisfy IEEE 519-2019 standards. Regarding efficiency and THD, the model outperformed single-phase boost PFC systems as well as non-PFC ones [72].

Boutoubat et al.'s [73] study investigated ways to control a wind energy conversion system (WECS). The author proposed using a Grid Side Converter (GSC) and regulating a Stator Side Converter (SSC) for MPPT as a means to stabilize DC voltage as well as improve the power factor. This would be achieved by building a cascade converter setup, thereby improving power quality and active power production [73]. Mohamed et al. [74] proposed a novel control strategy that combined a feed-forward Artificial Neural Network (ANN) and Model Predictive Control (MPC) for bi-level converters. The authors aimed to improve performance and voltage quality for diverse loads by decreasing the THD. By conducting simulations under different operational conditions, the authors demonstrated that the model showed reasonably good efficiency in comparison with standard MPC [74].

3.4 Study of a Three-Phase AC System

Figure 3.1 illustrates the three-phase AC usage system supplying loads, while Figures 3.4 depict the proposed novel dynamic error-driven tri-loop FLC applied to lower switching transients and current inrush excursions. This may also be applied to low-voltage systems for effective power/energy utilization and power quality improvement for the type of load depicted in [75], [56]. The AC three-phase system grid network depicted in Figure 3.1 comprises a synchronous generator (driven by source) that delivers the power to a local hybrid load (linear, induction motor, and DC ARC load) and is connected to an infinite bus through an 8 km transmission line. The AC system consists of the following:

A. Three-phase AC source.
B. Novel modulated filter-capacitor compensator (MFCC) scheme.
C. Hybrid nonlinear load.
D. Transformer.
E. Transmission line.

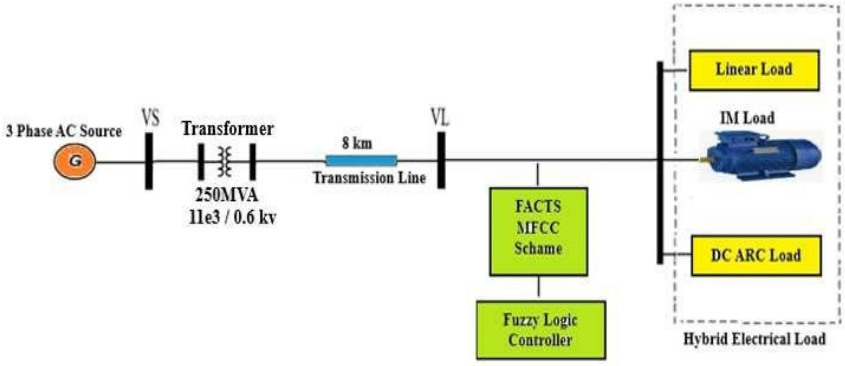

Figure 3.1 Single-Line Diagram of Sample AC System

Power transmission efficiency and the power factor of efficient power transmission is a cornerstone of the modern electrical grid. Minimizing losses and maintaining reliability play a crucial role in providing a stable and cost-effective electricity supply to end-consumers while also contributing to sustainable energy practices [76]. Active power loss reduction strategies with power factor regulation efforts can lead to a more efficient power transmission system [77], [39]. The best way to ensure high efficiency is to minimize the active power loss during the power transmission process. At the same time, regulating the power factor is crucial during power transmission, as it contributes substantially to transmission efficiency [78], [28].

Transmission efficiency:

$$\eta_T = \frac{\text{Receiving end power}}{\text{Sending end power}} \times 100 \quad (1)$$

$$= \frac{V_{R\,IR}\cos\phi R}{V_{S\,Is}\cos\phi S} \times 100 \quad (2)$$

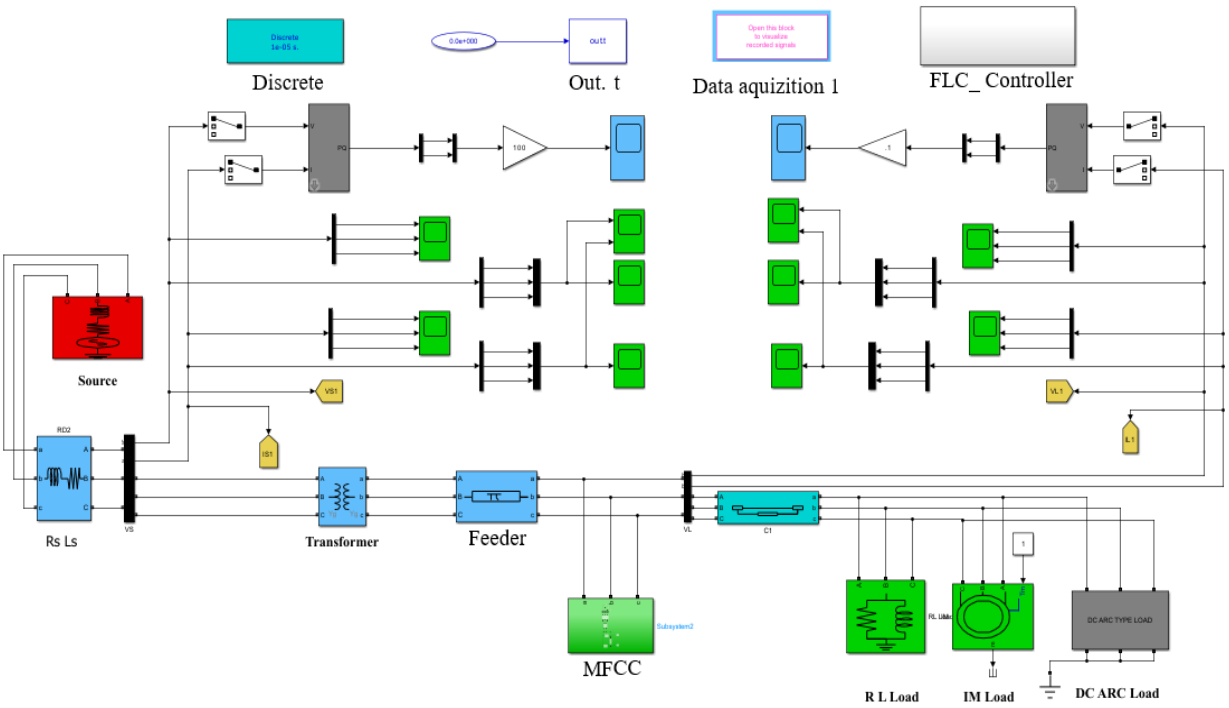

Figure 3.2 Three-Phase System with FLC and Hybrid Load

3.5 MFCC-Filter Compensator

FACTS technology is used to enhance the efficiency, reliability, and control of power transmission in AC systems. One of the aspects of FACTS is the harmonics mitigation and power quality improvement in three-phase systems. The IGBT switches used in this work are controlled by two complementary pulses, allowing the equivalent admittance of the MFCC circuit to be changed with different operating states. If switch S1 is opened and S2 is closed, the resistor and indicator will be connected into the circuit. If switch S1 is closed and S2 is opened, the resistor and inductor will be shorted. In this case, a three-phase capacitor bank will procure a capacitive admittance, as illustrated in Figure 3.3. The IGBT switches are controlled by a novel tri-loop dynamic error driven PID controller [79], [80], [81].

In this context, a FACTS system that incorporates a switchable type of capacitor bank can indeed play a crucial role in reducing system harmonics. The MFCC is also controlled to absorb ripples and reduce current oscillations [83]. The idea behind the dynamic controller is to maintain stable voltage and current levels in the system, feed the errors to the SPWM, and generate a series

of pulses whose widths are adjusted to create a waveform that resembles a sine wave. SPWM is commonly used in applications like motor drives and power inverters with the duty ratio and the error value for renewable energy systems [50]. The MFCC used and tested with a three-phase system is depicted in Figure 3.3. The MFCC control scheme is based on decoupled current and voltage components of the bus.

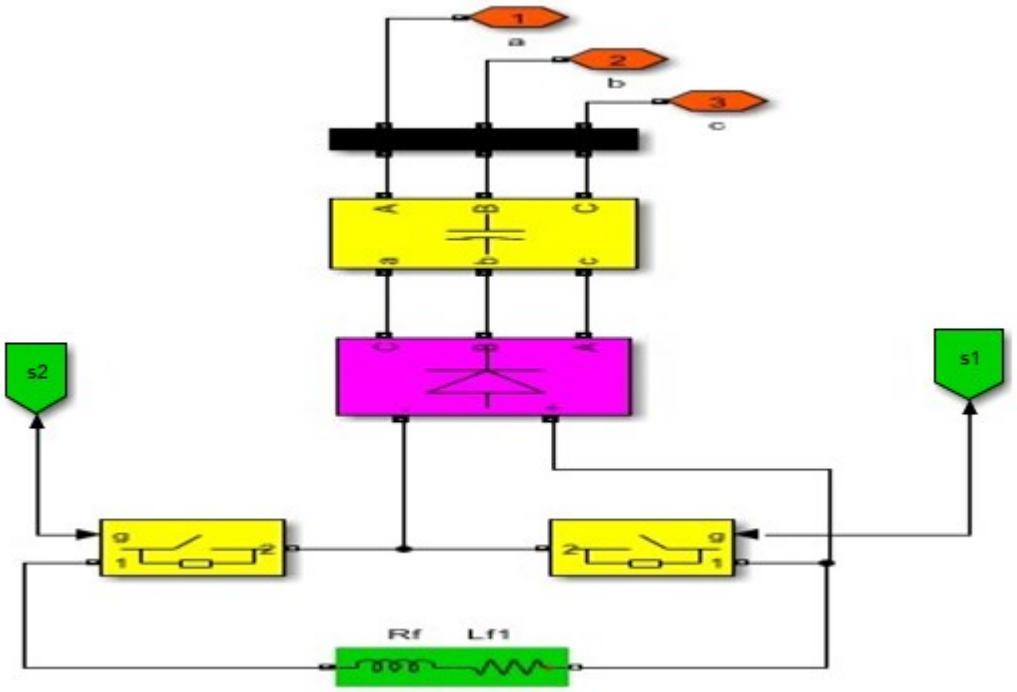

Figure 3.3 MFCC Switched Green Plug – Filter Compensator Scheme

The increased power with higher voltage and current ratings of power electronic converters used in an MFCC also allows for adequate sizing and optimized operation [47], [84]. In this work, the effectiveness of the MFCC scheme is fully validated using MATLAB/Simulink digital simulation. All the subsystem components are individual submodules that are linked to determine the overall system model. The simulation of the proposed scheme is carried out, and the dynamic performance of the system is tested for the proposed controller.

The MFCC must be connected across the bus terminal to maintain constant voltage to allow the operation of the voltage source converter (VSC) with two control loops, as shown in the Simulink model in Figure 3.2. The main duty of the capacitor bank is to feed the voltage path and current path (Figure 3.1). The input of control loop 1 is the dynamic voltage change in the bus,

which produces an error at recognizes the measured value; the error is then used for voltage adjustment. The input to loop 2 is the dynamic current bus, which has the same transfer function as the voltage loop [44], [85].

In recent years, renewables have been playing increasingly greater roles in the main grid. However, renewables tend to be intermittent, nonlinear, and fluctuating, and this affects their integration into the grid [86], [87]. One of the primary disadvantages of renewables is problems with inertia. Most renewables are disconnected from the main grid during fault conditions due to the negative impact on the reactive power [88], [89]. A key benefit of the proposed compensator is to use it with renewables to reduce the faulted condition impact on the main grid.

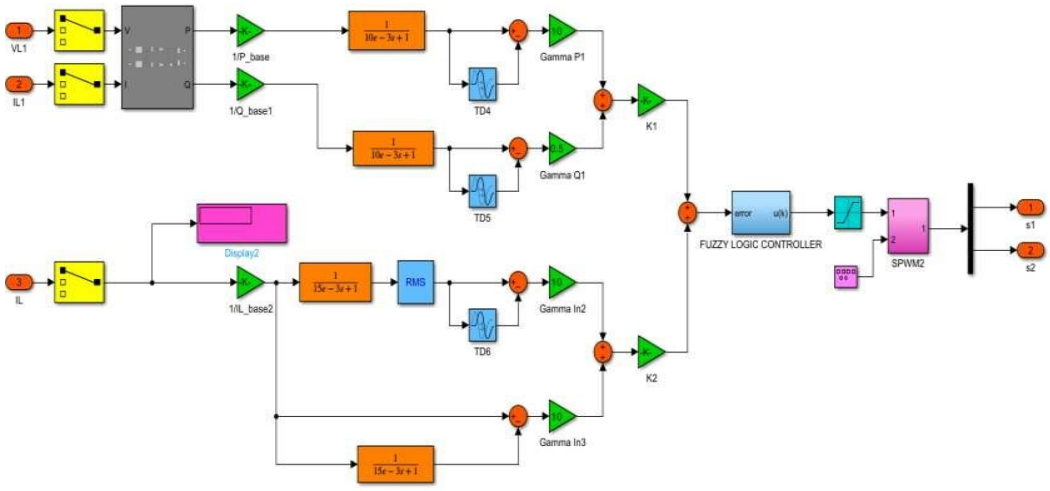

Figure 3.4 Dynamic Error-Driven Tri-Regulation Controller

3.6 Controller Design

Membership functions are the basic elements of the fuzzy logic controller. The present study uses triangular membership functions [86], [90], [77] whose input comes from the membership values of space necessary for the weight coefficients of each rule, determined based on minimums [26] – [35]. After determining the weight coefficients of the required unit of blurring, the rules for multiplying these values are sent to the processed parts. FLC uses the exact method of de-fuzzification unit values to obtain the central areas. FLC systems design then proceeds according to the logic block error feedback and input directly; it also is possible to perform data

processing by reference [83] – [91]. FLC will determine whether the limits of membership functions can be determined, as shown in Figure 3.5.

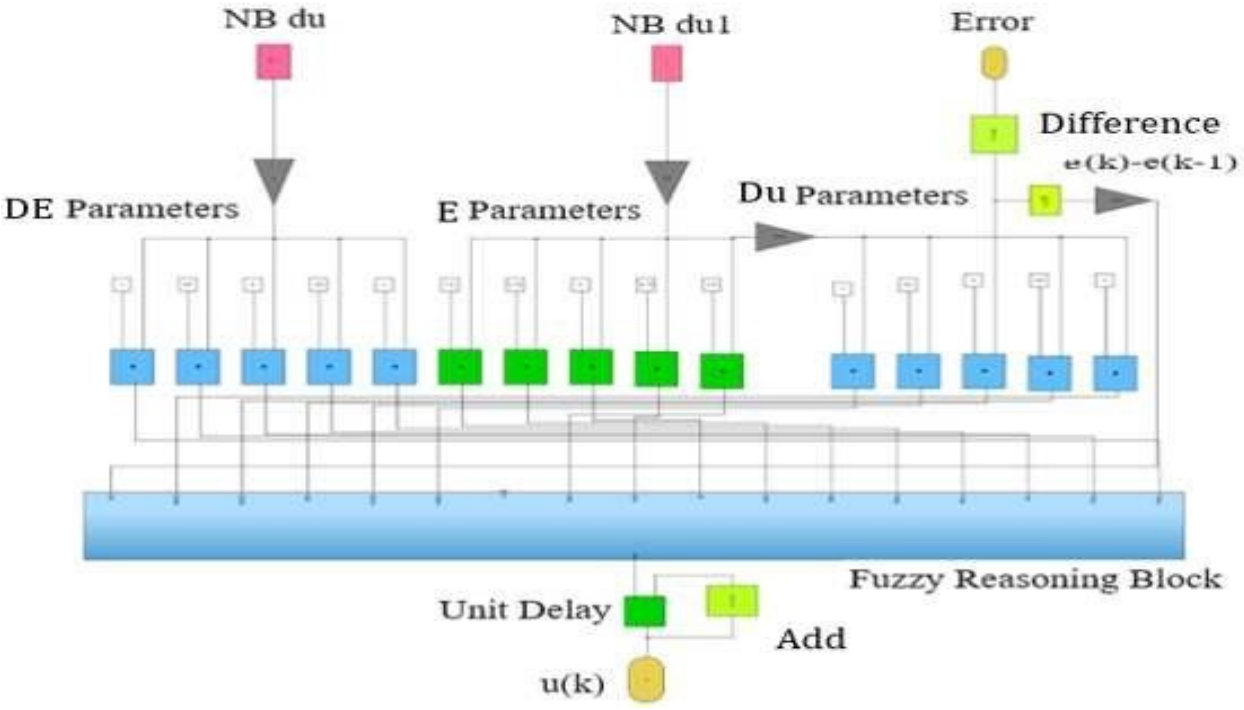

Figure 3.5 Fuzzy Logic Controller MATLAB/Simulink Block Model Structure

Figure 3.6 depicts a block diagram of the elements of linguistic control rule base and database. Rules are processed in the fuzzy defuzzification unit to influence the result, which is sent to mark out the next step, producing definitive results. In Figure 3.6, E(k) indicates the error signal and e(k-1) refers to the change of error in a sampling period. Additionally, M1, M2, and M3 are gain values, while Du(k) clarifies a previous value of unit output. D(k-1) and D(k) are then obtained and the system input is given. The variables are produced according to the rule base unit rule table.

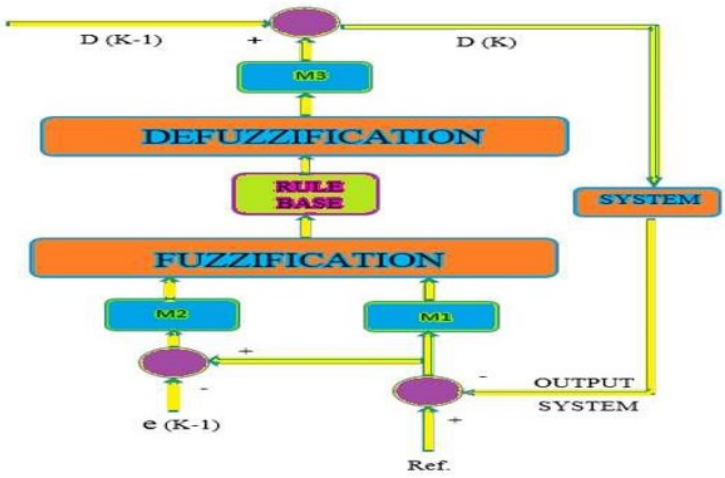

Figure 3.6 Structure of Fuzzy Logic Controller

A basic structure of fuzzy controller membership functions is used here, employing a selection of arbitrary functions of the membership triangle, trapezoid, sinusoid, Cauchy, bell, sigmoid, Gaussian types [45], [92]. FLC is usually the input variables, control error (e), and the duration of a sampling error change (Δe) form. Where is P: positive, Z: zero, PB: positive big, PS: positive small, NB: negative big and NS: negative big. According to these variables of the rule base unit, a rule table can be created, as presented in Table 3.1. A detailed description of the rules establishment is provided in [93], [94].

Table 3.1: FLC Rules (e-Δe): Rules-Assigned Matrix (5X5 = 25)

		Δe				
		NB	NS	Z	PS	P
e	PB	Z	PS	PS	PB	PB
	PS	NS	Z	PS	PS	PB
	Z	NS	NS	Z	PS	PS
	NS	NB	NB	NS	Z	PS
	NB	NB	NS	NS	NS	Z

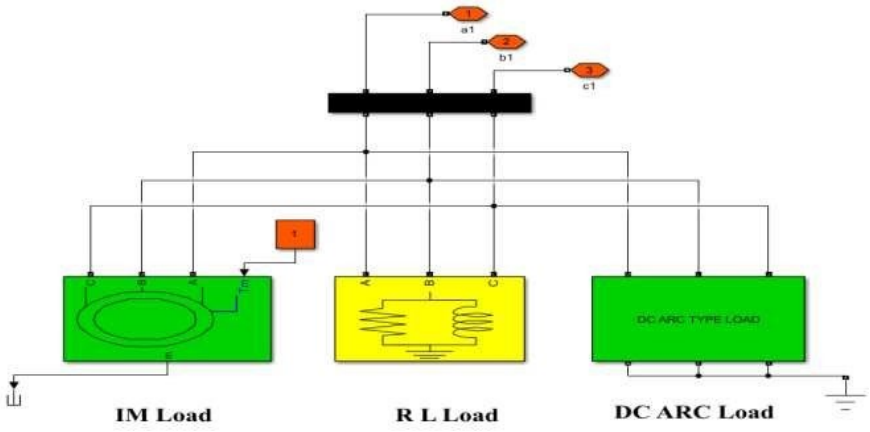

Figure 3.7 Hybrid Loads Fed by AC Smart Grid

3.7 Digital Simulation Results

Digital simulation results are obtained in a MATLAB/Simulink/Sim-Power software environment to verify the dynamic effectiveness of the introduced three-phase system for the proposed MFCC-based SFC scheme. The system feeding three types of industrial loads is presented in the following sections.

3.7.1 Normal Operating Conditions Using Time Scales from 0 to 0.4 Sec on a Step of 0.05 Sec

The integrated AC system model is dependent on hybrid load disturbances. The digital simulation dynamic responses at the source side are shown in Figure 3.8, while Figure 3.9 depicts the digital responses at the load bus without using the proposed filter. Figures 3.10 and 3.11 illustrate the dynamic responses at the source side and the load bus, respectively, after using MFCC. As seen from the figures, there is an improvement in the dynamic response after using the proposed filter.

Tables 3.2 and 3.3 present the changes in the voltage, current, and active and reactive power before and after using the filter. The results indicate that there is an improvement in the voltage, current, and reactive power and power factor, as indicated in Tables 3.8 and 3.9. This applies to two cases, based on using the MFCC-FACTS device. Table 3.2 shows the results at the source bus

with and without the MFCC filter as well as the results at the load bus. As seen from Table 3.3, there is a huge improvement in the voltage at the source bus (20%), with the voltage changing from 0.89 to 1.09, and at the load bus (19%), with the voltage changing from 0.91 to 1.09.

The current is also improved from 1.9 to 2.5 at the source bus, which means there is an increase in its value by 6 %; the increase in the current at the load bus is around 4%. Additionally, it is clear that the active and reactive power are improved at both the source and load bus. The active power is increased by 8% at the source bus and by 3% at the load bus, while the reactive power is increased by 19% at the source bus and by 7% at the load bus. However, special care should be taken in selecting the MFCC parameters to avoid possible parallel resonance with the induction generator or system inductance.

The obvious improvement in voltage, current, and power is impressive, but there is also a huge increase in the reactive power at the source bus. This increase is considered as an important advantage of MFCC, especially with the increasing penetration of renewable energy into the main grid. Up until now, most renewable energy sources have had a mostly negative impact on the grid during fault conditions. Using MFCC improves the performance of the system and increases its robustness, especially during fault conditions. Again, this is crucially important feedback, particularly in the presence of the renewable resources due to the low inertia during fault conditions because of the dependency on the asynchronous generators and converters that have zero inertia, which will affect the overall system performance.

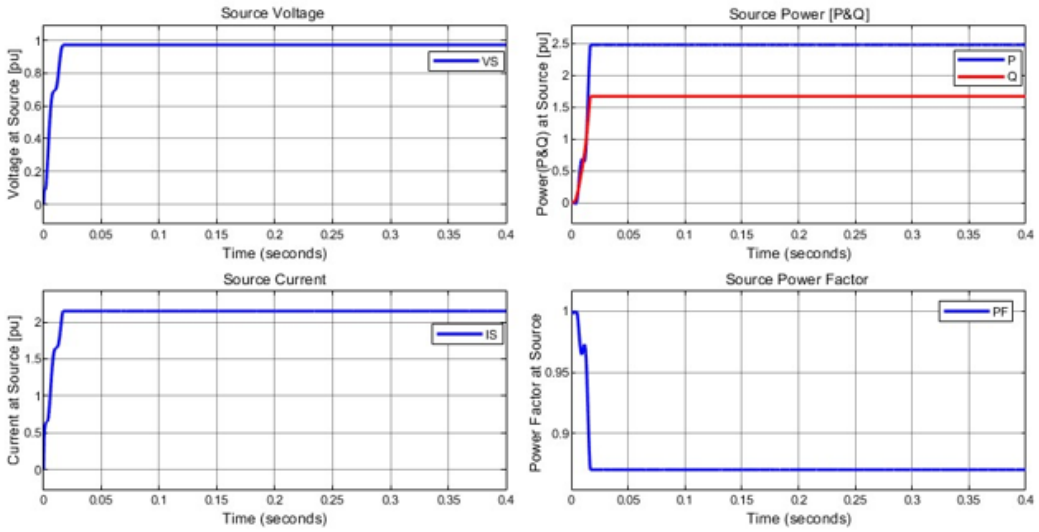

Figure 3.8 V, I, P (P&Q) and PF at Source Bus without MFCC Filter and Hybrid Load

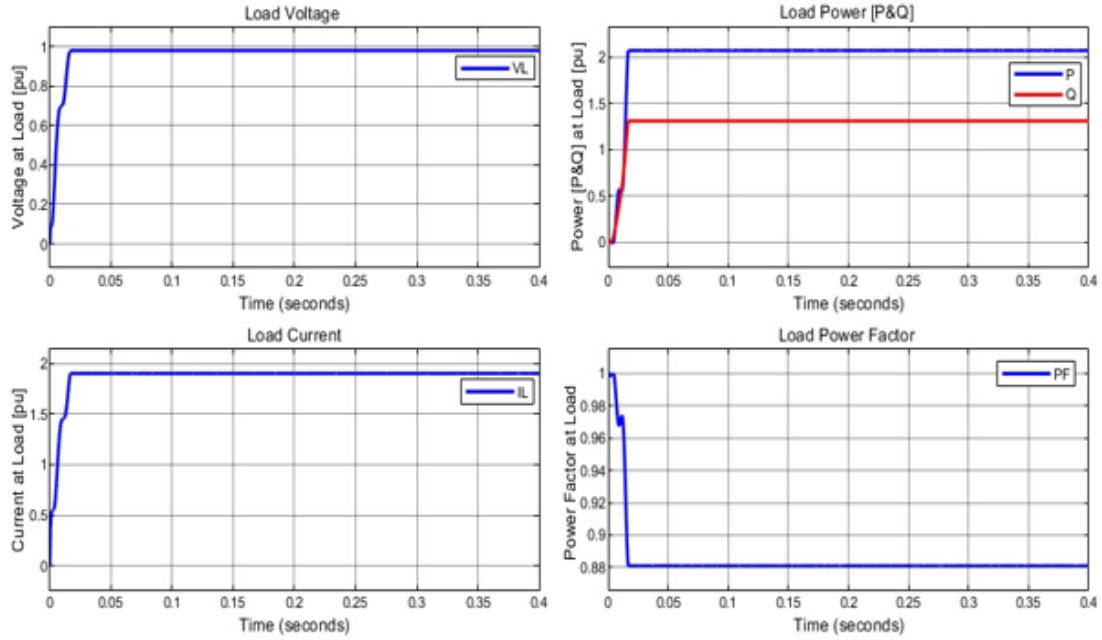

Figure 3.9 V, I, P (P&Q) and PF at Load Bus without MFCC Filter and Hybrid Load

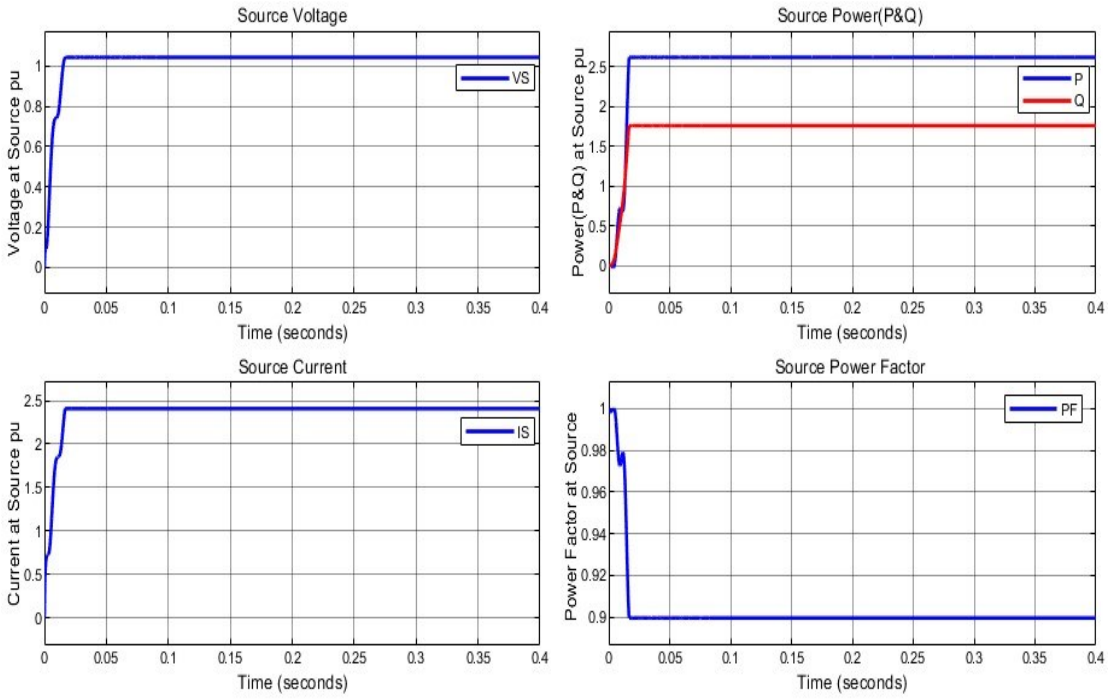

Figure 3.10 V, I, P (P&Q) and PF at Source Bus with MFCC Filter and Hybrid Load

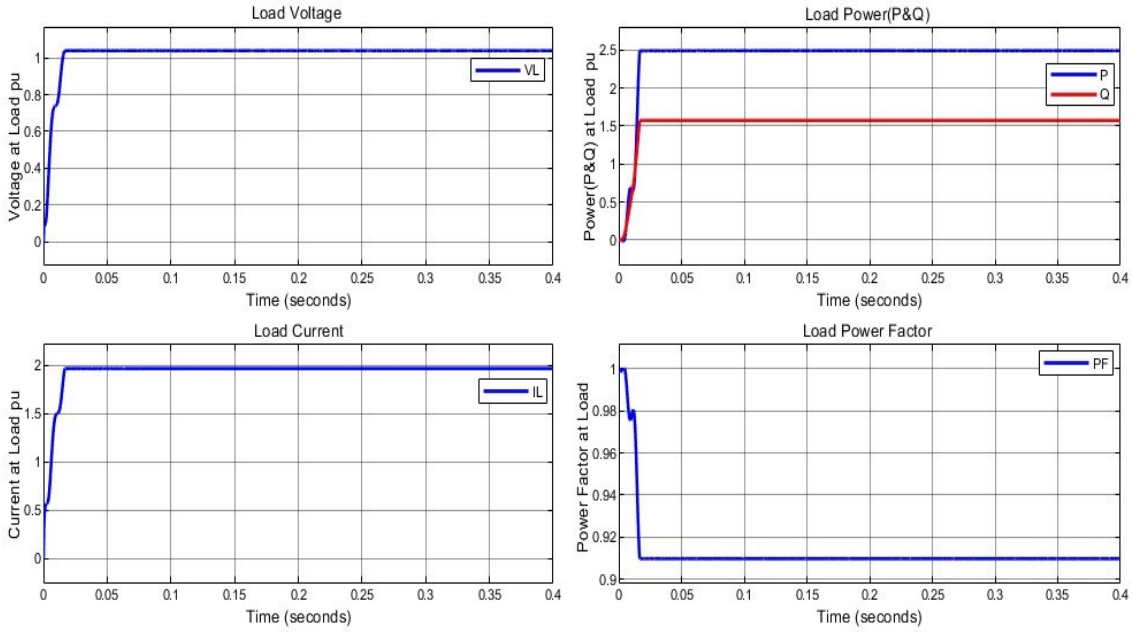

Figure 011 V, I, P (P&Q) and PF at Load Bus with MFCC Filter and Hybrid Load

Table 3.2: Dynamic Simulation Results without and with an MFCC Filter at Source Bus

Response Name	Without MFCC	With MFCC
Voltage at source Vs	0.89 pu	1.09 pu
Current at source Is	2.38 pu	2.4 pu
Active power at source bus (P)	2.5 pu	2.58 pu
Reactive power at source bus (Q)	1.52 pu	1.71 pu
Power factor at source bus (PF)	0.87 pu	0.90 pu

Table 3.3: Dynamic Simulation Results without and with MFCC Filter at Load Bus

Response Name	Without MFCC	With MFCC
Voltage at load VL	0.91 pu	1.09 pu
Current at load IL	1.95 pu	2 pu
Active power at load bus (P)	2.02 pu	2.5 pu
Reactive power at source bus (Q)	1.48 pu	1.55 pu
Power factor at source bus (PF)	0.88 pu	0.91 pu

Figures 3.12 and 3.13 show the Fast Fourier Transform (FFT) for the current and voltage at the source bus after using the filter and with the hybrid load.

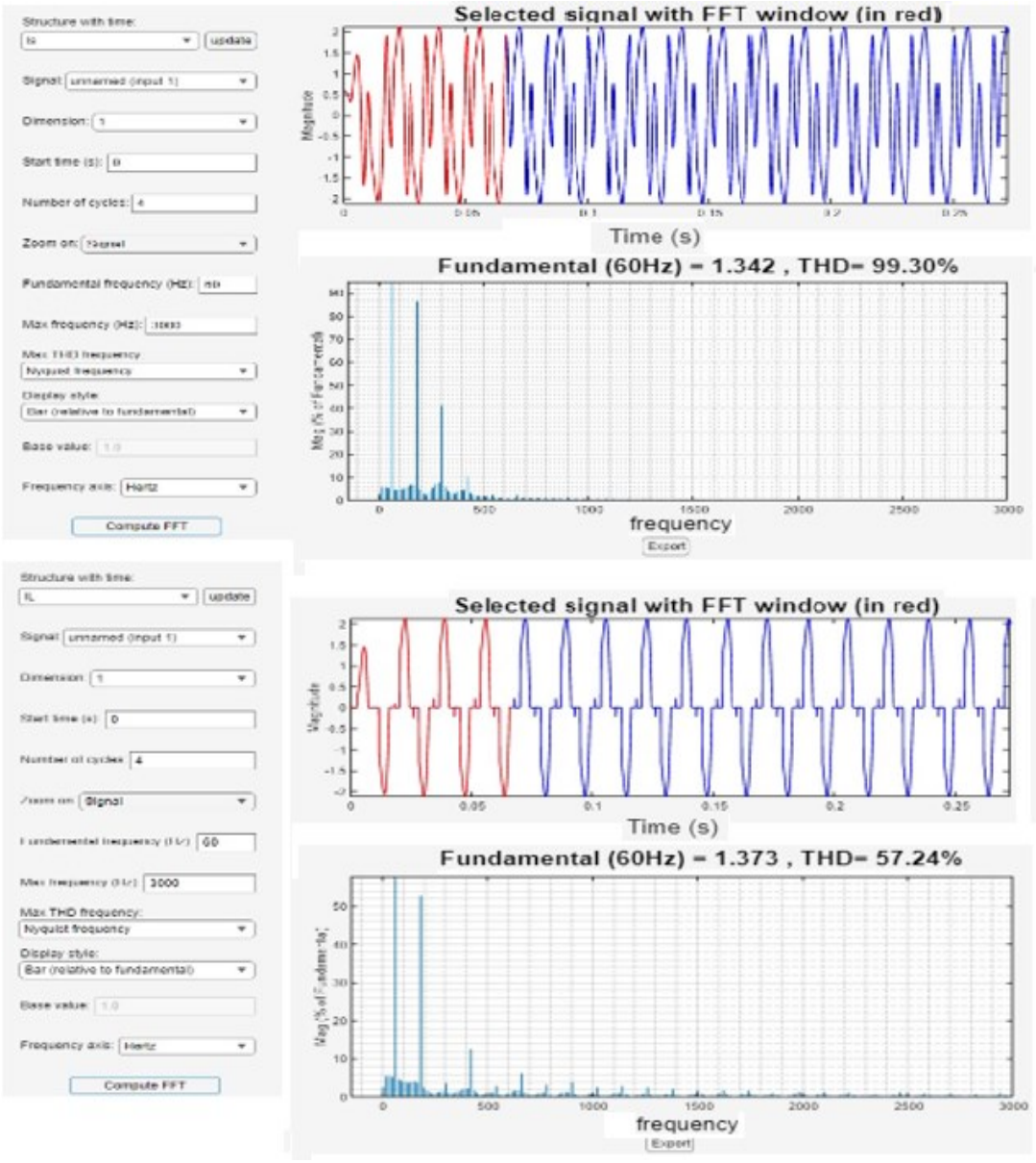

Figure 3.12 FFT for Current at Source & Load Bus with Filter and Hybrid Load

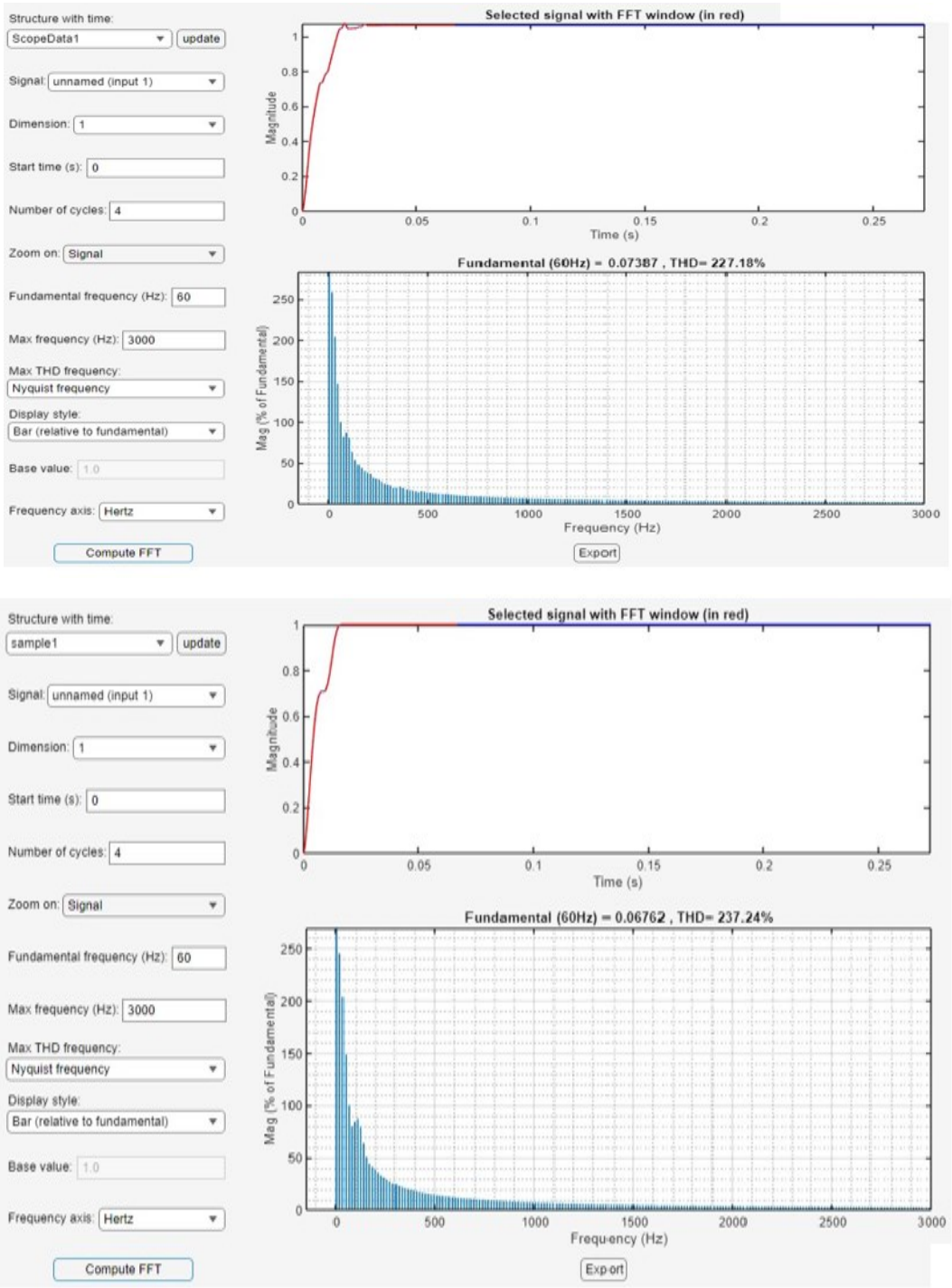

Figure 3.13 FFT for Voltage at Source & Load Bus with Filter and Hybrid Load

In the next section, the time scale is extended to 2 seconds to check whether there will be further change.

3.7.2 Hybrid Load with Extended Time Scale to 2 Seconds

As seen in Figures 3.14, 3.15, 3.16, and 3.17, the voltage, current, active, and reactive power is stable, and there is no fluctuation after adding the MFCC for both the source and the load bus.

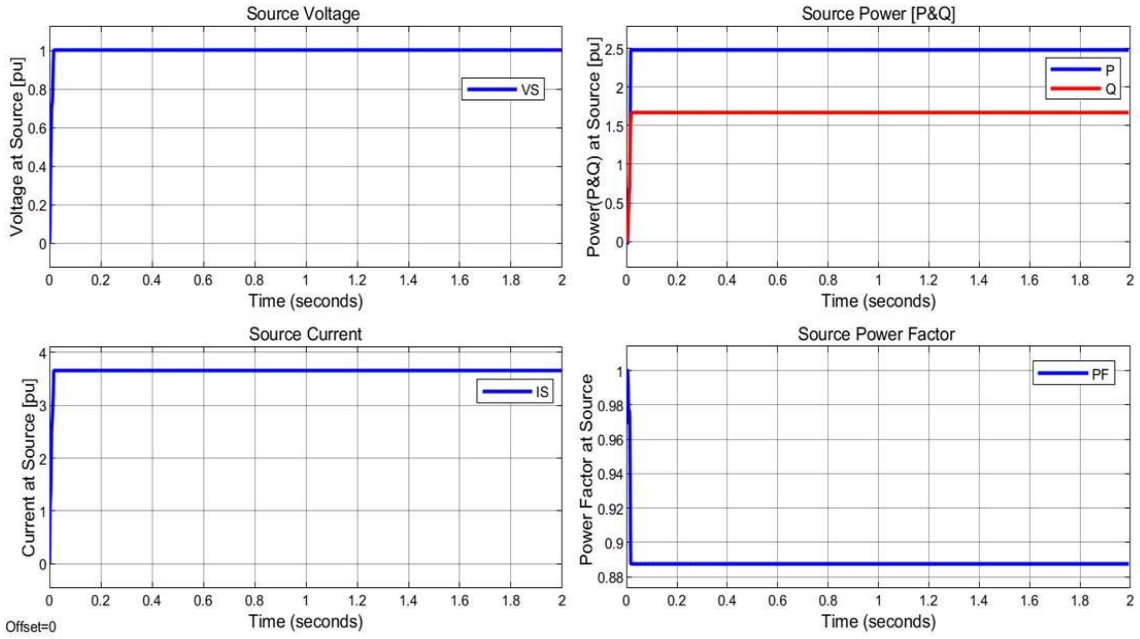

Figure 3.14 V, I, P (P&Q) and PF at Source Bus without Filter and Hybrid Load

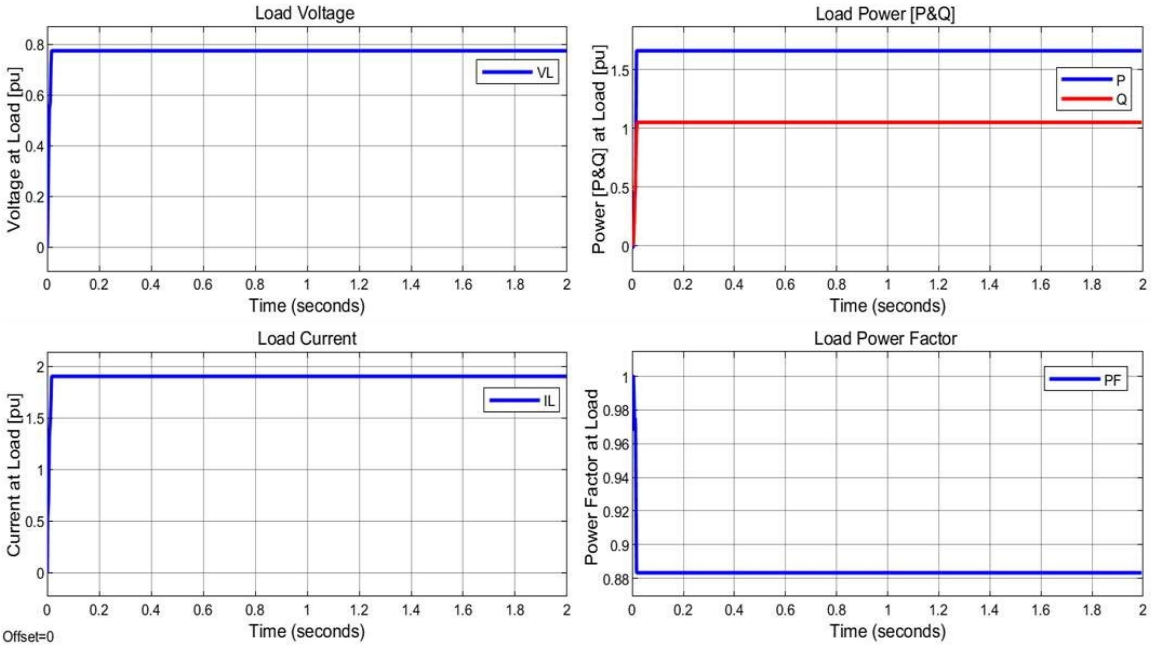

Figure 3.15 V, I, P (P&Q) and PF at Load Bus without Filter and Hybrid Load

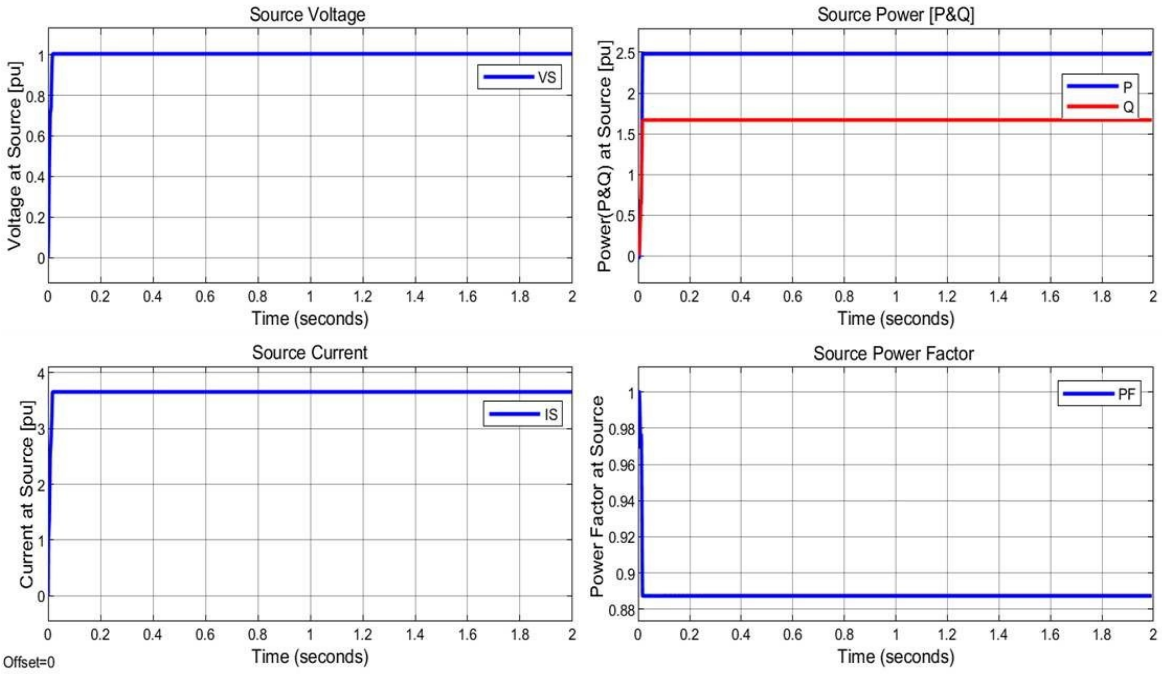

Figure 3.16 V, I, P (P&Q) and PF at Source Bus with Filter and Hybrid Load

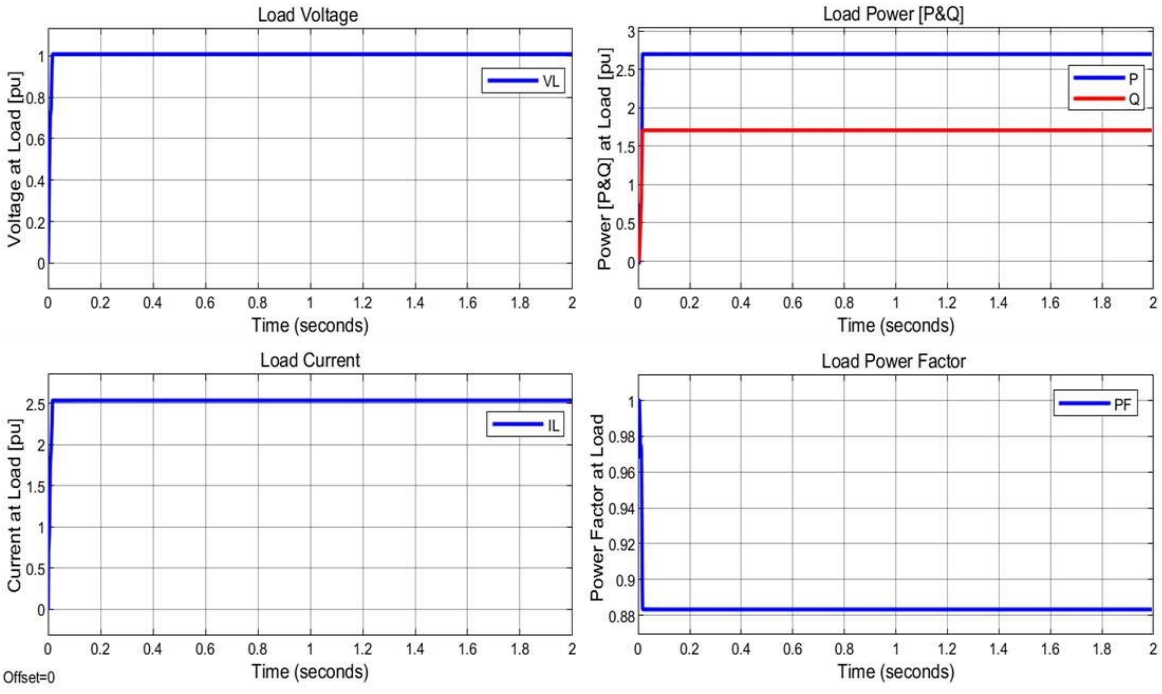

Figure 3.17 V, I, P (P&Q) and PF at Load Bus with Filter and Hybrid Load

Figures 3.18 illustrates the FFT for the current without a filter at the source and load buses.

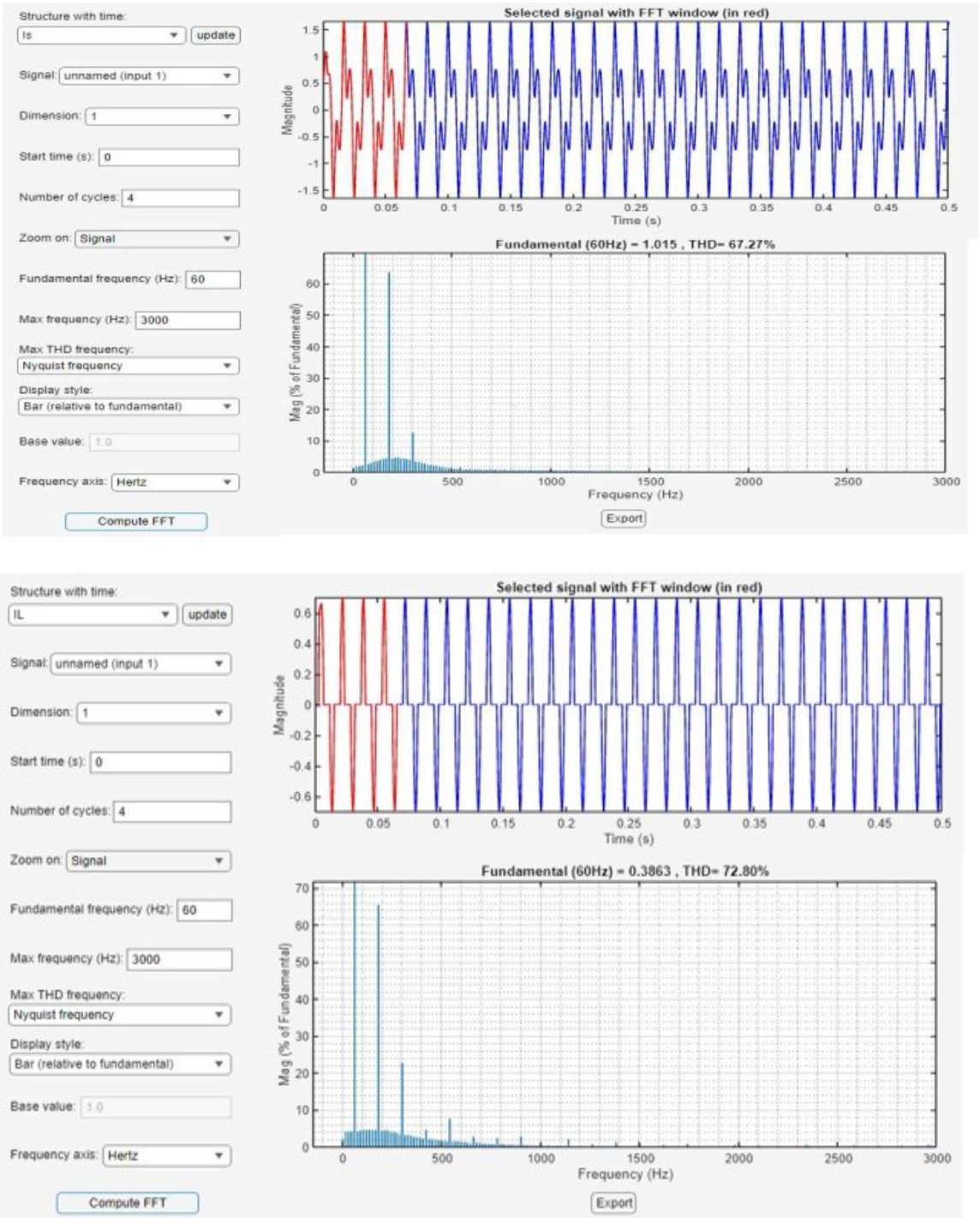

Figure 3.18 FFT for Current at Source and Load Bus without Filter for Hybrid Load

Figures 3.19 depicts the FFT for the voltage at the source and load buses.

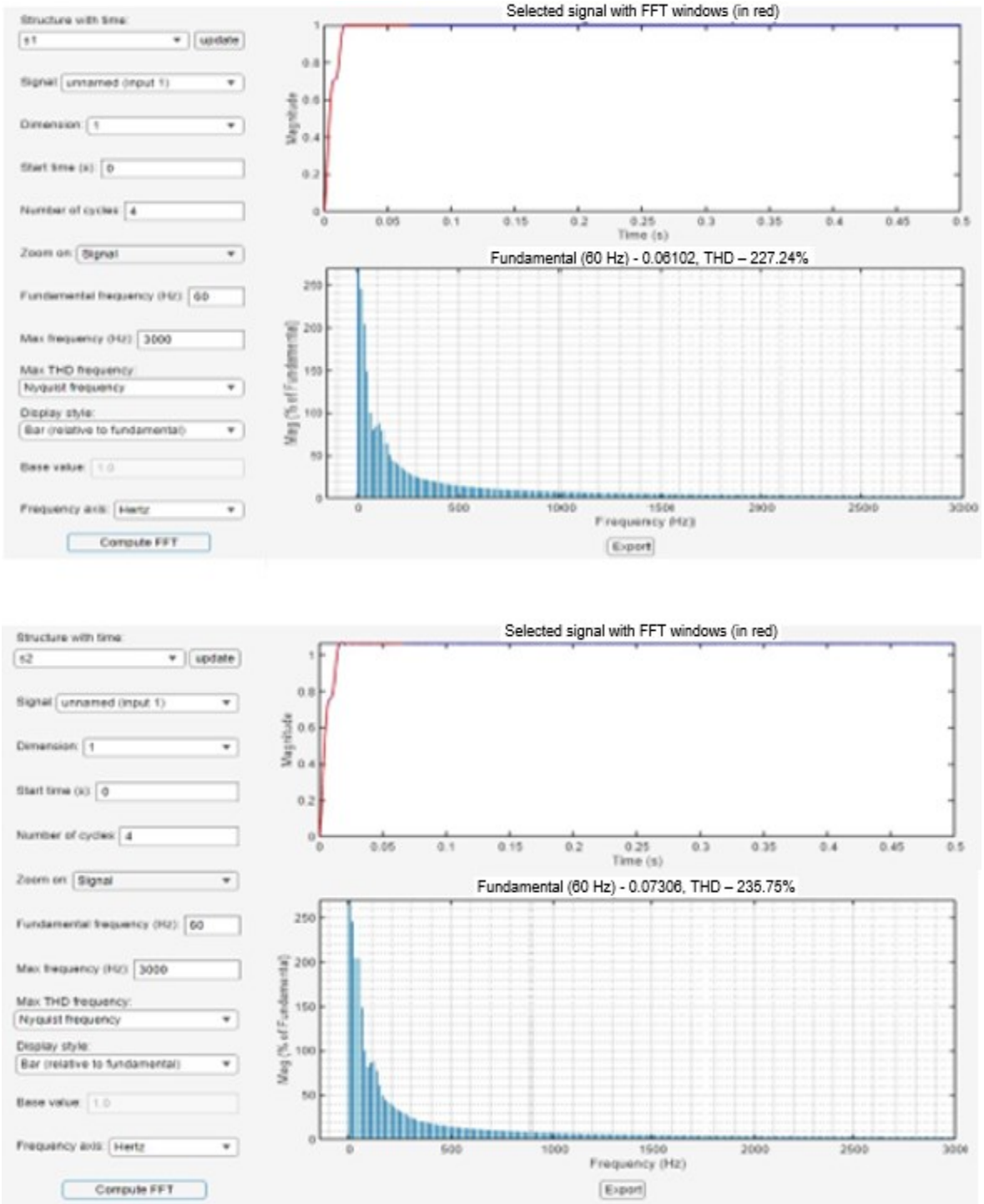

Figure 3.19 FFT for Voltage at Source and Load Bus without Filter for Hybrid Load

3.7.3 Load Changes with Open Circuit (OC) and Short Circuit (SC)

The following conditions are dictated to the grid to examine the AC grid's response to load excursions without and with the MFCC. Figures 3.20 to 3.25 show the results obtained with a hybrid load for voltage, current, active power (P), reactive power (Q), and power factor (PF) values with different cycle times of OC and SC at different time scales.

3.7.3.1. Time scale of 3 sec with OC of 0.1 sec and SC of 0.5 sec

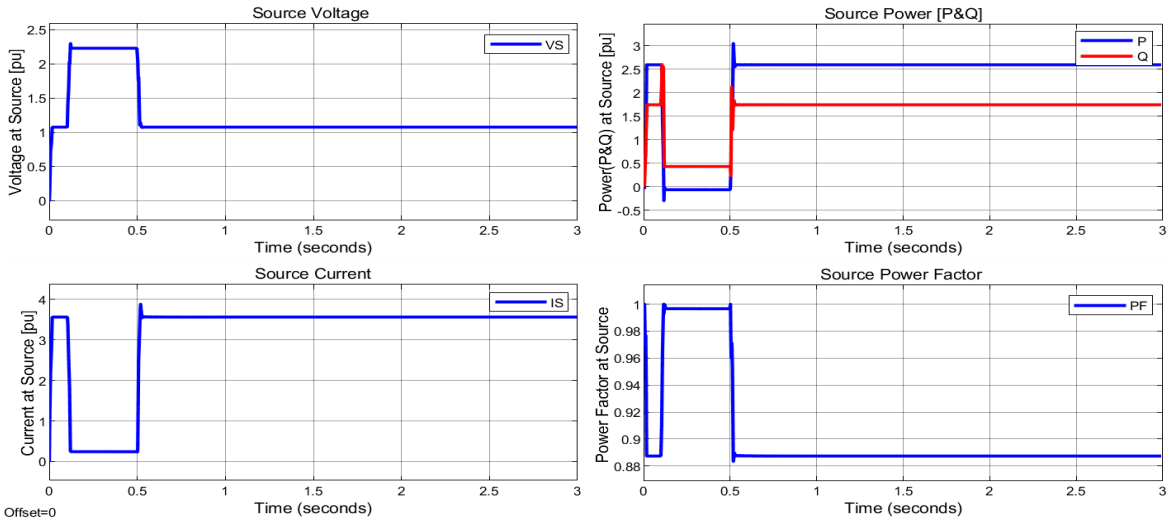

Figure 3.20 RMS V, I, P, Q, and PF at AC Source Bus Vs under Short-Circuit Fault

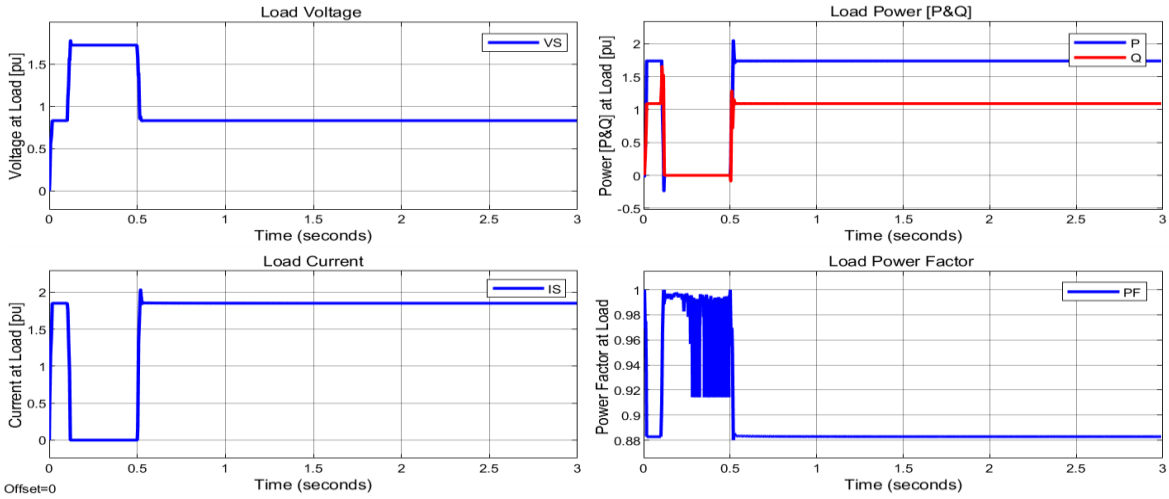

Figure 3.21 RMS V, I, P, Q, and PF at AC Load Bus VL under Short-Circuit Fault

3.7.3.2. Time scale of 2 sec with OC of 20 ms and SC of 100 ms

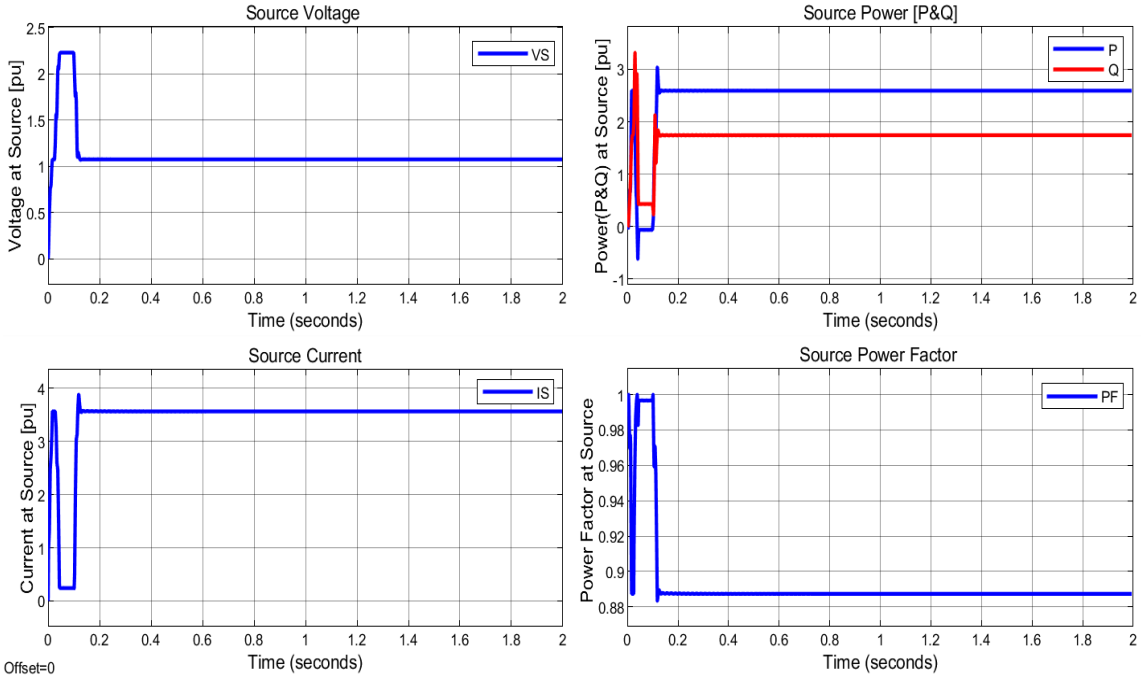

Figure 3.22 RMS V, I, P, Q, and PF at AC Source Bus Vs under Short-Circuit Fault

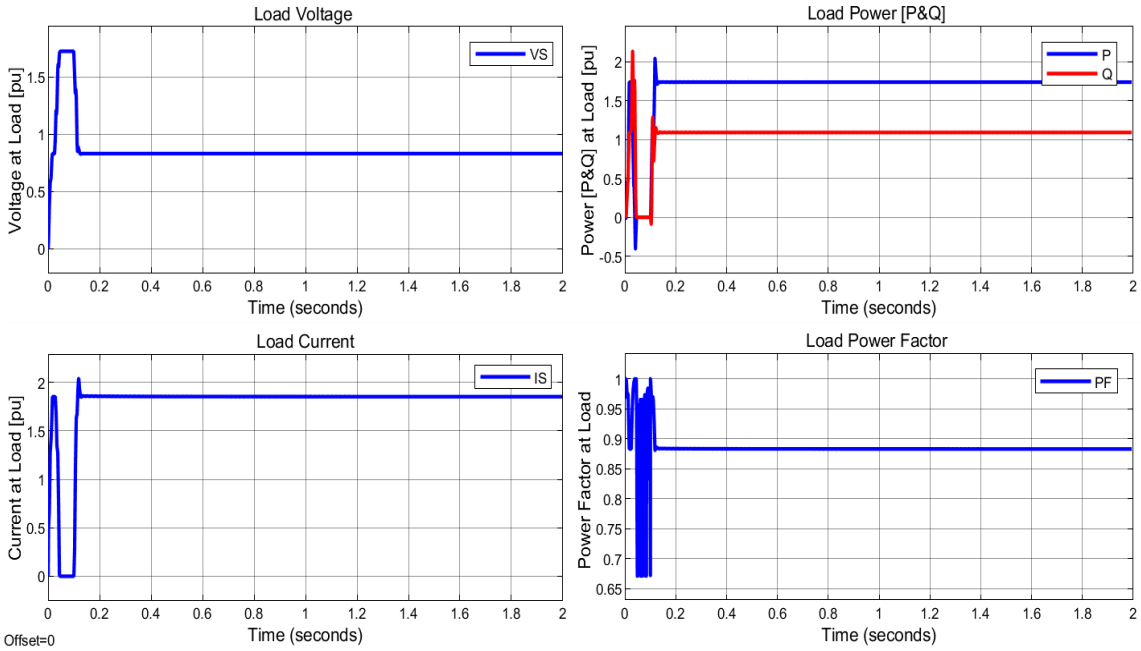

Figure 3.23 RMS V, I, P, Q, and PF at AC Load Bus VL under SC Fault

3.7.3.3. Time scale of 2 sec, with OC of 0.63 sec, and SC of 0.6 sec

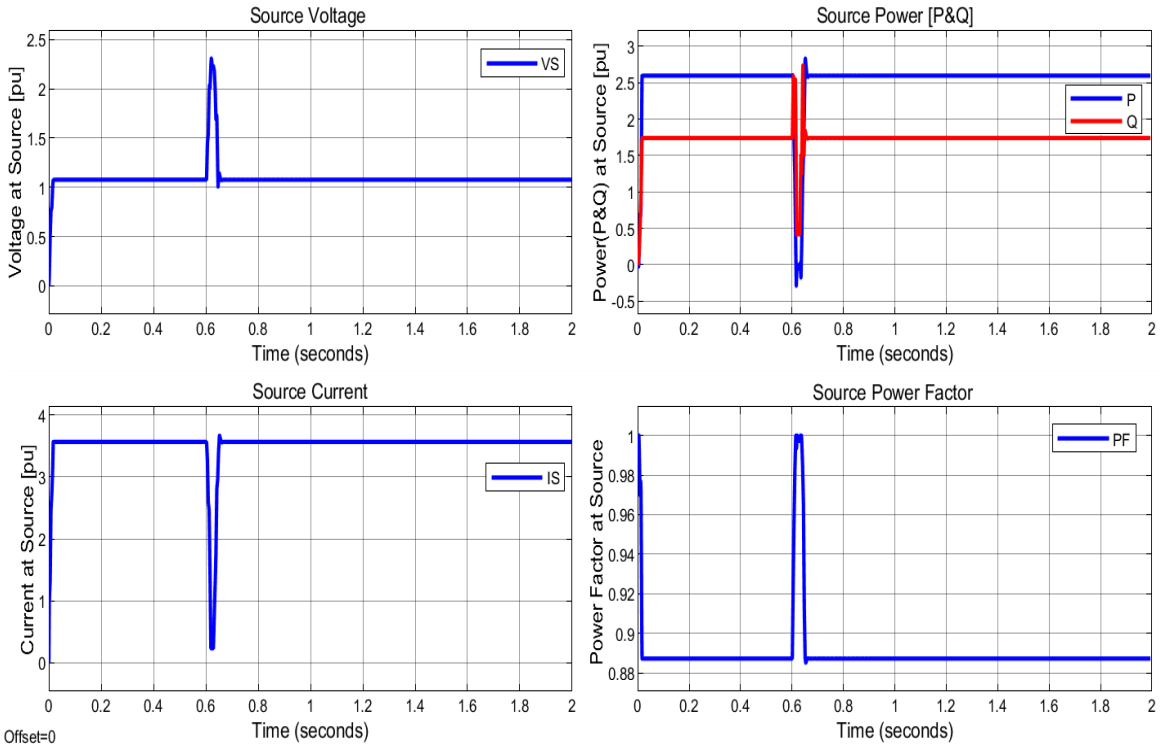

Figure 3.24 RMS V, I, P, Q, and PF at AC Source Bus Vs under OC for 0.63 sec and SC for 0.6s sec

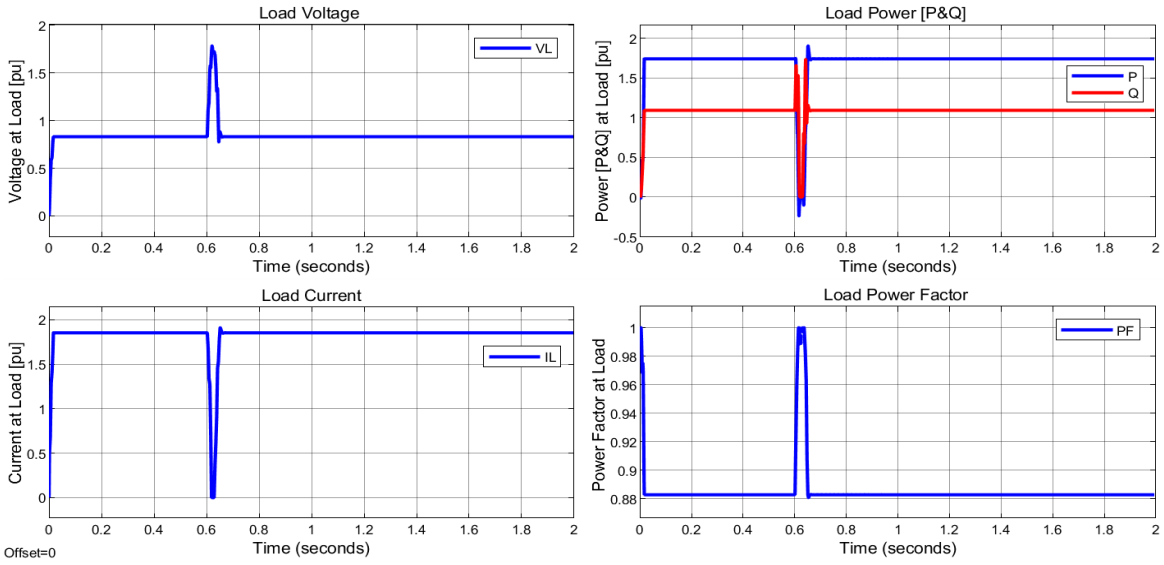

Figure 3.25 RMS V, I, P, Q, and PF at AC Load Bus VL under OC for 0.63 sec and SC for 0.6 sec

3.8 Conclusion and Chapter Summary

This chapter presented a new switched modulated capacitive filter compensation scheme for distribution/residential systems using nonlinear inrush loads. The SFC-PWM switched filter used a complementary switching of two IGBT/MOSFET to change action from a tuned arm low-pass filter to capacitive compensation. The SPWM pulse modulation was controlled online by a fuzzy logic multi-regulation loop, based on aggregate weighted loop error-weighted summation and configuration changes from capacitive compensation duty to power quality harmonics reduction of voltage and current transients. The proposed SFC/MFCC filter was validated using different loads, such as the DC ARC load, induction motor inrush loads, and common seal-type loads. The SFC/MFCC filter was shown to be effective in enhancing energy utilization and reducing harmonic contents in voltages and current at source and load buses while also improving the power factor at the source. The SFC/MFCC filter can be extended to various energy efficient, power quality applications in DC-AC micro grids, renewable energy utilization, motor drives, and battery charging schemes. The dual arm SPWM double-function SFC filter tuned arm and capacitive compensation is controlled online with a multi-regulation fuzzy logic controller.

Chapter 4: A Low-Impact V2H Battery-Charging Station Using an AC Green Plug Switched Filter Scheme

4.1 Abstract

This chapter proposes a switched/modulated capacitor filter approach for optimizing electric vehicle (EV) and vehicle-to-house (V2H) battery-charging stations. The proposed method employs a classical optimized type-2 fuzzy logic controller (FLC). Multi-mode charging modes are modified to enable super-fast charging and enhanced power quality while reducing voltage transients on the DC side and inrush currents and harmonics on the AC side. An inter-coupled AC-DC capacitor interface equipped with dual complementary switching modes is utilized by the modulated filter to enable capacitive compensator pulsing and dual operational modes for the tuned arm filter. The aim of the proposed switched inter-coupled AC-DC filter compensation strategy is to achieve EV-enhanced electrical power usage by mitigating AC-DC voltage transients and inrush currents.

The work presents a dual-action switched capacitor-tuned filter and reactive compensator scheme. The dual-action complementary switched filter/capacitor compensator is controlled by a multi-loop regulation controller to ensure effective measured action based on the global errors sum of the voltage and current/power loops. The novelty of the work lies in using a multi-loop weighted error action to carry the Pulse-Width Modulation (PWM) power width modulation/duty cycle ratio based on slow-changing dynamic/inrush loads. The results demonstrate the importance of the proposed scheme for improving overall system efficiency and quality. The proposed scheme is tested and validated under different operating conditions, proving its effectiveness.

4.2 Introduction

In vehicle-to-home (V2H) systems, electric vehicles have the advantage of environmental stability, along with lower costs, grid stability, emergency back-up power, energy cost reduction, and environmental sustainability [95], [57]. The adoption of EVs is being driven by factors such as climate changes concerns, air and noise pollution reduction, cost savings on fuel, and the steady movement away from fossil fuels towards clean energy [55]. Governments offer incentives for

people and private companies to develop and purchase EVs, shifting the focus to research and development related to EVs to improve its performance and reduce its cost [96], [97].

DC fast-charging systems for EVs have become one of the most popular charging systems due to their ability to charge EVs quickly. These systems can supply high-voltage DC power directly to the vehicle's battery, allowing for faster charging times. EV charging systems play a crucial role in facilitating the widespread adoption of electric vehicles by providing convenient and efficient ways to charge EVs batteries. V2H system can quickly charge an EV with direct current from the storage battery and can supply the electricity from the EV back to the household. EV charging systems are infrastructures and equipment which provide power supply to power battery of electric vehicle, and mainly include battery exchange and a charging pole as well as a standalone charging station [98].

According to industry standards, the charging of a battery involves a power factor correction (PFC) loop and a two-stage system. Both EVs and plug-in hybrid electric vehicles (PHEVs) rely heavily on power generation systems. Over the past decade, PHEVs have received special research attention due to their potential in replacing fossil fuel-powered vehicles [76], [99]. An EV's engine configuration determines the vehicle's classification as either a PHEV or a battery-electric vehicle (BEV). Vehicles that combine the features of PHEVs and BEVs are called plug-in hybrids (PEVs) [100], [101].

The world's increasing population and industrialization is leading to higher levels of air pollution, prompting the auto industry to focus on vehicles that reduce pollutants (e.g., hydrocarbons, carbon dioxide, etc.). However, only EVs can be a zero-emission [102]. This feature comes at the price of performance and ability to travel long distances without recharging. To offset these challenges, manufacturers are currently producing vehicles that combine good performance with reduced emissions, which are known as hybrid EVs (HEVs) [103]. In HEVs, the electric motor powered by a separate battery pack helps accelerate the gas-fired engine. One main advantage of HEVs over gas-generated vehicles is its ability to use the battery to recycle heat energy for other p.u.rposes, such as regenerative braking [83] – [104].

In a Flexible Alternating Current Transmission System (FACTS) device, the power flow is managed and controlled by electronics-based devices connected to electrical grids. FACTS devices have been demonstrated to be a highly efficient approach for enhancing power system quality.

They typically employ a fuzzy logic control system in a PWM dynamic switching/regulation strategy that uses EV battery-charging systems to optimize both power consumption and quality [94]. FACTS devices offer numerous advantages compared to other devices like type-2 fuzzy logic controllers (FLC). FACTs are characterized by their reduced costs, simplicity of use, and ease of adaptability when loads are uncertain and/or contain unknown process dynamics or mathematical modelling.

EV charging requires appropriate infrastructure, including stations for charging and battery exchange [56], [55]. FACTS devices aim to enhance the power factor and power systems quality while removing line current harmonics. The present thesis has developed a new hybrid filter compensator design for PHEVs for use within a buck-boost converter [105]. This FACTS-based device is controlled by quad-loop multi-zonal dynamic controllers and categorized under the V2G and V2H families of devices. To attain optimal charging performance, a quad-loop error-driven controller has been developed to assist the DC/DC buck-boost chopper [106], [107]. The proposed device is depicted in Figure 4.1.

As shown in the figure, a buck-boost regulator controlling the line current waveform and DC-link voltage level comprises the first stage, and the DC/DC converters usually comprise the second stage [108]. The battery charger at the AC/DC front-end determines the performance, so it is important to choose a topology that fulfills not only with input current harmonics but also with PFC regulatory requirements. Typically, battery chargers in PFC applications have a boost topology that utilizes a buck-boost section and AC/DC rectifier as a diode bridge [109], [110].

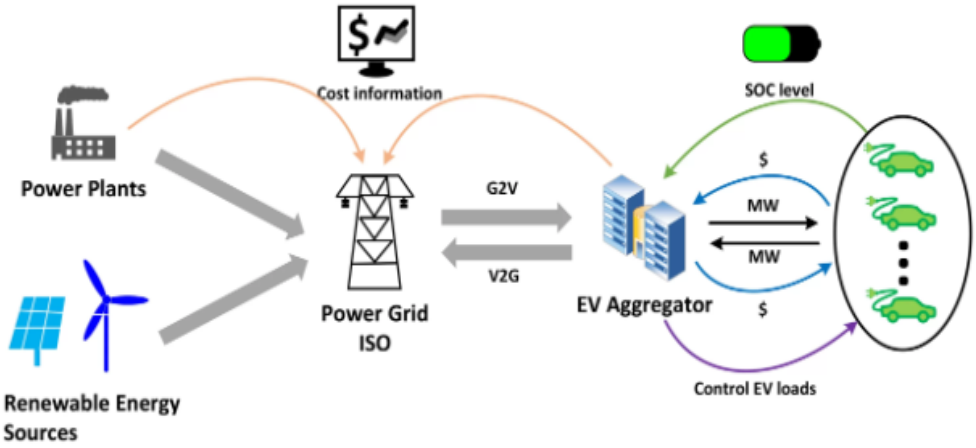

Figure 4.1 Vehicle-to-Home (V2H)

This chapter proposes a novel low-cost FACTS dynamic voltage scaling (DVS)/general purpose (GP) device that is validated in a MATLAB/Simulink software environment using a type-2 FLC to stabilize voltage and deliver energy efficiently and securely to the load. The proposed FACTS-DVS/GP scheme incorporates switches for dynamic error-driven control, which results in enhanced response. The work also compares a mobile/EV battery charger performance both with and without the MFCC-FACTS device for testing improvements in power quality, power factor, and harmonics reduction.

4.3 Literature Review

In [111], different V2H scenarios were considered using a multi-port converter-driven charging station and DC power production. The work investigated vehicles as battery energy storage systems and/or backup generators using DC bus design for optimal extraction from solar panels for DC power sources. Additionally, a hysteresis control pulse-width modulation (PWM) approach was utilized to control the charger station. Through simulations, the authors demonstrated that their control scheme easily supports energy management.

In [112], the authors presented a control scheme that uses an EV battery for an inverter to minimize depletion. The proposed technique incorporates a bridgeless bidirectional flyback converter, operated via solar charging, plug-in charging, and emergency inverting. The results from the simulations support the authors' claims that their proposed scheme can power critical loads and reduce grid stress in peak hours. The authors in [113], proposed a logarithmic hyperbolic cosine robust sparse adaptive filter algorithm for controlling grid-tied off-board chargers using a photovoltaic (PV) interface. The work demonstrated that algorithms offer optimal dynamic performance, as they can track key features of the load current in the shortest time. In this chapter, a bi-directional buck-boost converter enables EVs to be charged and discharged using different functionalities (e.g. V2H, G2V, V2G, etc.) and a hardware unit undergoes testing in dynamic conditions (e.g., load-switching, and different PV insulations). The obtained results conform to IEEE standards for total harmonic distortion.

In [114], the authors present a novel multi-functional charger using solar energy to power an EV. Various operational modes are considered, including grid connection and disconnection, selected by a synchronization/switching algorithm. Along with supplying power to/from the

grid/car, the proposed charger can also drive local loads, with simulation results demonstrating its usefulness in EVs. Also, the authors introduce a resonant capacitor selector that can be combined with a supply voltage changer to resolve issues related to narrow range power control. Both the proposed converter and controller satisfy IEEE standards.

In [115], a high frequency inverter that uses inductive power transfer is proposed for wireless EV charging. This solution also helps to reduce carbon emissions. The authors provided results that validate their proposed scheme. Meanwhile, in [116], a dual-active bridge was suggested to charge EVs in a V2H scenario. In this scheme, the inp.u.t current can be regulated via an AC-DC converter, with the overall aim of enhancing the power factor. Both the battery voltage and current can be regulated with an isolated DC-DC converter.

A new three-phase four-wire inverter scheme was proposed for V2H application. The extra leg of the inverter helps to suppress the voltage oscillation in the outp.u.t waveform. By introducing the concept of virtual resistance, resonance phenomenon is damped. This results in improved functionality of V2H architecture. The performance of the inverter is also investigated with different types of loads [117].

In [118], the authors proposed a single-stage EV charger as a way to offset the double conversions, such as DC to DC and DC to AC. The single stage can enhance both the battery and outp.u.t voltage and a logic control were developed for switching between load types. In addition, a one-leg shoot-through approach is proposed in the same work for modulation, as it aids in reducing insulated-gate bipolar transistor (IGBT) losses caused by switching and conducting. The authors' experimental results indicate that the charger provides a reasonable alternative.

In [119], a novel capacitor-less bi-directional EV charger is presented that has applications in both V2H and V2G operational modes, featuring smooth transition between the modes as well as low voltage. The proposed charger's DC-DC converter stage can also function as an AC-DC transformer with zero cross-switching on full load swings. The authors report 95.6% efficiency 95.6% for their proposed device at a 900W charging mode.

Finally, in [120], the authors proposed a novel EV charger that operates in four modes: power exchanges between PV arrays, EV batteries, and the grid. During power feeding, the charger can maintain a power factor of unity because the controller is responsible for making the decisions

about power sharing between the grid and solar arrays. In addition to offering superb dynamic level and steady-state performance, the proposed charger can operate on 230V 50Hz.

4.4 System Description

Figure 4.2 depicts a battery-charge system that has no inter-coupled hybrid filter compensator (HFC) FACTS, while Figure 4.3 presents the proposed modulated filter capacitor compensator-switched filter compensator (MFCC-SFC) system. MFCC-SFC has two electronic switches that are controlled by using a type-2 FLC. As can be seen, both schemes have a full wave bridge rectifier to convert AC supply voltage into DC and incorporate a DC-DC buck-boost converter for increasing the DC voltage. Although cells in battery-powered devices can be stacked to achieve higher voltage, some high voltage applications are unable, due to space constraints, to house a sufficient cell stack. However, buck-boost converters can decrease cell count while also increasing the voltage. Figure 4.2 shows that a free-wheeling diode is connected to loads both in parallel and reverse, thus removing any negative voltage in the load and helping to supply a smooth current. Furthermore, the DC-DC buck-boost converter switch can be switched ON or OFF using a PWM pulse signal with a multi-loop weighted modified sliding mode controller. The DC-DC buck-boost converter output can then charge a high ampere-hour battery.

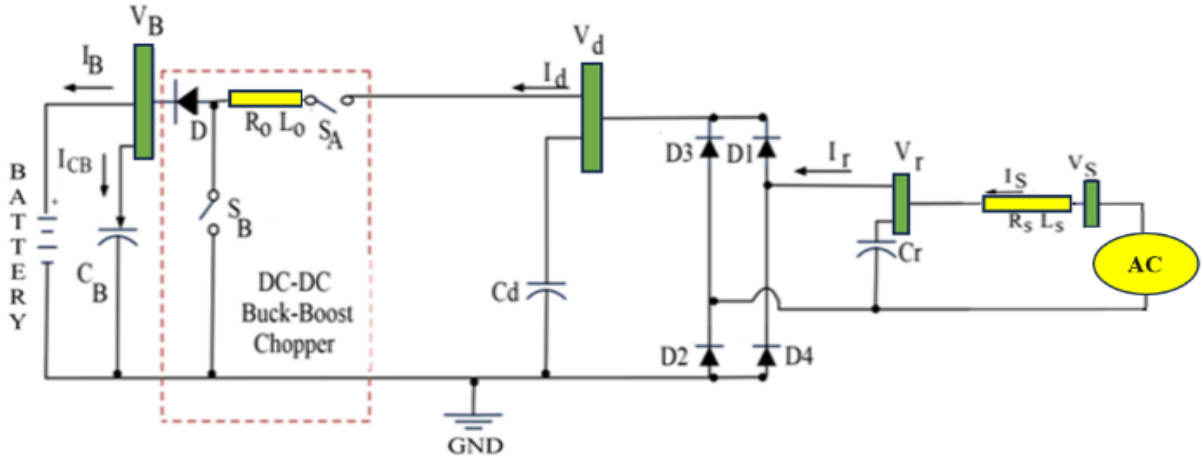

Figure 4.2 Basic Scheme for EVs without MFCC-SFC

V2H schemes is used for charging localize cars batteries at home and usually used for small size charger. To improve power quality, reduce line current harmonics, and boost the power factor,

a modified filter-hybrid filter compensator (MFHFC) can be connected in parallel to the full wave rectifier. Figure 4.3 illustrates the MFHFC, showing how it combines two shunt capacitors and a tuned arm shunt filter. Figure 4.3 indicates the PWM-produced switching pulses (P1and P2) caused by the control of the switches S_A and S_B. As can be seen, the complementary switching PWM pulses can modify the filter topology of FACTS-MFCC as follows:

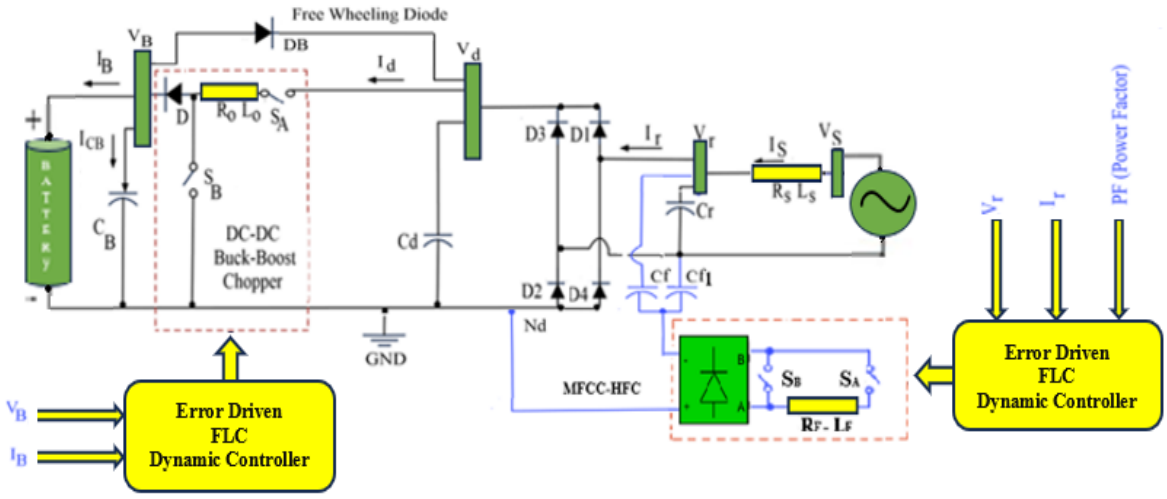

Figure 4.3 Proposed FACTS-Based (MFCC-SFC) V2H Battery-Charging Scheme for EVs

First: When pulse 1 and pulse 2 present as high and low, respectively, the resistor and inductor are cut off, and the shunt capacitor provides the AC system with appropriate shunt capacitive compensation to increase the power factor.

Second: When pulse 1 presents as low and pulse 2 as high, both the inductor and resistor are incorporated as a tuned arm filter in the circuit for harmonics reduction.

4.5 Type-2 Fuzzy Logic Controller

Type-2 fuzzy logic is an extended version of type-1 fuzzy logic, with an aim to capture the uncertainties related to defining the type-1 fuzzy membership function. To perform this task, a footprint of uncertainty is introduced in type-1 fuzzy sets. This footprint of uncertainty is bound between the upper and lower fuzzy membership functions. Thus, any data from the real world will now have two degrees of membership when mapped using interval type-2 fuzzy sets [121]. This completes the fuzzification process.

The fuzzified lower and upper degrees of membership are operated on rule-base and all the rules are evaluated in sequence. Now, since we have more encoded information, defuzzification cannot be directly performed. Therefore, a type of reduction method is introduced to mitigate the complexity of the algorithm. Many types of reduction algorithms are available, with the Karnik-Mendel approach being the most widely used method. However, this algorithm is more complicated, so some computationally less expensive methods have also been proposed. After the type of reduction, crisp value is generated through the same defuzzification methodology, as is the case with type-1 fuzzy logic. In our work, we used triangular membership functions to represent upper and lower fuzzy sets, as depicted in Figure 4.4 [122].

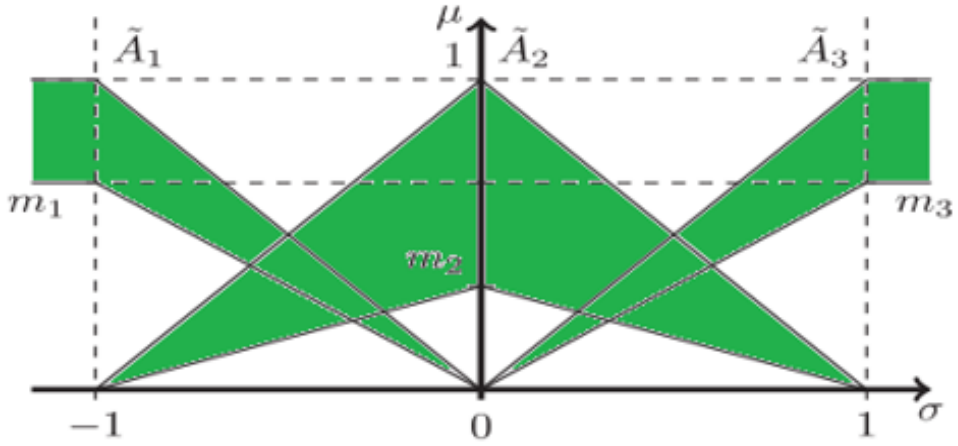

Figure 4.4 Triangular IT2-FSs

The rule structure of each S1-IT2-FLC is as follows:

Ri: IF σ is $\widetilde{A}_i$ THEN φ is B_i, $i = 1,2,3$ (4.1)

$\bar{\mu}_{\tilde{A}_i}$ can be described in terms of an upper membership function.
$\underline{\mu}_{\tilde{A}_i}$ can be described in terms of the lower membership function.
σ is the standard deviation.
$\boldsymbol{B_i}$ is crisp consequents 1,2,3.

The equations type-2 fuzzy logic are described as:

$$\varphi = \begin{cases} m_1 = m_3 = 1 - \alpha \\ m_2 = \alpha \end{cases} \quad (4.2)$$

where $m_1, m_2\ and\ m_3$ represent the height of the lower membership function.
Eq. (4.2) describes the fuzzy rule base:

$$\varphi = \frac{\varphi^{'} + \varphi^{r}}{2} \tag{4.3}$$

while Equation (4.3) describes the type of reduction mechanism of type-2 fuzzy control, as shown in Figure 4.4. In the figure, $\varphi^{'}$ and φ^{r} are the endpoints of the type of reduced set, which are described as follows:

$$\begin{cases} \varphi^{l} = \frac{\sum_{i=1}^{L} \overline{\mu}_{\tilde{A}_i}(\sigma) B_i + \sum_{i=L+1}^{N} \underline{\mu}_{\tilde{A}_i}(\sigma) B_i}{\sum_{i=1}^{L} \overline{\mu}_{\tilde{A}_i}(\sigma) + \sum_{i=L+1}^{N} \underline{\mu}_{\tilde{A}_i}(\sigma)} \\ \varphi^{r} = \frac{\sum_{i=1}^{R} \underline{\mu}_{\tilde{A}_i}(\sigma) B_i + \sum_{i=R+1}^{N} \overline{\mu}_{\tilde{A}_i}(\sigma) B_i}{\sum_{i=1}^{R} \underline{\mu}_{\tilde{A}_i}(\sigma) + \sum_{i=R+1}^{N} \overline{\mu}_{\tilde{A}_i}(\sigma)} \end{cases} \tag{4.4}$$

where L & r are switching points.

Equation (4.4) describes the type of reduction mechanism of type-2 fuzzy controller, as illustrated in Figure 4.5:

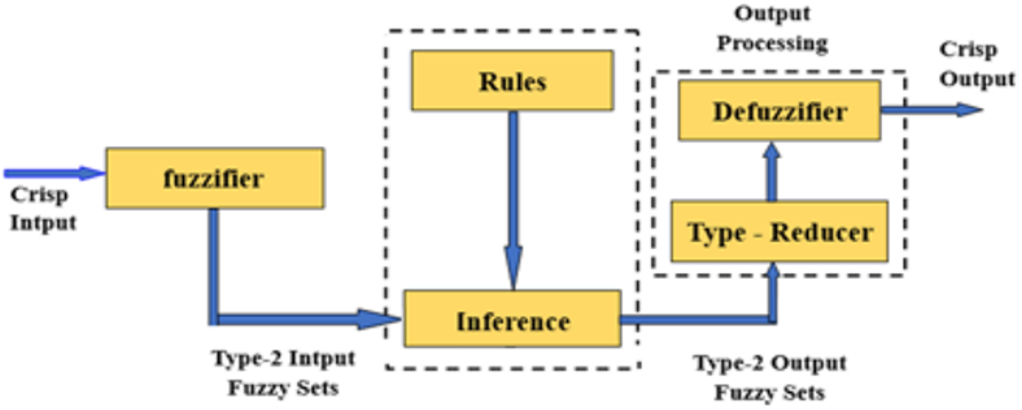

Figure 4.5 General Type-2 Fuzzy Information Processing

4.6 Lithium-ion Battery

EVs, especially high-performance ones, rely on Lithium-ion batteries. Compared to other rechargeable batteries on the market, Lithium-ion products provide a high number of charge/discharge cycles as well as high specific energy and are relatively cheap. These features make Lithium-ion batteries better options compared to nickel metal hydride and silver zinc batteries. However, due to their relative scarcity in the commercial market, Lithium-ion batteries need to be assembled as cells in series/parallel configurations to achieve the desired battery sizes [123].

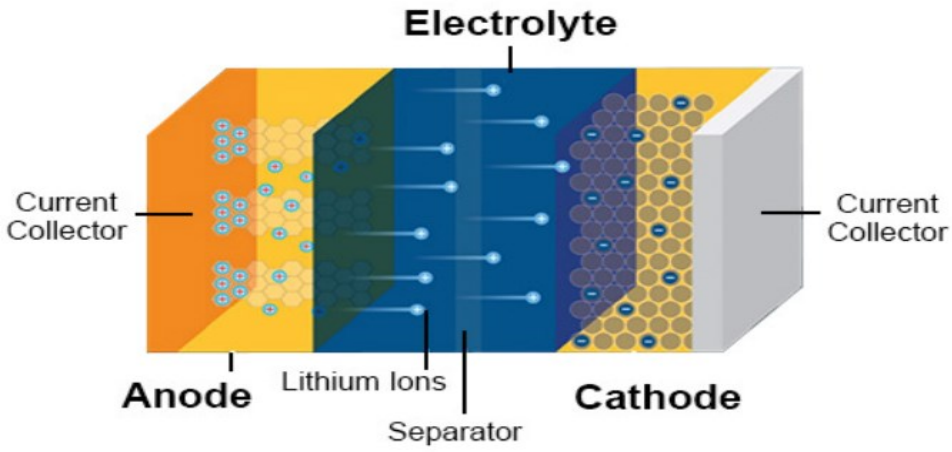

Figure 4.6 Diagram of Lithium-ion Battery

This factor, along with some emerging safety issues, can make it difficult to create efficient and dependable battery packs for EVs. Added to these problems is that rechargeable lithium-ion battery charge and discharge can be highly complex electro-chemical processes to model mathematically or to examine electro-chemically.

Figure 4.6 depicts a rechargeable lithium-ion battery. As can be seen, the models shown in the figure have great precision because the equations are dependent on internal chemical reactions. Equation (3) expresses the battery's electro-motive force (EMF). As shown in Figure 4.6, the model includes the measured battery voltage at the terminals V_{bat} along with the product (at that moment in time) of the current and equivalent over-potential resistance [124].

$$EMF(SOC) = V_{bat}(t) - i(t) \times R_{overpotential}\ (SOC) \quad (4.5)$$

SOC estimation method: The SOC is defined as the average concentration of lithium-ions in cathode over its maximum concentration.

$$SOC = \frac{\text{Avarage concentration of Lithium ion in cathode}}{\text{Maximum concentration of Lithium ion in cathode}} \quad (4.6)$$

Hence,

SOC_{min} greater than 0 & SOC_{max} less than 1

$$SOC = \frac{SOC_k - SOC_{min}}{SOC_{max} - SOC_{min}} \quad (4.7)$$

where,

SOC_k is the amount of energy present at time k.

$$SOC = \frac{Q_{remain}}{Q_{rated}} x\ 100 \quad (4.8)$$

The Lithium battery can be obtained by the ampere-hour integration method, which can be expressed by the following formula:

$$SOC(t) = \left(SOC_{(t_0)}\right) + \frac{1}{Q_N}\int_{t_0}^{t_0+t} I_{bat}\, d\tau \text{ x } 100\% \quad (4.9)$$

The SOC of the Lithium battery can be obtained by the ampere-hour integration method, which can be expressed by the following formula:

$$SOC(t) = (SOC(t_0) - \int_{t_0}^{t} \frac{\eta I d\tau}{Q_N} X\ 100\% \quad (4.10)$$

$$SOC(t) = SOC_{(t_0)} - \frac{I(t)}{Q_N} \quad (4.11)$$

where:

I_{batt} is the charging and discharging current of the battery.

V_{bat}= battery voltage (V)

Q_N is the capacity of the Lithium battery.

There are various ways to measure the EMF of a battery, either directly or indirectly, and it is strongly correlated with the battery's state of charge (SOC). The battery is charged and discharged at a low current rate using the voltage relaxation method, afterwards used to allow the battery to reach equilibrium by relaxing (resting) for a while [125].

4.7 MFCC-SFC

In AC systems, FACTS technology can be used to boost reliability, efficiency, and power transmission control. In fact, improvements in power quality and in harmonics mitigation are the key FACTS features and use IGBT switches controlled by dual complementary pulses. This allows Mel Energy Spectrum Dynamic Coefficients (MEDC) circuit equivalent admittance to be modified from different operating states [126]. For instance, when switches S1 and S2 are open, the inductor and resistor are circuit-connected, but when the switches are closed, the inductor and resistor are shorted. The result is a capacitive admittance occurring within the capacitor bank as shown in Figure 4.7. The tri-loop dynamic error-driven Type-2 FLC can control IGBT switches [35]. It is worth noting that a FACTS system with a switchable capacitor bank can drastically decrease system harmonics, as MFCCs are programmed to mitigate ripples and thereby reduce current oscillations [78], [127].

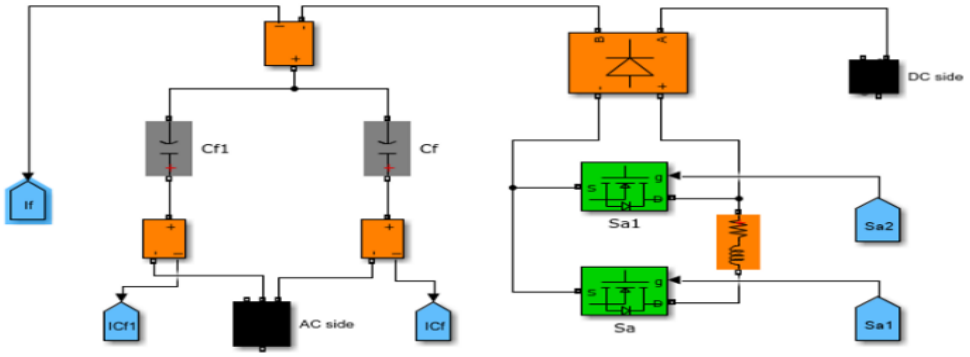

Figure 4.7 MFCC – SFC Switched Green Plug – Filter Compensator Scheme

This MFCC strategy uses the bus's separated voltage and current components. Sine-triangle pulse-width modulation (SPWM) has been widely employed in recent years, especially in renewable energy applications [103]. These include power inverters with the error value and duty ratio [59].

The aim of the dynamic controller is to maintain stable current and voltage levels while transmitting any mistakes to the SPWM. The SPWM then generates adjustable-width pulses in a series, creating a mimic of sine waveforms (see Figure 4.7). The power electronic converters that are used in MFCCs feature improved the power due to higher current and voltage ratings, resulting in optimal efficiency in operation and appropriate sizing [74]. The proposed technique is simulated using a MATLAB/Simulink-2023 digital simulation environment, and the system's dynamic performance is tested and validated with the proposed controller based on different operating conditions. A key benefit of the proposed compensator is its ability to pair with renewables to reduce the impact of faulty states on the grid [66].

4.8 Simulation Results and Discussion

Digital simulation results based on a MATLAB/Simulink/Sim-Power software environment is used to verify the dynamic effectiveness of the introduced type-2 FLC and the proposed MFCC-based battery-charging V2H scheme with an SOC of 50% for EV systems, as illustrated in Figure 4.8 and in the following subsections:

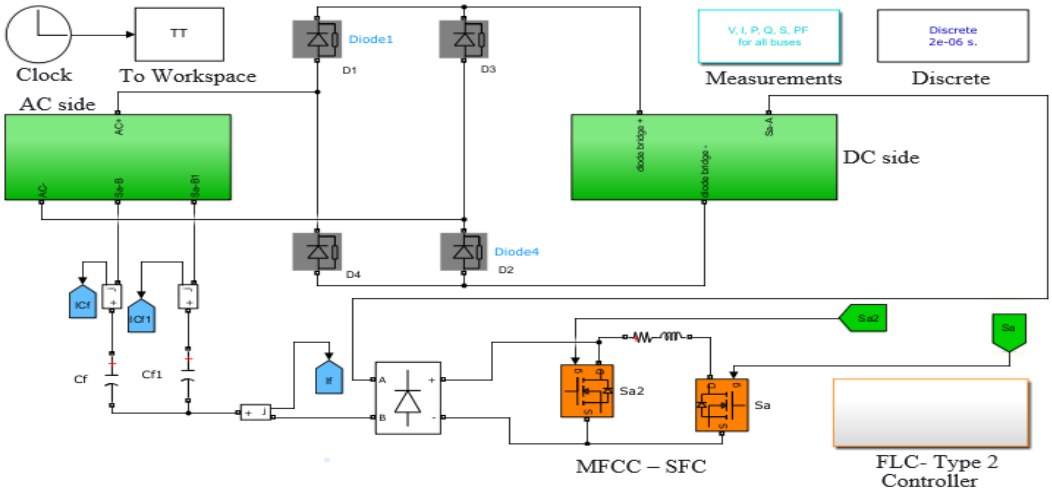

Figure 4.8 Hybrid Filter Compensator (HFC) for V2H Battery-Charging SOC 50% using FLC, without/with MFCC-SFC

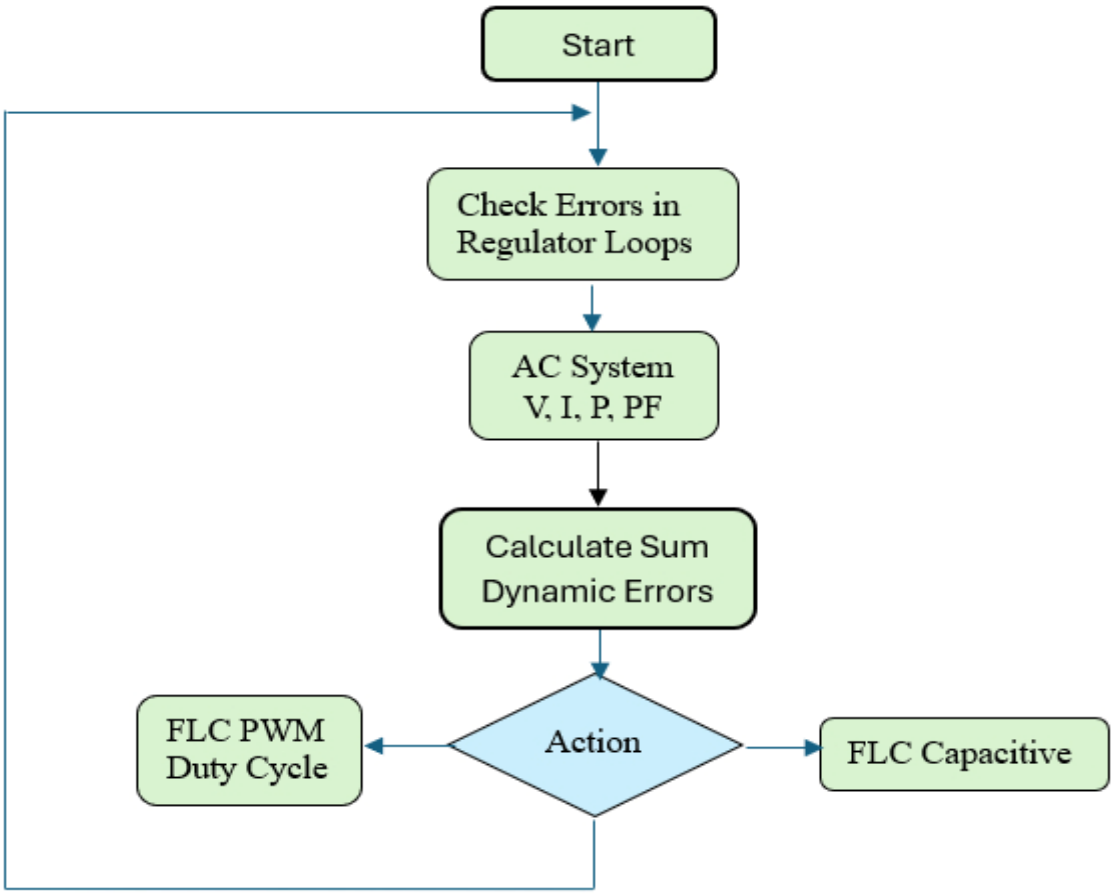

Figure 4.9 Flowchart of Dual-Mode Switched Filter with FLC

The errors are checked first in the regulator loops and are based on voltage, current, power, and power factor signals. The sum of the dynamic errors is then calculated and fed to the controller, which then takes one of two actions: to use either the FLC PWM duty cycle or the FLC capacitive compensation filter direction. The controller acts on dynamic errors and adjusts the duty cycle ratio for either the tuned arm filter or the capacitive compensation action. Next, the errors in the regulator loops are checked and step k+1 is added for each step. The control cycle is again repeated and the dynamic changes are reviewed to determine whether the dynamic duty cycle ratio is on or off. The looping continues for each controller time step until the required performance is reached. As shown in Figure 4.9, the controller is modified at each control time step at 5-10 times the largest system time constant.

4.8-1 FLC without and with MFCC – SFC at normal operating condition case

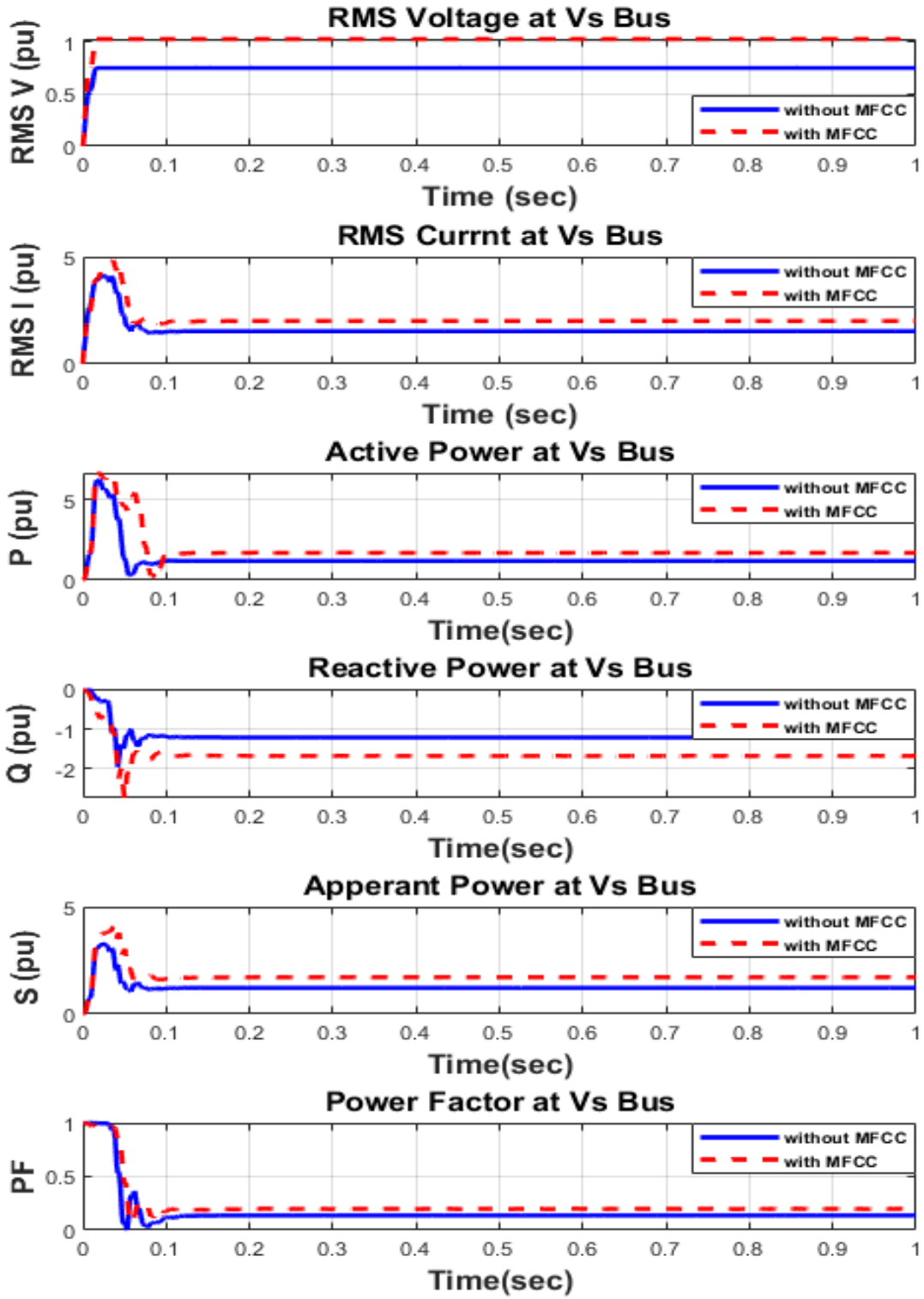

Figure 4.10 RMS V, I, P, Q, S & PF at Vs Bus with and without MFCC-SFC Compensator

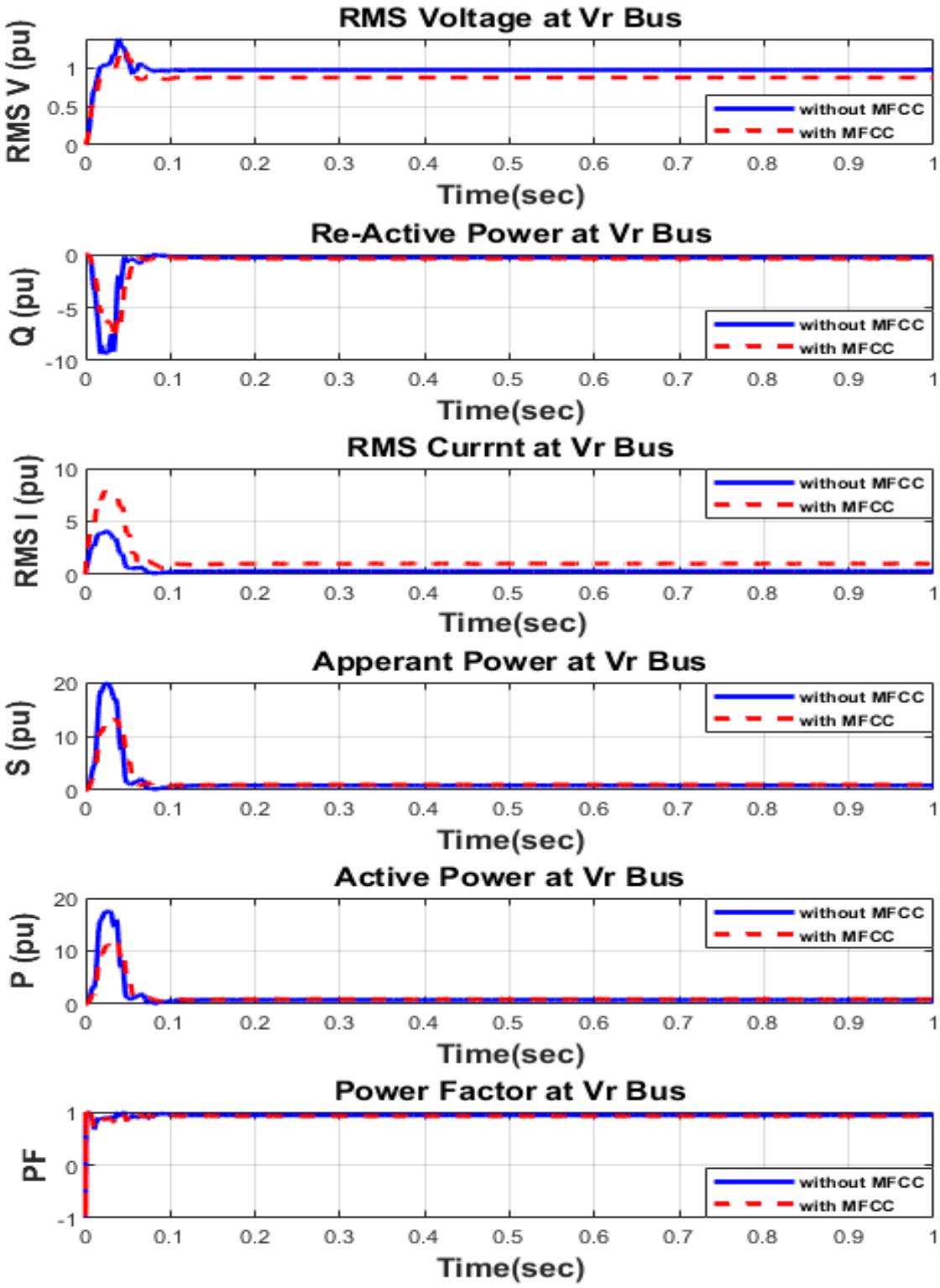

Figure 4.11 RMS V, I & P, Q, S, and PF at Vr Bus with and without MFCC-SFC Compensator

Table 4.1: Voltage, Current, and Active Power Values at AC Buses

Buses	Vs (pu)			Vr (pu)		
	Vs	Is	Ps	Vr	Ir	Pr
Without MFCC	0.8	1.75	1.0	1.0	0.6	1.5
With MFCC	1.0	2.0	1.1	0.85	0.8	1.65
Improvement	0.2	0.25	1.0	0.15	0.2	0.15
% Improvement	20%	25%	10%	15%	20%	15%

The digital simulation results using MATLAB/Simulink-2023 for the proposed MFCC-SFC with normal operating case conditions at the AC side of the system are illustrated in Figures 4.10 and 4.11. (RMS V, I and P, Q, S, PF) which is RMS voltage and Current, and Active power, Reactive Power and Power factor at source bus Vs. As shown, the dynamic response of the root mean square (RMS) voltage at the Vs bus for the voltage is relatively constant at around 0.8 pu without the proposed MFCC and 1.0 pu with the MFCC for most of the time, except for a few seconds during the switching. Also, the figure shows that the RMS current is more variable than the voltage, but it is generally between 1.7 pu and 2 pu when the proposed MFCC is inserted and it has a less value compared to without the situation without the MFCC, which improves the voltage profile. On the other hand, the reactive power at the Vs is relatively constant at around 0.15 seconds, and the reactive power at the source bus is decreased. This improves the power factor from 0.2 to 0.3, as shown in Figure 4.10. As well, the active power is enhanced from 1.0 to 2.0 pu with MFCC, as presented in Table 4.1 and Figure 4.10.

Figure 4.11 shows that there is an improvement in the RMS current from 1.2 pu to 2 pu when the proposed MFCC is inserted at the Vr bus. There is also an enhancement in the power factor. Table 4.1 presents the current, voltage, and active power changes of the AC-side system buses without and with inserting the proposed MFCC-SFC. It is clear that after using the proposed MFCC-SFC, there is an improvement in the voltage as well as the active power and a reduction in the reactive power, which is reflected in an improvement in the power factor.

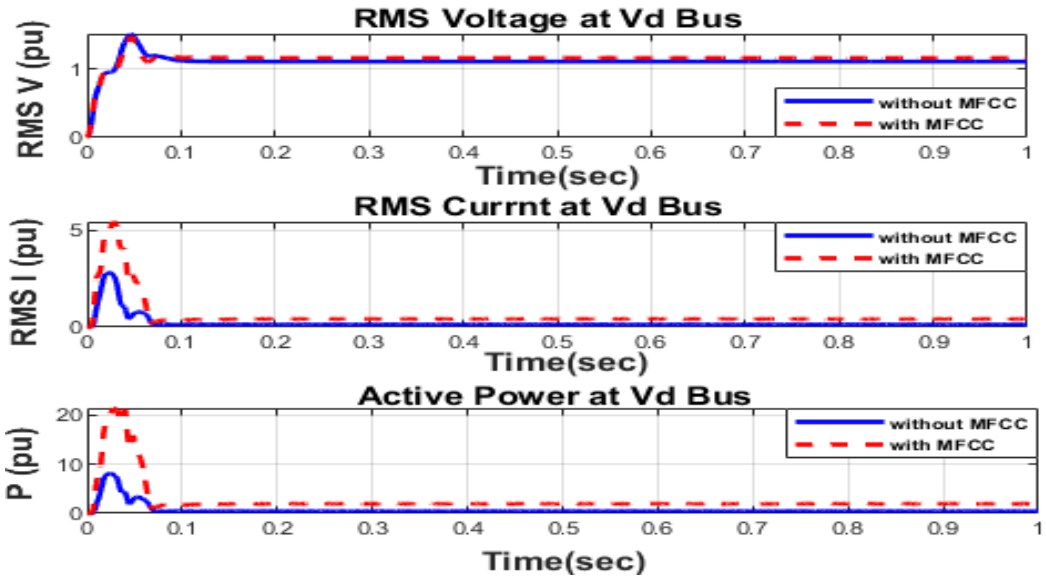

Figure 4.12 RMS V, I & P at Vd Bus with and without MFCC-SFC Compensator

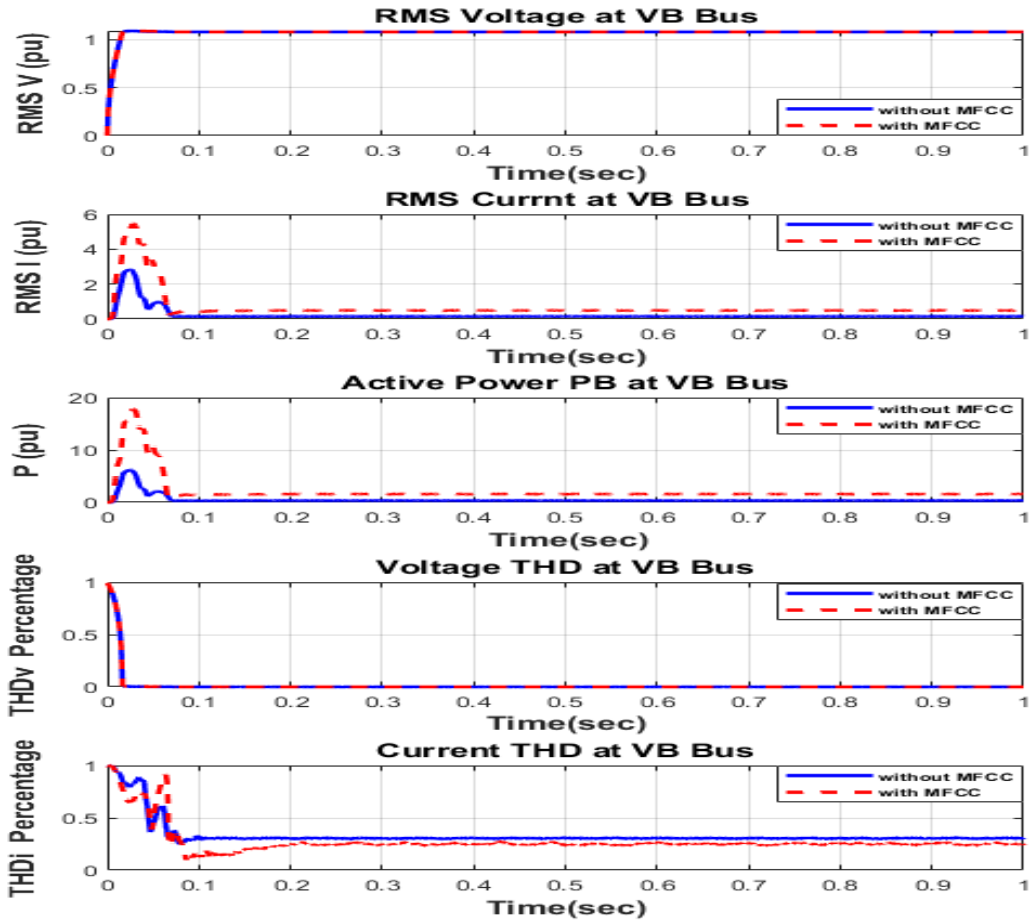

Figure 4.13 RMS V, I & P, THDv, and THDi at VB Bus without and with MFCC-SFC Compensator

Table 4.2: Voltage, Current, and Active Power Values at DC Buses

Buses	Vd (pu)			VB (pu)		
	Vd	Id	Pd	VB	IB	PB
Without MFCC	1.2	0.3	1.75	1.1	0.3	1.5
With MFCC	1.25	0.5	2.0	1.11	0.5	1.75
Improvement	0.05	0.2	0.25	0.01	0.2	0.25
% Improvement	5%	20%	25%	1%	20%	25%

Figures 4.12 and 4.13 depict the DC side of the charging scheme system for both Vd and VB buses. The dynamic responses of the RMS voltage, current, and active power are shown in Figure 4.12. From the figures, it is clear that there is an improvement in the voltage, current and active power at Vd bus with the introduction of the proposed MFCC. The results are summarized in Table 4.2. Figure 4.13 illustrates the improved active power and RMS current at the VB bus after using MFCC. The changes in the values of the voltage, current, and power are compared with and without MFCC and displayed in Table 4.2.

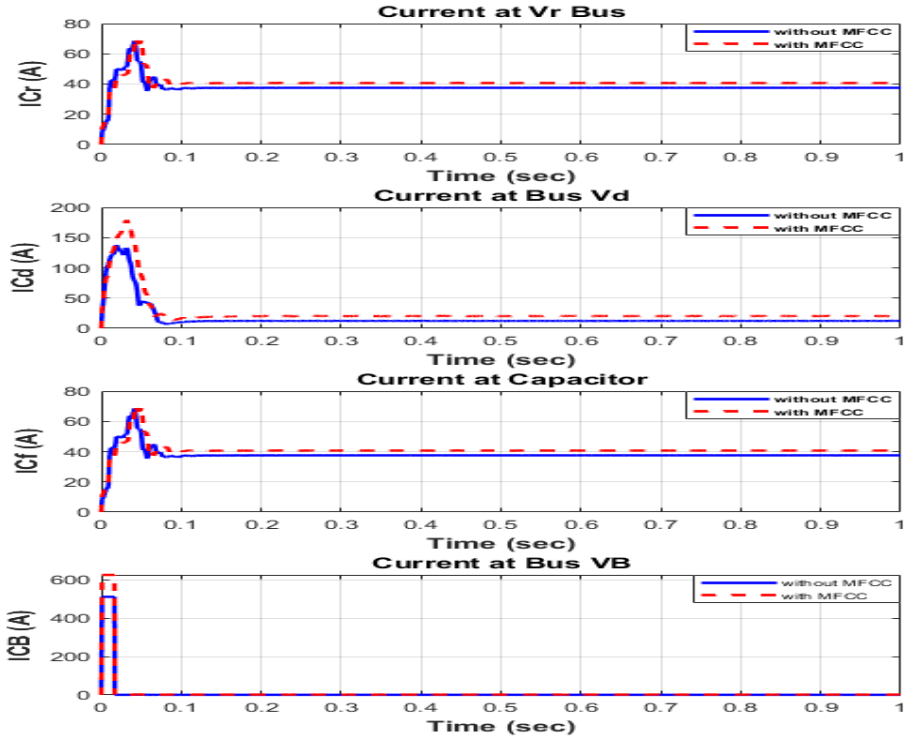

Figure 4.14 Currents ICr, ICd, ICf & ICB at VB Bus without and with MFCC-SFC Compensator

The currents ICr, ICf, ICd, and ICB at the VB bus without and with the MFCC-SFC compensator are shown in Figure 4.14. Figure 4.17 illustrates in 3-D the RMS current, RMS voltage, and active power at Vs, Vr, Vd, and VB buses with and without the proposed MFCC-SFC compensator. Figure 4.18. illustrates the improvement in RMS voltage and RMS current at the charging scheme side of the VB bus after using MFCC-SFC.

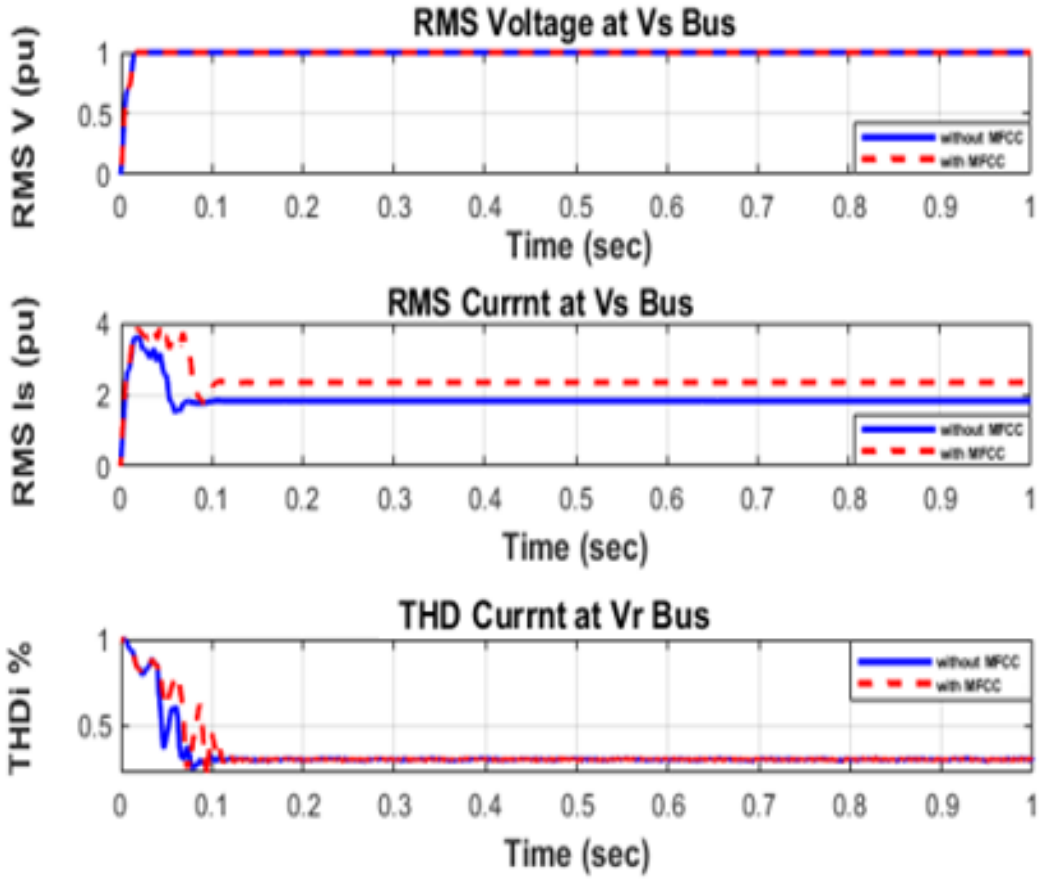

Figure 4.15 RMS Voltage, RMS Current IB & Current THD at Source Bus with and without MFCC-SFC Compensator

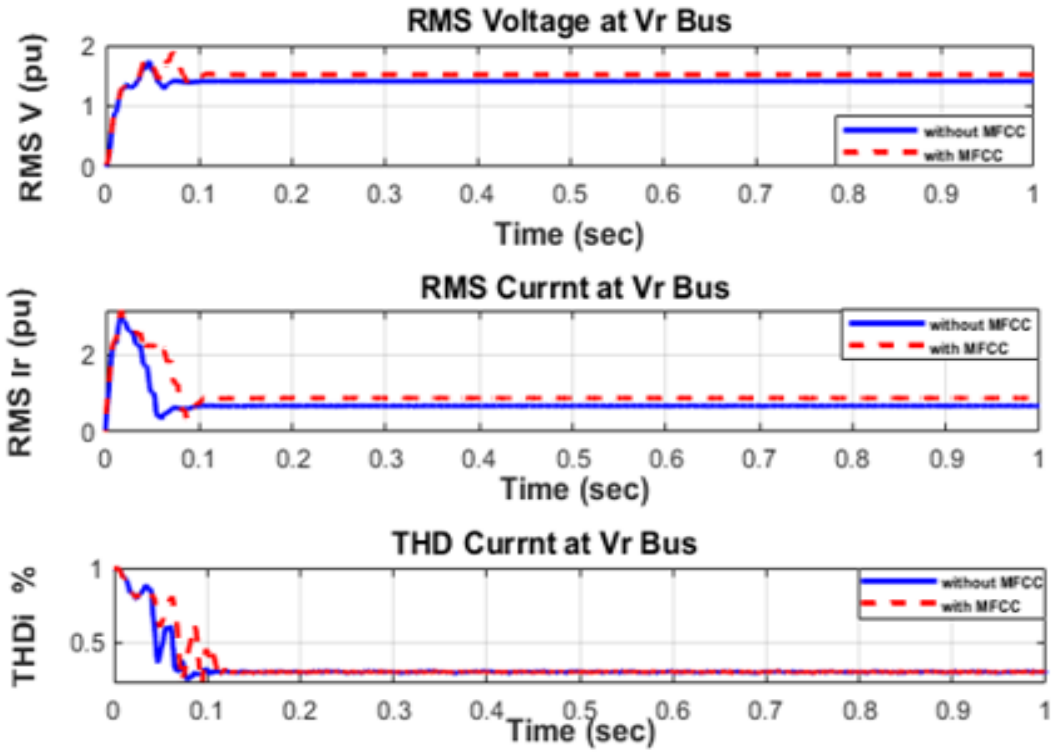

Figure 4.16 RMS Voltage, RMS Current IB & Current THD at Vr Bus with and without MFCC-SFC Compensator

Table 4.3: RMS Voltage, RMS Current, and THD of Current at AC Buses

Buses	Vs (pu)			Vr (pu)		
	RMS v (pu)	RMS i (pu)	THDi %	RMSv (pu)	RMSi (pu)	THDi %
Without MFCC	1.0	2.0	1.0	1.2	0.85	0.25
With MFCC	1.01	2.25	1.01	1.25	1.0	0.27
Improvement	0.01	0.25	0.01	0.05	0.15	0.02
% Improvement	1%	25%	1%	5%	15%	2%

Figures 4.15 and 4.16 illustrate the digital simulation results for the proposed MFCC-SFC with normal operating case conditions at the AC source side of the system for both Vs and Vr buses, performed in a MATLAB Simulink environment. According to the figures, the dynamic response of the RMS voltage at the Vs bus is reasonably consistent, at roughly 1.0 pu without the proposed MFCC and 1.01 pu with the proposed MFCC. The only exception to the consistency occurs a few seconds during switching. Moreover, there is a 1% improvement in the voltage magnitude after adding the proposed MFCC. Also, the figures show that the RMS current is more variable than the voltage, but it is normally between 2 pu and 2.25 pu with the suggested MFCC and has a lower value without MFCC. The current profile improvement is higher than the voltage profile by 25%. On the other hand, the THD of the current at the AC source side at Vs is relatively constant at roughly 0.01. This improves the system at the source AC side, while the THD of the voltage goes to the zero level, which is considered ideal for the system, as illustrated in Figure 4.15.

Figure 4.16 indicates that installing the suggested MFCC at the Vr bus improves the RMS current magnitude by 15% (0.85 pu to 1 pu). It also improves the voltage magnitude by 5%, reflecting an improvement of the power factor. Thus, the RMS current, RMS voltage, total harmonic distortion of the voltage (THDv) at zero level, and total harmonic distortion of the current (THDi) are improved. THDi changed by 2% in the Vr bus of the AC side system after using the proposed MFCC-SFC. Therefore, it is obvious that employing the indicated MFCC-SFC improves the power factor, which translates into an improvement in the power quality of the proposed system, as presented in Table 4.3.

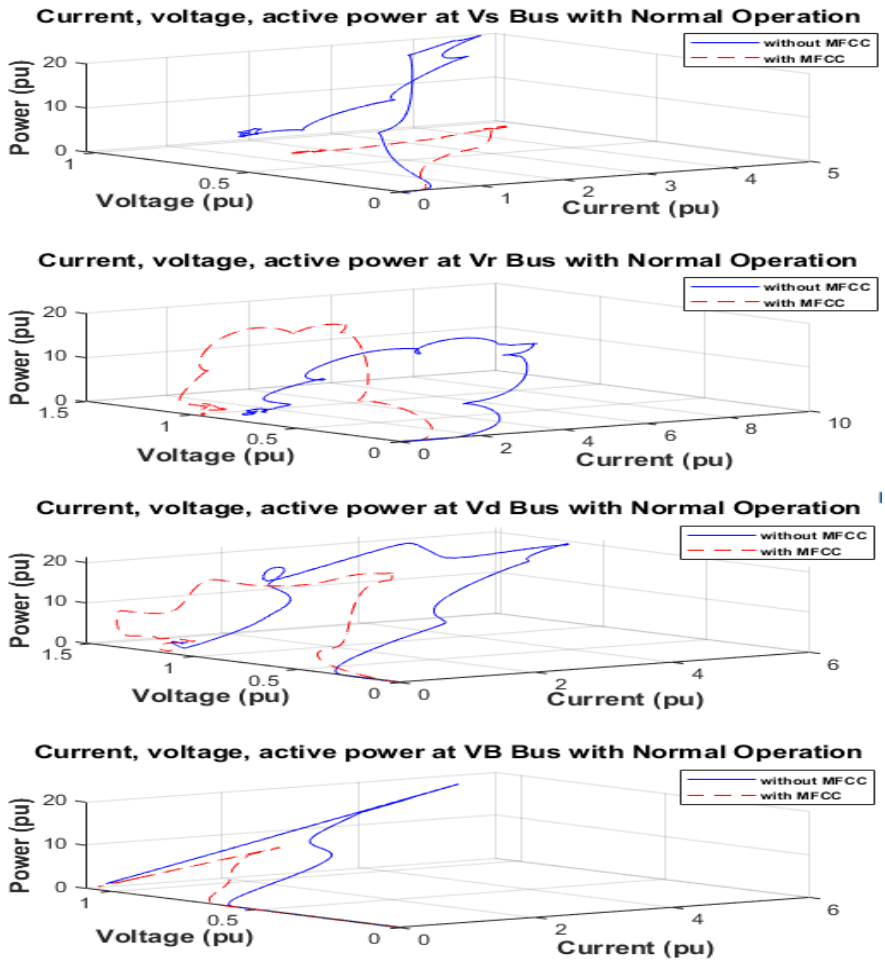

Figure 4.17 Current, Voltage, & Active Power at Vs, Vr, Vd, V_B Buses without and with MFCC-SFC Compensator

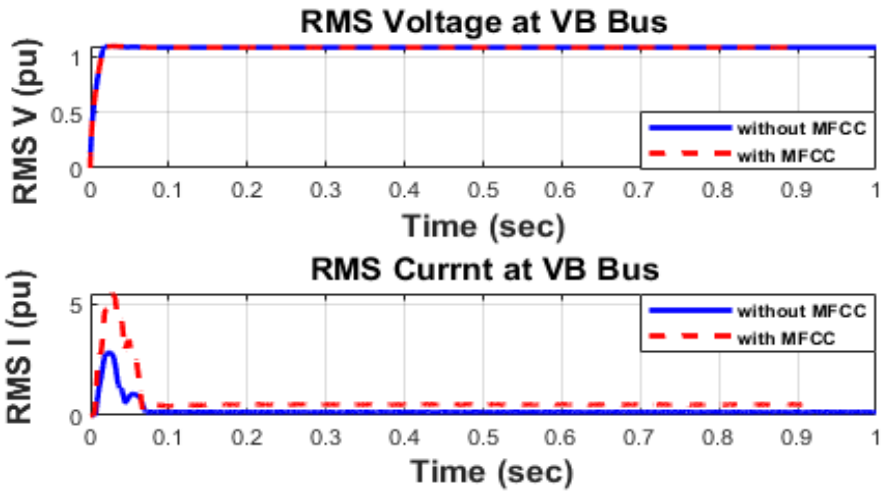

Figure 4.18 RMS Current I_B & RMS Voltage VB at Source Bus with and without MFCC-SFC Compensator

4.8-2 FLC without and with MFCC – SFC for Short-Circuit Fault Operating Case

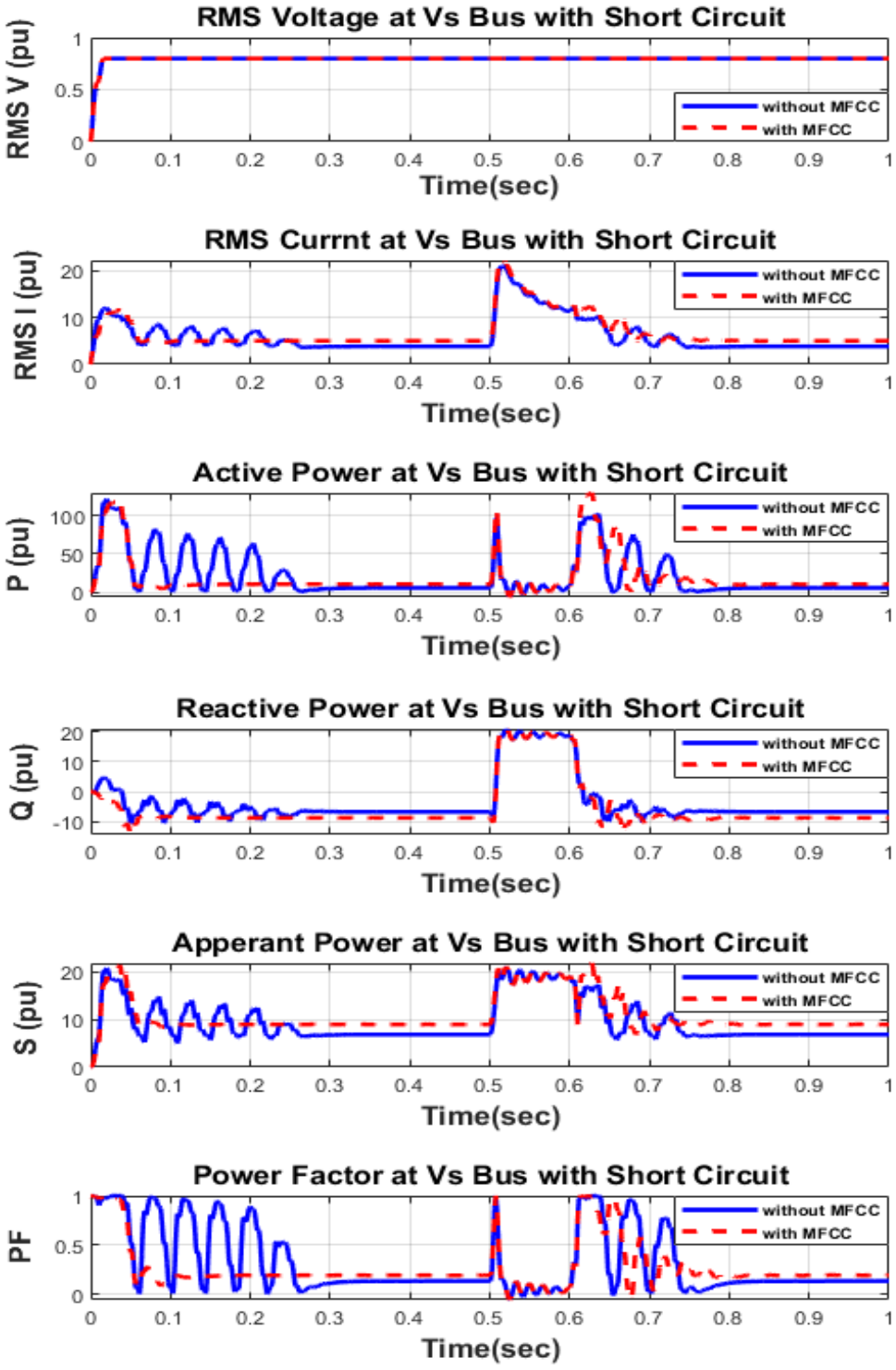

Figure 4.19 RMS V and I & P, Q, S, and PF at Vs Bus under SC Fault without and with MFCC-SFC Compensator

The digital simulation dynamic responses at the DC side for both the Vd and VB buses are shown in Figures 4.19 and 4.20 on the AC side, without and with the proposed filter. We can conclude from the response to all figures that the dynamic response and power quality for all buses at both the AC and DC sides have been improved. Also, the power factor during the short-circuit fault with the charging system scheme in key buses has less fluctuation when the proposed filter is used, especially in the AC source bus.

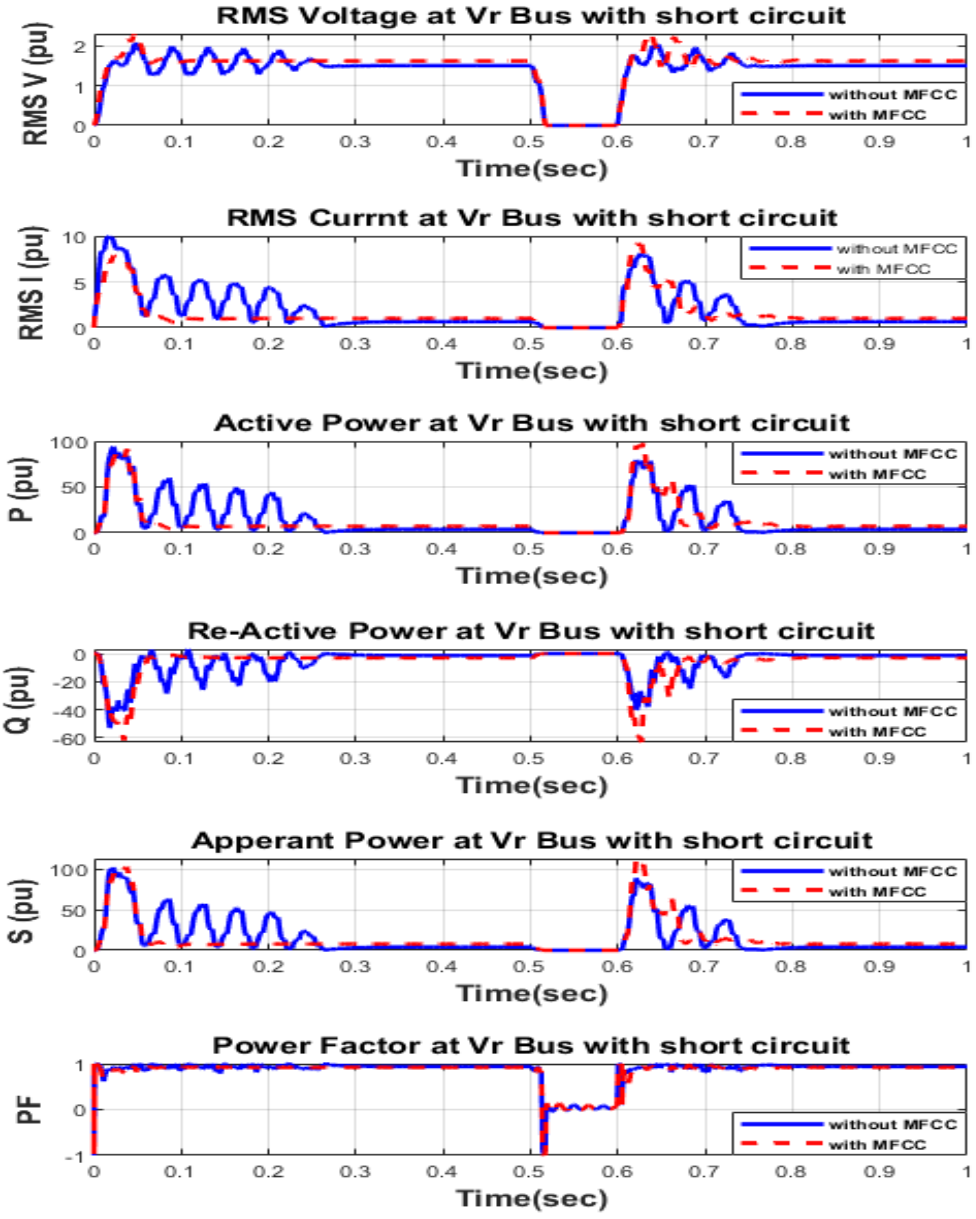

Figure 4.20 RMS V and I & P, Q, S, and PF at Vr Bus under SC Fault without and with MFCC-SFC Compensator

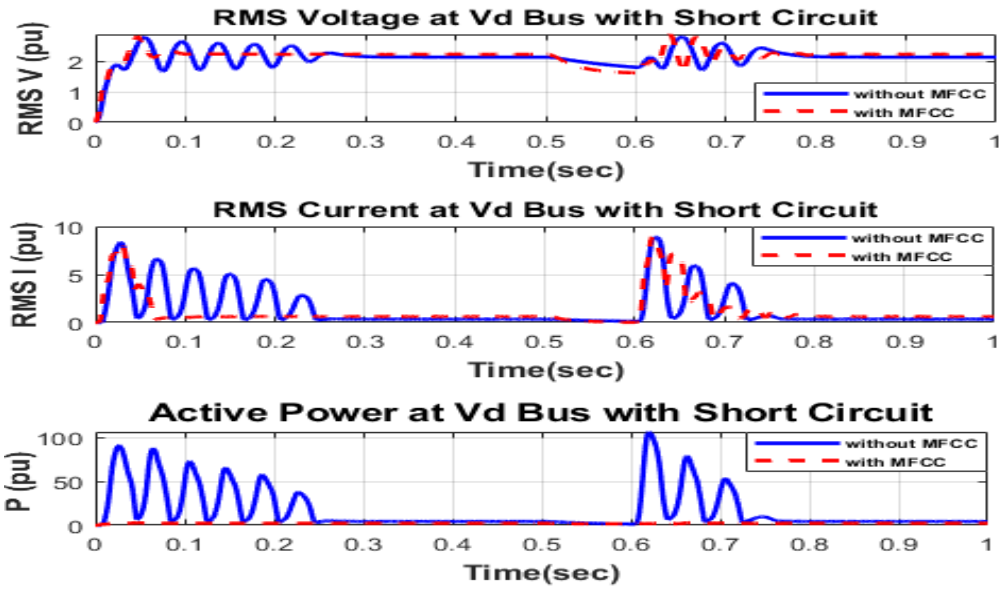

Figure 4.21 RMS V and I & P at Vd Bus under SC Fault without and with MFCC-SFC Compensator

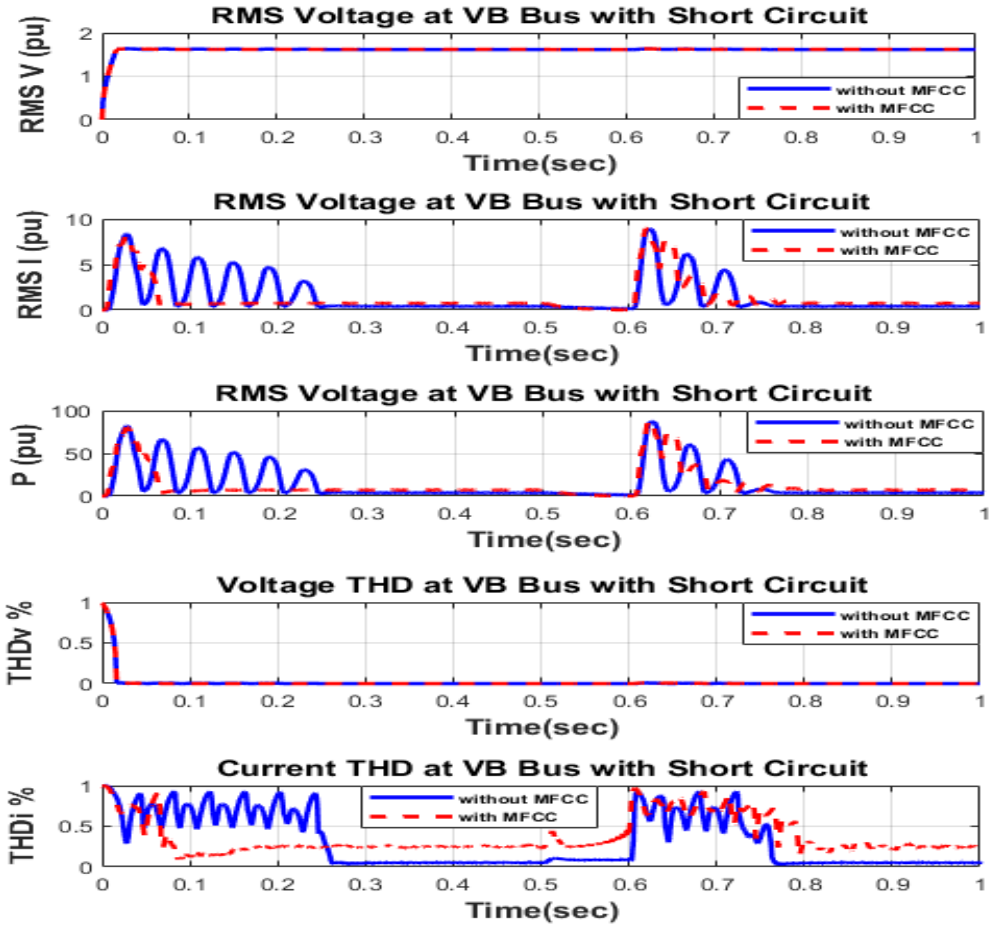

Figure 4.22 RMS V and I & P, THDv, and THDi at VB Bus under SC Fault without and with MFCC-SFC Compensator

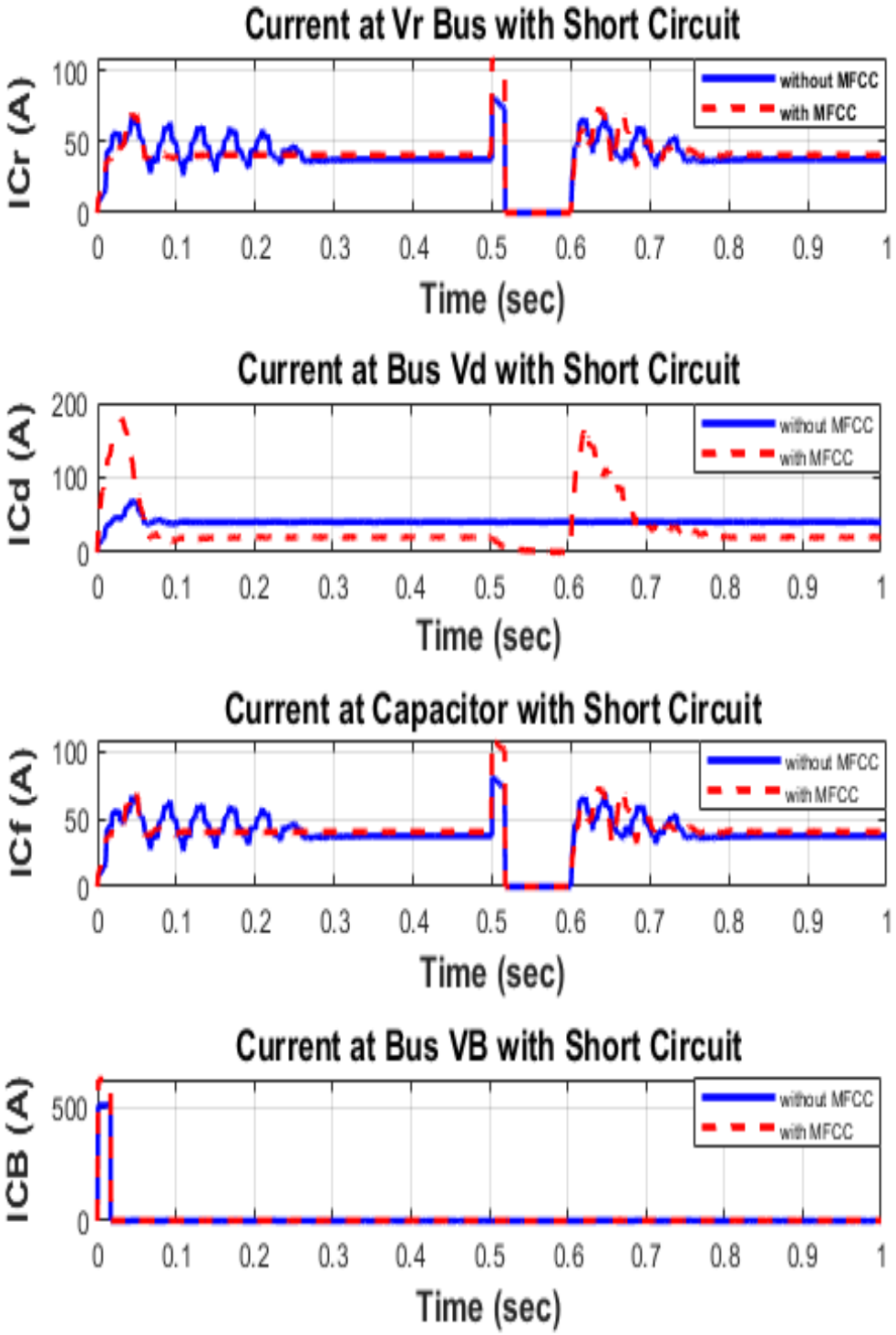

Figure 4.23 Currents ICr, ICf, ICd & ICB at VB Bus under SC Fault without and with MFCC-SFC Compensator

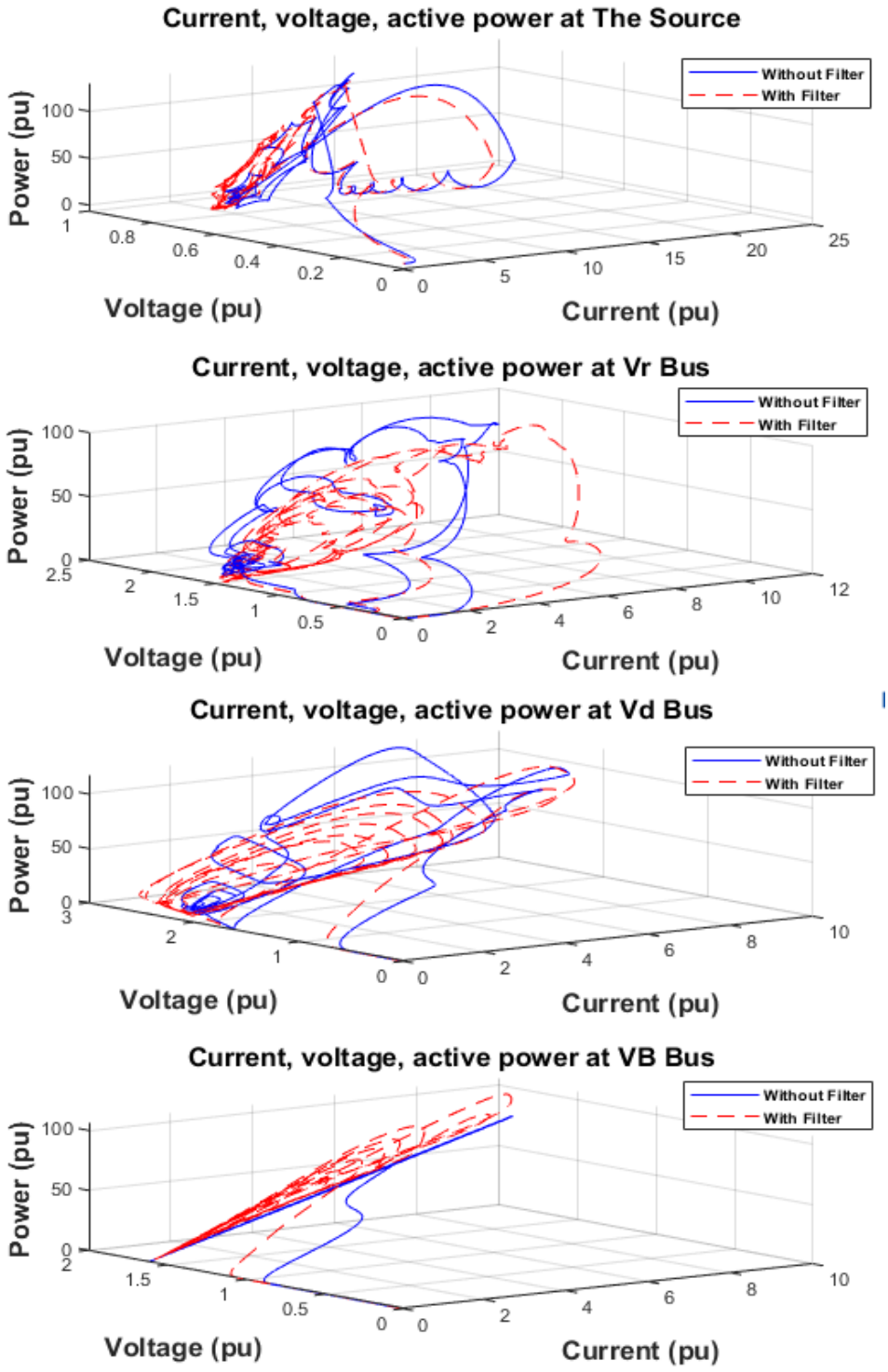

Figure 4.24 Current, Voltage, and Active Power at Vs, Vr, Vd, VB Buses without and with MFCC-SFC Compensator

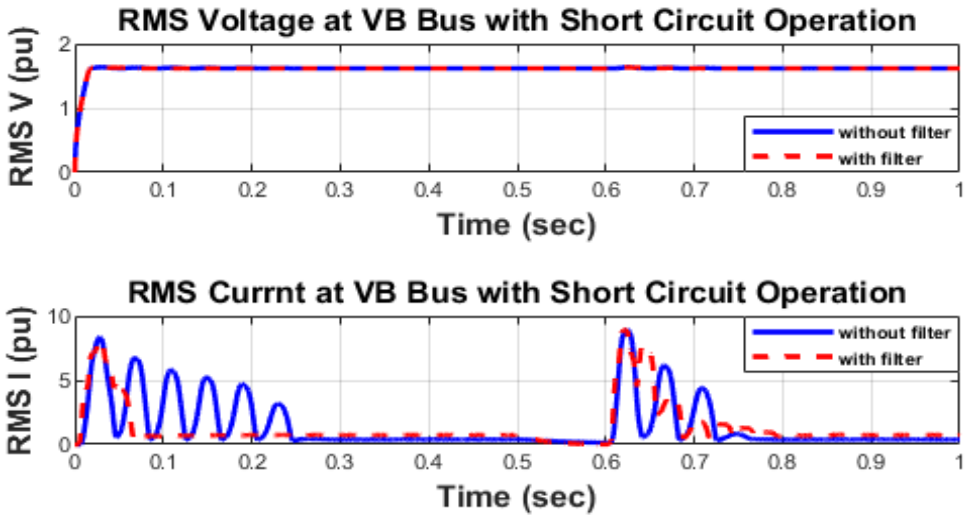

Figure 4.25 RMS (Current and Voltage) at VB Bus under SC Fault without and with MFCC-SFC Compensator

The digital simulation results, which form a crucial aspect of our study, are applied at the 50% SOC case to verify the dynamic effectiveness of the proposed MFCC-SFC scheme for the H2V battery-charging system. This case utilizes digital simulation software under short-circuit conditions at 200 ms, based on a scale of 1 second on the AC side (Vs & Vr) buses. The digital simulation dynamic responses at the DC side for both (Vd and V_B) buses are depicted in Figures 4.21 and 4.22.

As presented in Figure 4.23, the results are comprehensive, which presents all currents for the short-circuit operating condition without and with MFCC-SFC. Figure 4.24 further demonstrates the thoroughness of our approach, showing the 3D view during the short-circuit condition for RMS current, RMS voltage, and active power at all system buses without and with the proposed MFCC-SFC scheme. This level of detail instills confidence in the results. Figure 0.25 shows the improvement of RMS voltage and RMS current at the charging scheme side of the V_B bus.

4.8-3 FLC without and with MFCC–SFC for OC Fault Operating Case at 100 ms

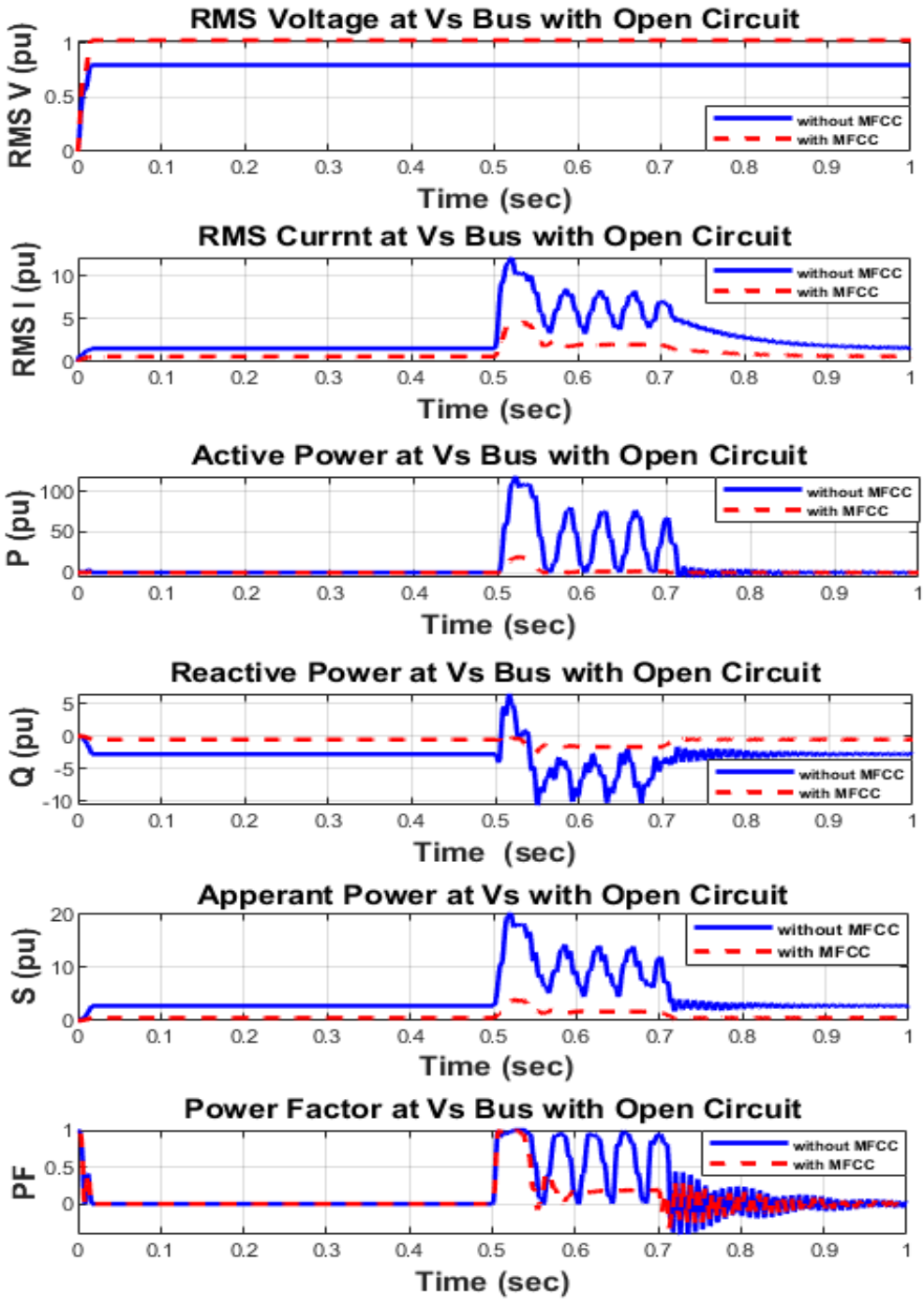

Figure 4.26 RMS V and I & P, Q, S and PF at Vs Bus under OC Fault without and with MFCC-SFC Compensator

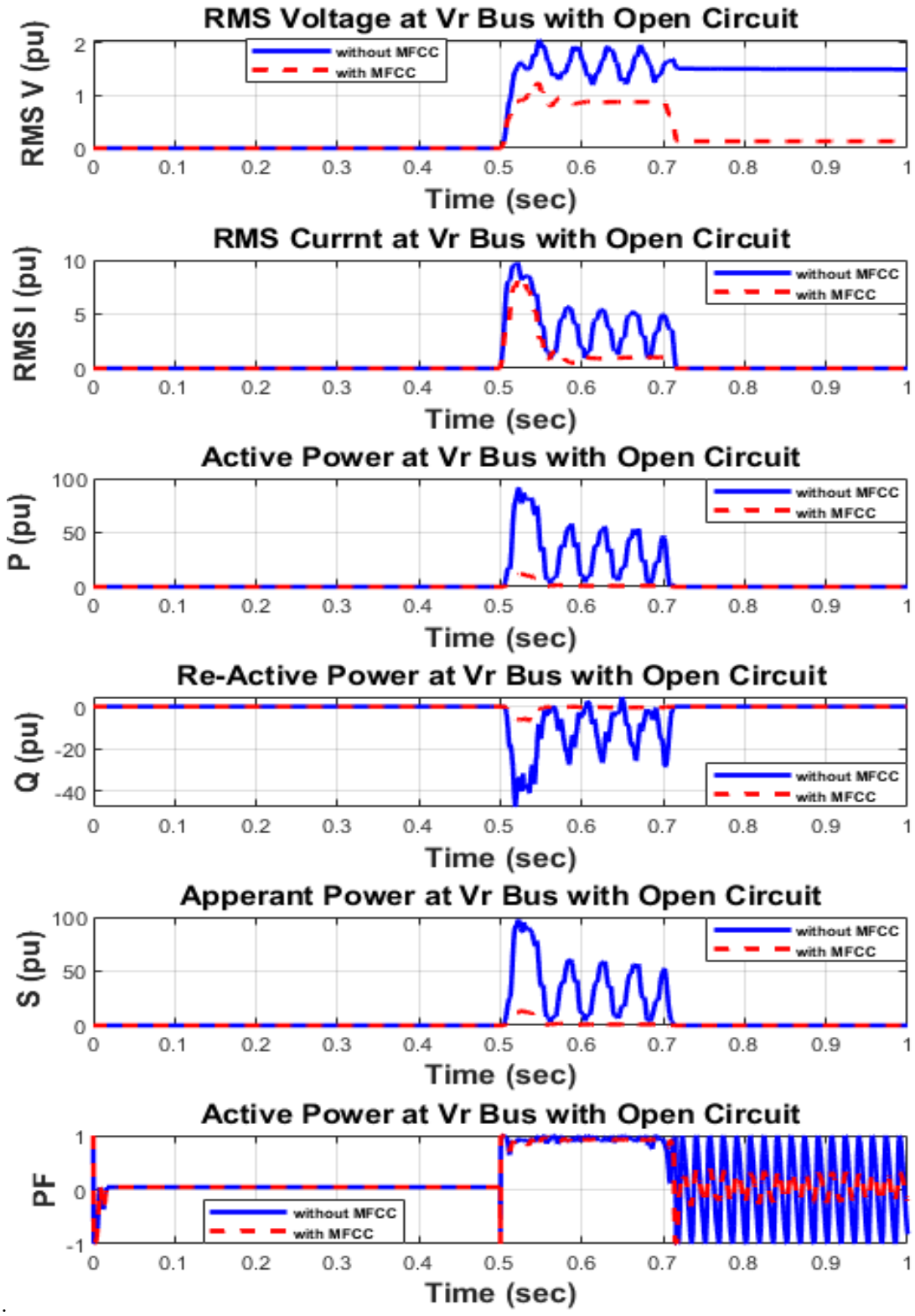

Figure 4.27 RMS V and I & P, Q, S and PF at Vr Bus under OC Fault without and with MFCC-SFC Compensator

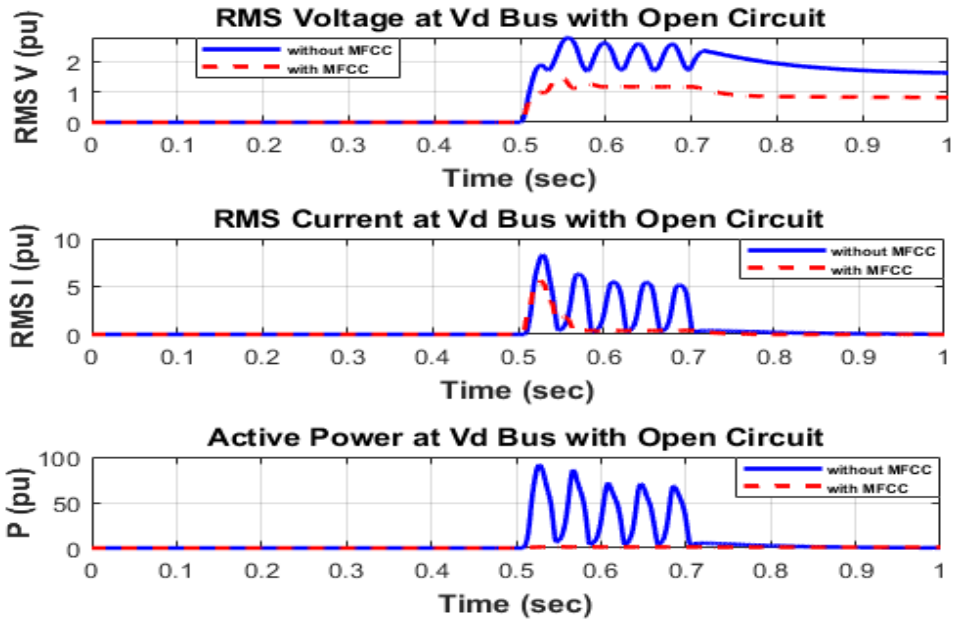

Figure 4.28 RMS V and I & P at Vd Bus under OC Fault without and with MFCC-SFC Compensator

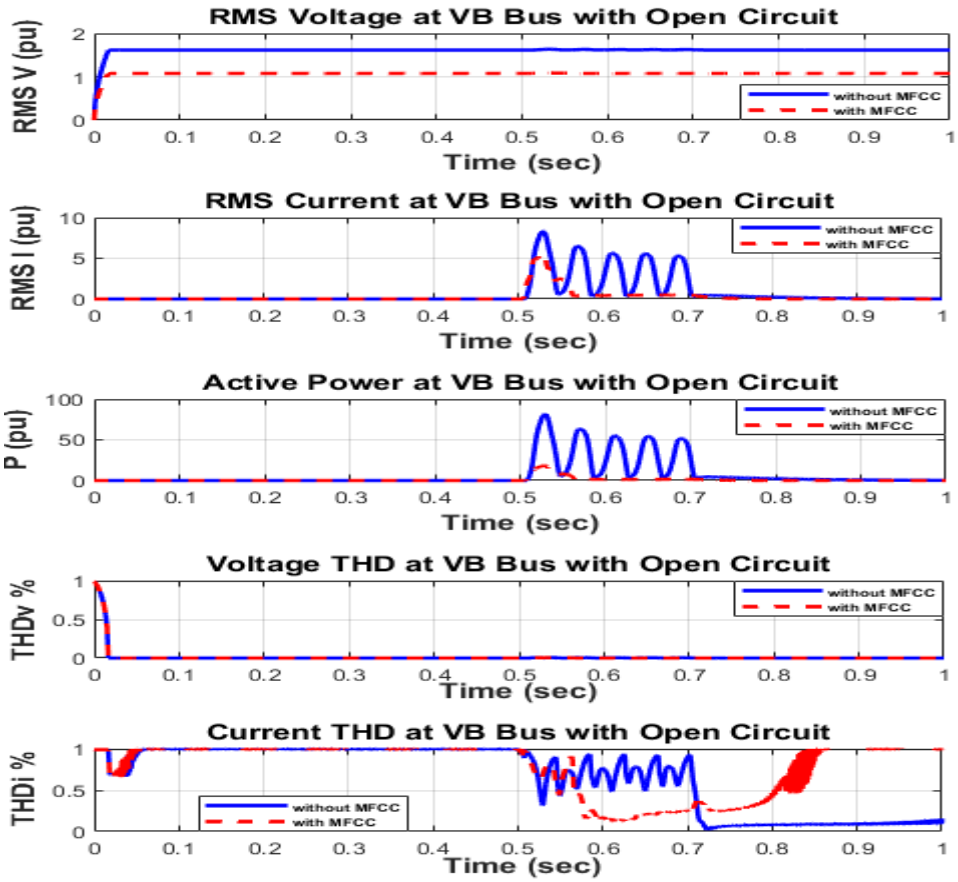

Figure 4.29 RMS V and I & P, THDv, and THDi at VB Bus under OC Fault without and with MFCC-SFC Compensator

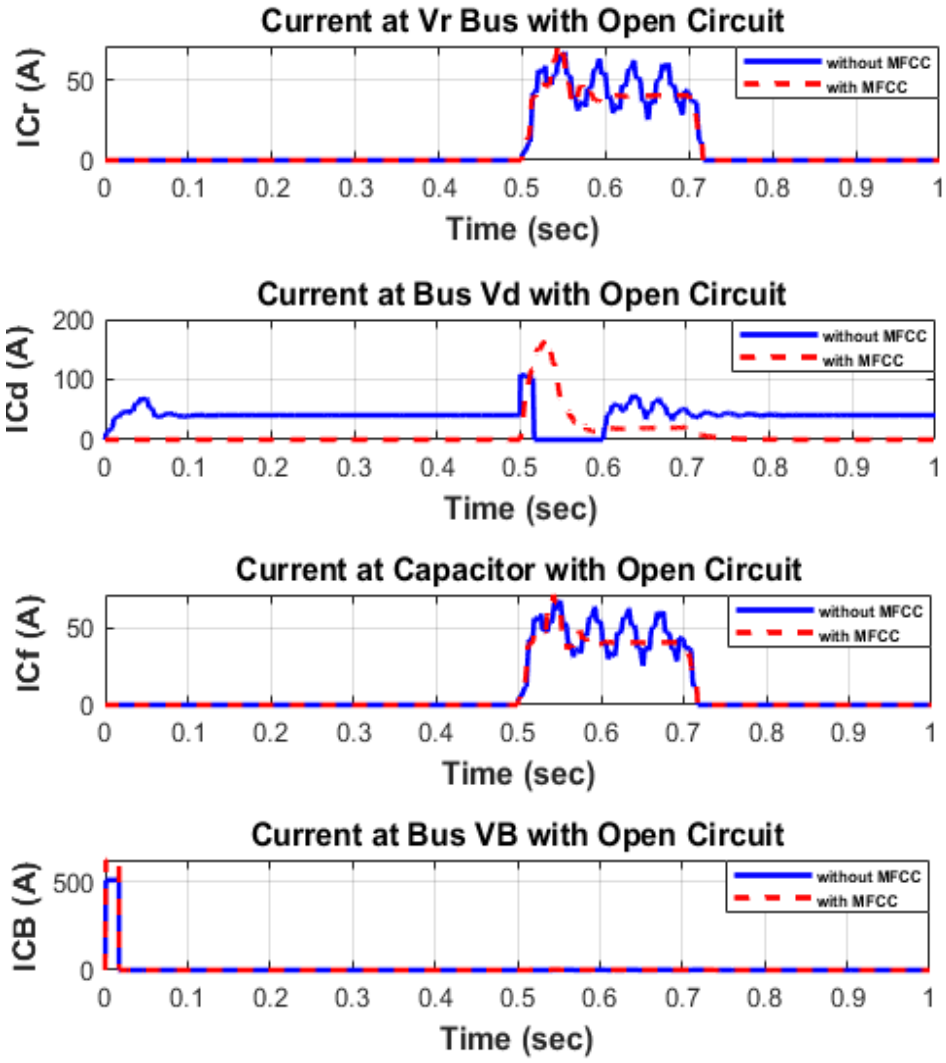

Figure 4.30 Currents ICr, ICf, ICd & ICB at VB Bus under OC Fault without and with MFCC-SFC Compensator

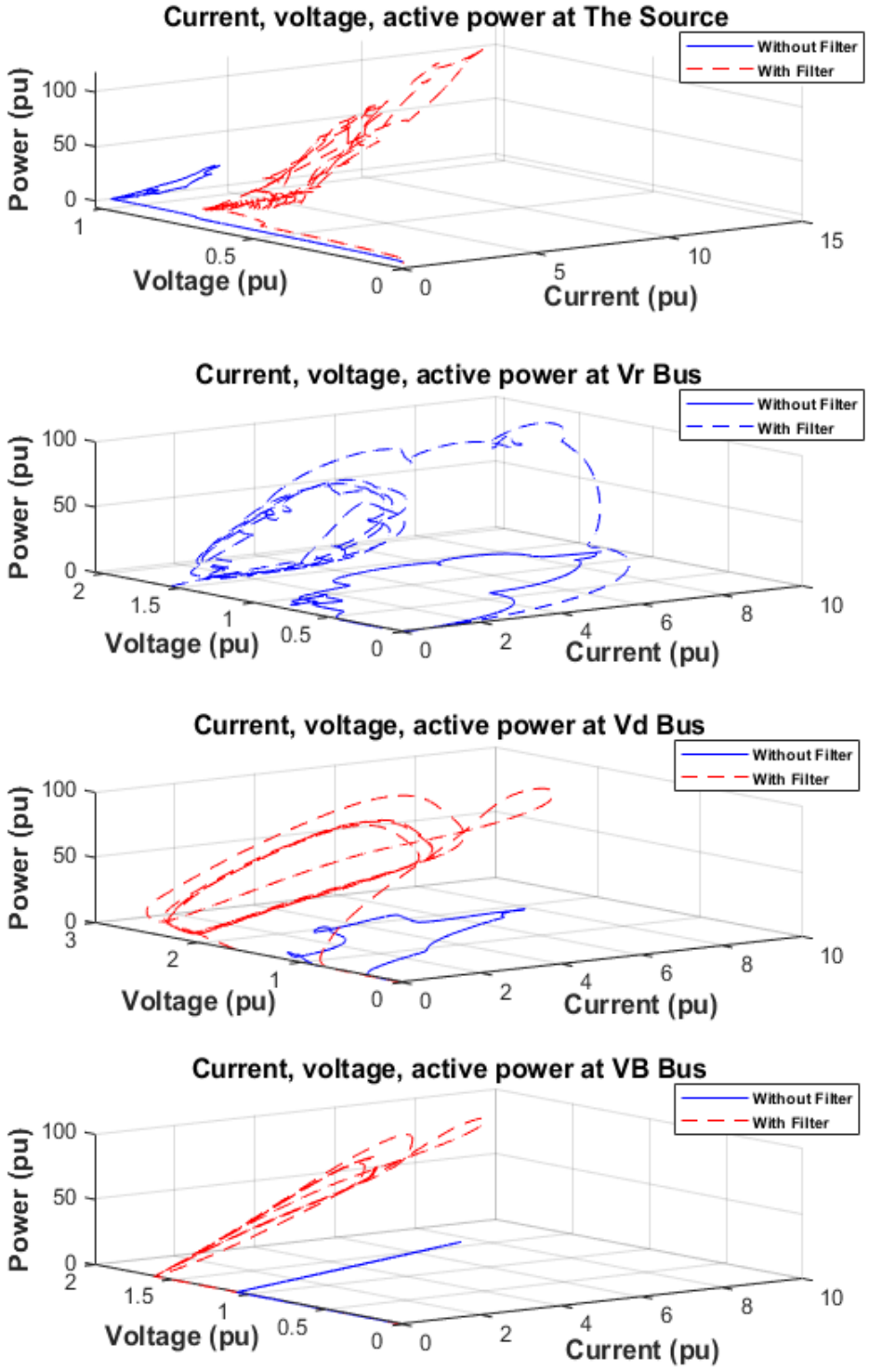

Figure 4.31 Current, Voltage, and Active Power at Vs, Vr, Vd, and V_B Buses under OC Fault without and with MFCC-SFC Compensator

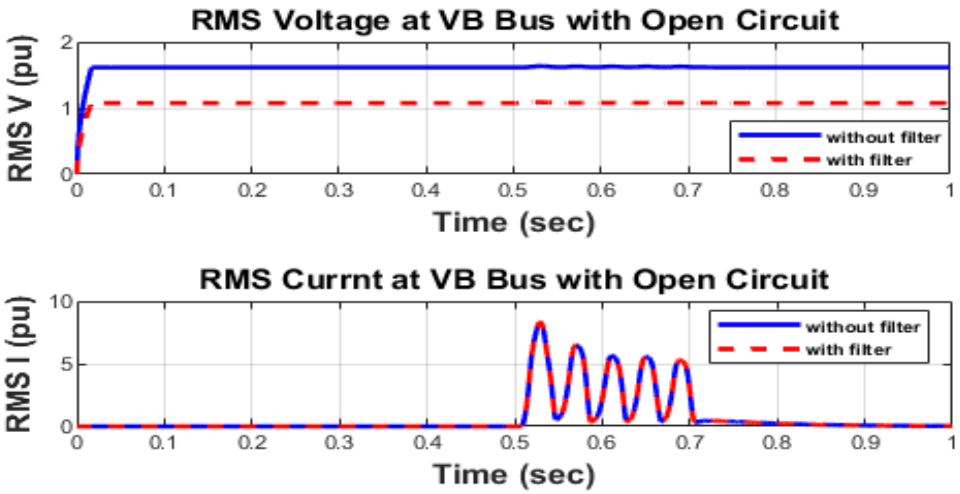

Figure 4.32 RMS (Current and Voltage) at VB Bus under OC Fault without and with MFCC-SFC Compensator

To validate the effectiveness of the proposed low-cost MFCC-SFC scheme for the H2V battery-charging system at 50% SOC, the models are tested under OC conditions at 100 ms of the AC grid at scale 1 sec on the AC side (Vs and Vr) buses. It is clear from Figures 4.25 to 4.30 that the dynamic response of the system is more stable with the proposed control schemes, even under OC fault conditions. The results of the simulation under OC conditions show an improvement in the power factor and reduction of the inrush currents, as seen in Figures 4.26 and 4.27, and in Figures 4.28 and 4.29 on the AC side. Additionally, it can be seen that the dynamic response and the power quality for all buses at both AC and DC sides have been enhanced. The power factor during the OC fault condition with the charging system scheme at buses has less fluctuation compared to the power factor without the proposed compensator.

Figure 4.30 shows all currents with OC fault operating conditions without and with MFCC-SFC, while Figure 4.31 illustrates in 3D the SC of the RMS current, RMS voltage, and active power at all buses without and with the proposed MFCC-SFC. Figure 4.32 depicts an enhancement of the RMS voltage stability at 1.0 pu and RMS current at the charging scheme side of the V_B bus. In the evaluation of power fluctuations before the buck-boost converter, it is observed that the fuzzy logic type-2 controller achieved a remarkable level of stability. This finding indicates that the controller effectively regulates power input, ensuring a relatively steady and controlled power level.

4.9 Total Harmonic Distortion , THD Analysis

Total harmonic distortion represents the harmonics in voltage and current waveforms. To better understand the voltage and current load bus's harmonic effects, we provide our results showing the voltage and current THD of the load bus without and with MFCC-SFC as a function of time. The rate of THD has increased for constant series compensation, as can be seen in Figure 4.33 and Figure 4.35 because nonlinear loads are used on power systems. However, our proposed MFCC-SFC works with a function to obtain optimal power factor and low THD and harmonics at the DC side in order to improve our system. The proposed AC-MFCC filter acts as a green plug device that reduces the THD of voltage and current low-order harmonics, improves the power factor, ensures fewer inrush source currents, and reduces DC bus transient overvoltage. As shown in Figures 4.34 and 4.36, the THD of current and voltage in the load bus side is improved by using MFCC-SFC. For how to THD calculated:

THD: Ratio of the RMS of the harmonic content to the RMS of the Fundamental:

$$\text{THD} = \sqrt{\frac{\text{sum of square of amplitudes of all harmonics}}{\text{square of amplitudes of fundamental}}} \quad \text{x } 100 \tag{4.12}$$

- Voltage THD:

$$\% \text{ THD} \quad \frac{\sqrt{V_2^2+V_3^2+\cdots+V_N^2}}{\sqrt{V_1^2}} \quad \text{X } 100 \tag{4.13}$$

- Current THD:

$$\% \text{ THD} \quad \frac{\sqrt{I_2^2+I_3^2+\cdots+I_N^2}}{\sqrt{I_1^2}} \quad \text{X } 100 \tag{4.14}$$

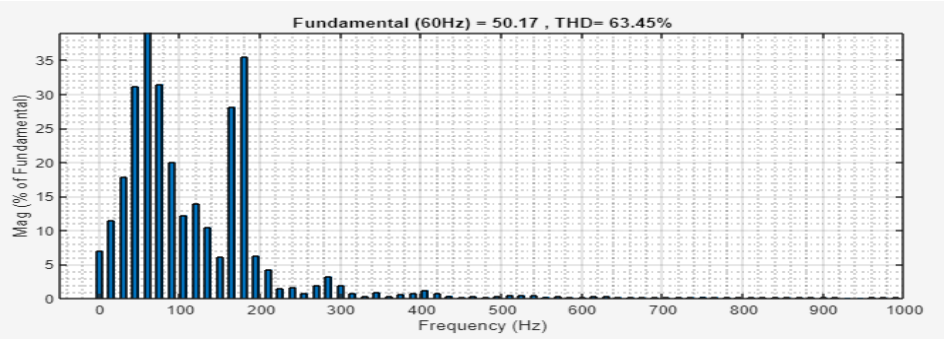

Figure 4.33 FFT Analysis of Voltage without MFCC-SFC for Changing Operation

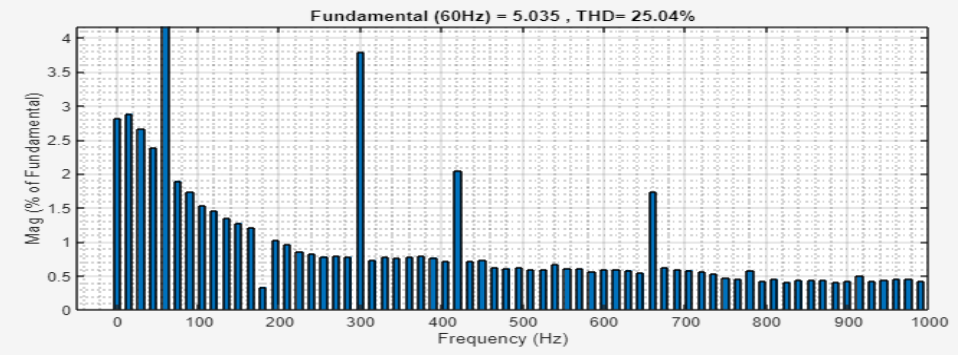

Figure 4.34 FFT Analysis of Voltage with MFCC-SFC for Changing Operation

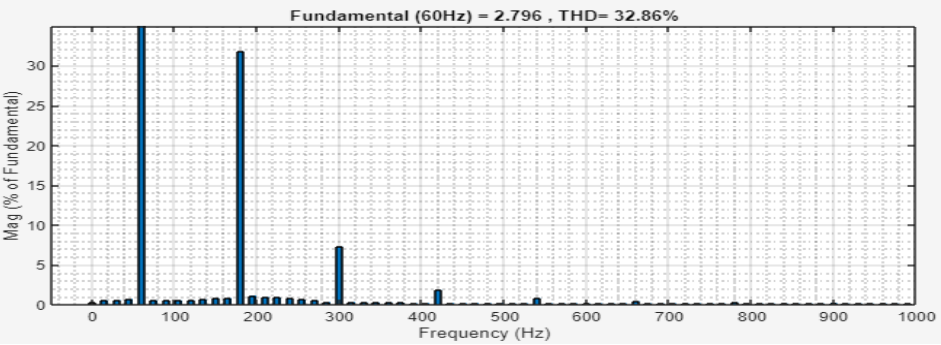

Figure 4.35 FFT Analysis of Current without MFCC-SFC for Changing Operation

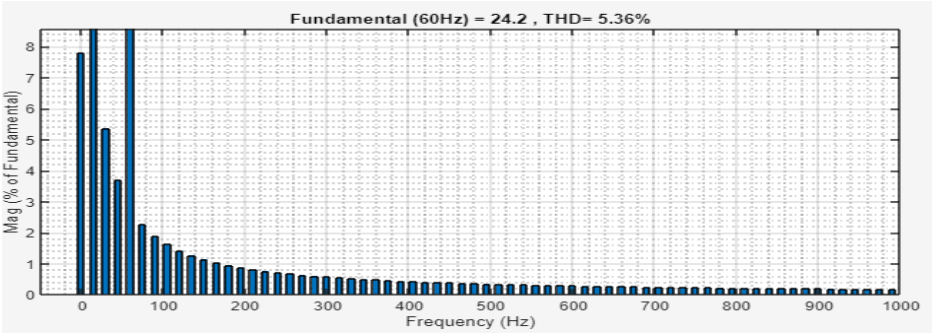

Figure 4.36 FFT Analysis of Current with MFCC-SFC for Changing Operation

4.10 Novelty of Proposed Switched/Modulated Filter Scheme

The proposed AC green plug switched filter scheme is an extended version of a family of modulated filters using new inter-coupled AC-DC configuration and capacitive compensation devices [128]. The distinction is in using a multi-loop, multi-regulation, duty cycle, and PWM switching duty cycle ratio based on the total summed error for control and switching of the dual action modes of the tuned arm filter and reactive compensation coping with slow dynamic varying nonlinear and inrush motorized loads. The improvement is in ensuring a fast-acting modified control scheme. The combined action also reduces DC-side inrush charging currents and improves DC-side power factor, while reducing AC-side supply harmonics.

Moreover, the family of AC green plugs/modulated filters represents a low-cost alternative method compared to other active power filters schemes and static compensation devices. The filter duty is controlled by flexible fast-acting summed errors of different weighted loops and multi-functional regulators. This chapter presented a new effective inter-coupled AC green plug-switched filter with a fast-acting fuzzy logic multi regulation multi-loop controller to ensure better dynamic performance in comparison to other published families of modulated power filters /AC green plugs. The proposed work is done by using AC voltage, current and power measured signals in weighted loops to generate the final summed error that regulate the duty cycle ratio online as necessitated by nonlinear inrush current loads.

4.11 Validation of the Proposed Work

To validate the proposed work, the performance of the model is compared with a benchwork done in that area. Table 4.4 presents a comparison between the proposed work done in this chapter and previous work. As seen in the table, there is an improvement of around 20% for the proposed work related to RMS_V compared to the previous work, which is 5% after using the filter. RMS_I also improved 20% in the proposed work after adding the filter, compared to the previous work, which was 12%. Additionally, the active power and power factor improved 15% and 10%, respectively, after adding the filter. This compares with improvements of only 7% and 5%, respectively, from the previous work. As well, THD_V and THD_I improved by 38.41% and 27.5%, respectively, compared to 32.89% and 20%, respectively, for the previous work done. Thus

it can be concluded that adding the proposed filter in this work made a significant improvement in performance compared to that in previous work.

Table 4.4: Comparison Between the Proposed and Other Similar Applications

OPERATING MODE	PREVIOUS WORK						CURRENT WORK					
CONTROLLER TYPE	WPID						FLC-TYPE-2					
FILTER TYPE	FACTS-DTS-GP						MFCC - SFC					
OUTPUT SIGNAL	RMSV (PU)	RMSI (PU)	P (PU)	PF	THDV %	THDI %	RMSV (PU)	RMSI (PU)	P (PU)	PF	THDv %	THDI %
WITHOUT FILTER	0.95	0.7	0.35	0.8	120.31	104.82	0.80	0.7	0.85	0.9	63.45	32.86
WITH FILTER	1.0	0.82	0.42	0.85	87.42	87.42	1.0	0.9	1.0	1.0	25.04	05.36
Improvement	0.05	0.12	0.07	0.05	32.89	17.4	0.2	2.0	0.15	0.1	38.41	27.50
% Improvement	5%	12%	7%	5%	32.89	17.4	20%	20%	15%	10%	38.41	27.50

4.12 Conclusion

This chapter presented a novel modulated green plug AC-side filter compensation scheme for V2H stations. The scheme was controlled using a type-2 fuzzy logic optimized controller to control two electronic switches. The V2H scheme was assessed and tested under various operating conditions, including SOC (50%) for open- and short-circuited conditions and hybrid weighted battery-charging modes. The modulated/switched filter capacitor compensation and tuned arm filter was validated as effective, low-impact, and efficient. The presented switched dual modified filter capacitive compensation scheme is considered a new extension to micro DC-AC utilization grids and energy storage schemes, including virtual energy systems and static transformer less voltage stabilization systems using PV fuel cell and Lithium-ion battery storage systems.

Throughout the chapter, the proposed scheme displayed its effectiveness in dealing with different operating conditions and demonstrated its importance in improving the overall system quality and performance. Its high response is encouraging when dealing with renewables

integration into the utility grid. The AC green plug switched filter compensation scheme ensures improved AC power quality, reduced AC-side harmonics, and AC-DC decoupling, thus reducing inrush currents and transient voltage excursions on DC and AC interface buses.

Furthermore, the novel dual-action multi-loop regulators indicated that they could ensure effective control of tuning/compensation level for slow varying/motorized/nonlinear reactive type loads. The simple low-cost structure of the parallel shunt switched modulated filter was greatly enhanced in this work by the fast-acting multi-loop regulation scheme. The novelty of the research lies in the use of weighted multi-loop time-scale-decoupled controller error used to activate the multi-regulator fast-acting controller. The same fast-acting weighted control scheme is now being extended to AC-DC energy storage and V2G battery charging/smart grid systems, including Virtual Inertia Systems (VIS)/static synchronous dynamic voltage stabilization battery-based schemes for use in smart grids and interfaced wind/ PV/Lithium-ion battery storage and combined AC-DC grid systems.

Chapter 5: A Novel AC Green Plug – Switched Filter Scheme for Low-Impact Efficient V2G Battery-Charging Stations

5.1 Abstract

In this chapter, a novel switched/modulated capacitor filter scheme is proposed for enhancing vehicle-to-house (V2G) battery-charging stations utilized in electric vehicles (EVs). The novel approach is tested on two controllers with a classical optimized PID controller. The technique, which employs modified multi-mode weighted charging modes for fast charging, improved power quality, and minimal inrush currents, results in reduced voltage transients on the DC side and less harmonics on the AC side. An inter-coupled DC-AC capacitor interface that features dual complementary switching modes is used by the switched modulated filter as a way to provide optimal pulsing in both the tuned-arm filter and capacitive compensator modes of operations. This switched inter-coupled AC-DC filter compensation approach leads to enhanced power usage in EVs, along with lower AC-DC voltage transients and inrush currents.

5.2 Introduction

Micro-grids use energy storage systems for the integration of renewable energy sources, including intermittent ones. Batteries built for electric vehicles (EVs) can serve as storage devices for micro-grids during the charging (i.e., plugged-in) phase. The majority of personal transportation vehicles are idle for up to 22 hrs a day. During their "idle" time, EVs have the potential to contribute to micro-grid energy management either through: 1) the storing of energy during surplus in (G2V) exchange, or 2) giving energy to the grid during demand, which is known as V2G. However, when used in the general power grid, V2G still has some issues that make it impractical in the short term, such as highly complex control needs and the large number of EVs that would be required for the approach to be effective [129].

On the other hand, even with these issues, V2G can be implemented in micro grids relatively easily with the use of wind power, solar power, micro-turbine power, and other forms of renewable energy. Such a system would be independent and controllable as well as built from micro-sources and other loads able to supply small-scale local energy needs (e.g., heat and

electricity). One challenge in this set-up is the lower level of inertia in micro grids that can cause fluctuations in both the network and the load. Moreover, due to inherent instabilities and discontinuities in renewable energy sources, voltage sagging, and outages are an ongoing concern. Therefore, it is crucial to develop viable energy storage systems that will enhance the micro-grids' power quality [56].

Flexible alternating current transmission system (FACTS) electronics-based devices are used for controlling and managing power flow in electrical grids. They are currently the best approach on the market for enhancing power quality. FACTS uses fuzzy logic controls for p.u.lse width modulation (PWM) dynamic switching/regulation for EV battery charging systems, with the aim of optimizing both power consumption and quality. This scheme has numerous advantages compared with other proportional-integral-derivative (PID) controllers, such as low price, operational simplicity, and ease of adaptability, especially when faced with an uncertain load of an unknown process dynamic or mathematical model with regard to power quality. The necessary infrastructure for FACTS includes charging stations, charging poles, and battery exchange stations, all of which would be needed to provide a power source for EV battery charging [57].

In this research, a dynamically regulated flexible alternating current transmission system (FACTS) is proposed to improve both the power factor and power quality and to remove line current harmonics. This device uses a novel hybrid filter compensator design developed for a buck-boost converter in PHEVs. The FACTS device presented in this work is controlled using a quad-loop multi-zonal dynamic controller and is related to both the V2G and V2H device families. The proposed devices are illustrated in Figure 5.1. Additionally, aiming to achieve the best charging performance, a quad-loop error-driven controller has been developed for the DC/DC buck-boost chopper [130].

Developing, producing, and delivering reliable and stable sources of electricity is the primary goal of power system operation using plug-in vehicles (PEVs) as a power source via V2G smart scheme innovations would benefit these systems by contributing to this goal. In the plug-in period, PEVs save enormous amounts of electrical energy. Hybrid PEVs (PHEVs) are currently the main focus of research in this field [83], [131], but other types of EVs are also receiving heightened attention. The main issues facing the use of EVs in micro grids are power quality and challenges around peak demand and high energy absorption. Unpredictability caused by dynamic

behaviors is also an ongoing concern [77]. Still, the advantage of integrating EVs into micro-grids far outweighs the disadvantages. In one especially promising scheme, V2G is used in frequency and voltage regulation services. It is worth noting that all EVs incorporate an electric motor that is built into the drivetrain. Furthermore, EV classification is determined by configuration, the three main ones being battery-electric vehicles (BEVs), PHEVs), and plug-in hybrids (PEVs) that combine BEVs and PHEVs [132].

The overall benefits of EVs, such as reduced energy costs and environmental sustainability, are improved through V2G systems. For example, using the direct current from the back-up storage battery, the system is able to quickly charge an EV while also returning its produced energy to the home source. Many different factors, ranging from economic to environmental, have been driving the successful adoption of EVs. The main factors include reduced reliance on traditional (i.e., fossil) fuels, improved air quality, and less noise pollution [133].

The growth of the automotive industry has led to the development of smart cars and other products, but it is also contributing to air pollution. To address pollution issues caused by vehicles, automakers are aiming to reduce gaseous pollutants like carbon dioxide and hydrocarbons and to build the only type of vehicle that has zero emissions, which is EVs [134]. However, despite their constant promotion by industry and government, EVs have gained little popularity with consumers due to their performance challenges, the main one being their need to be recharged after relatively short distances. Environmentalists, on the other hand, generally support EVs but hope that this type of vehicle can improve its performance by combining its zero-emissions attribute with the driving performance of traditional vehicles.

In the meantime, one available bridge between traditional and electric vehicles is the hybrid electric vehicle, which combines good performance with reduced pollution levels [135]. In HEVs, an electric motor with a separate battery pack helps to accelerate the gas-fired engine. Unlike traditional cars, HEVs can recycle heat energy and use it for storage purposes, e.g., regenerative braking [103]. Proponents of V2G suggest that this feature can be used to return energy back to the micro-grid in a network, thereby assisting in grid stabilization. This feature makes EVs even more attractive to environmentalists [136]. Speeding up the charging time required for EVs involves collaborating with a V2G power matrix (V2G), as was investigated in [137], [138]. with the authors finding that utilizing a bi-directional charger provided the best solution. However,

because the cost of replacing batteries in EVs can be prohibitively expensive, industry is still approaching bi-directional EV charging devices with caution, as they tend to reduce battery life [139].

The authors in [140] demonstrated a device for battery-charging standards that involves a two-stage AC/DC power rectifier converter that has a power factor correction loop (PFC). The first stage comprises a buck-boost regulator, which controls the line current waveform and DC-link voltage level. One of the DC/DC converters is the second stage [141]. Furthermore, because the AC/DC front-end is considered the most important part of the battery charger, choosing a topology to satisfy both power factor corrections and inp.u.t current harmonics regulations is crucial. Boost topology is the most frequently used design for battery chargers in PFC applications. For a diode bridge, this design uses buck-boost sections after AC/DC rectifiers [124], [111].

In this chapter, we present a novel low-cost FACTS-MFCC-SFC device. The proposed device is then validated in a MATLAB-Simulink-2023b software environment using a PID controller for voltage stabilization and power delivery to the load. This FACTS-MFCC-SFC device uses switches for implementing dynamic error-driven control strategies, thereby achieving improved response. The study also compares mobile/EV battery-charger operation both with and without the MFCC-FACTS device, testing for power quality, harmonic reduction, and power factor correction.

5.3 Literature Review

In alignment with Khalid et al. (2019), the increasing deployment of EV charging stations within the utility grid is identified as a source of power-quality issues, affecting both large and small consumers. The conversion of AC power to DC power by EV chargers introduces harmonics into the grid, leading to electrical and thermal overloading of distribution transformers and impacting their lifespan. Despite the benefits such as high vehicle-to-wheel and well-to-wheel efficiency, and reduced greenhouse gas emissions, EVs also pose challenges like negative impacts on renewable energy resources, grid stability, supply-demand balance, utility system assets, voltage, current harmonics, and losses [142].

Chakraborty et al.'s (2019) study focused on designing and assessing DC-DC converter topologies for Battery Electric Vehicles (BEVs) and Plug-in Hybrid Electric Vehicles (PHEVs).

They compare these topologies across various parameters, such as output power, component count, switching frequency, electromagnetic interference (EMI), losses, effectiveness, reliability, and cost. The Multidevice Interleaved DC-DC Bidirectional Converter (MDIBC) emerges as the most suitable option for high-power BEVs and PHEVs due to its advantageous characteristics like low input current ripples, output voltage ripples, and electromagnetic interference, along with bidirectionality, high efficiency, and reliability. However, for low-power electric vehicles (<10 kW), alternatives like the Sinusoidal Amplitude Converter, Z-Source DC-DC converter, and boost DC-DC converter with resonant circuit are recommended due to their soft switching, noise-free operation, low switching loss, and high efficiency. The study also explores the potential integration of wide band gap semiconductors (WBGSs) in DC-DC converters for BEVs, PHEVs, and Fast Charging Stations (FCHARs), aiming to assist automotive engineers and PE converter designers in selecting the appropriate converter topology to achieve projected power density growth [143].

In [114], the authors presented a novel multi-functional charger that uses solar energy to power EVs. The researchers discussed different operational modes, such as grid connection/disconnection, selected by a switching and synchronization algorithm. Along with supplying V2G or G2V power, the proposed solution is able to drive local loads, with results indicating that the charger is viable for use in EVs [114].

Similarly, Mastoi et al. (2022) discussed the global transition to electric vehicles (EVs), emphasizing the need for advanced charging station infrastructure development alongside distributed energy generation units and supportive government policies. The work examined key factors for planning EV charging infrastructure, current scenarios, the impact of EVs on grid integration, and optimal allocation provisioning. It also addressed research and developments in charging station infrastructure, challenges, and standardization efforts, while discussing future trends such as renewable energy procurement and the benefits of EVs to grid technology. Unified norms and standards for EV charging and grid integration are emphasized, along with an examination of existing infrastructure aspects in terms of power, communication, control, and coordination [144].

In [109], the researchers offered details on a novel control scheme that used EV batteries as inverters to prevent the so-called depletion phenomenon. Their approach uses a bridgeless bi-directional flyback converter operated in plug-in, solar, and emergency inverting modes. Results

from the experiments supported the technique for powering critical loads, especially during peak stress hours [109]. More recently, Hemavathi and Shinisha (2022) reviewed current and future trends in EV battery-charging methodologies and the roadmap for EV adoption in India, discussing various conventional and advanced battery charging methods, power topologies, and levels of EV charging stations. They underscored the importance of integrated renewable energy (RE) with EV charging architecture and optimized energy management algorithms to address uncertainties from transmission power grids. Future research directions for power electronics-based solutions related to RE integration, energy storage, and smart grid technologies are outlined, with an emphasis on the crucial role of charging capability in addressing climate change and range anxiety [145].

In similar work, Rahman et al. (2022) highlighted the impact of integrating EVs into existing distribution lines on power quality and grid stability, noting challenges related to the mobile nature of EV charging loads and opportunities presented by renewable energy integration. They delved into the impact of EV integration on component and system levels, focusing on power quality, grid pollution, EV load location, existing load distribution, and EV charging load distribution. The chapter advocated for smart charging/coordinated charging to achieve higher EV penetration with minimal grid reinforcement [146].

In [147], the authors developed a new logarithmic hyperbolic cosine robust sparse adaptive filter algorithm for controlling grid-tied off-board chargers using a PV interface. The work showed how algorithms provide optimal dynamic performance through tracking the load current's fundamental component over a short period of time. Also in the same work, the authors proposed a bi-directional buck-boost converter for charging and discharging various EV modes for functionalities like V2G, V2H, G2V, PV2G, and PV2V. The hardware unit was then subjected to different dynamic conditions through load switching and varying the PV insulation. The obtained results showed good agreement with IEEE standards [147].

Mohammadi, Nazri, and Saif proposed a bidirectional charging control strategy for Plug-in Hybrid Electric Vehicles (PHEVs) based on the stochastic nature of daily mileage and arrival/departure times. This strategy aims to regulate battery charge connected to the grid and control the voltage and frequency of the power grid during charging time, contributing to peak reduction and power quality improvement [148].

In summary, these studies collectively address various aspects of electric vehicle charging infrastructure, including converter topologies, power quality issues, grid integration challenges, and charging control strategies, providing valuable insights for researchers and industry professionals in the field. Furthermore, research on EV charging stations presented by other studies emphasizes the importance of technical measures like ancillary power reserves and demand-side energy management to ensure stability. They suggest leveraging renewable energy sources to sustain power peaks induced by charging demand and discuss various control strategies for optimal performance. Additionally, the potential of Vehicle-to-Grid (V2G) technology in alleviating grid integration issues and providing auxiliary services is explored, highlighting the significance of smart grid integration, efficiency, and low cost as growth strategies for V2G.

5.4 System Description

This study demonstrates a dynamically controlled flexible alternating current transmission system to eliminate line current harmonics and increase power quality and power factor. The FACTS device described in this work is related to both the V2G and V2H device families and is controlled by a quad-loop multi-zonal dynamic controller. A quad-loop error-driven controller has also been developed for the DC/DC buck-boost chopper with the goal of achieving the best charging performance [149]. The proposed devices are illustrated in Figure 5.1.

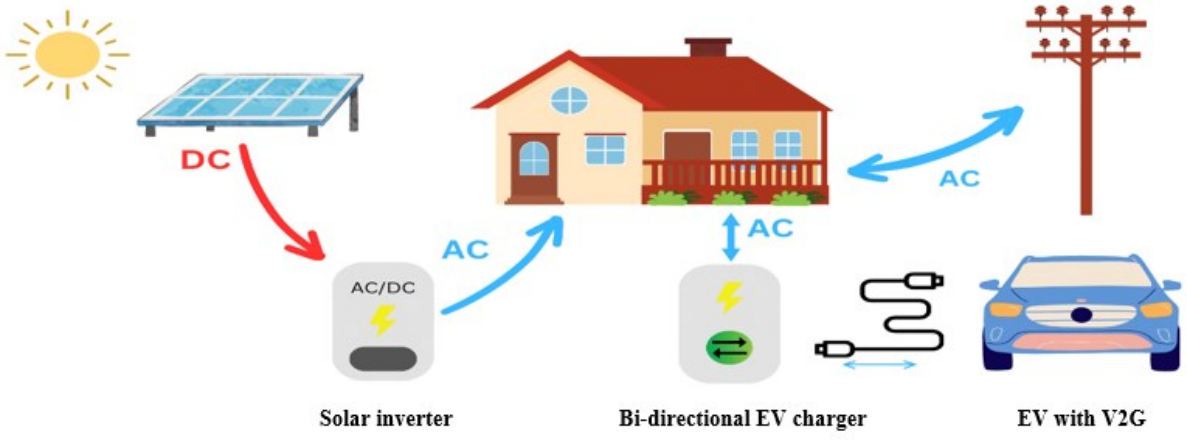

Figure 5.1 Block Diagram of Vehicle-to-Grid (V2G)

The battery-charge scheme with no inter-coupled Hybrid Filter Compensator (HFC) FACTS and the proposed scheme are shown in Figures 5.2 and 5.3, respectively. As can be seen, both schemes have a full wave bridge rectifier that converts AC supply voltage into DC. To increase the DC voltage, a DC-DC buck-boost converter is then used, as cells are typically stacked in series in battery-powered devices to achieve higher voltage. Due to space constraints, however, some high voltage applications are unable to accommodate a large enough cell stack. Buck-boost converters can be used in these cases to reduce cell number of cells but still raise the voltage [150]. In the presented scheme, a free-wheeling diode connects to loads in both parallel and reverse, thus removing negative voltage in the load and helping to supply a smooth current [151]. To turn the DC-DC buck-boost converter switches (SA and SB) ON and OFF, a pulse signal formed from pulse-width modulation (PWM) is used. The PWM modulating signal is generated by the multi-loop weighted modified Sliding Mode Controller (SMC). A high ampere-hour battery can be charged using output from the DC-DC buck-boost converter.

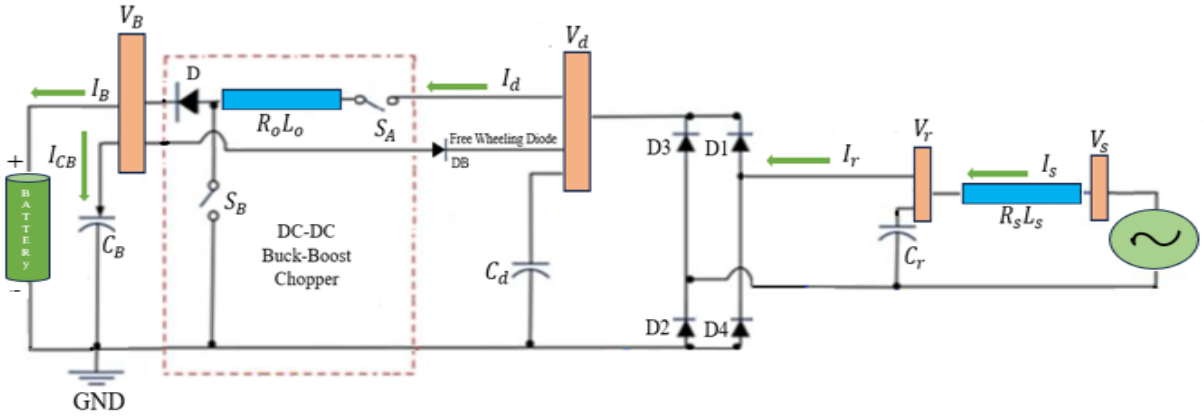

Figure 5.2 Basic Scheme for Electric Vehicles without MFCC-HFC

V2G schemes is a large scheme charging station it can be powered by local grid, PV, wind or all the above. Furthermore, to decrease line current harmonics while also improving the power factor and quality, a Modified Filter-Hybrid Filter Compensator (MF-HFC) can be connected in parallel to the full wave rectifier, as illustrated in Figure 5.2. The MF-HFC combines two shunt capacitors with a tuned arm shunt filter. Figure 5.3 illustrates how the switching pulses P1 and P2, which are produced from PWM, can control switches SA and SB. As shown, the complementary switching PWM pulses can alter the FACTS (MF-HFC) filter topology in a couple of ways. First,

during an event when (P1) is high and (P2) is low, both the resistor and inductor are cut off. The shunt capacitor then provides the AC system with any shunt capacitive compensation needed to increase the power factor. Second, the resistor and inductor are incorporated as a tuned arm filter into the circuit in order to decrease the harmonics in cases where pulse (P1) is too low, or pulse (P2) is too high.

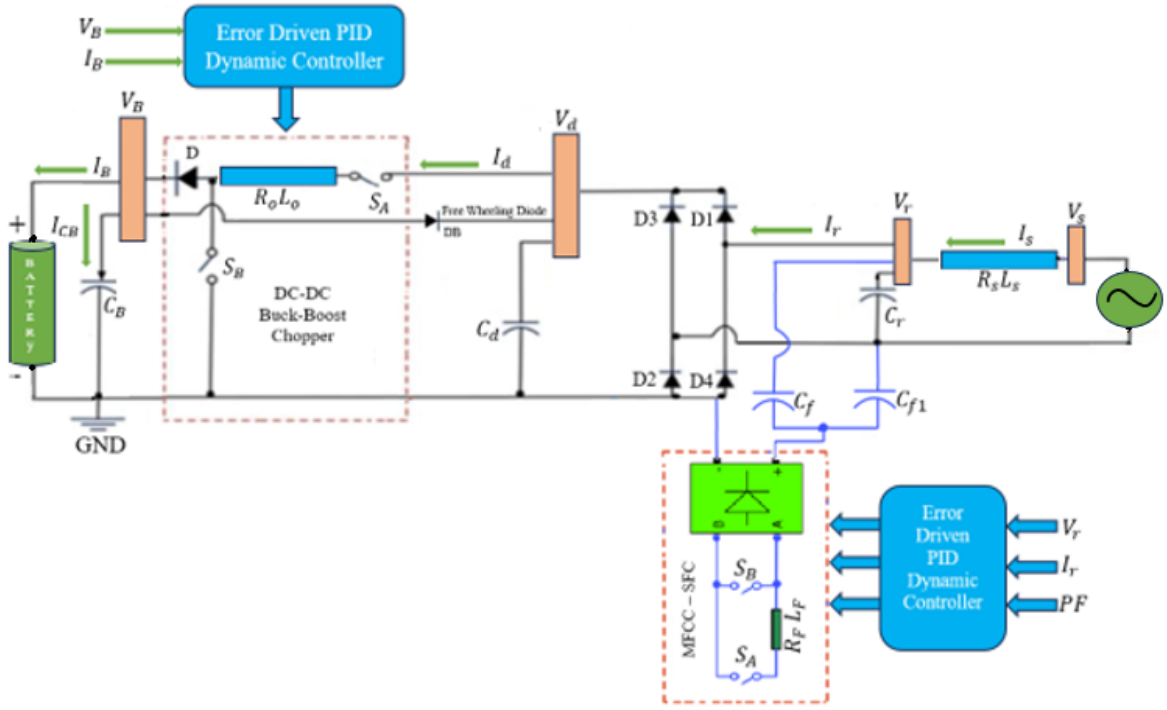

Figure 5.3 Proposed FACTS-Based (MFCC-HFC) V2G-Battery-Charging Scheme for Electric Vehicles

5.5 PID Dynamic Error-Driven Controller

To stabilize shared DC and AC buses, we use a novel tri-loop error-driven PID dynamic target practice controller. The dynamic regulation loops ensure energy efficiency as well as decreased current ripple content [152]. To obtain the desire features, i.e., ease of hardware implementation, fast dynamic response, and insensitivity to changing parameters and external conditions, the parameters of the dynamic controller are optimizable both on- and off-line [105]. The need to address multi-objective duties of adequate filtering and capacitive compensation for

power factor improvement and reduced transients and inrush currents necessitates using a complex time-scaled, multi-loop, multi-regulator weighted summed errors.

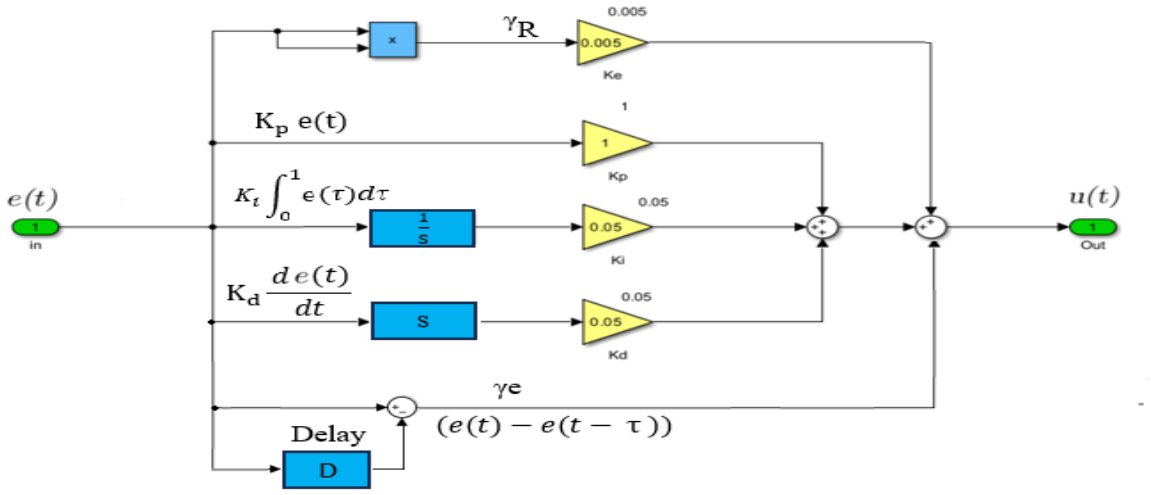

Figure 5.4 Novel Modified PID Dynamic Controller with Error Squared and Rate Compensation Loops

In the modulating control signal (Figure 5.4), the PWM switching block can be regulated using a PID dynamic controller, with the global error signal for an input. Quick dynamic response along with robust large excursion damping can be guaranteed by utilizing PID dynamic controllers, which feature error-sequential activation supplementary loops [107]. As presented in Figure 5.5 and Figure 5.6, the dynamic quad-loop controller is comprised of two primary loops and two sub-loops. The primary loops are for monitoring any inaccuracies that may occur within the bus's current or voltage readings at the diode bridge's AC and DC sides, while the sub-loops are for tracking any inaccuracies that may occur. Off-line guided trial and error is employed to select the controller's values for time delay and scaling. This approach ensures not only a quick response but a negligible number of errors overall [129]. The novel tri-loop regulation set-up at the common DC bus is able to mitigate any inrush, dynamic, abrupt, excursion changes that may manifest in the bus voltage and current. Meanwhile, loop-weighing factors ensure loop decoupling in a dominant voltage stabilization loop.

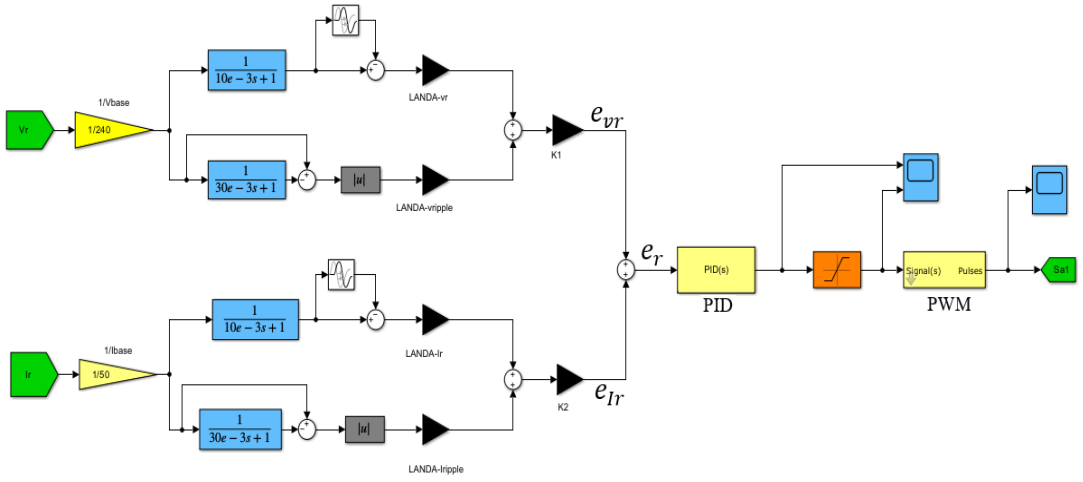

Figure 5.5 Dynamic Tri-Loop Regulator A for the AC HFC Filter Compensator

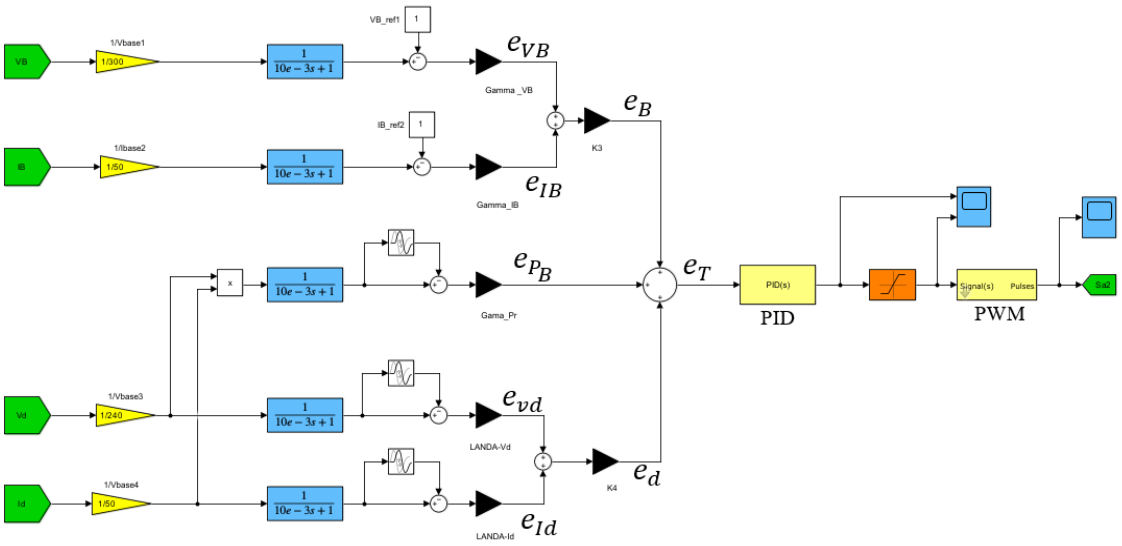

Figure 5.6 Dynamic Tri-Loop Regulator B for Buck-Boost DC-DC Battery Charging Chopper

This approach uses modulated filter capacitive compensator optimized switching according to system requirements. Additionally, for the green plug filter, a fast PWM-modulated switching system made up of a dynamic multi-regulation time descaled error-driven controller is employed [153].

The operation of the weighted PID controller specifically for two extra added loops error squared fast loop and error rate and how settings and gain selected.

WPID control is a modify two extra loops:

1. using the error square loop to improve the dynamics and fast response.
2. An incremental error type loop.

Effecting derivative action to compensate for the time lag in the control system, the delay in this loop T is selected base on the sampling period of the controller.

By alternating between static capacitive compensation and the tuned arm filter, this topology ensures dynamic interface bus voltage regulation, along with decreased ripple content of the inrush current and lower damped voltage transients. These circumstances may result from load-switching, wind scheme variations, the charging and discharging of self-excited capacitor banks, and/or short-term SC and OC faults.

The SFC filter change role from capacitive compensation to tuned arm Filtering based on weighted multi revulsion error with time scaling to control duty cycle ration and compensation time based on the dynamics of the nonlinear loads and inrush currents. Minimal transient over voltages is damped by the tuned arm filter mode of operation.

The novel controller has three loops: voltage stabilization loop error, dynamic power loop error, and current loop limiting error. Note that the first loop controller inputs represent the voltage and current values, V_r and I_r, prior to and after the filter, respectively. The loop serves to decrease the incidence and scale of bus voltage deviations to a unity voltage level ($V_{m_{ref.}}$) from a reference voltage level. To achieve this aim, the loop controller makes a comparison of the reference value and the current/voltage for MFCC-HFC (both sides). The result of the comparison represents the first signal error (e_r) for the PWM, as expressed in Equations (5.1), (5.2), and (5.3):

$$e_r = \Upsilon_{v_r}(e_{v_r}) + \Upsilon_{vB}(e_{vB}) \tag{5.1}$$

So that,

$$e_{v_r} = \left(\frac{V_{m_{ref}} - V_r\left(\frac{1}{1+ST_1}\right)}{V_{m_{base}}}\right) \tag{5.2}$$

$$e_{vB} = \left(\frac{V_{m_{ref}} - V_B\left(\frac{1}{1+ST_1}\right)}{V_{m_{base}}}\right) \tag{5.3}$$

The inputs of the second loop controller are the measured currents and voltage of both sides of the MFCC-HFC. The idea behind this loop of the controller is limiting the inrush current and dynamic rms current changes, i.e., during the fault conditions. Accordingly, the loop controller compares the currents of both side of MFCC-HFC with a reference value (I_m); hence, the output of this comparison will be the second signal error (e_d) of the PWM, as given in Equations (5.4) to (5.6).

$$e_d = \Upsilon_{v_d}(e_{v_d}) + \Upsilon_{I_d}(e_{I_d}) \tag{5.4}$$

So that,

$$e_{v_d} = \frac{e_{vd}}{I_{m_{base}}} \left(\frac{1}{1+ST_1}\right)\left(1 - \frac{1}{1+ST_2}\right) \tag{5.5}$$

$$e_{I_d} = \frac{I_d}{I_{m_{base}}} \left(\frac{1}{1+ST_1}\right)\left(1 - \frac{1}{1+ST_2}\right) \tag{5.6}$$

The inputs of the third loop controller are the measured currents and voltages of bus e_{I_B}. This loop reduces the impacts of the dynamic changes of power under load changes and sudden excursions. Accordingly, the loop controller compares the measured voltage (V_B), current (I_B), and the calculated power(V_B) * (I_B) with their reference values and feeds the third error e_B to the PWM module, as given in Equations (5.7) to (5.10):

$$e_B = \Upsilon_{v_B}(e_{v_B}) + \Upsilon_{I_B}(e_{I_B}) \tag{5.7}$$

So that,

$$e_{v_B} = \frac{I_{m_{ref}} - V_B\left(\frac{1}{1+ST_1}\right)}{I_{m_{base}}} \tag{5.8}$$

$$e_{I_B} = \frac{I_B}{I_{m_{base}}} \left(\frac{1}{1+ST_1}\right)\left(1 - \frac{1}{1+ST_2}\right) \tag{5.9}$$

$$e_{P_B} = \left(\frac{V_B}{V_{m_{base}}} \bullet \frac{I_B}{I_{m_{base}}}\right)\left(1 - \frac{1}{1+ST_2}\right) \tag{5.10}$$

where γV_B is the loop error gain for the voltage, γI_B is the loop error gain for the current, and γP_B is loop error gain for the power. Also, e_{I_B} , e_{v_B}, e_{P_B} , and e_{V_d} are the current limiting loop error before the MFCC-HFC, voltage stabilization loop error, synthesis dynamic power loop error, and current limiting loop error before the MFCC-HFC, respectively. Consequently, a total error e_T is calculated from the three errors of the control system, which are the combination of the voltage

stabilization loop error (e_r), the current limiting loop error (e_d), and the synthesis dynamic power loop error (e_B), as illustrated in Equations (5.11) to (5.14), respectively. This error in terms of generating the switching pulses to the GP-SFC in accordance with the duty ratio and the error value. Also, K_1, K_2, K_3 and K_4 are selected weightings for the three separate regulation loops to allow adjustment of the control burdens.

$$e_{T} = e_r + e_d + e_B \tag{5.11}$$

So that,

$$e_r = e_R \bullet k_1 \tag{5.12}$$

$$e_d = e_D \bullet k_2 \tag{5.13}$$

$$e_B = e_B \bullet k_3 \tag{5.14}$$

A proportional integral derivative controller processes the difference between the signals to obtain the phase angles (delta) required to drive the error to 0. Finally, the control signal of the PWM of the MFCC-HFC scheme has the following form u(t) in the time domain for the PID controller.

$$u(t) = K_1\, e_T(t) + K_2 \int_0^t e_T(t)dt + K_3 \frac{(d(e_T)(t))}{dt} \tag{5.15}$$

where e_T (t) is the selected system error, u(t) is the control variable, Kp is the proportional gain, Ki is the integral gain, and Kd is the derivative gain. In this work, the Tri loop error-driven controller is used with a traditional PID controller, where the PID controller gains (K_1, K_2, and K3) are based on a trade-off between design goals such as total error minimization and step-by-step trials [154]. The control gains and weightings were selected of line to minute an error squared objective function over a for is fixed settling time and the final form u(t) in the time domain for the PID controller as shown:

$$u(t) = Kp\, e_T(t) + Ki \int_0^t e_T(t)dt + Kd \frac{(de_T(t))}{dt} + \gamma R\,(et(t))^2 + \gamma e\,(et(t) - et(t\ -\tau\ ))] \tag{5.16}$$

5.6 Lithium-ion Batteries

In EVs, Lithium-ion batteries are considered a key component for high performance. These rechargeable batteries provide a high number of charge/discharge cycles and high specific energy in comparison with other batteries. Lithium-ion batteries are also very reasonably priced. Such considerations make Lithium-ion batteries a better choice than alternatives such as nickel metal hydride or silver zinc. However, only small-size Lithium-ion batteries are currently available in the commercial marketplace. Accordingly, Lithium-ion batteries are usually used in series/parallel assembly configurations, but this raises issues around safety, especially in EVs [122].

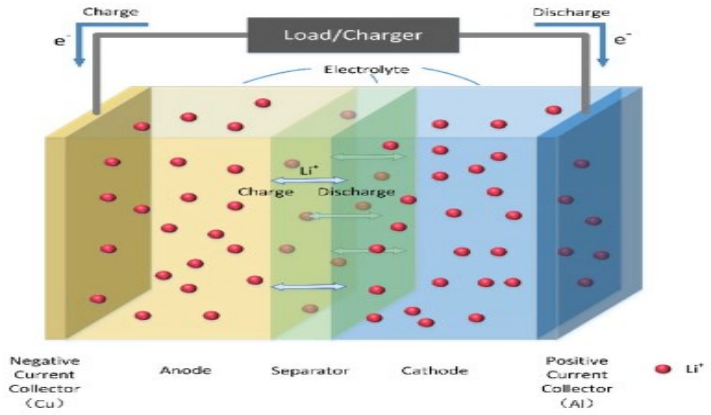

Figure 5.7 Diagram of Lithium-ion Battery [154]

Another challenge with Lithium-ion batters is their charge and discharge, which involves highly complex electro-chemical processes. These need to be modelled mathematically and then examined based on an electro-chemical perspective. In addition, the equations rely on the battery's internal chemical reactions, which means that the models need to be precise.

Equation (5.17) presents a model showing the measured battery voltage at the terminals (V_{batt}), the battery's electro-motive force (EMF), and the current and equivalent over-potential resistance of the product for that moment in time. Figure 5.67 presents a rechargeable Lithium-ion battery [155].

$$\mathrm{EMF(SOC)} = V_{\mathrm{batt}}(\mathrm{t}) - \mathrm{i(t)} \bullet R_{\mathrm{overpotential}}\,(\mathrm{SOC}) \tag{5.17}$$

SOC estimation method:

The SOC is defined as the average concentration of lithium ions in cathode over its maximum concentration.

$$\mathrm{SOC} = \frac{\text{Avarage concentration of Lithium ion in cathode}}{\text{Maximum concentration of Lithium ion in cathode}} \tag{5.18}$$

Hence,

$\mathrm{SOC_{min}}$ greater than 0 & $\mathrm{SOC_{max}}$ less than 1

$$\mathrm{SOC} = \frac{\mathrm{SOC_k} - \mathrm{SOC_{min}}}{\mathrm{SOC_{max}} - \mathrm{SOC_{min}}} \tag{5.19}$$

where,

$\mathrm{SOC_k}$ is the amount of energy present at time k.

$$\mathrm{SOC} = \frac{\mathrm{Q_{remain}}}{\mathrm{Q_{rated}}} x\ 100 \tag{5.20}$$

A Lithium battery can be obtained by the ampere-hour integration method, which can be expressed by the following formula:

$$\mathrm{SOC(t)} = \left(\mathrm{SOC}_{(\,t_0)}\right) + \frac{1}{\mathrm{Q}_N}\int_{t_0}^{t_0+t} \mathrm{I_{bat}}\, d\tau\ x\ 100\% \tag{5.21}$$

We can also express the formula of the equivalent circuit model of the battery as:

$$\mathrm{SOC(t)} = \mathrm{SOC}_{(\,t_0)} - \frac{\int_{t_0}^{t} \mathrm{I}\, dt}{\mathrm{Q}_N} \tag{5.22}$$

$$\mathrm{SOC(t)} = \mathrm{SOC}_{(\,t_0)} - \frac{\mathrm{I\,(t)}}{\mathrm{Q_N}} \tag{5.23}$$

Where,

I_{bat} is charging and discharging the current of the battery.

Q_N is the capacity of the lithium battery.

There are various ways to measure the EMF of a battery, either directly or indirectly, and it is strongly correlated with the battery's state of charge. The battery is charged and discharged at a low current rate using the voltage relaxation method, after which the battery is allowed to reach equilibrium by relaxing (i.e., resting) for a while. The SOC was not estimated directly, but through the use of weighted voltage, current, and power dynamic compensation. The results show that the battery-charging controller can dynamically deal with changes using combined mode voltage, current, and power-weighted compensation [156].

5.7 MFCC – Modulated/Switched Filter Compensation

In power transmission, FACTS technologies can be utilized in AC systems for boosting reliability, efficiency, and control. As mentioned previously, FACTS-enabled devices improve power quality and reduce harmonics through IGBT switches controlled via two complementary pulses [125]. The equivalent admittance of an MFCC circuit is then easily modified using different operating states. So, for instance, when switches S1 and S2 are open, the indicator and resistor are connected with the circuit. However, when switches S1 and S2 are closed, the indicator and resistor are shorted, leading to a capacitive admittance in the capacitor's bank.

This result is illustrated in Figure 5.8, which shows a tri-loop dynamic error-driven PID controller. Such considerations make Lithium-ion batteries a better choice than alternatives such as nickel metal hydride or silver zinc. However, only small-size Lithium-ion batteries are currently available in the commercial marketplace. Accordingly, Lithium-ion batteries are usually used in series/parallel assembly configurations, but this raises issues around safety, especially in EVs [126].

The modulated filter MFCC-SFC implemented the DC/DC converter stage using pulse with modulation, duty-cycle modulation, and the bandpass to address the different complex versions of DC-DC converter interface topologies, including transformer coupled isolated and non-isolated buck-boost types. On the other hand, a FACTS system that has a switchable capacitor bank would be able to reduce system harmonics significantly. Such an MFCC could be programmed as well to

reduce current oscillation and absorb ripples [55], [96]. This MFCC control strategy uses components from a bus's separated current and voltage.

As explained in [105], SPWM has already been incorporated into renewable energy applications, including power inverters and motor drives that have a duty ratio and error value. The main idea for a dynamic controller is to enable stable current and voltage levels in a system, with all mistakes transmitted to an SPWM. The SPWM then generates pulse series that have adjustable widths, creating waveforms that resemble a sine wave (see Figure 5.8).

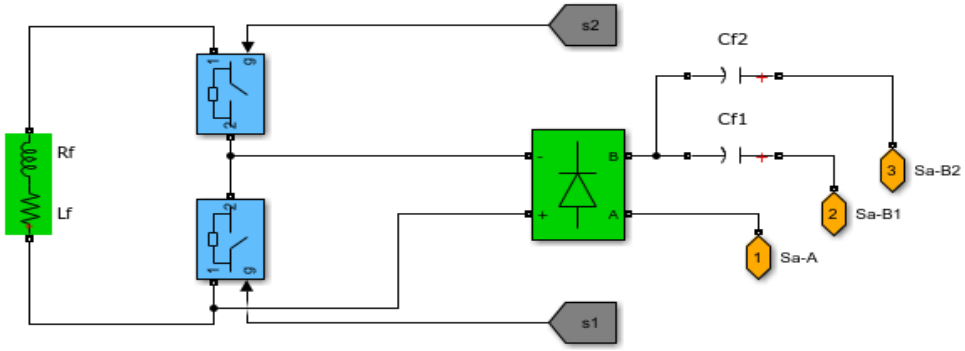

Figure 5.8 MFCC-SFC Switched Green Plug-Filter Compensator Scheme

Furthermore, the power electronic converters used in an MFCC show enhanced power abilities, leading to greater current and voltage ratings. These features result in efficient operation as well as appropriate sizing [79]. MATLAB/Simulink-2023b digital simulation is used in this research to validate the MFCC approach. One key advantage of the proposed compensator is that the impact of faulty states in the main grid can be decreased when used with renewables. The MFCC acts as a modulated admittance and point of connection near nonlinear loads. The duty cycle ratio is adjusted online using the multi-regulation total error to ensure dynamic matching to the fast and slow-acting nonlinear variations. The dual function of tuned arm filter is complemented by the adjusted capacitive compensation level for nonlinear reactive-type loads, motorized inrush loads, and cyclical-type loads. The proposed AC filter functions as a green plug device that reduces the THD of the voltage and current low order harmonics, improves the power factor, and mitigates inrush source currents and DC bus transient over voltages. The MFCC-HFC is an effective low-cost tool combining filtering and capacitive compensation that replaces the need for active power filters and D-STATCOM reactive compensation devices.

5.8 Operation of Modulated/Switched Filter Compensation, MFCC

The number of nonlinear loads in a modern electrical distribution system has increased exponentially. Examples of these loads include power supply, rectifier equipment, home appliances, and adjustable speed drives (ASD). The harmonic currents produced by the loads may become highly substantial as their number increases. However, numerous power system issues, such as distorted voltage waveforms, equipment overheating, malfunctioning system protection, excessive neutral currents, flickering lights, inaccurate power flow metering, etc., can be caused by these harmonics. By taking a reactive current component from the distribution network, they also lessen efficiency. FACT-MFCC can be used to solve these issues.

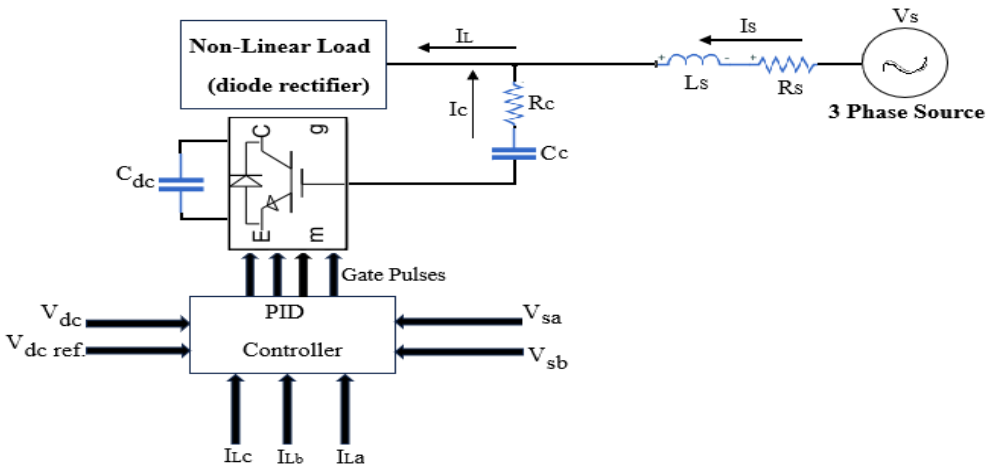

Figure 5.9 Structure of an MFCC Filter

Nonlinear loads in parallel are mostly connected via a current source. Conventionally, the MFCC is configured to inject reactive and harmonic compensation currents in response to reference current calculations. The injected currents are meant to cancel the harmonic and reactive currents drawn by the nonlinear loads. In recent years, a current-source-inverter (CSI)-based MFCC filter has been used and established as an acceptable choice for the control scheme [157]. This scheme is straightforward and easy to install, as it determines the necessary compensatory currents simply by sensing line currents. It uses a conventional PID for the generation of a reference current, as shown in Figure 5.9. For this system, the instantaneous load current can be written as:

$$i_l = \sum_{n=1}^{\infty} I_n \sin(n\omega t + \phi_n)$$
$$i_l = I_1 \sin(n\omega t + \phi_1) + [\sum_{n=1}^{\infty} I_n \sin(n\omega t + \phi_n)] \quad (5.24)$$

Both basic power and reactive power, including harmonic power, make up the load power. The power of the instantaneous load can be expressed as:

$$P_{l(t)} = i_s(t) \times V_s(t) \quad (5.25)$$

$$P_l(t) = V_m \sin^2 \omega t \times \cos \phi_1 + V_m I_1 \sin \omega t \times \cos \omega t \times \sin \phi_1 + V_m \sin \omega t \times [\sum_{n=1}^{\infty} I_n \sin(n\omega t + \phi_n)] \quad (5.26)$$

$$P_l(t) = P_f(t) + P_r(t) + P_h(t) \quad (5.27)$$

where $P_f(t)$ is the fundamental component of power, and

$P_r(t)$ is the reactive power and $P_h(t)$ represent harmonic power.

From this equation, we can see that the only real power drawn by the load is:

$$P_f(t) = V_m I_1 \sin^2 \omega t \times \cos \phi_1 = V_s(t) \times i_s(t) \quad (5.28)$$

The source current drawn from the main after compensation should be sinusoidal, which is represented as:

$$i_s(t) = \frac{P_s(t)}{V_s(t)} = I_1 \cos \phi_1 \sin \omega t == I_{max} \sin \omega t \quad (5.29)$$

If the reactive power line conditioner provides all the reactive and harmonic power, the source current will be sinusoidal and in phase with the utility voltage [124]. Using the load current as a guide, MFCC evaluates the fundamental and accounts for the reactive and harmonic components.

5.9 Results Simulation and Discussion

MATLAB/Simulink/Sim-Power digital simulation results are used to verify the proposed PID controller's dynamic effectiveness as well as the effectiveness of the proposed MFCC-based battery charging V2G scheme, given as a SOC of 50% in EV systems. We tested the hybrid filter compensator (HFC) for V2G battery-charging 50% SOC using a PID controller, without and with MF-HFC. The simulated setup is illustrated in Figure 5.10 below.

5.9.1 Without and with Filter for Normal Operation

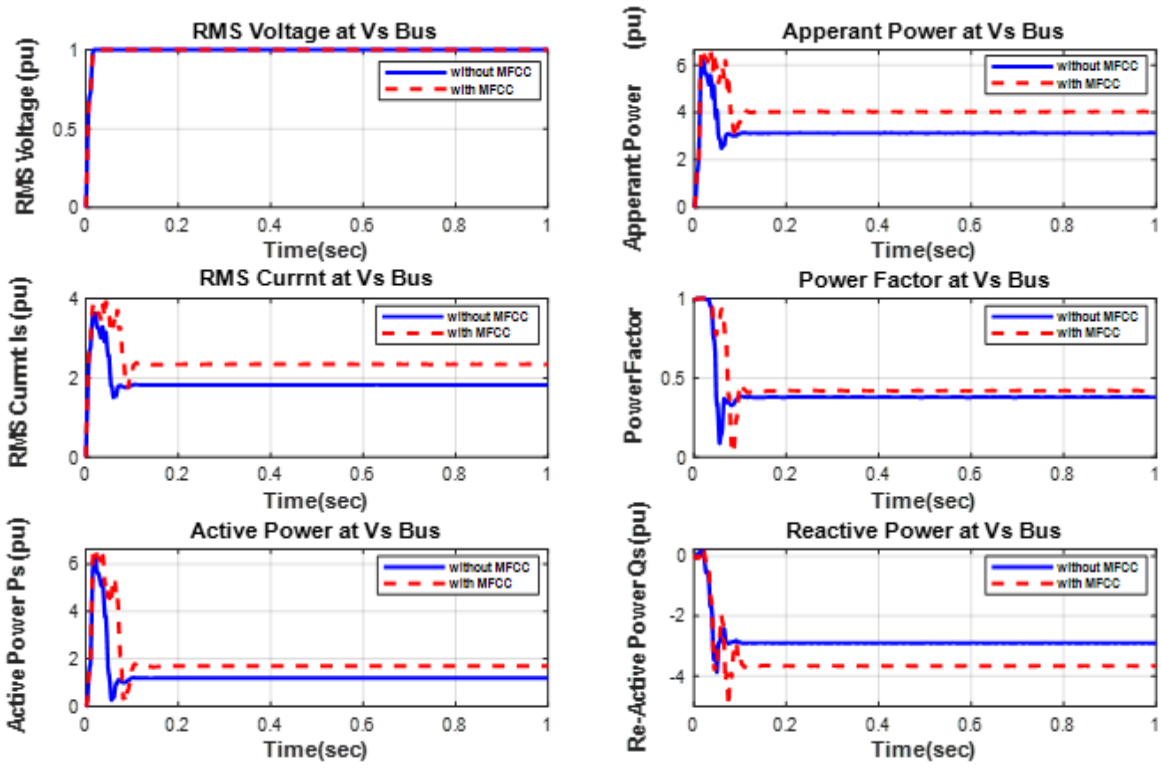

Figure 5.10 RMS V, S, I, PF and Ps & Q, S and PF at Vs Bus without and with MFCC-HFC Compensator

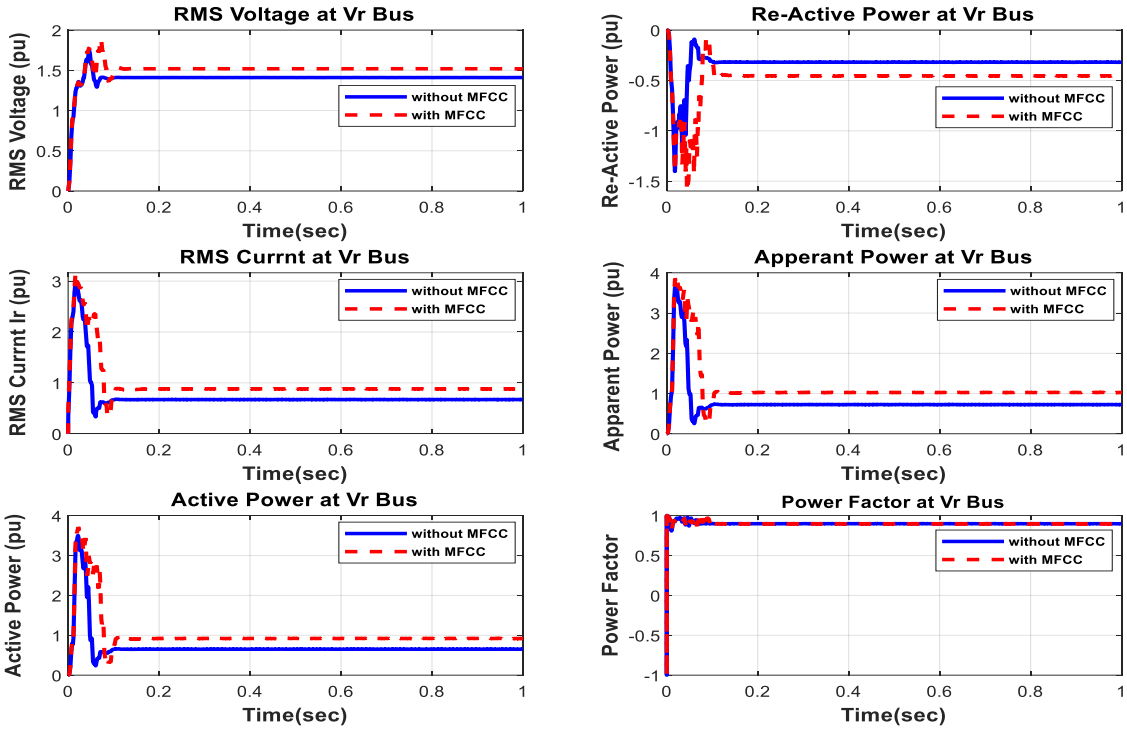

Figure 5.11 RMS V and I & P, Q, S and PF Vr Bus without and with MFCC-HFC Compensator

Table 5.1: Voltage, Current, and Active Power Values at AC Buses

Buses	Vs (pu)			Vr (pu)		
	Vs	Is	Ps	Vr	Ir	Pr
Without MFCC	0.95	1.90	1.75	1.40	1.80	0.80
With MFCC	1.00	2.50	1.90	1.50	1.95	1.00
Improvement	0.05	0.60	0.15	0.10	0.15	0.20

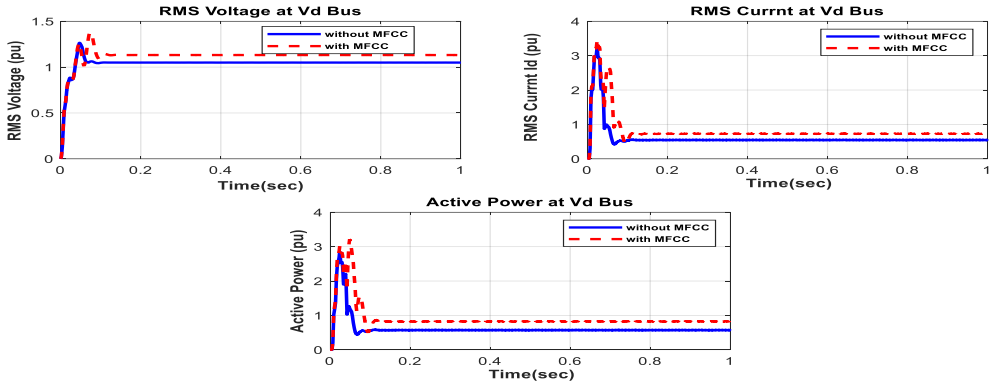

Figure 5.12 RMS V and I & P at Vd Bus without and with MFCC-HFC Compensator

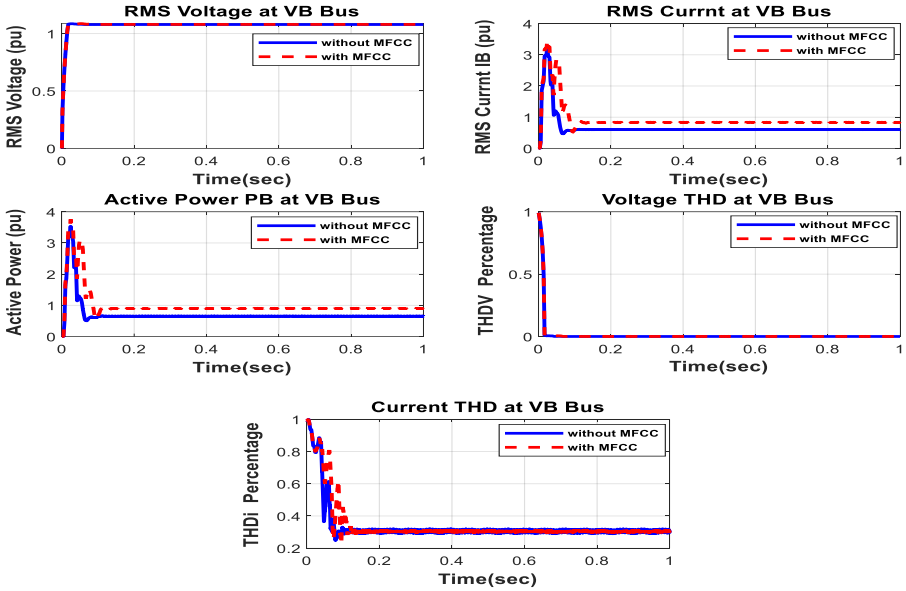

Figure 5.13 RMS V and I & P, THDv, and THDi at VB Bus without and with MFCC-HFC Compensator

Table 5.2: Voltage, Current, and Active Power Values at DC Buses

Buses	V_d (pu)			V_B (pu)		
	Vd	Id	Pd	V_B	I_B	P_B
Without MFCC	1.01	0.70	0.75	0.97	0.80	0.80
With MFCC	1.10	0.80	0.90	1.00	0.90	0.99
Improvement	0.09	0.10	0.15	0.03	0.10	0.19

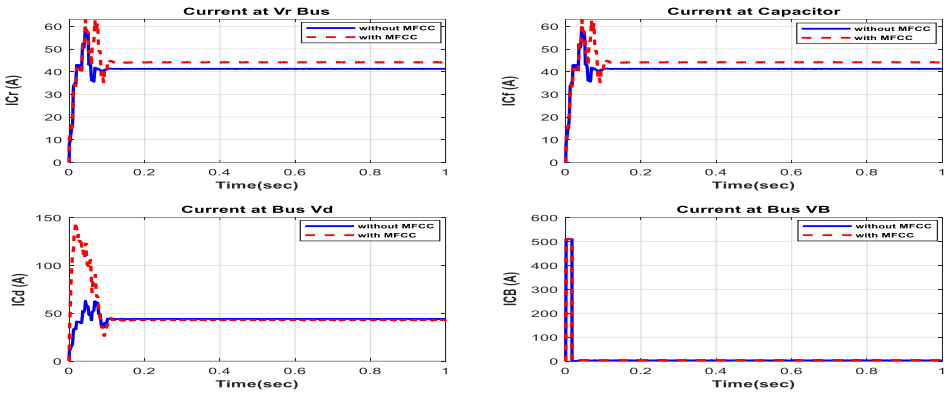

Figure 5.14 Currents ICr, ICf, ICd & ICB at VB Bus without and with MFCC-HFC Compensator

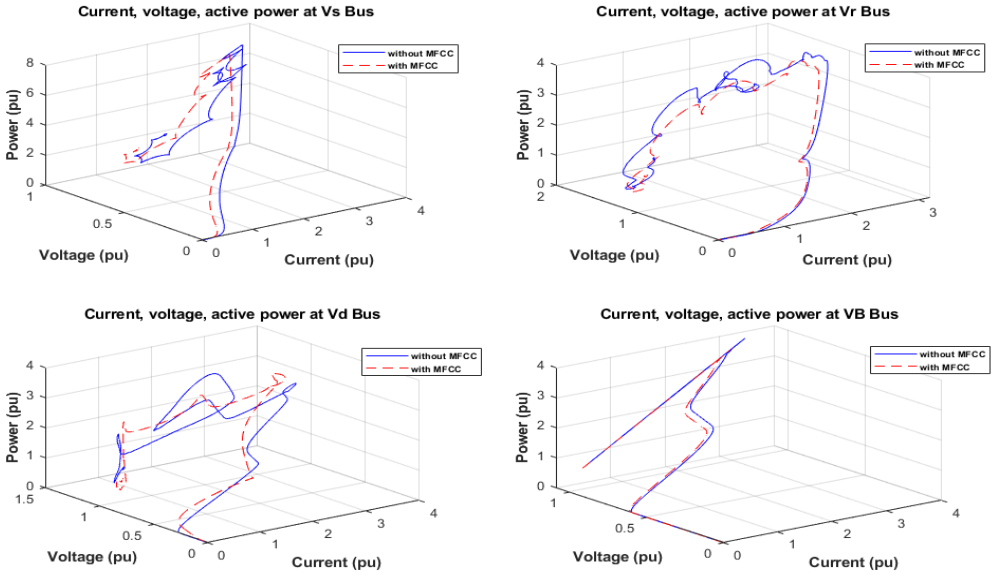

Figure 5.15 Current, Voltage & Active Power @ Vs, Vr, Vd, VB Buses without and with MFCC-HFC Compensator

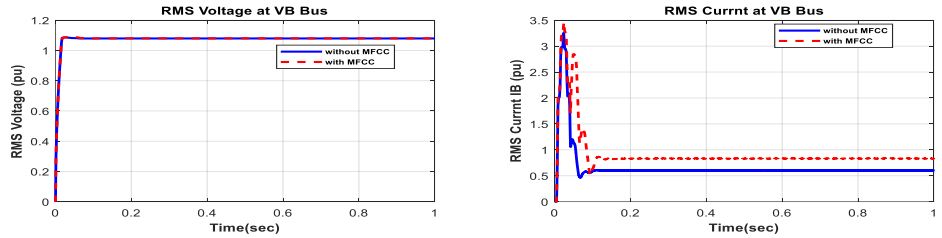

Figure 5.16 RMS Current IB & RMS Voltage VB at Source Bus without and with MFCC-HFC Compensator

MATLAB/Simulink digital simulation is used for the proposed MFCC-HFC at normal operating conditions. Figures 5.10 and 5.11 show the system's AC side. As can be seen, the RMS voltage's dynamic response for the sending end bus (Vs) reveals that the measured voltage is around 0.95 pu when operating without the proposed MFCC and is around 1.0 pu when operating with the MFCC. The figures also indicate that the RMS voltage is less variable than the RMS current, remaining around 1.9 pu and 2.5 pu, respectively, when involving the suggested MFCC. In addition, the graph illustrates how the Vs bus reactive power remains relatively constant near the 0.18 second and how the reactive power at the source bus is reduced. These dynamics boost the power factor up to 0.3 pu from 0.4 pu, as presented in Figure 5.11.

Table 5.1 shows how the active power is boosted to 1.75 pu from 1.95 pu when MFCC is applied. In Figure 5.11, we can see a clear improvement in the RMS current (1.8 pu to 1.95 pu) when the proposed MFCC is added at the Vr bus. The same figure also shows an obvious power factor enhancement. Table 5.1 presents improvement values for active, voltage, and current power on the AC-side system buses, both without and with involving the suggested MFCC-HFC strategy.

In Figures 5.12 and 5.13, the charging system's DC side is shown with Vd and VB buses. In Figure 5.12, the RMS active, current, and voltage power's dynamic response reveals obvious enhancements at the Vd bus when the MFCC approach is involved. Table 5.2 presents the same findings. In Figure 5.13, there is also evidence of improved active power and RMS current at the V_B bus when the MFCC approach is applied. These values are then compared in Table 5.2.

Figure 5.14 shows the currents IC_r, IC_f, IC_d and IC_b at the V_B bus without/with the MFCC-HFC compensator. The figure also illustrates RMS voltage, RMS current, and active power three-dimensionally at the V_s, V_r, V_d, V_B buses with/without the involvement of the MFCC-HFC compensator. Figure 5.16 demonstrates some improvement in RMS current and voltage in the charging scheme side of the V_B bus when the proposed MFCC-HFC is involved.

5.9.2 Total Harmonic Distortion Analysis of Voltage and Current

Total harmonic distortion is the harmonics in waveforms of voltage and current. We provide our results showing the voltage and current THD of the load bus without and with FACTS-MFCC-HFC as a function of time. The rate of THD has increased for constant series compensation because nonlinear loads are used on power systems; however, our proposed FACTS-MFCC-HFC is

working with a function to get an improved power factor and low THD and harmonics at the DC side only to improve the system performance. The proposed AC filter acts as a green plug device that reduces THD of voltage and current for a low order of harmonics, improved power factor, fewer inrush source currents, and less DC bus transient over-voltages. The THD of the current at the load bus side is improved, as shown in Figures 5.17 (A) without the FACTS device and in Figure 5.17 (B) with the FACTS device. As can be see, the improvement is 25.98%. Figure 5.18 (A) shows the THD of the current without the FACTS device and Figure 5.18 (B) with the FACTS device. By employing the FACTS-MFCC-SFC, the improvement is 38.99% [125], [55].

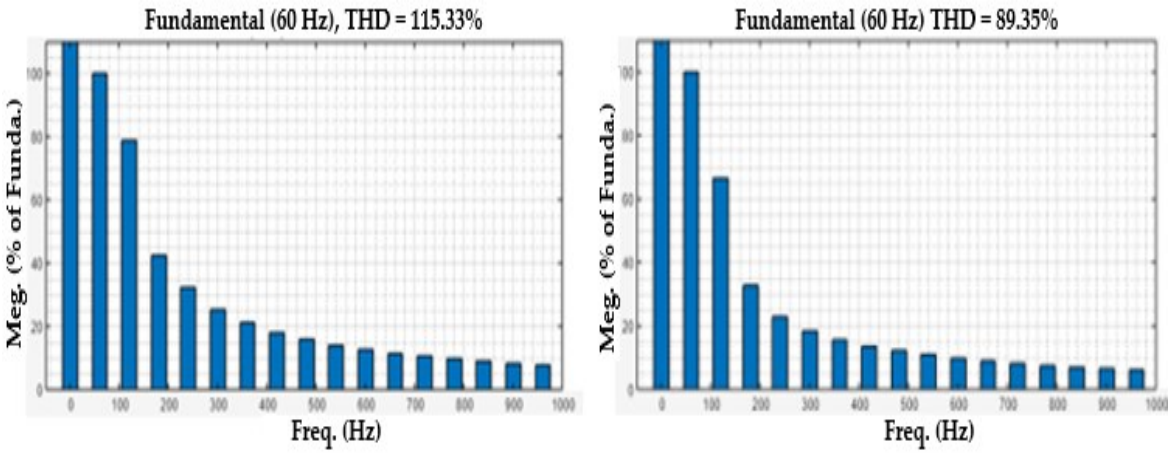

A B

Figure 5.17 (A) THD Voltage at load Bus without FACTS-MFCC-HFC for Load-Changing Operation
(B) THD Voltage at Load Bus with FACTS-MFCC-HFC for Load-Changing Operation

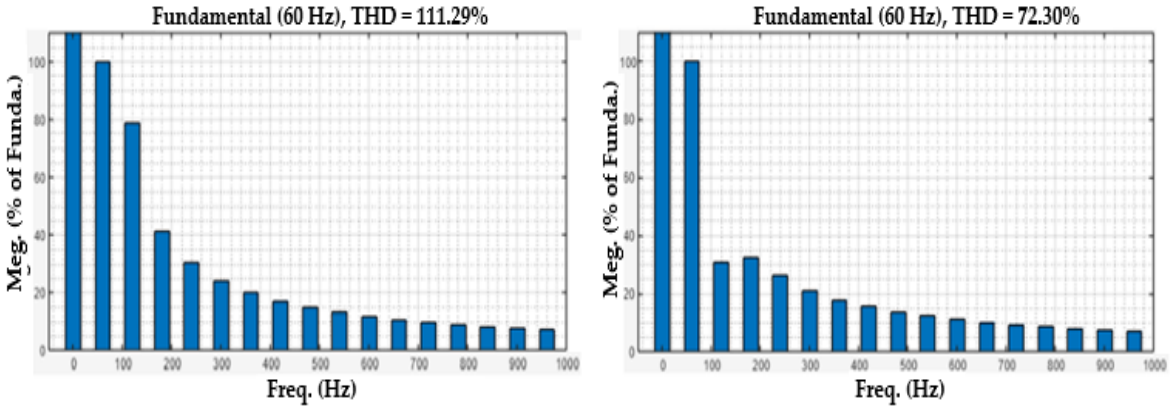

A B

Figure 5.18 (A) FFT Analysis of Current at Load Bus without FACTS-MFCC-HFC for Load-Changing Operation
(B) FFT Analysis of Current at Load Bus with FACTS-MFCC-HFC for Load Changing Operation

5.9.3 Without and with Filter for Short-Circuit Fault Operation

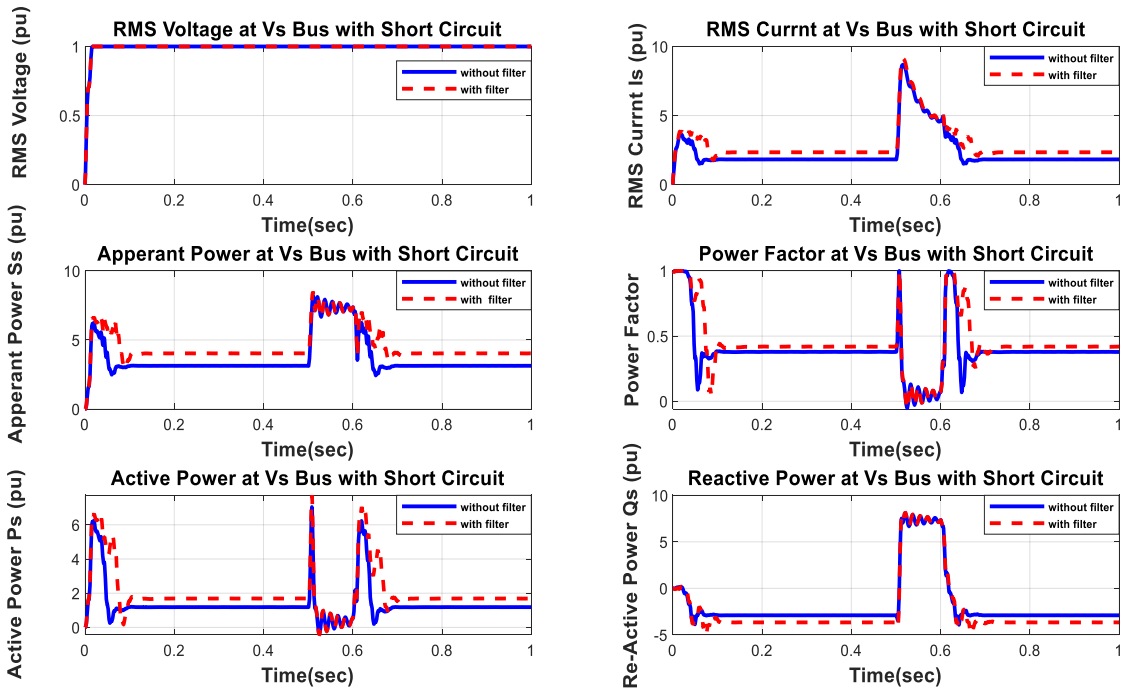

Figure 5.19 RMS V, S, I, PF and P & Q at Vs Bus under SC Fault with and without MFCC-HFC Compensator

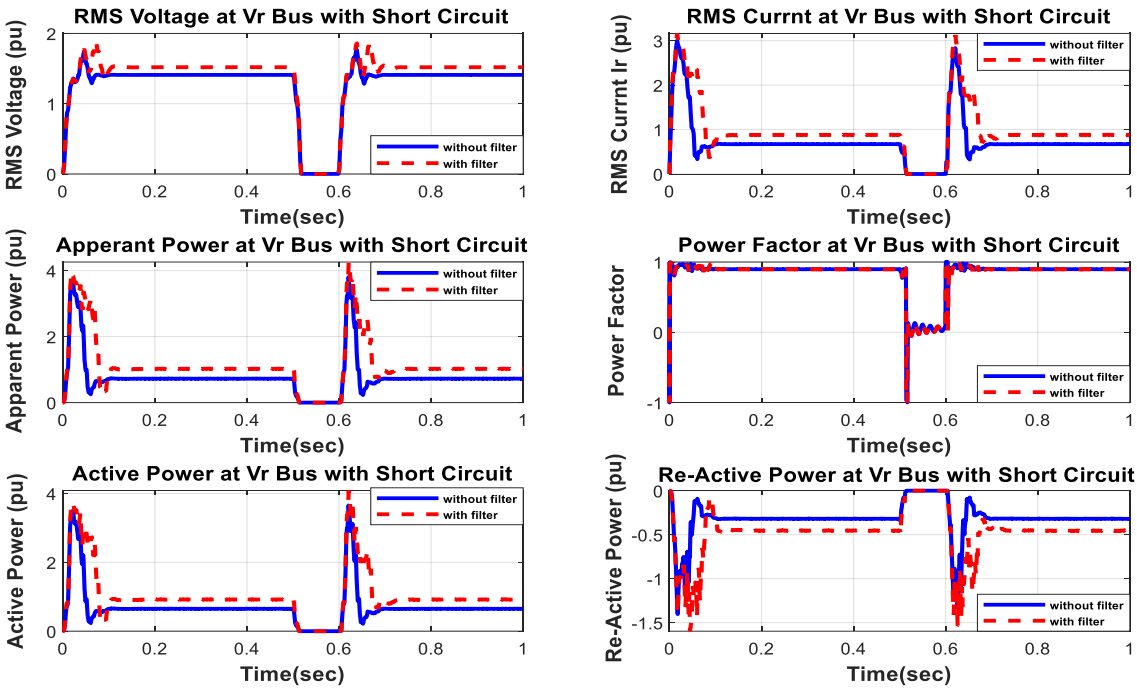

Figure 5.20 RMS V, I, P, Q and S & PF, at Vr Bus under SC Fault with and without MFCC-HFC Compensator

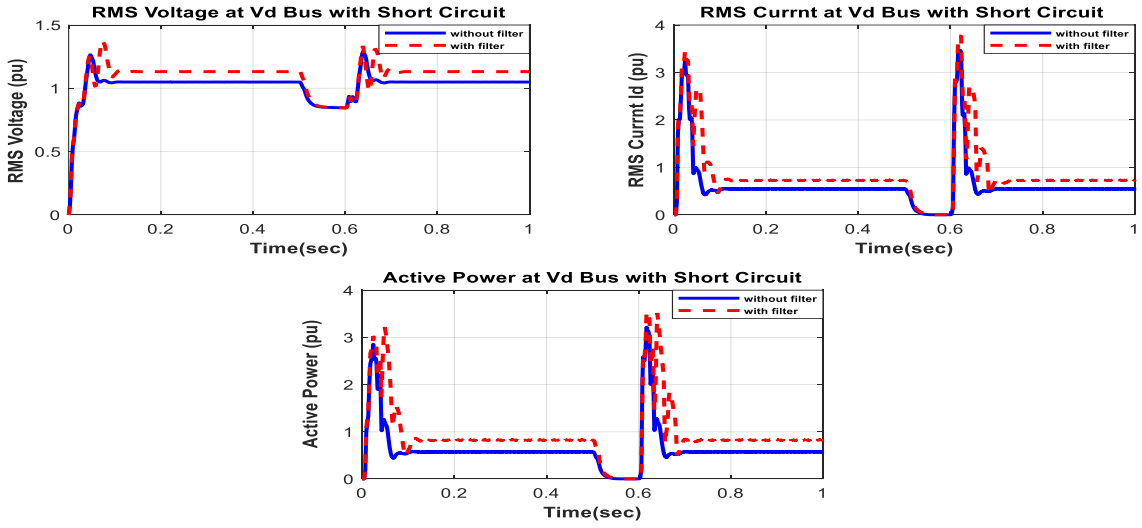

Figure 5.21 RMS V and I & P at Vd Bus under SC Fault with and without MFCC-HFC Compensator

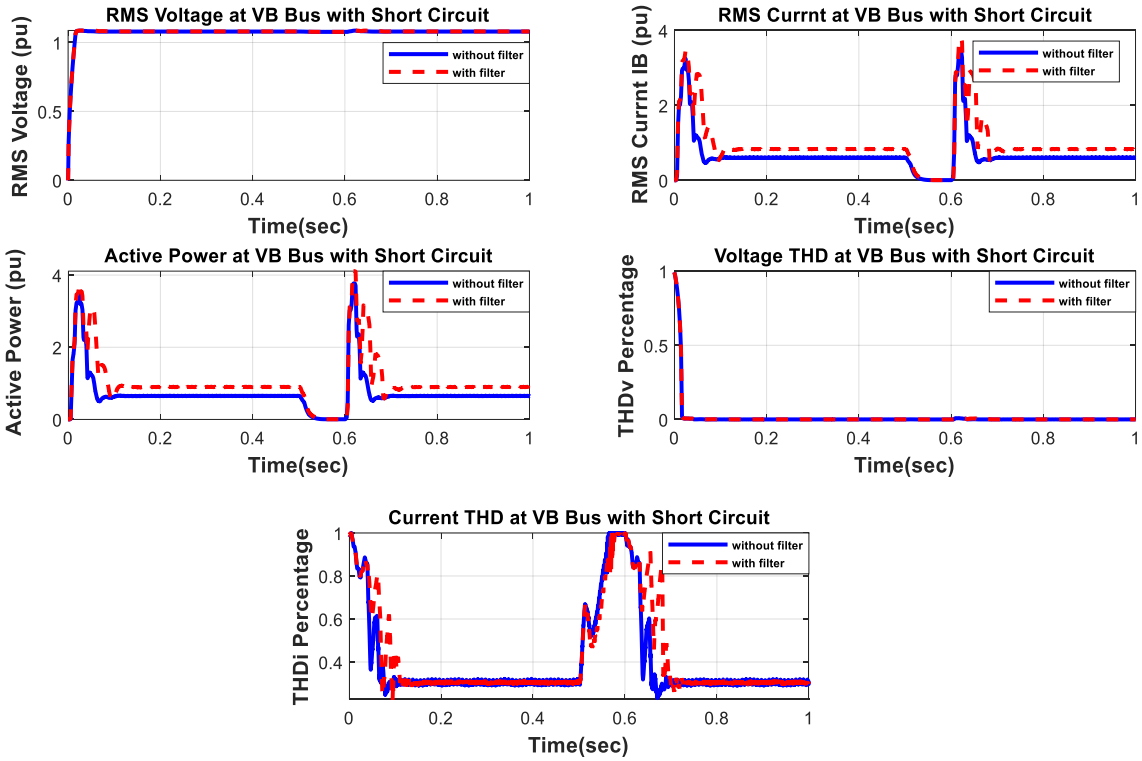

Figure 5.22 RMS V and I & P, THDv, and THDi at VB Bus under SC Fault with and without MFCC-HFC Compensator

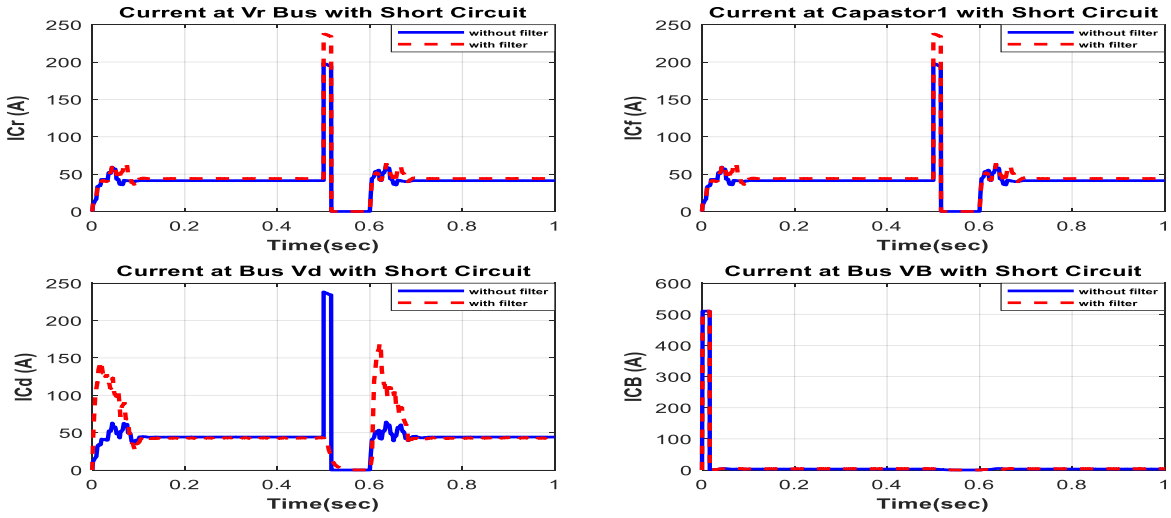

Figure 5.23 Currents ICr, ICf, ICd & ICB at VB Bus under SC Fault with and without MFCC-HFC Compensator

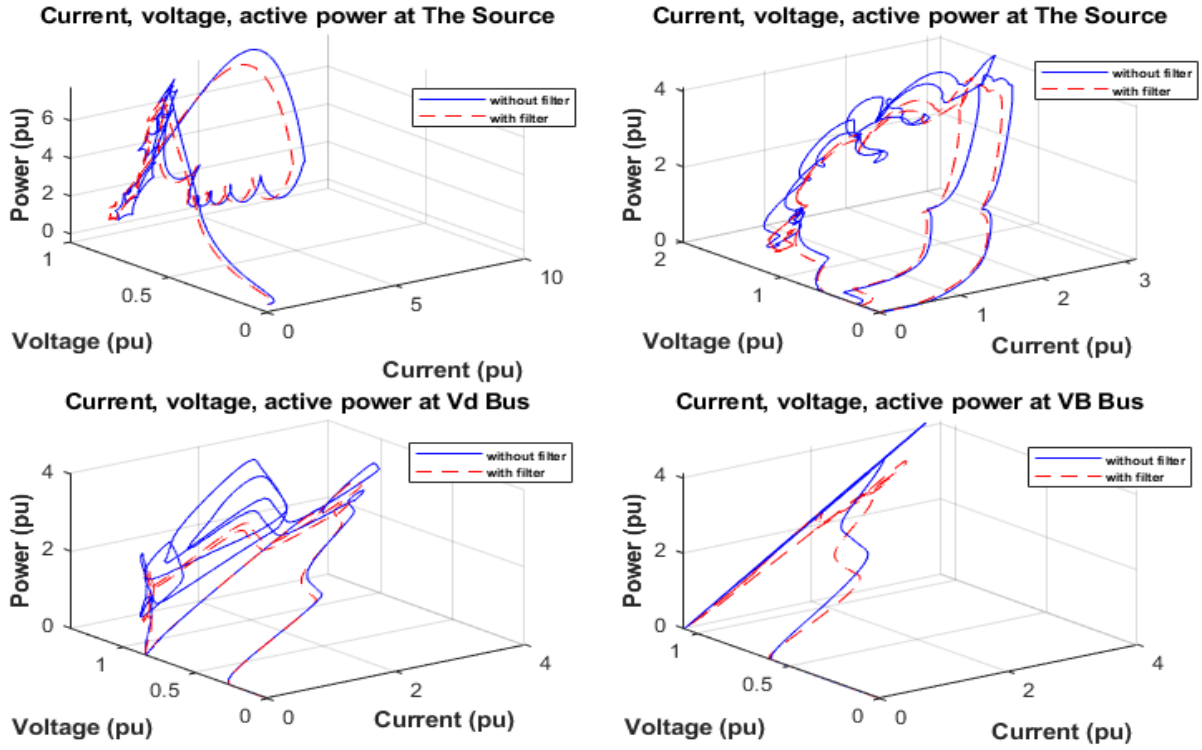

Figure 5.24 Current, Voltage, & Active Power at Vs, Vr, Vd, and VB Buses under SC Fault with and without MFCC-HFC Compensator

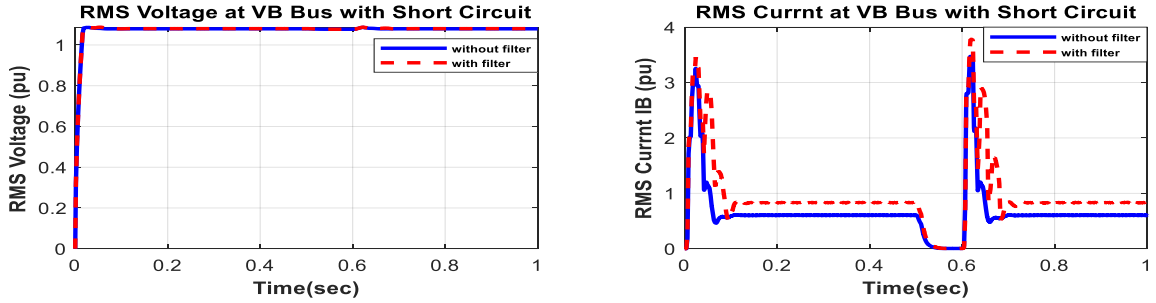

Figure 5.25 RMS Current IB & RMS Voltage VB at Source Bus under SC Fault with and without MFCC-HFC Compensator

A MATLAB/Simulink/Sim-Power software environment is used to verify the proposed MFCC-HFC scheme's dynamic effectiveness in a V2G battery-charging system operating at 50% SOC. The digital simulation operated in an open circuit of 200 ms and at a scale of 1 second for buses on the AC side (V_s & V_r). On the DC side, the digital simulation dynamic responses for the

V_d and V_B buses are presented in Figures 5.21 and 5.22. In Figures 5.19 and 5.20, the digital responses for both buses on the AC side are shown without/with the suggested filter. Also, the figures show that the power quality and dynamic responses of all buses (AC and DC sides) have been significantly improved. As can be seen, there is reduced fluctuation in the power factor of key buses when operating in open-circuit fault conditions with the proposed charging strategy, particularly the AC bus.

Figure 5.23 illustrates the currents during open-circuit operation without/with the MFCC-HFC compensator, while Figure 5.24 presents a 3D view of OC for RMS voltage, current, and active power for all system buses without/with the MFCC-HFC scheme. In Figure 5.25, we can see how the RMS voltage and current have improved on the V_B bus-charging scheme side.

5.9.4 Without and with Filter for Open-Circuit Fault Operation

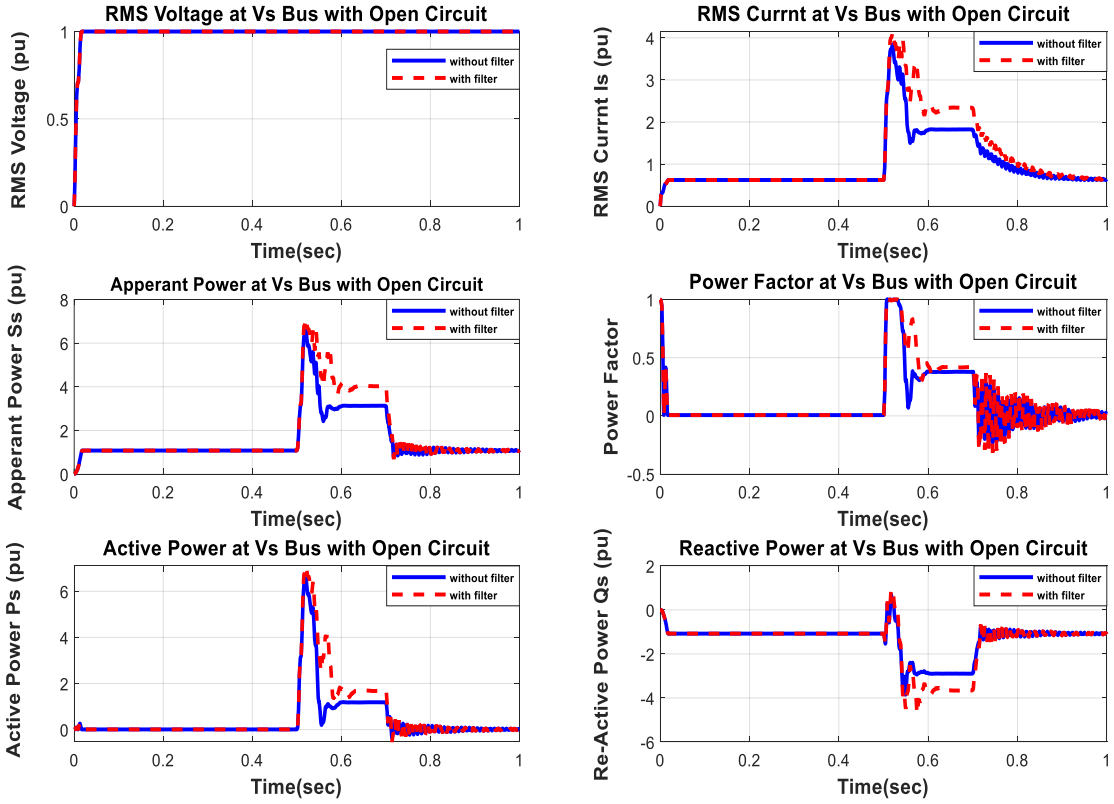

Figure 5.26 RMS V amd I & P, Q, S, and PF at Vs Bus under OC Fault with and without MFCC-HFC Compensator

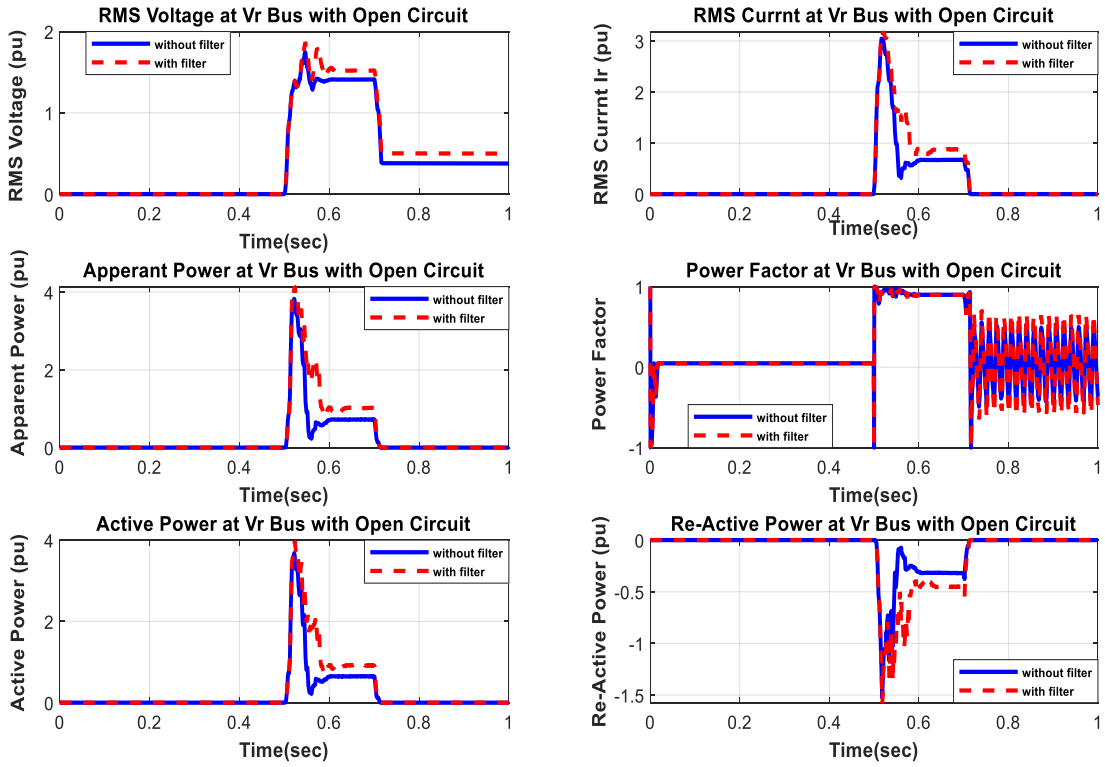

Figure 5.27 RMS V and I & P, Q, S and PF at Vr Bus under OC Fault with and without MFCC-HFC Compensator

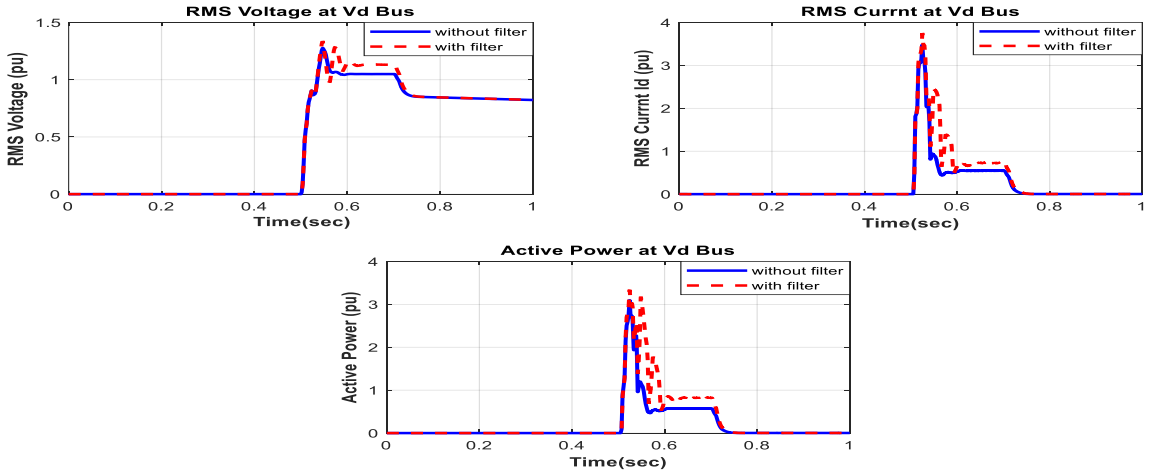

Figure 5.28 RMS V and I & P at Vd Bus under OC Fault with and without MFCC-HFC Compensator

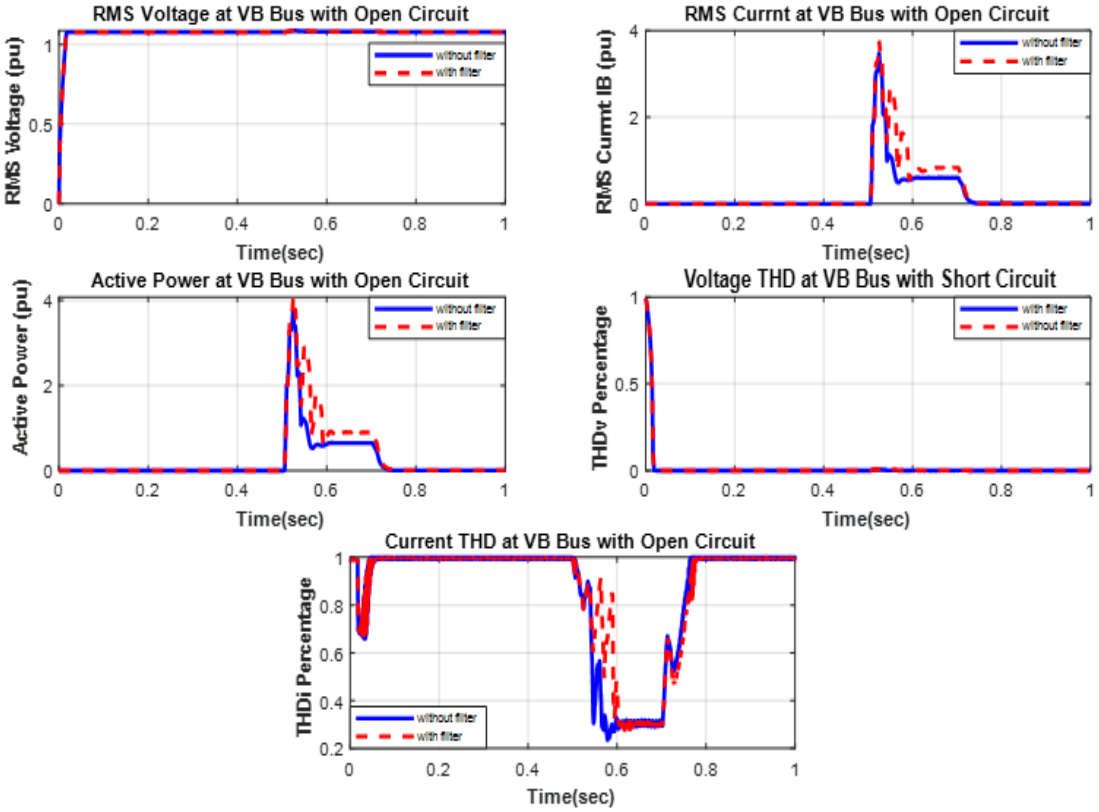

Figure 5.29 RMS V and I & P, THDv, and THDi at VB Bus under OC Fault with and without MFCC-HFC Compensator

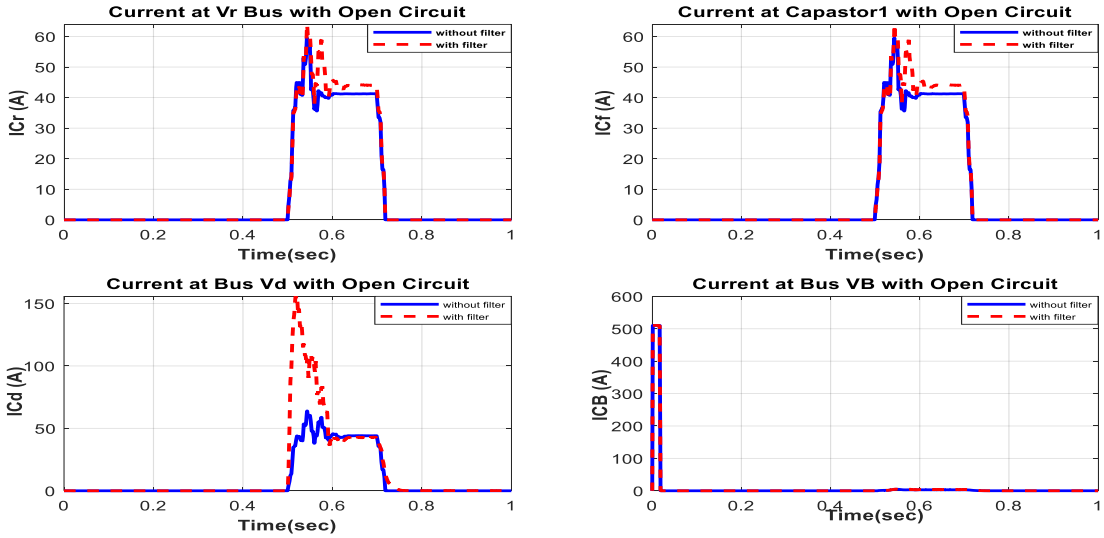

Figure 5.30 Currents ICr, ICf, ICd & ICB at VB Bus under OC Fault with and without MF-HFC Compensator

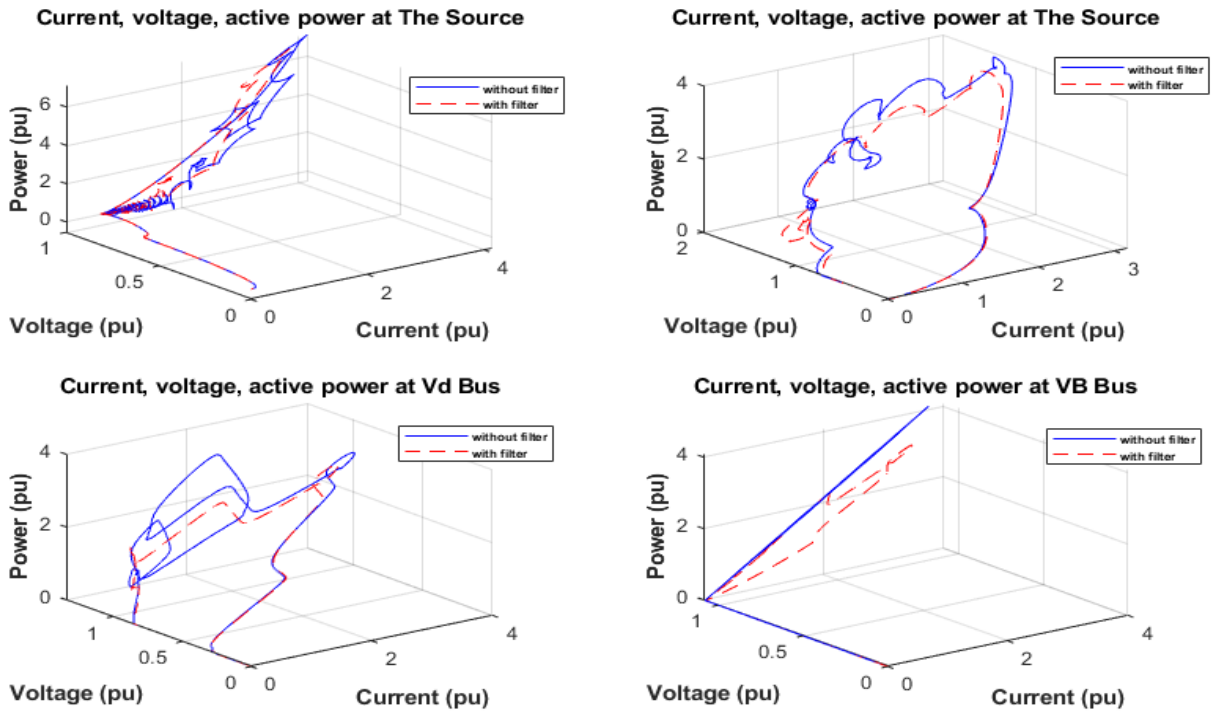

Figure 5.31 Current, Voltage & Active Power at Vs, Vr, Vd and VB Buses with and without MFCC-HFC Compensator

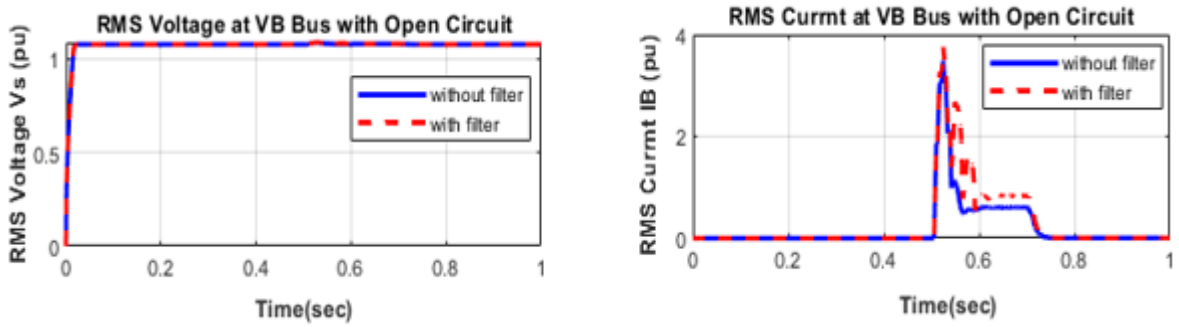

Figure 5.32 RMS (Current & Voltage) at VB Bus under OC Fault with and without MFCC-HFC Compensator

The MFCC-HFC scheme's effectiveness in V2G battery-charging systems at 50% SOC was tested for validation. The models were employed for a short-circuit condition case (100 ms of the AC grid) using a 1-second scale at the AC side for V_S and V_r buses. The simulation was tested for efficiency of energy use and dynamic stabilization, using the proposed control schemes as a

means to stabilize the smart grid in short-circuit fault operation changing conditions. The results indicate an improvement in the power factor as well as a reduction in the inrush currents under short-circuit conditions on the AC side (see Figures 5.26-5.29). For all buses, the power quality and dynamic response on both the DC and AC sides are enhanced and there is reduced fluctuation in the power factor during short circuit fault.

Figure 5.30 illustrates the short-circuit fault operation currents both with and without the MFCC-HFC scheme, while Figure 5.30 depicts a 3D schematic showing the SC of RMS voltage, current, and active power for the system buses with/without the proposed MFCC-HFC approach. In Figure 5.33, the image shows an enhanced RMS current and voltage stability (1.0 pu) on the V_B bus-charging scheme side. From the figures, it can be seen that evaluating power fluctuations prior to the introduction of the buck-boost converter reveals a significant increase in the stability level of the PID controller. Based on this finding, it is clear that the power input is effectively regulated by the PID controller, thereby providing a controlled and steady power level.

5.10 DC-DC Converter Interference Scheme

The chapter explored a simple DC-DC topology using pulse width modulation switching. Other complex topologies can be utilized in isolated and non-isolated transformer coupled stages. The fast-acting controller requires minimum DC-DC converter stages to reduce interface cost and switching losses. The modulated filter MFCC-SFC implemented a DC-DC converter pulse width duty cycle modulation, though it did not address the different complex versions of DC-DC converter interface topologies, including transformer coupled isolated and non-isolated buck-boost types. As validated via simulations, the simple DC-DC converter structure demonstrated comparability with fast-acting multi-loop, multi-regulator controllers, with minimal inrush current and transient over-voltages [158].

5.11 Conclusion and Future Work

This chapter presented a low-cost, modulated, AC-side filter compensation strategy intended for use with V2G stations. The scheme is easily controlled using a PID-optimized controller device. The novel MFCC-HFC was validated under different operating conditions, using 50% SOC for open- and short-circuit conditions and hybrid weighted battery-charging modes. The

results showed the effectiveness of the tuned arm filter and modulated/switched filter-capacitor compensator. The approach also showed, under testing, reduced rippling, and fast modulation when SPWM was applied.

The proposed novel modified/switched filter-capacitor compensation method was tested on energy storage for micro-AC-DC utilization grids, including virtual energy systems that use PV fuel cells and Lithium-ion battery storage systems. Additionally, the technique was simulated on static transformer-less voltage stabilization systems. The results clearly demonstrated not only the low cost and efficiency of the proposed technique, but also its enhanced AC power quality, reduced harmonics on the AC side, and AC-DC decoupling. The outcome of these improvements was a reduction in transient voltage excursions and inrush currents in the system's AC and DC interface buses. The novel inter-coupled AC-DC PWM-switched/modulated filter compensation scheme can be extended to new applications using micro DC-AC grids, including energy storage systems, virtual inertia machines, and dynamic static synchronous machines.

Chapter 6: An Efficient Shunt-Modulated AC Green Plug Switched Filter Compensation Scheme for Nonlinear Loads

1.1 Abstract

Nonlinear loads are a a crucial component of power system grids. However, they also pose an ongoing challenge due to harmonics injection. The present chapter tackles this issue with a novel modified green plug/switched filter compensation scheme using fuzzy logic controllers. This innovative scheme utilizes dual action pulse width modulation to ensure switching functions from harmonics reduction and capacitive compensation for inrush nonlinear type AC loads. The scheme's multi-loop regulations and online switching effectively handle dynamic-type slow-acting inrush, motorized, and other rectifier type-nonlinear loads, enhancing the power factor and power quality at source and load buses, and reducing total harmonics distortion at key source and sensitive nonlinear load buses.

A simulation model in the MATLAB/Simulink-2023b software environment demonstrates the efficiency of the proposed FACTS technique. The modulated dual-mode switched filter/capacitive compensation scheme controlled by a fuzzy logic controller ensures less harmonic distortion and improved voltage stabilization. The results show that voltage, current, active power, reactive power, power factor regulation, and effective energy utilization are achievable with the designed Flexible AC Transmission System – Modulated Filter Capacitor Compensation – Switched Filter Compensator (FACTS-MFCC-SFC). The switched modulated AC green plug filter significantly improves power quality and enhances the power factor in the case of inrush and nonlinear loads.

1.2 Introduction

Over the past two decades, power quality issues have become increasingly prevalent in electrical power transmission and distribution systems. More and more devices are being connected to microgrids, while at the same time modern distribution systems contribute to power quality issues, including harmonics distortions in the grids. Key sources of harmonics in modern distribution systems include motor drives, electric vehicle chargers, compact fluorescent lamps,

LEDs, and inverters utilized as interfaces for storage systems and Distributed Generation (DG) units [159]. Flexible Alternating Current Transmission Systems (FACTS) devices offer a viable solution to improve power quality by addressing various issues such as long- and short-duration voltage variations, voltage imbalance, waveform distortion, voltage fluctuation, and power frequency variations, primarily caused by loads connected to electric supply systems. Power outages, generator malfunctions, frequency control challenges, and unplanned prolonged blackouts are among the most commonly encountered issues. Modern automation and industries rely on sensors, microprocessors, relays, and other sophisticated electrical equipment. While these devices enable complex operations, they are highly sensitive to power quality. As a result, utilities, customers, and load device suppliers all face financial implications [160].

The advantageous point of the proposed scheme is its performance by adding the fuzzy logic control type-2 scheme that reduces harmonics and improves the power factor while also reducing transient over-voltage conditions with FACTS-MFCC-SFC [161]. Various capacitor banks, including fixed, switched, and modulated types, have been widely deployed in modern electrical systems to mitigate feeder active and reactive power losses and enhance the system response to events like faults, load switching, and short circuits [158]. Fixed power filters, known for their cost-effectiveness and simple structure, are commonly used in industrial networks to enhance power quality [162]. However, these fixed-parameter power filters and capacitor banks may have limited effectiveness for dynamic loads and can potentially lead to resonance issues in certain scenarios [163].

This chapter introduces an innovative AC switched filter compensation method employing dual-action pulse width modulation. The novel approach facilitates the switching functionality for both harmonics reduction and capacitive compensation and is particularly suitable for addressing inrush-type nonlinear AC loads. The novel multi-loop regulations and online switching mechanisms are designed to effectively mitigate the effects of dynamics and thus reduce the impact of inrush currents [164]. This compensation strategy aims to improve the power factor and power quality at source and load buses and reduce total harmonic distortion at critical source and sensitive nonlinear load buses.

Moreover, this chapter delves into type-2 fuzzy logic, an advancement from type-1 fuzzy logic, which addresses uncertainties in defining membership functions by introducing an

uncertainty zone between upper and lower membership functions. This enables each data point to possess two degrees of membership when mapped, using interval type-2 fuzzy sets managed by governing rules. However, direct defuzzification becomes impractical due to added encoded data, necessitating reduction techniques to simplify algorithm complexity [165]. We utilize the defuzzification process from type-1 fuzzy logic to generate crisp values, employing triangle membership functions in our study. Shifting to dynamic controllers, we explore their enhanced functionality with additional loops operating in an error-sequential manner.

Our research also investigates an innovative tri-loop regulation setup at the common source bus, strategically addressing changes in voltage and current. Leveraging a modulated filter capacitive compensator and a fast PWM-modulated switching system, we effectively reduce voltage transients and minimize inrush current ripple, addressing various scenarios arising from load-switching and short-term faults [166]. The fuzzy logic controller is flexible, as it can deal with hidden nonlinearities in the loads and other inrush transient load behaviors. The flexibility is boosted by fast response and tolerance to hidden nonlinear load dynamics [167].

In addition, the chapter presents a novel low-cost FACTS-MFCC-SFC device that will improve system performance. The proposed device is validated in a MATLAB-Simulink-2023b software environment using a type-2 FLC controller for voltage stabilization and power delivery to the load. This FACTS-MFCC-SFC device employs switches for implementing dynamic error-driven control strategies, thereby achieving improved response. The chapter also compares the operational quality both with and without the MFCC-FACTS device and tests for harmonic reduction, power quality, and improvements in the power factor correction.

1.3 Literature Review

Chao et al. [168] delved into the limitations of passive filters in LCC-HVDC projects, particularly regarding harmonic filtering and system impedance dependence. They introduced Hybrid Active Power Filters (HAPF) as a versatile solution offering high controllability and effective compensation for various harmonics, flicker suppression, and reactive power compensation. Unlike passive filters, HAPF's characteristics remain stable regardless of system impedance, mitigating resonance risks. The adaptive function enables automatic harmonics tracking and compensation, as evidenced by its successful application in the Fujian Guangdong

DC interconnection project, indicating its suitability for high-voltage environments and future DC projects [168]. In a different vein, Wang et al. presented a TPMP Si & SIC hybrid inverter coupled with a specialized compensating current modulation strategy. This approach effectively addressed large low-frequency harmonic currents, showcasing high efficiency and comparable performance to all SIC-MOSFET inverters. The proposed hybrid inverter offered cost savings and compact filter volumes, validated by simulation results [169].

Furthermore, Catata et al. [170] explored the presence of stroke components in the electrical grid and proposed in-line adaptive filters for DC-link voltage control loops. These filters aimed to mitigate stroke frequency components from Synchronous Reluctance Generators (SRG), reducing distortion in grid current waveforms. Experimental results demonstrated the effectiveness of these adaptive filters in adapting to SRG stroke frequencies and minimizing distortion, particularly when integrated with voltage compensators [170]. Similarly, Singh et al. [171] addressed harmonic currents generated by nonlinear loads and evaluated the performance of a Shunt Active Power Filter (SAPF) in power distribution systems using MATLAB/Simulink. They implemented SAPF with a combination of hysteresis current control (HCC) and Pulse Width Modulation (PWM) Generator, effectively maintaining total harmonic distortion (THD) of supply currents below specified limits [171].

Meanwhile, Lima et al. [172] proposed an adaptation to existing switching rule design methods to address time-varying nonlinearities in Shunt Active Power Filters (APF). This modification aimed to improve harmonics compensation and power factor correction when dealing with nonlinear loads, outlining future research directions for extending the approach to three-phase systems and minimizing sensor information requirements [172]. Working in the same field, Lin et al. [173] tackled limitations in traditional high-power APFs using IGBT by proposing a novel approach employing Proportional-Integral (PI) and repetitive control with shorter sampling times. Simulation results demonstrated improved harmonic compensation with higher switching frequencies, ensuring accurate compensation even for high-order harmonics and dynamic load changes [173].

Daftary et al. [174] focused on modeling and simulating hybrid active power filters to reduce the kVA rating of shunt active power filters, leading to improved power quality and reduced VA rating. Their findings suggested the potential of hybrid power filters to enhance power quality

in grid systems [174]. Finally, Nolasco et al. [175] introduced an automatic power quality diagnosis method based on the online estimation of voltage and current total harmonic distortions indices. This method utilized a fuzzy system to assess the impact of harmonic distortions on power quality, providing linguistic and quantitative diagnoses without requiring external expertise [175].

1.4 System Description

A single-line diagram of an AC system study of a three-phase AC system supplying loads is shown in Figure 6.1. Figure 1.4 shows the FACTS-MFCC-SFC scheme of the AC three-phase system grid network. It uses MATLAB/Simulink software to illustrate the novel dynamic error-driven tri-loop FLC applied to lower switching transients, current inrush excursions, as well as in the low voltage utilization system. The aim is to improve power/energy utilization and power quality for the load-type depicted in [56].

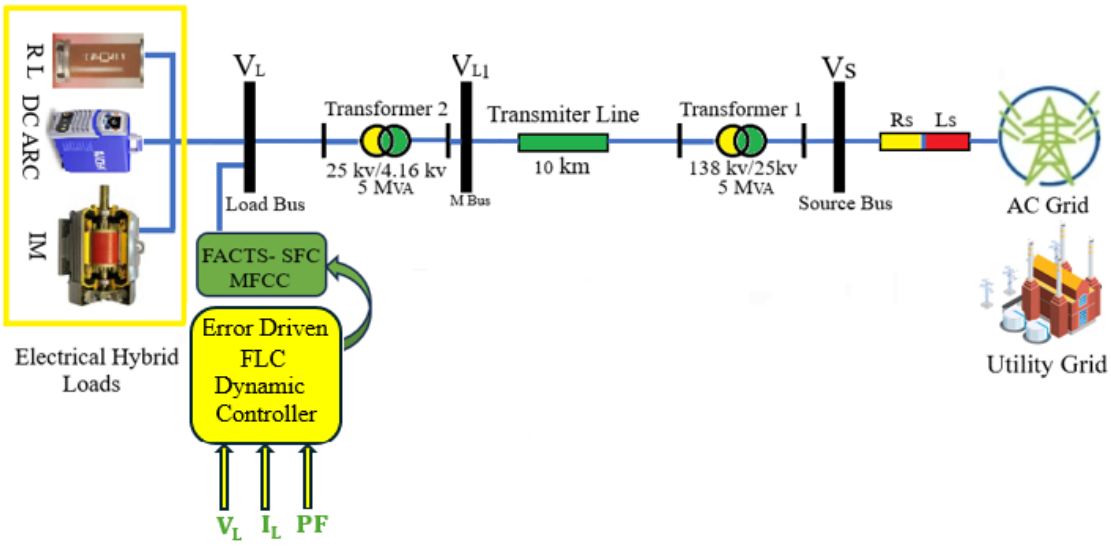

Figure 6.1 AC Grid System with Hybrid Loads and Interface Hybrid FACTS-Switched Filter

The single-line diagram study of a three-phase AC system consists of a synchronous generator (driven by the source) that delivers the power to a local hybrid load (linear, DC ARC, or induction motor load) and is connected to an infinite bus through a 10 km transmission line. The main components of the AC system are:

- Three-phase AC Grid Source.
- Rs Ls are source resistor and indictor.
- DC ARC Load.
- IM is induction motor Load.
- Novel modulated filter-capacitor compensator MFCC-SFC filter scheme.
- Novel dynamic error-driven tri-loop type-2 FLC.
- Three different electrical hybrid nonlinear loads.
- Transformers for voltage change from 138 kv to 25kv and then 25kv to 4.16 kv.

The best way to ensure high efficiency is to minimize active power loss during the power transmission process. Active power loss reduction strategies with power factor regulation efforts can lead to a more efficient power transmission system [39]. At the same time, regulating the power factor is crucial during power transmission, as it contributes substantially to transmission efficiency [78]. Minimizing losses and maintaining reliability play a crucial role in providing end-consumers a stable and cost-effective electricity supply while also contributing to sustainable energy practices [176].

The power obtained at the receiving end of a transmission line is generally less than the sending end power due to active power losses in the line resistance. The ratio of the receiving end power to the sending end power of a transmission line is known as the transmission efficiency of the line, as shown in Equation 6.1.

$$\% \text{ T. E., } \eta_T = \frac{\text{Receiving end power}}{\text{Sending end power}} \text{ X } 100 \tag{6.1}$$

$$= \frac{V_R I_R \cos\phi_R}{V_S I_S \cos\phi_S} \text{ X } 100 \tag{6.2}$$

where:

V_R, I_R are the receiving end voltage and current.

$cos\phi_R$ is the receiving end power factor (lagging).

V_S, I_S are the sending end voltage and current.

$cos\phi_S$ is the sending end power factor.

1.5 FACTS-MFCC-SFC Scheme

The proposed low-cost FACTS-MFCC-SFC dynamic voltage stabilization device is a member of the switched capacitor compensator and modulated switching/modulated power filter family [125]. Using a double-switched shunt capacitor bank and two shunt-linked fixed capacitors for the proposed FACTS-MFCC-SFC minimizes the overall harmonics distortion and improves the power quality and power factor. Moreover, the system's ground is linked to a tuned arm filter to improve the overall performance. The FACTS-MFCC-SFC device has two modes of operation: a capacitive compensation mode and a tuned arm filter mode that utilizes the controlled IGPT switches S1 and S2, as shown in Figure 6.2.

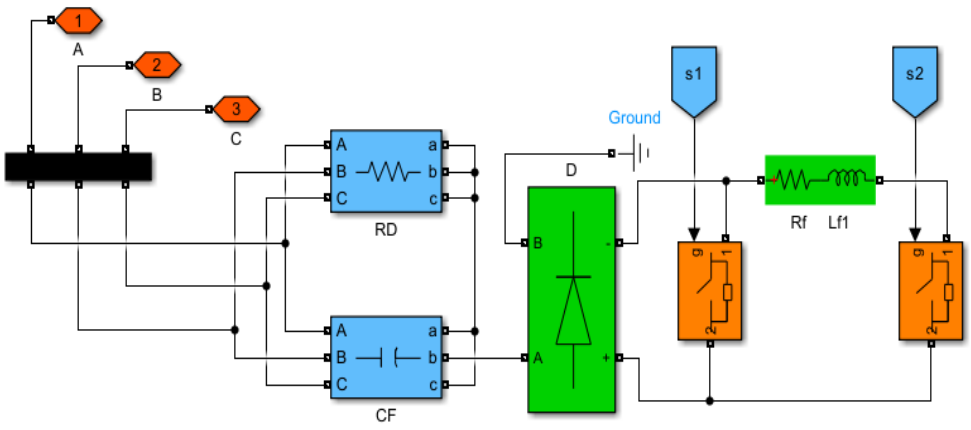

Figure 6.2 MFCC-SFC Device

The MFCC filter acts as a modulated admittance and point of connection, usually near nonlinear loads. The duty cycle ratio is adjusted online using the multi-regulation total error to ensure dynamic matching to fast and slow-acting nonlinear variations. The dual function of the tuned arm filter is complemented by the adjusted capacitive compensation level for nonlinear reactive loads, motorized inrush loads, and cyclical load.

1.6 Type-2 Fuzzy Logic Controller

The fuzzy logic controller is flexible, which enables it to easily deal with hidden nonlinearities in the loads and other inrush transient load behaviors. The flexibility is boosted by fast response and tolerance to hidden nonlinear load dynamics [166]. The purpose of type-2 fuzzy logic, which is an expanded form of type-1 fuzzy logic, is to capture the ambiguities involved in defining type-1 fuzzy membership functions.

To perform this task, a footprint of uncertainty is introduced in the type-1 fuzzy sets between the upper and lower fuzzy membership functions. Consequently, when mapping real-world data using interval type-2 fuzzy sets, any such data will now have two degrees of membership [120]. The fuzzified lower and upper membership levels function according to rules, and each rule is assessed sequentially. Since there is an additional encoded data, defuzzification cannot be accomplished directly. As a result, a particular kind of reduction technique is presented to lessen the algorithm's complexity.

There are many other kinds of reduction algorithms, such as the Karnik-Mendel technique. However, as this and similar techniques are highly complex, we propose a computationally less expensive approach. The same defuzzification process used for type-1 fuzzy logic is used to generate crisp value following this kind of reduction. In our study, we have represented upper and lower fuzzy sets using triangle membership functions, as shown in Figures 1.6 and 6.5 [177], [178]. The main loops are used to monitor errors in the voltage or current of the bus, and the controller's time-delay and scaling parameters are chosen using offline guided trial and error.

Using the innovative tri-loop regulation set-up at the common source bus, it is possible to mitigate any inrush, dynamic, sudden excursion changes that may appear in the bus voltage and current. At the same time, loop decoupling in a dominant voltage stabilization loop is guaranteed by loop-weighing factors. This methodology ensures a prompt reaction and minimal errors [107]. Furthermore, using a modulated filter capacitive compensator, this method takes advantage of optimal switching based on system requirements. A fast PWM-modulated switching system consisting of a dynamic multi-regulation time-descaled error-driven controller is used for the green plug filter [179]. This design provides lower damped voltage transients, reduced inrush current ripple content, and dynamic interface bus voltage regulation by alternating between static

capacitive compensation and the tuned arm filter. These situations can result from load-switching, fluctuations in the wind pattern, self-excited capacitor banks within the system, and/or short-term in the SC and OC faults.

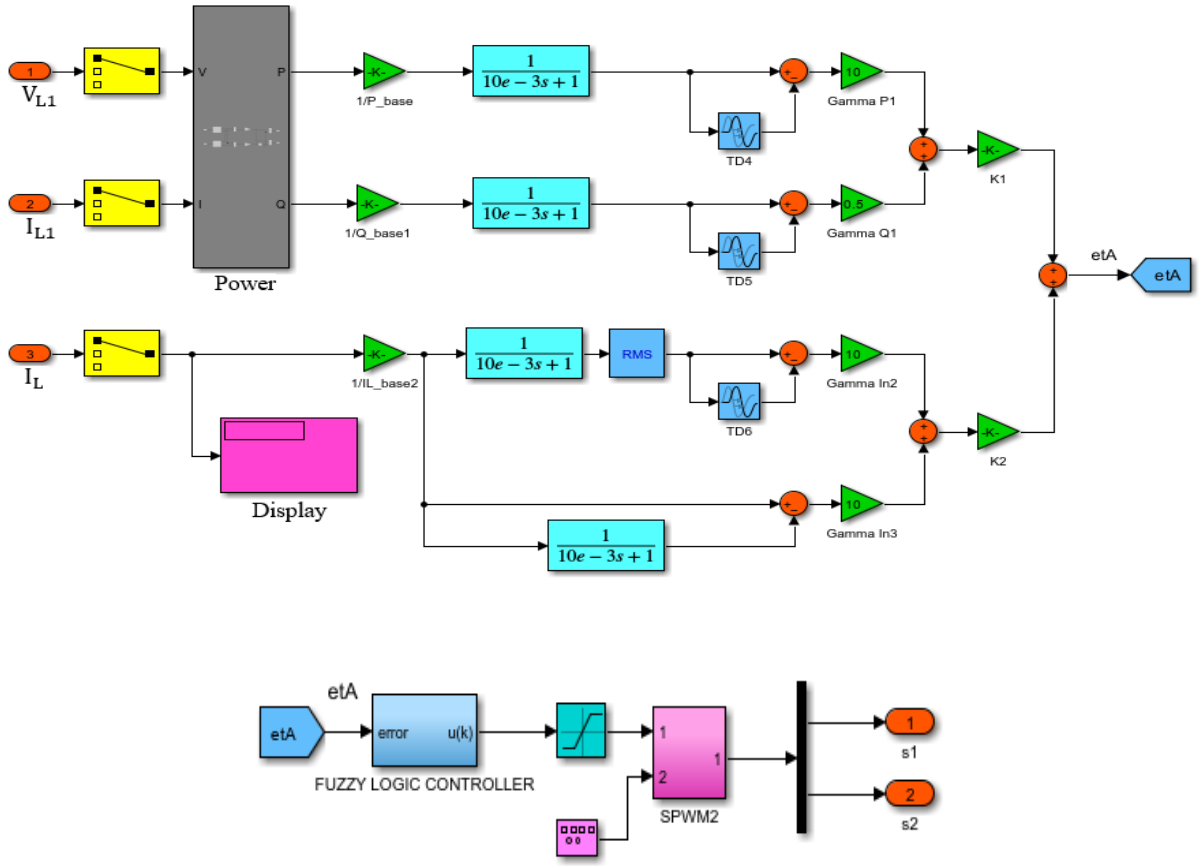

Figure 6.3 Dynamic Tri-Loop Tri-Regulation Controller for the AC SFC Filter Compensator

In the simulation, dynamic controllers with extra loops are activated in an error-sequential method. The dynamic quad-loop controller is made up of two main loops and two sub-loops, as shown in Figure 6.1. The inputs and/or outputs of the interval type-2 FLC are represented by interval type-2 fuzzy sets [152], [180]. Real-time robot FLC design is made possible using interval type-2 FLC, which simplifies the calculations compared to general type-2 FLC, which is computationally demanding [181]. The structure of an interval type-2 FLC and the fuzzifier, inference engine, rules-based, type-reducer and a de-fuzzifier are shown in Figure 1.6.

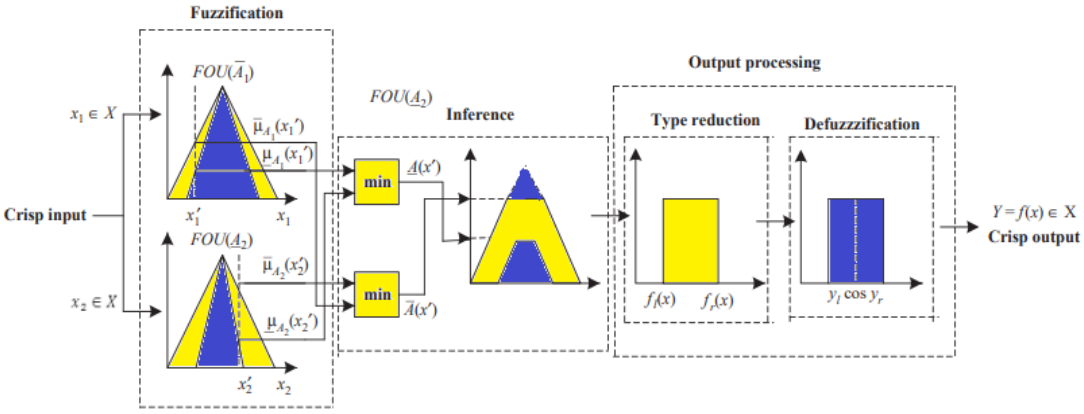

Figure 6.4 Structure Flow of Interval Type-2 Fuzzy System

The inputs for type-2 fuzzy sets are created by fuzzifying the crisp inputs from the input sensors. Since singleton fuzzification is easy to apply and works well with embedded processors and real-time applications, it is typically employed in interval type-2 FLC applications [182]. The inference engine and the rule base are illustrated in Figure 6.5:

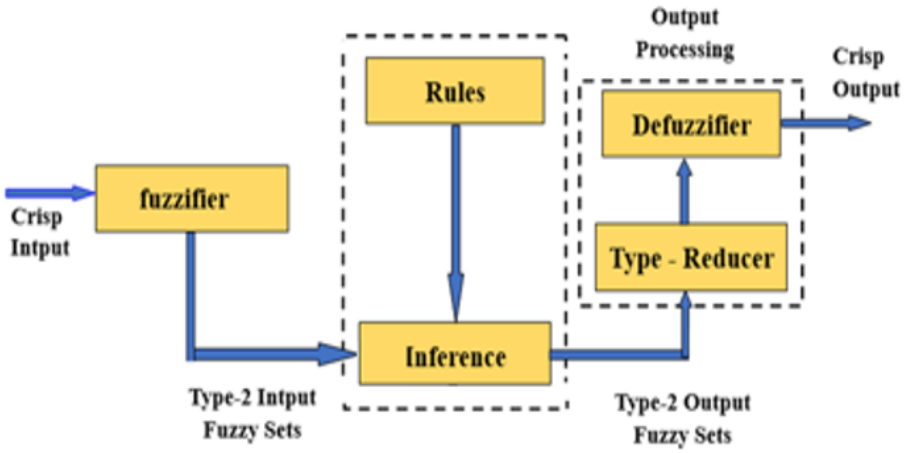

Figure 6.5 Type-2 Fuzzy Information Processing

Fuzzy Logic is classified into classical fuzzy logic or modified fuzzy logic including type-2 fuzzy logic and multistage fuzzy logic controller. Type-2 and multistage fuzzy logic controller are more effective for uncertain dynamic system and unknow model parameters.

1.7 Simulation Results and Discussion

Figure 6.6 shows the sample research AC system along with various supplementary FACTS-MFCC. It is connected to the infinite bus 138KV, substation bus through the 10 km feeder and consists of a local hybrid load, which includes linear, nonlinear, and induction motor type loads. Appendices A and B show the unified AC system, FACTS-MFCC, and the dynamic control parameters, respectively.

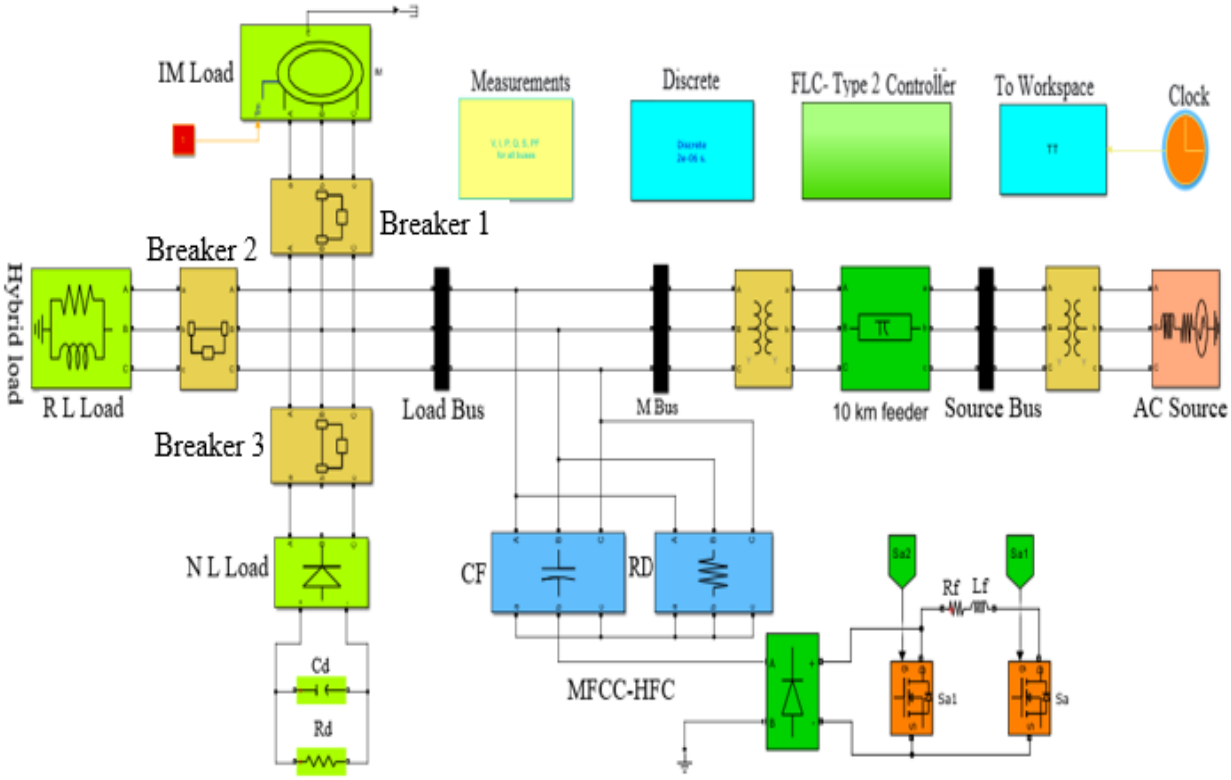

Figure 6.6 Radial AC Study System with FACTS-MFCC at Load Bus

6.7-1 V, I, P, Q and PF at Source Bus with Short-Circuit Operation

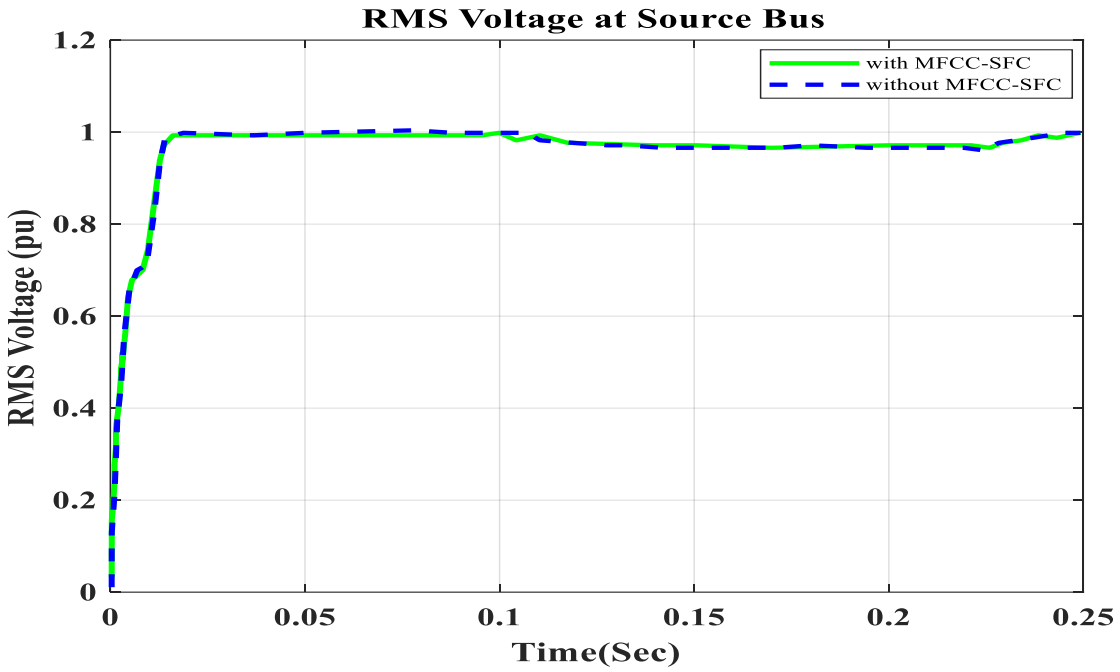

A. RMS Voltage Waveform

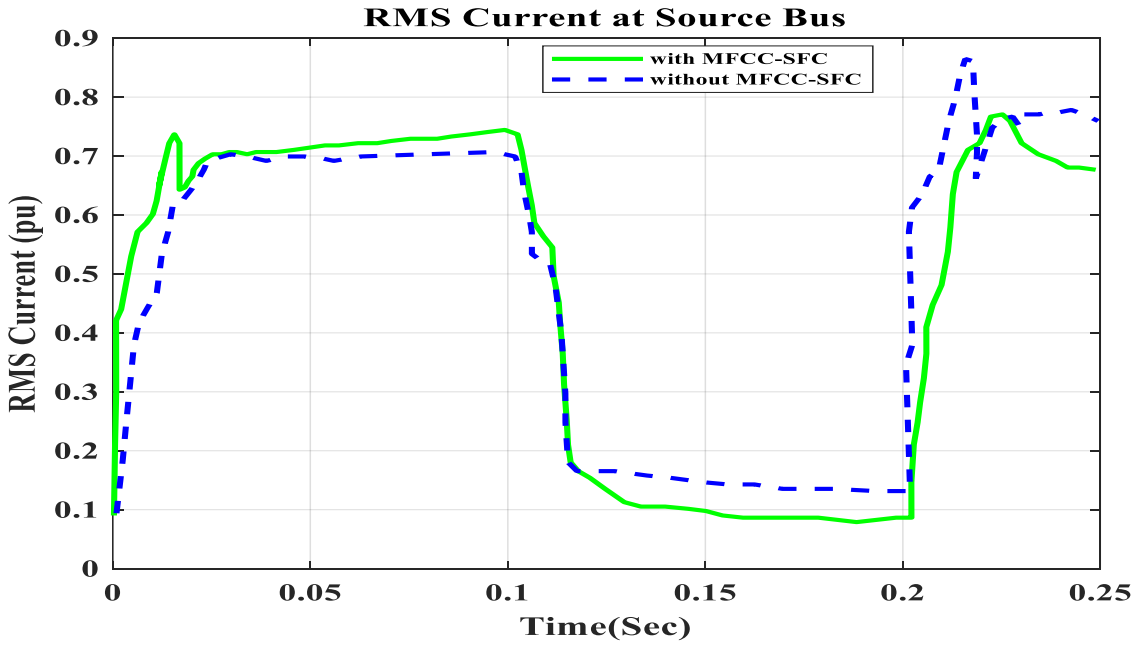

B. RMS Current Waveform

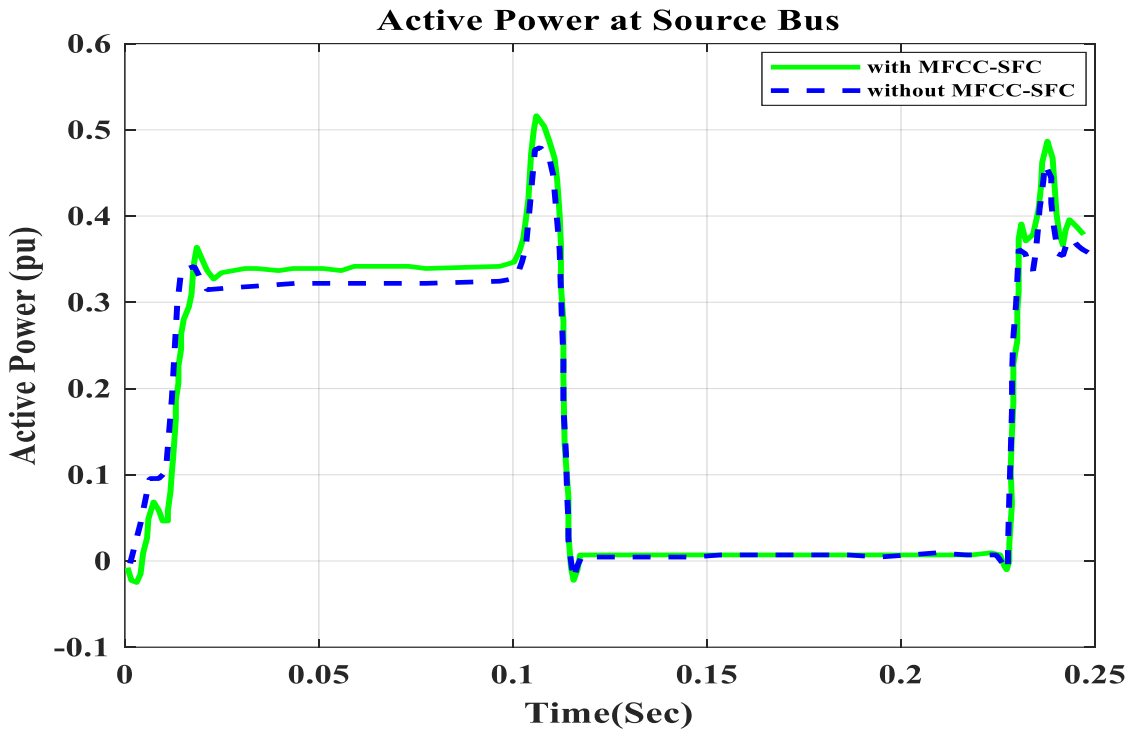

C. Active Power Waveform

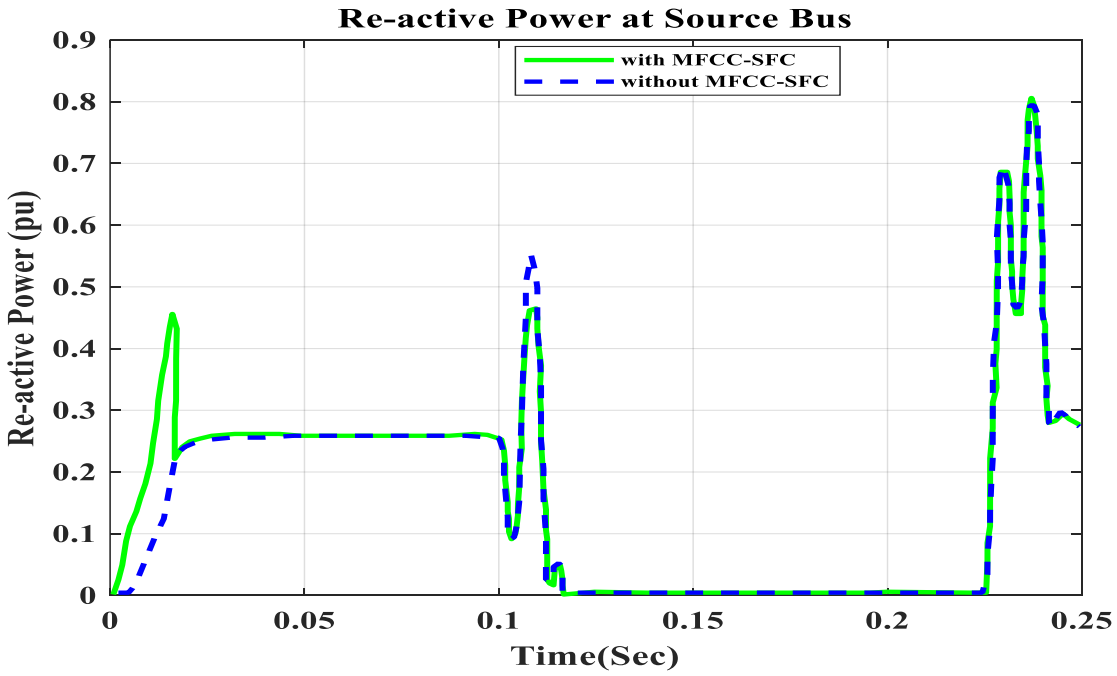

D. Reactive Power Waveform

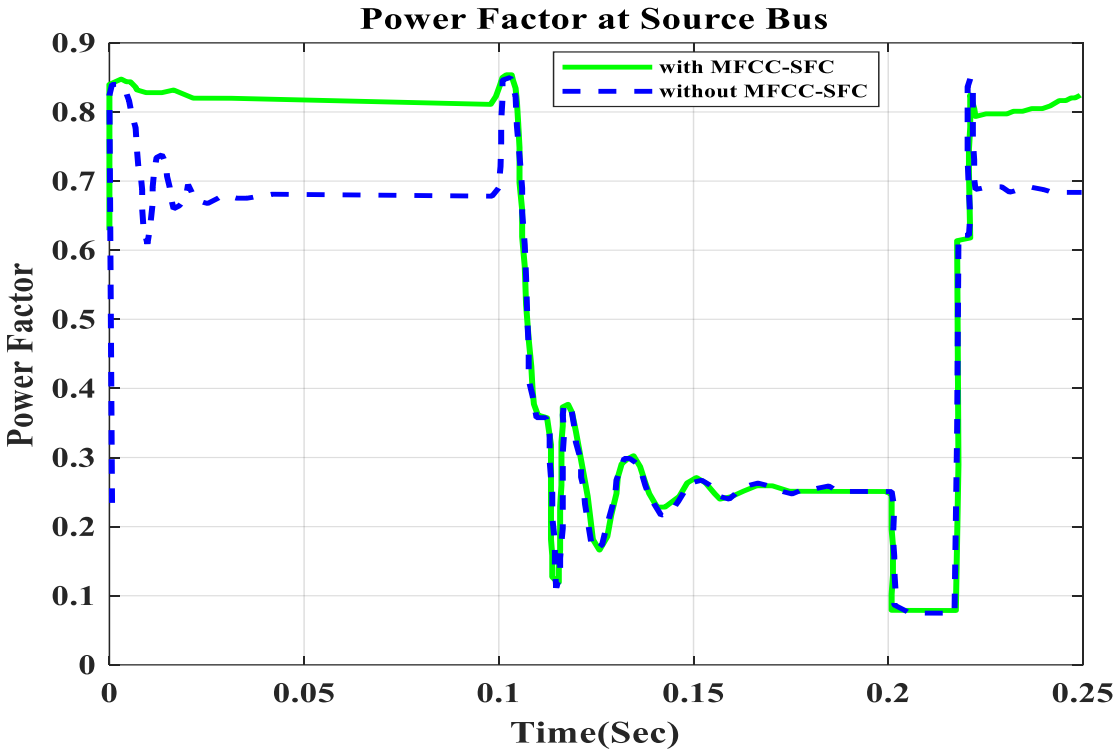

E. Power Factor Waveform

Figure 6.7 V, I, P, Q, and PF at Source Bus with Short-Circuit Duration of 100 to 200 ms. A) RMS Voltage Waveform. B) RMS Current Waveform. C) Active Power Waveform. D) Reactive Power Waveform. E) Power Factor Waveform at Source Bus.

6.7-2 V, I, P, Q, and PF at Load Bus with Short-Circuit Operation

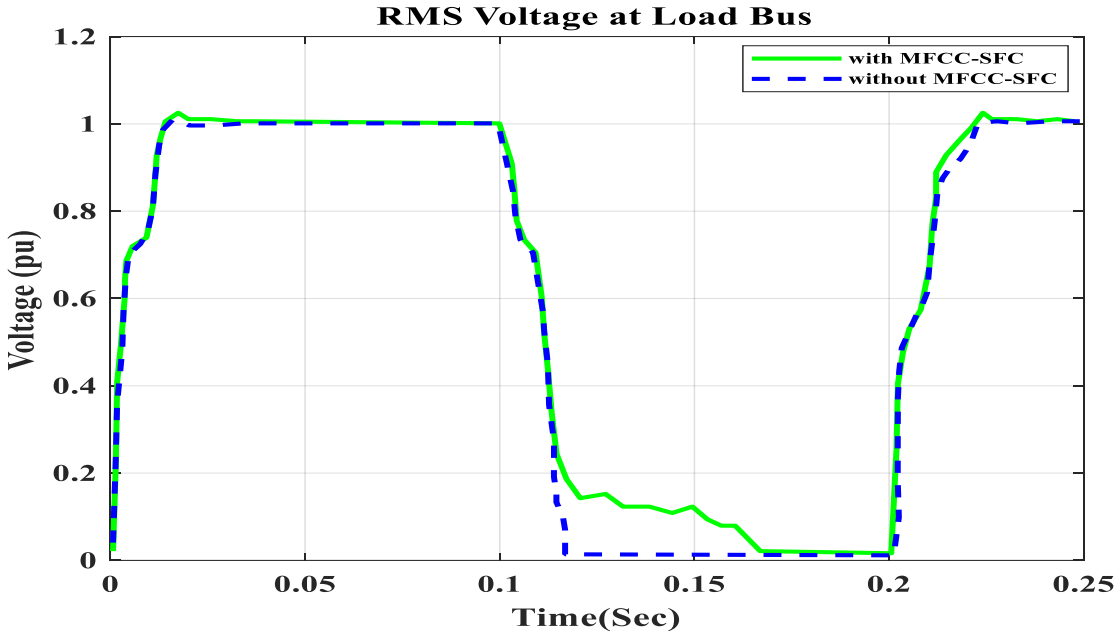

A. RMS Voltage Waveform

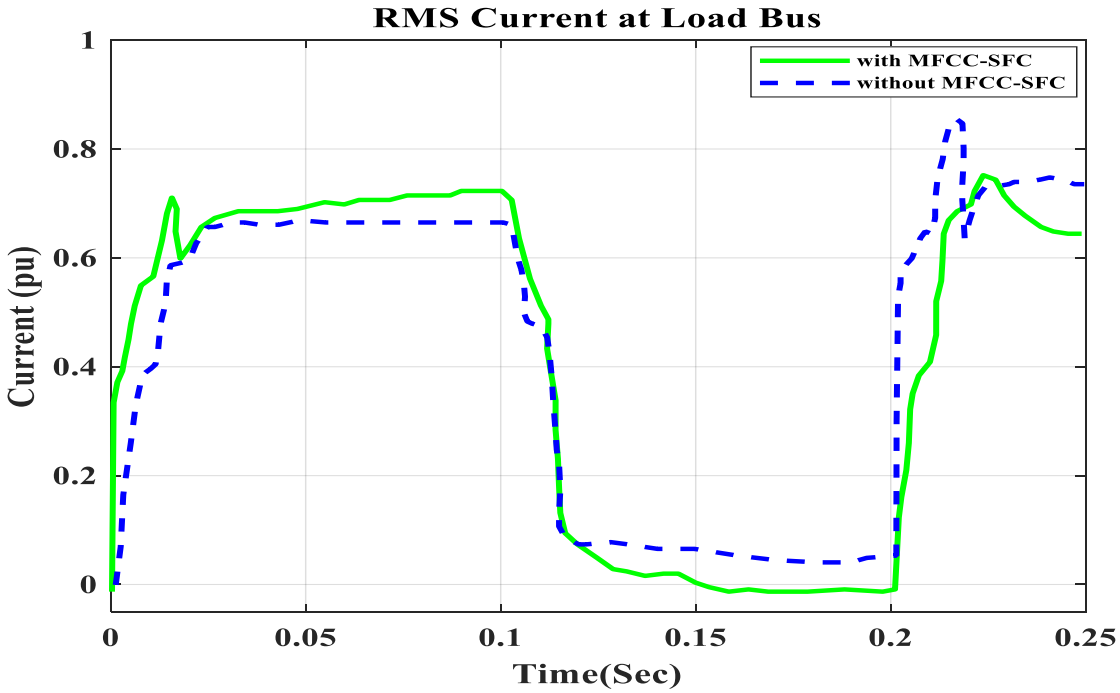

B. RMS Current Waveform

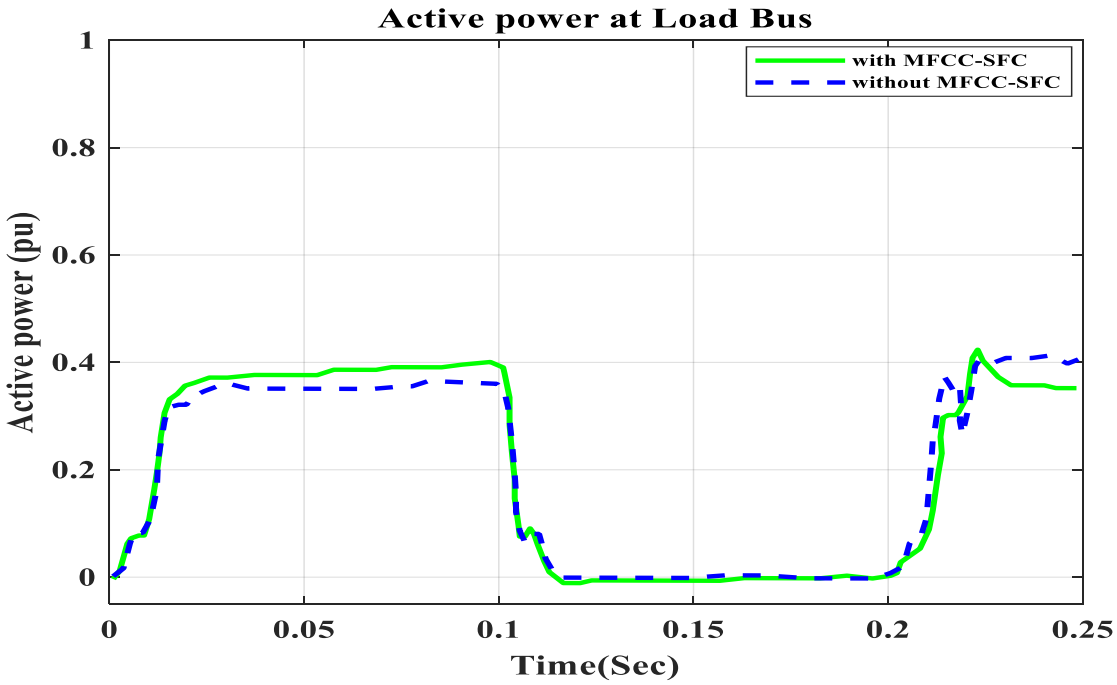

C. Active Power Waveform

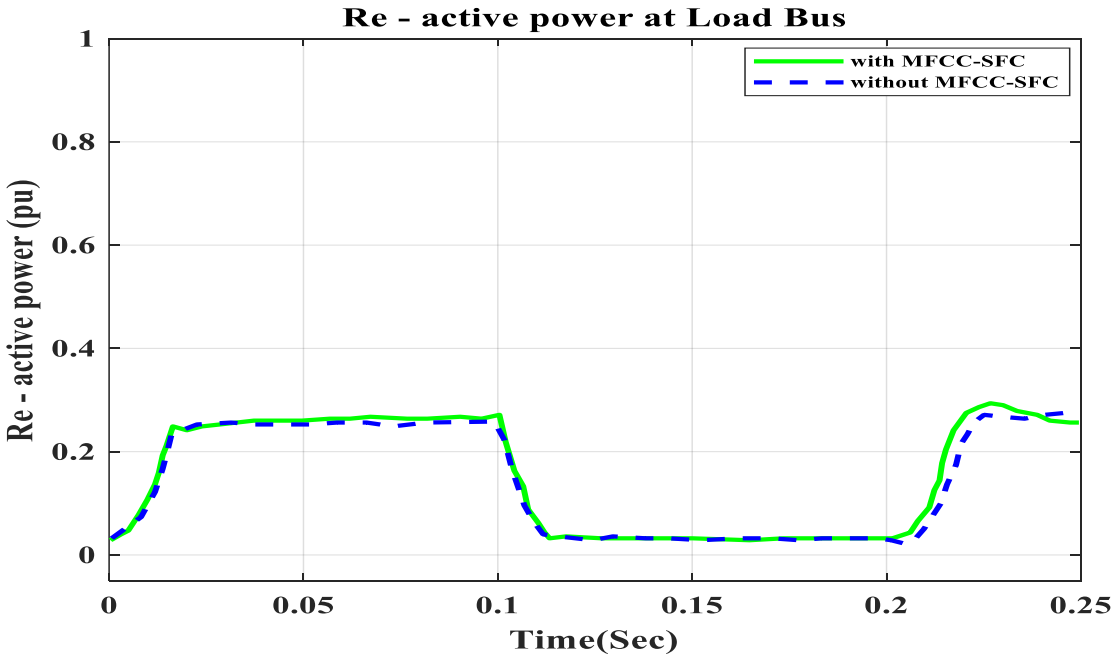

D. Reactive Power Waveform

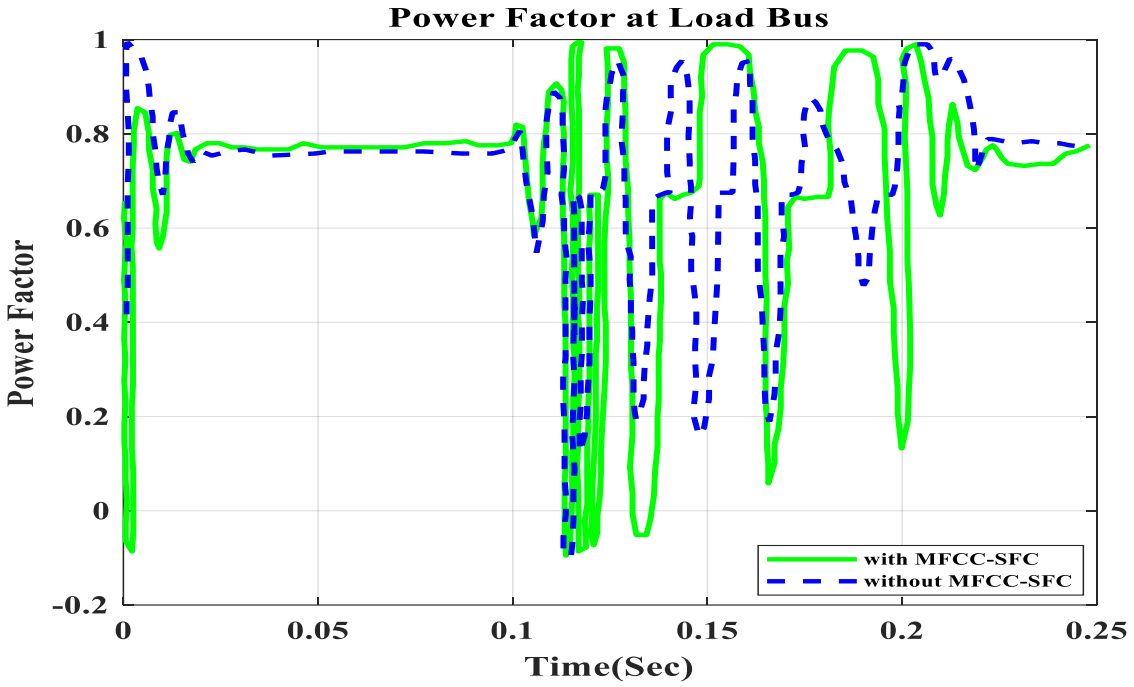

E. Power Factor Waveform

Figure 6.8 V, I, P, Q, and PF at Load Bus with Short-Circuit Duration of 100 to 200 ms. A) RMS Voltage Waveform. B) RMS Current Waveform. C) Active Power Waveform. D) Reactive Power Waveform. E) Power Factor Waveform at Load Bus.

Table 6.1: Voltage, Current, Active Power, and Power Factor Values at Source and Load Buses without and with MFCC Device under SC

Buses	Source Bus, Vs (pu)				Load Bus, V_L (pu)			
	V	I	P	PF	V	I	P	PF
Without MFCC	1.0	0.7	0.46	0.68	1.0	0.65	0.35	0.75
With MFCC	1.01	0.75	0.52	0.82	1.05	0.7	0.3	0.79
Improvement	0.01	0.05	0.06	0.14	0.05	0.05	0.05	0.04
% Improvement	1%	5%	6%	14%	5%	5%	5%	4%

6.7-3 V, I, P, Q, and PF at Source Bus with Open-Circuit Operation

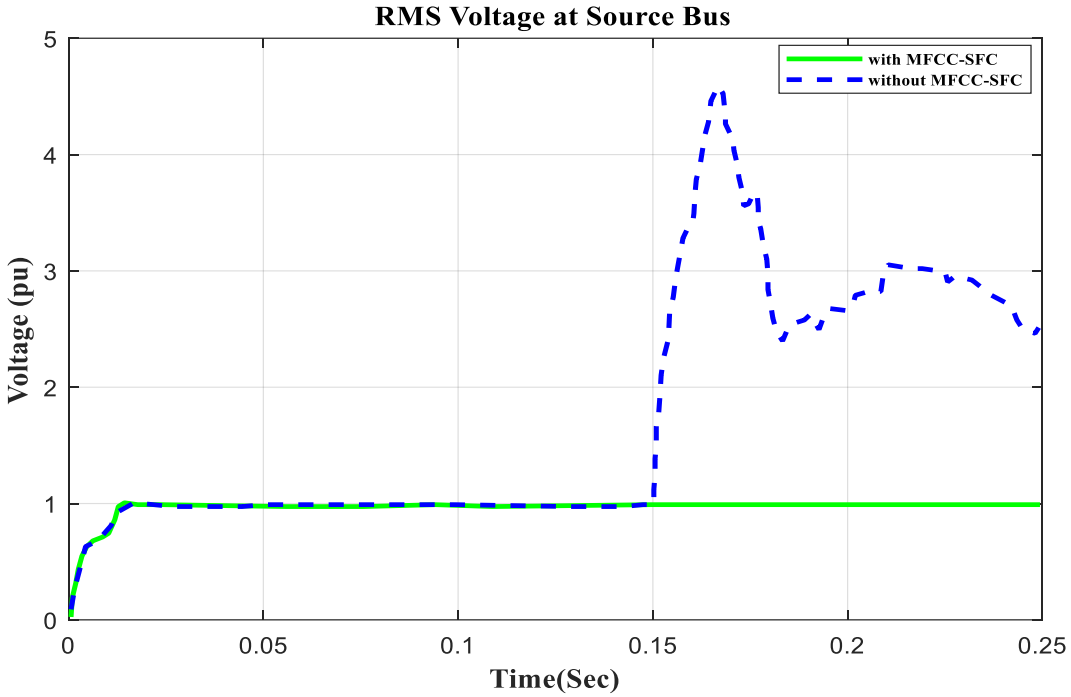

A. RMS Voltage Waveform

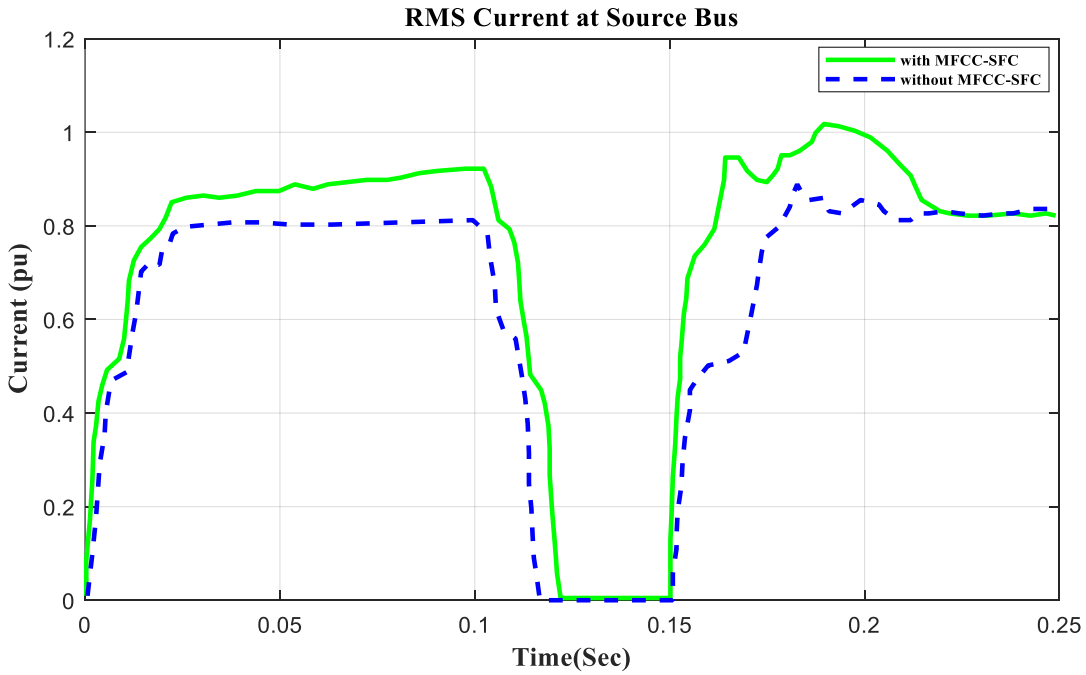

B. RMS Current Waveform

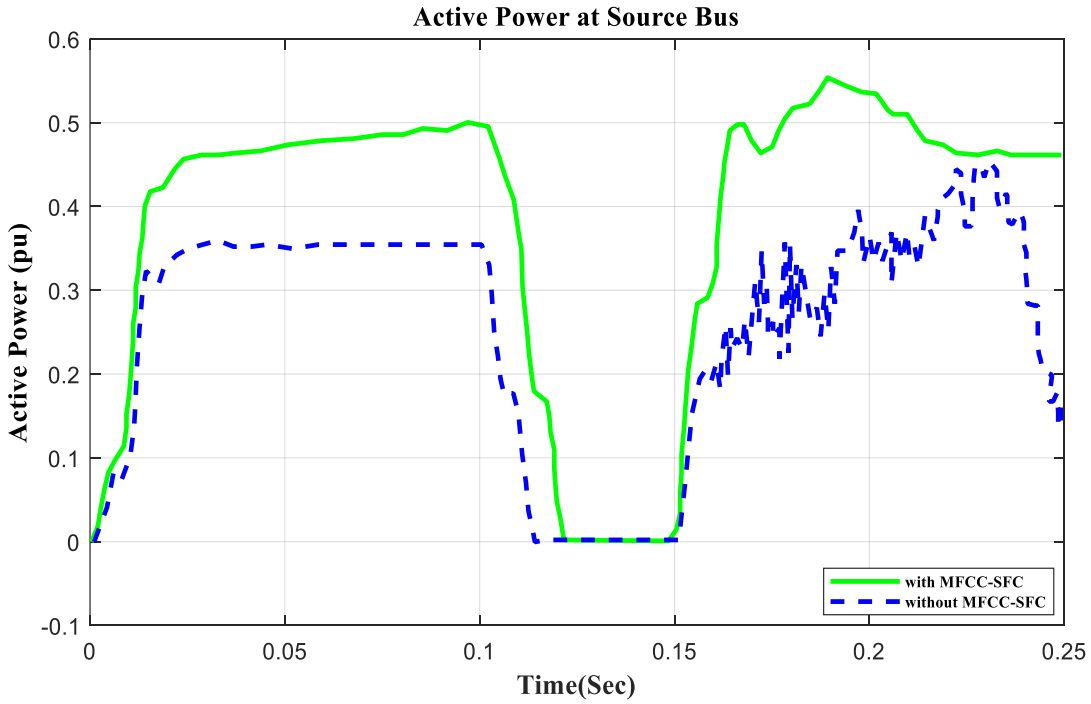

C. Active Power Waveform

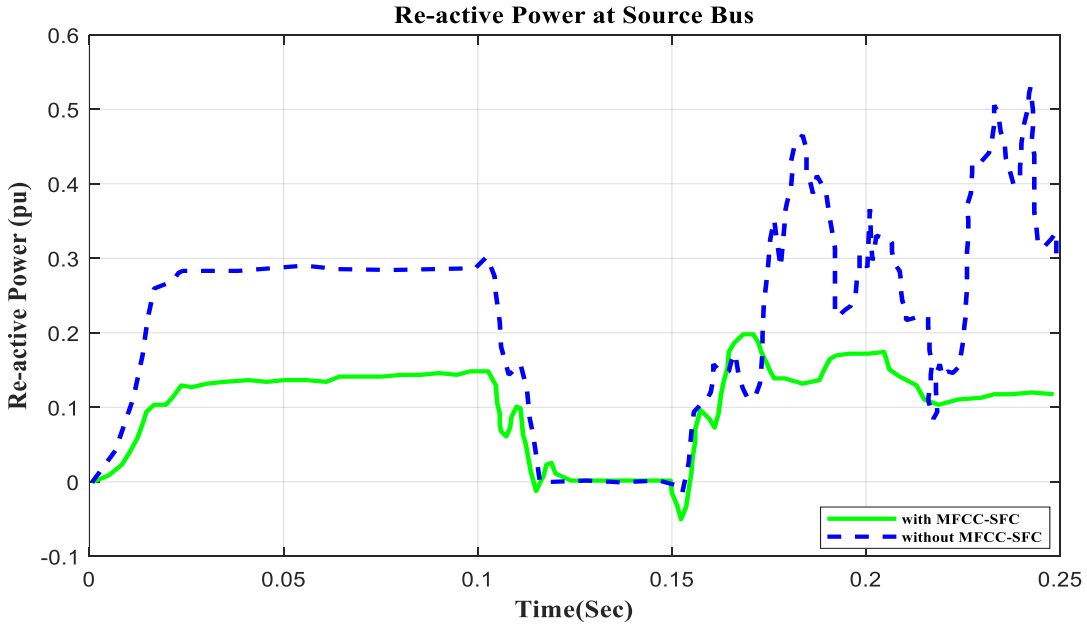

D. Reactive Power Waveform

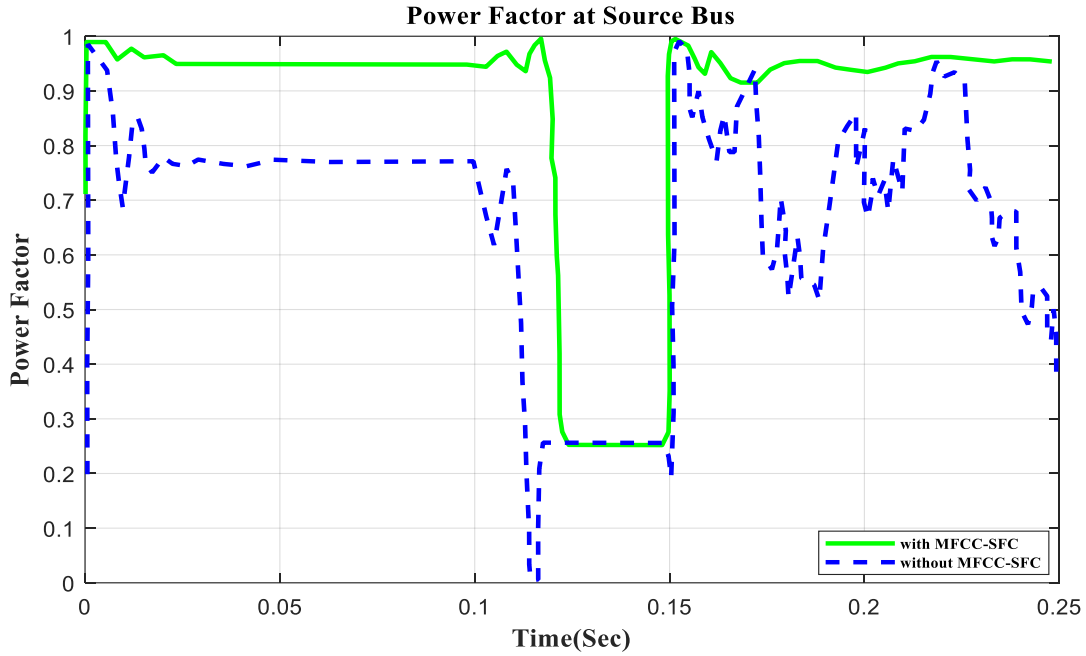

E. Power Factor Waveform

Figure 6.9 V, I, P, Q, and PF at Source Bus with Open-Circuit Duration of 100 to 150 ms. A) RMS Voltage Waveform. B) RMS Current Waveform. C) Active Power Waveform. D) Reactive Power Waveform. and E) Power Factor Waveform at Source Bus.

6.7-4 V, I, P, Q, and PF at Load Bus with Open-Circuit Operation

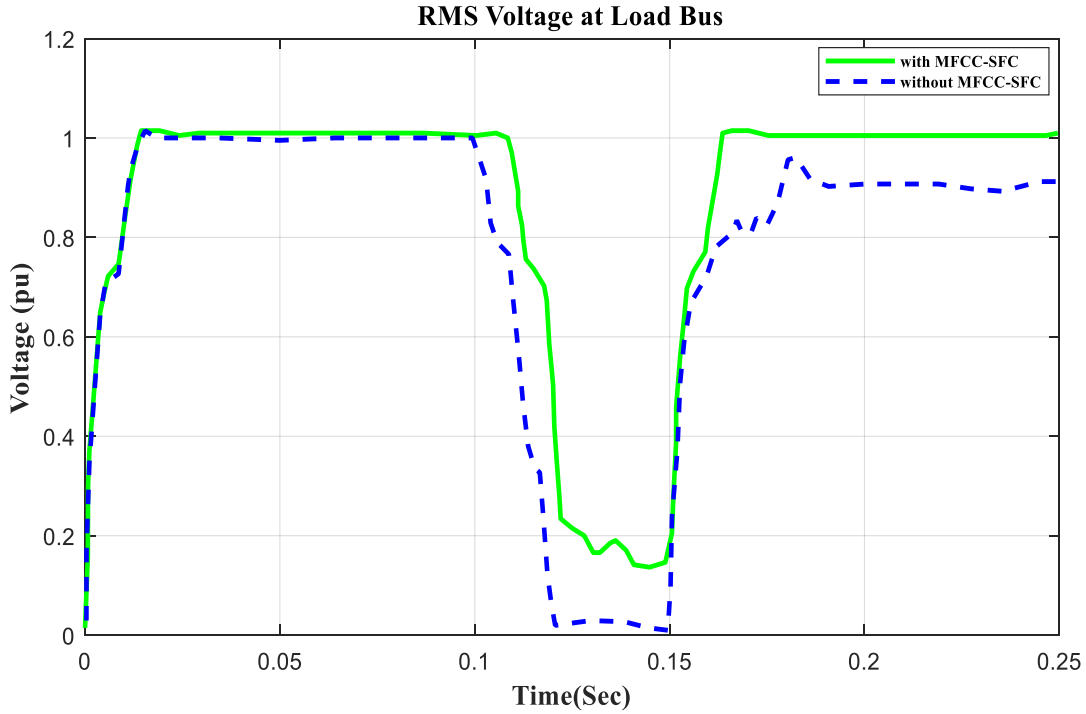

A. RMS Voltage Waveform

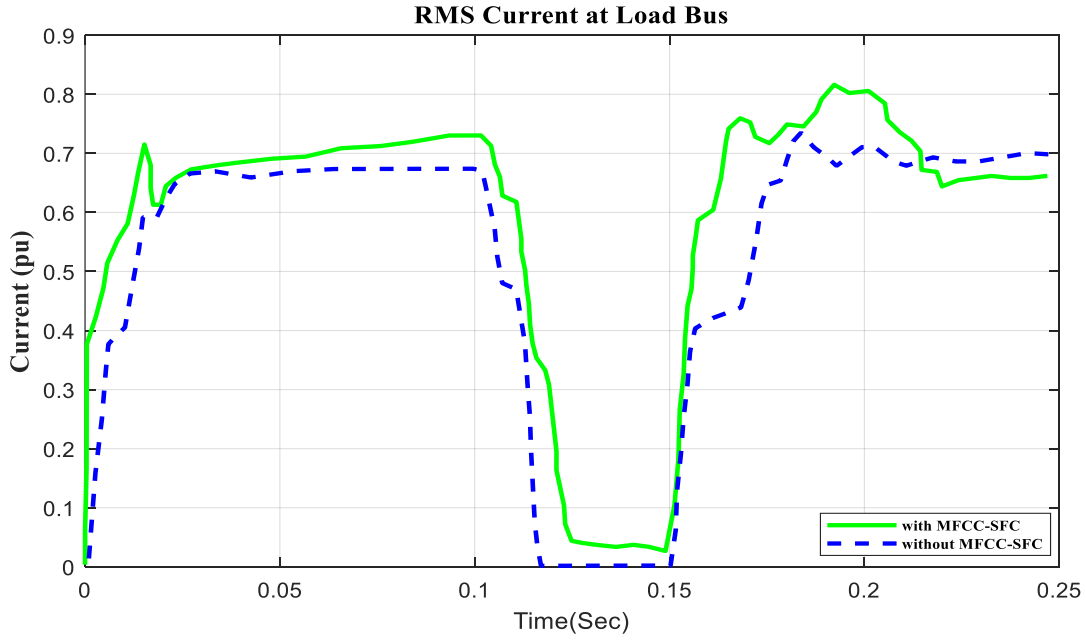

B. RMS Current Waveform

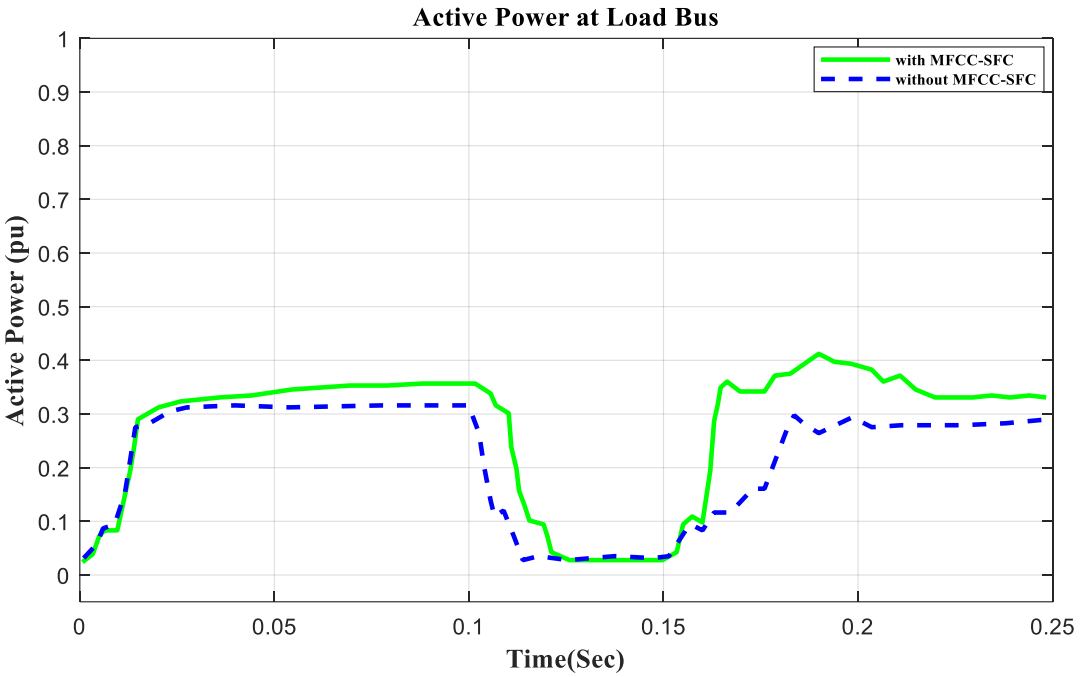

C. Active Power Waveform

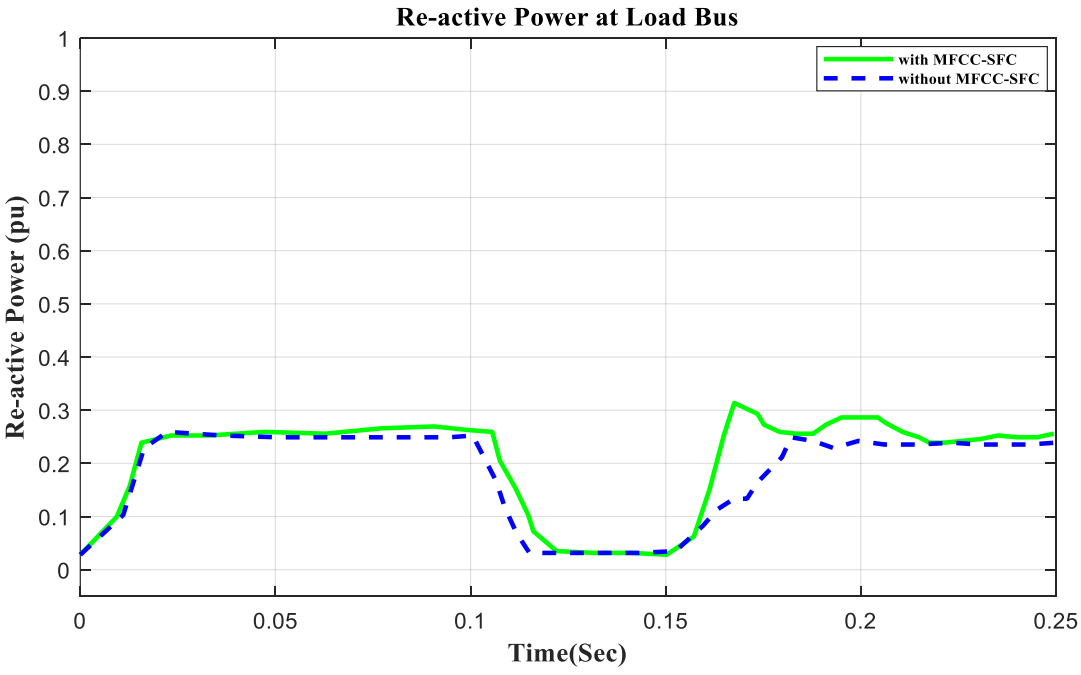

D. Reactive Power Waveform

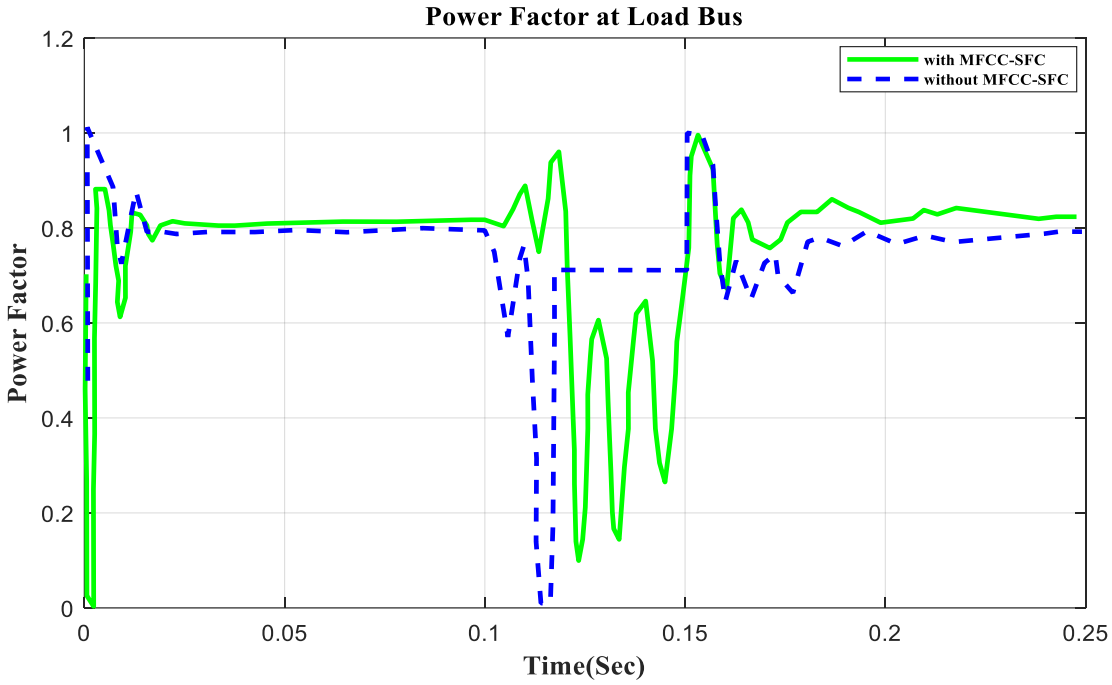

E. Power Factor Waveform

Figure 6.10 V, I, P, Q, and PF at Load Bus with Open-Circuit Duration of 100 to 150 ms. A) RMS Voltage Waveform. B) RMS Current Waveform. C) Active Power Waveform. D) Reactive Power Waveform. E) Power Factor Waveform at Load Bus.

Table 6.2: Voltage, Current, Active Power, and Power Factor Values

Buses	**Source Bus, Vs (pu)**				**Load Bus, VL (pu)**			
	V	**I**	**P**	**PF**	**V**	**I**	**P**	**PF**
Without MFCC	1.0	0.8	0.35	0.78	0.8	0.68	0.3	0.8
With MFCC	1.01	0.9	0.5	0.98	1.0	0.75	0.4	0.98
Improvement	0.01	0.1	0.15	0.2	0.2	0.05	0.1	0.18
% Improvement	1%	10%	15%	20%	20%	7%	10%	18%

6.8 Application of Open-Circuit Condition

In this section, we demonstrate the altering of a critical parameter through an open circuit close to the load. All digital simulations were performed in the MATLAB/Simulink-2023b software environment, which introduced a three-phase open circuit to both buses (source and load) of the AC grid at time 100 ms. It was cleared after 150 ms. Figures 6.9 and 6.10 demonstrate the outcomes of the simulations under the open-circuit situation. As can be seen, both buses now have better dynamic response and power quality. Additionally, there are minimal fluctuations in the power factor in open-circuit faults with FACTS-MFCC-SFC in essential buses, particularly the source bus.

6.8-1 V, I, P, Q, and PF in Infinite Bus

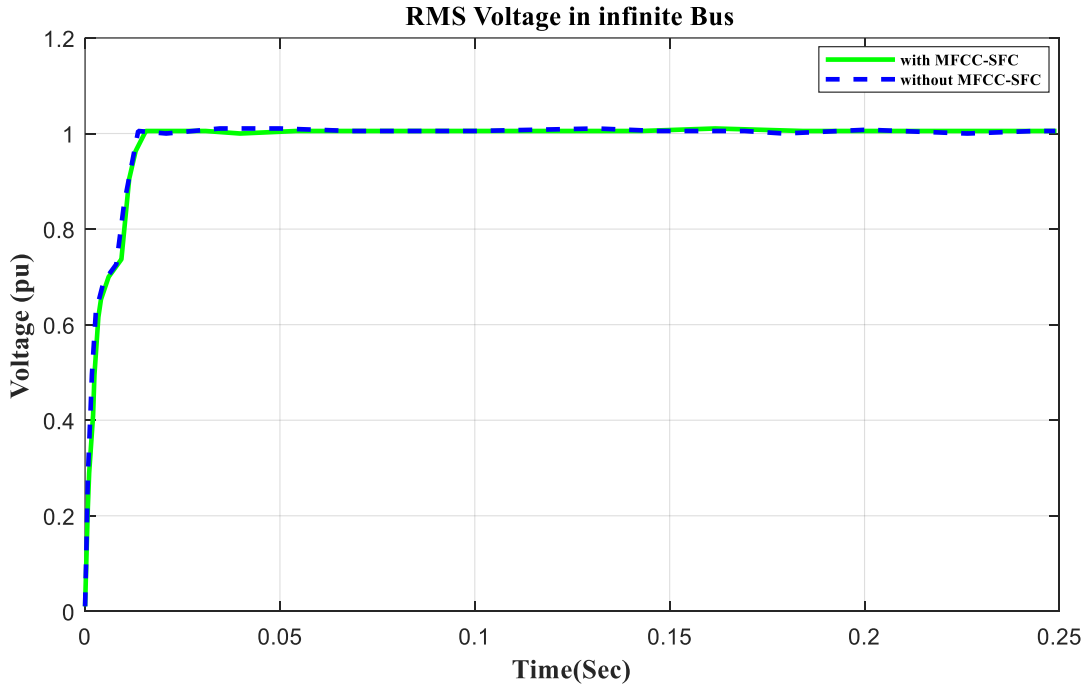

A. RMS voltage waveform

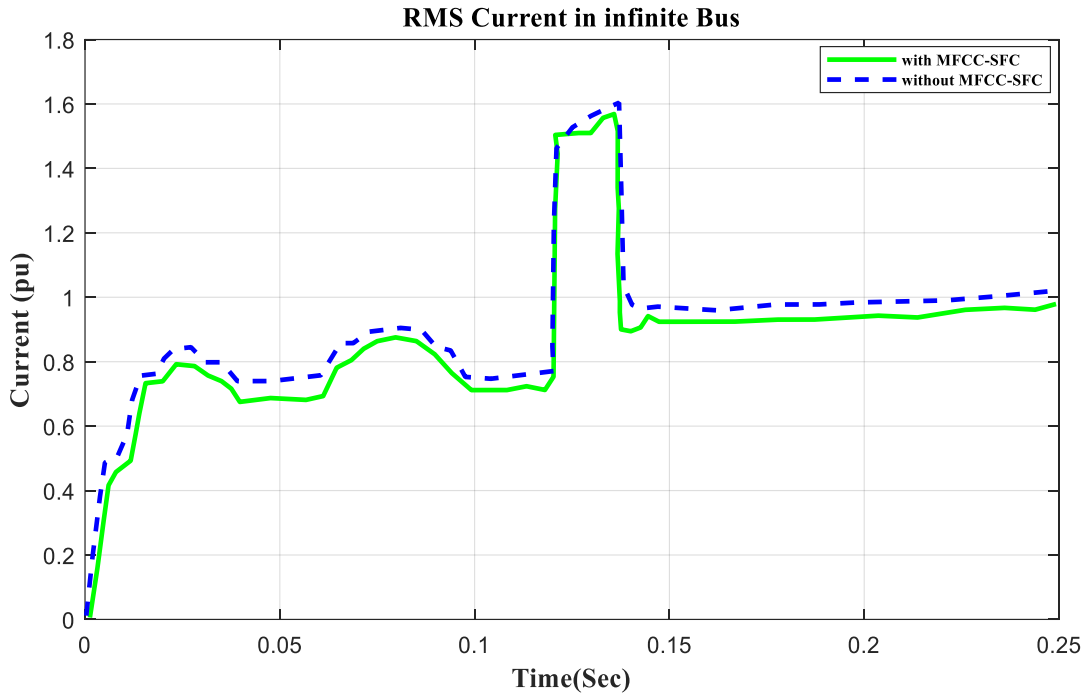

B. RMS Current Waveform

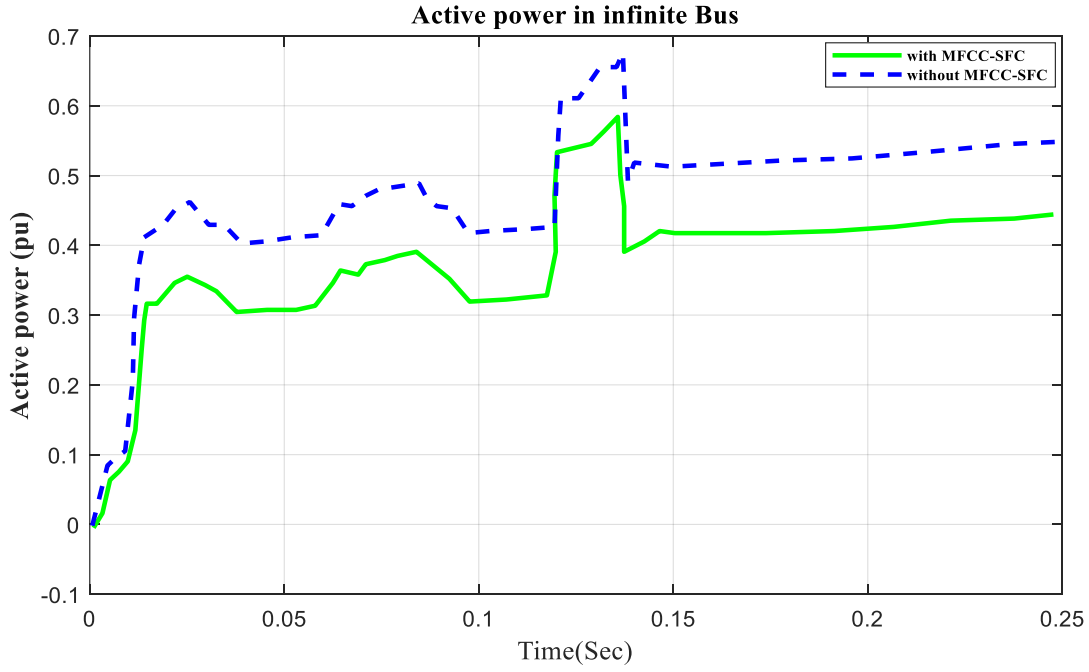

C. Active Power Waveform

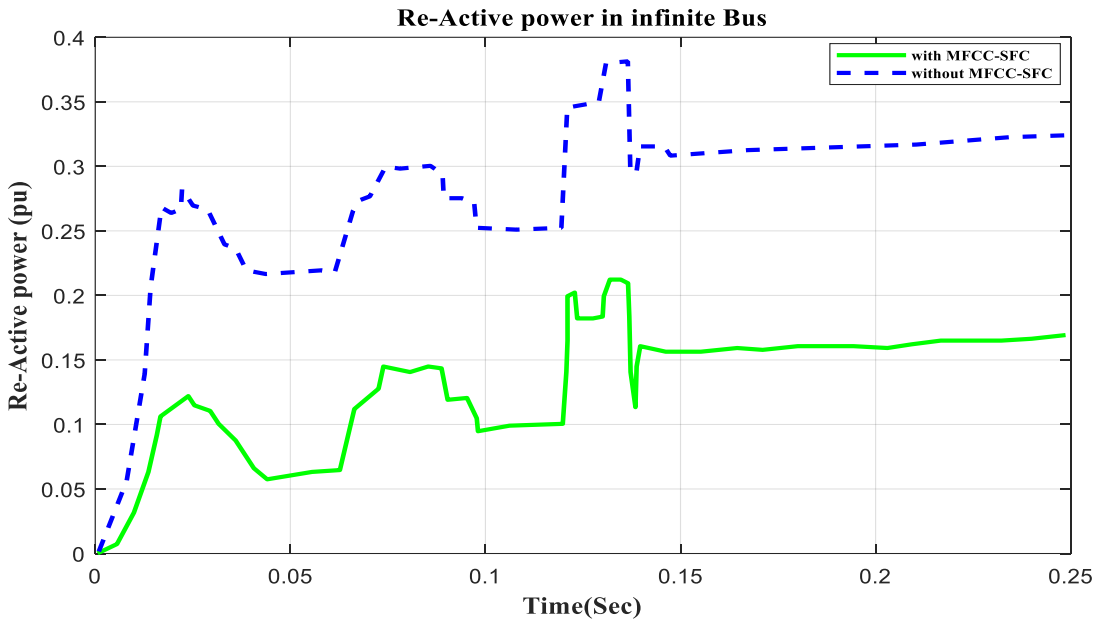

D. Reactive Power Waveform

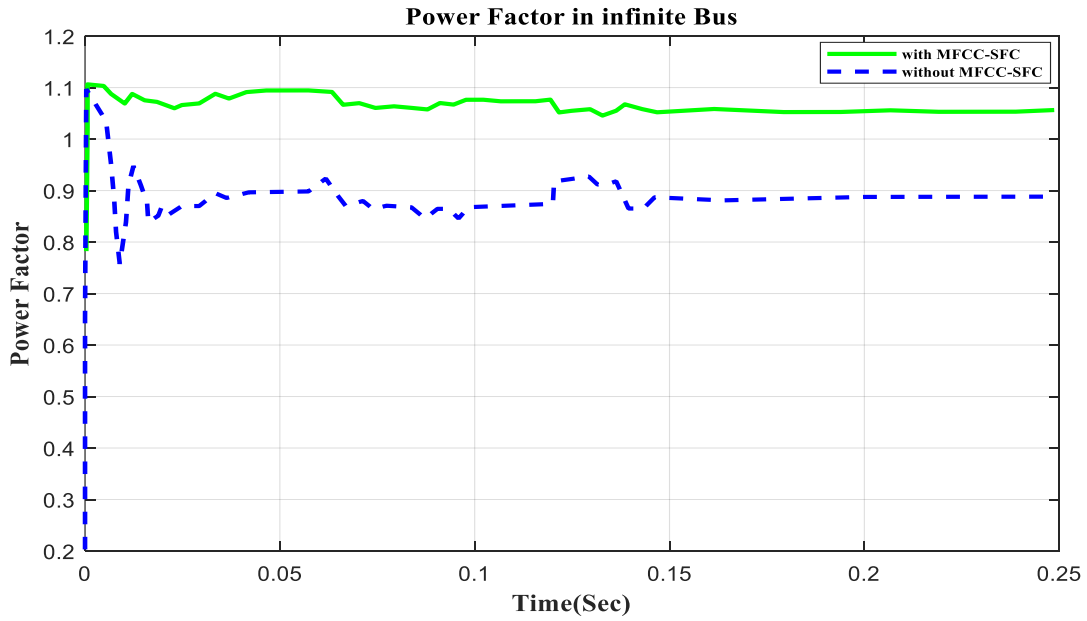

E. Power Factor Waveform

Figure 6.11. V, I, P, Q, and PF at Infinite Bus with Open-Circuit Duration of 100 to 150 ms. A) RMS Voltage Waveform. B) RMS Current Waveform. C) Active Power Waveform. D) Reactive Power Waveform. E) Power Factor Waveform in Infinite Bus.

6.8-2 V, I, P, Q, and PF in Load Bus

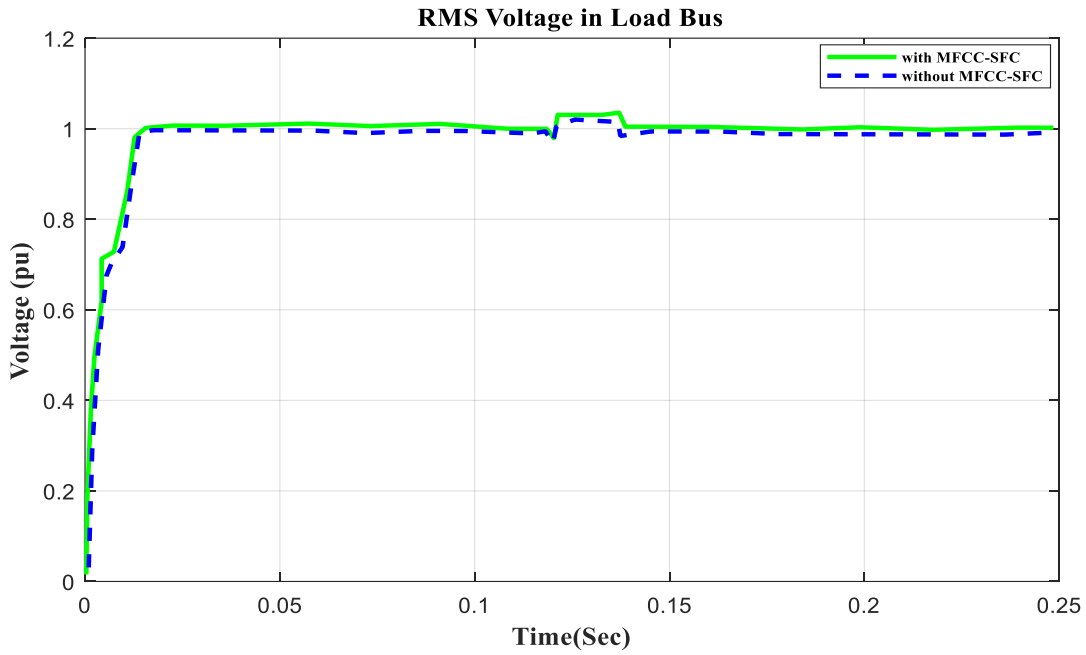

A. RMS Voltage Waveform

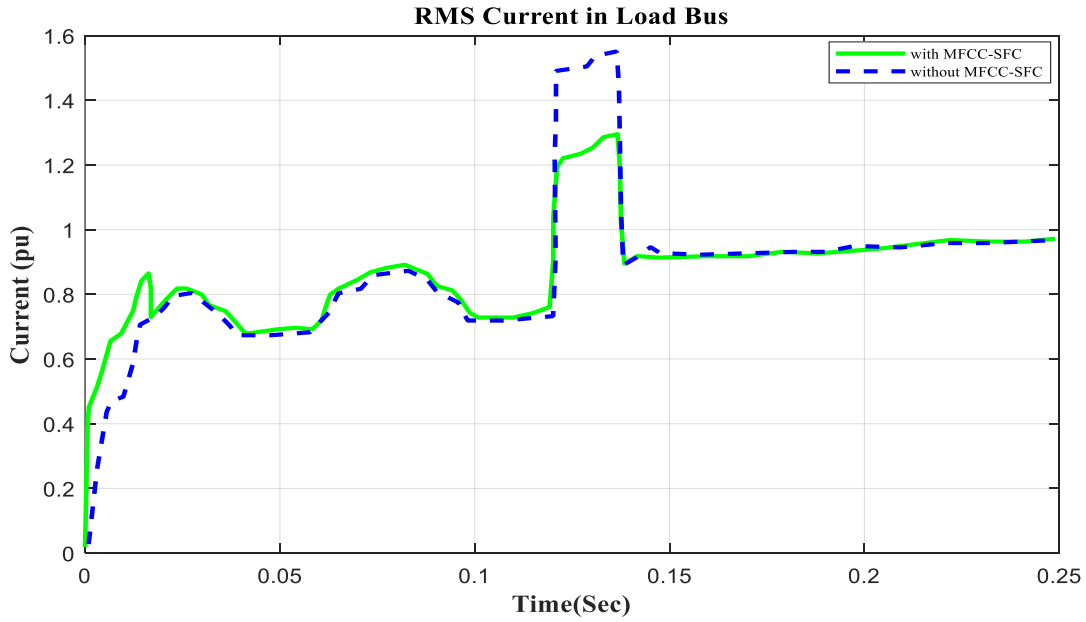

B. RMS Current Waveform

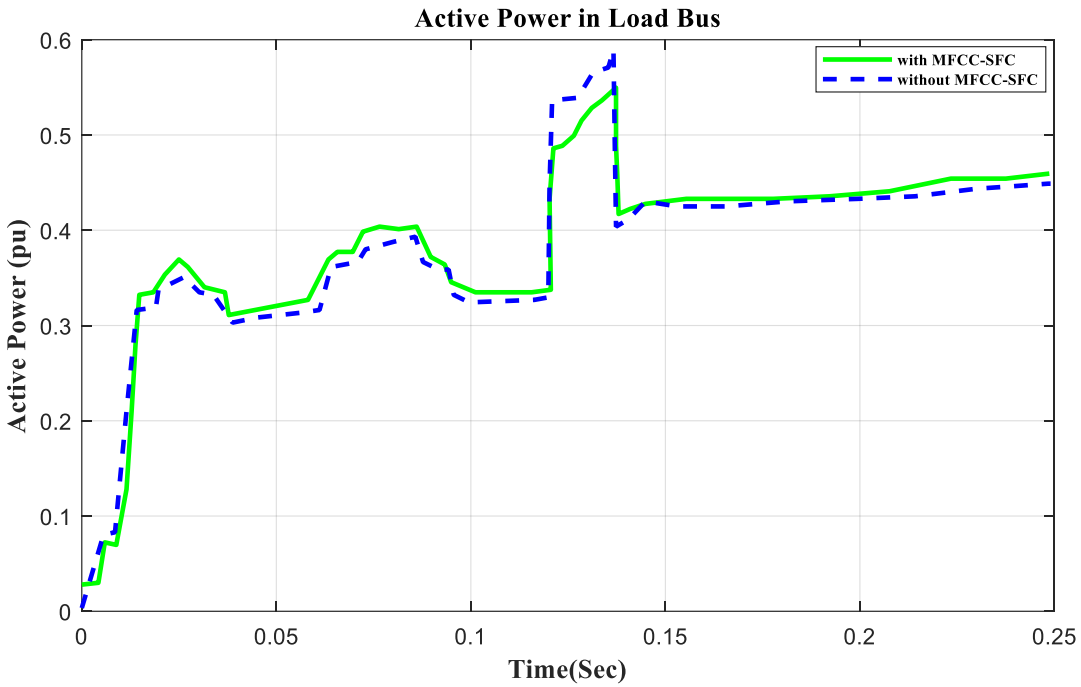

C. Active Power Waveform

\

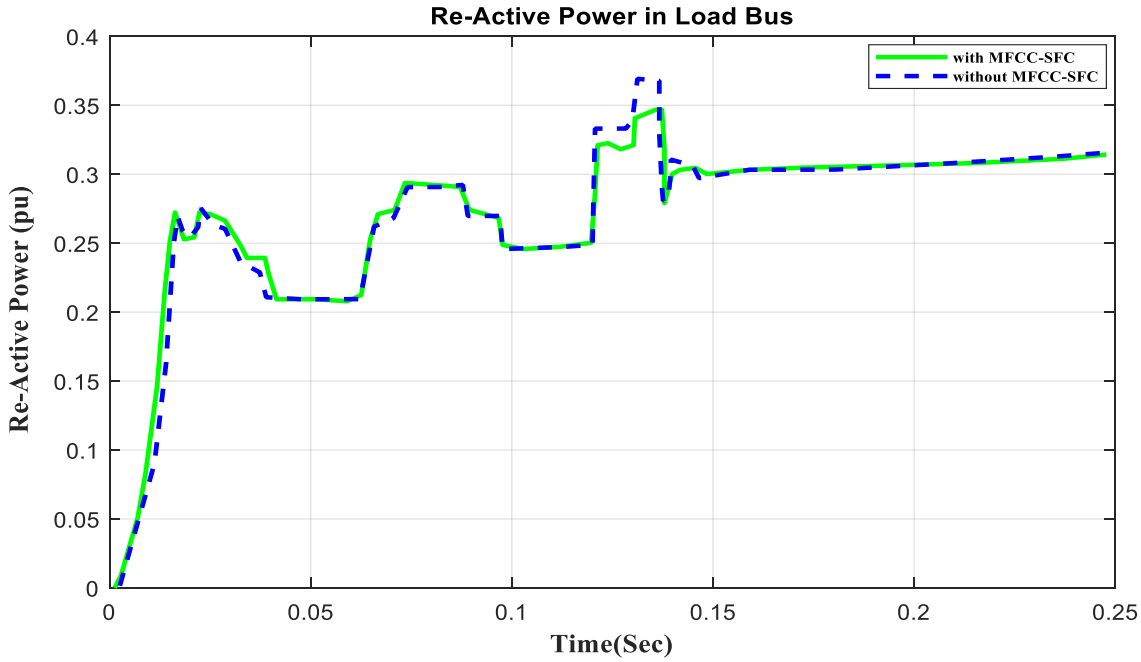

D. Reactive Power Waveform

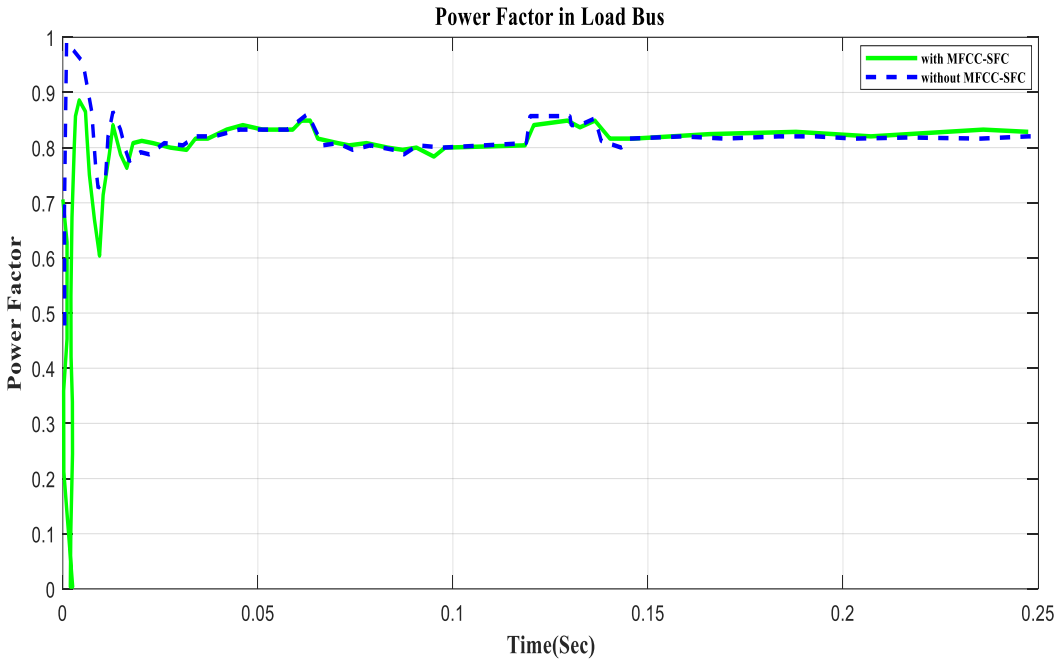

E. Power Factor Waveform

Figure 6.12. V, I, P, Q, and PF at Load Bus with Open-Circuit Duration of 100 to 150 ms. A) RMS Voltage Waveform. B) RMS Current Waveform. C) Active Power Waveform. D) Reactive Power Waveform. E) Power Factor Waveform in Load Bus.

6.9 Open and Closed Circuits

We used the breakers ON/OFF, as seen in the Simulink model and the position of the breaker in series, to close to ground at open circuit and parallel at short circuit. The operations for both open circuit and short circuit were done at the AC source and load bus. The duration of the short circuit was 100 to 200 ms and that of the open circuit was 100 to 150 ms, as presented in Tables 6.1 and 6.2. Additionally, Figure 6.7 shows the V, I, P, Q, and PF at source-side under short-circuit operation, and Figure 6.8 shows the V, I, P, Q, and PF at load-side under short-circuit operation of 100 to 200 ms. Finally, Figure 6.9 illustrates the V, I, P, Q, and PF at source-side under open-circuit operation, and Figure 6.10 depicts the V, I, P, Q, and PF at load-side under open-circuit operation of 100 to 150 ms.

6.10 Application of Short-Circuit Condition

To demonstrate that the low-cost FACTS-MFCC scheme dynamic stabilization and efficient energy utilization functions as intended, the proposed control schemes for stabilizing the host smart grid under short circuit, open circuit, and other conditions are tested. All of our digital simulations were performed in the MATLAB/Simulink-2023b software environment, which introduced a three-phase short circuit to the load bus of the AC grid at time of 100 ms and cleared after 200 ms. Figures 6.7 and 9.8 demonstrate the outcomes of the simulations under the short-circuit situation. As can be seen, the FACTS-MFCC-SFC scheme has improved its efficiency in lowering inrush currents during short- and open-circuit failures, which helped to enhance the power factor and stabilize the bus voltages in the case study.

6.11 Hybrid Load Variations

The grid is subjected to the following situations in order to study how the AC grid reacts to load excursions both with and without the FACTS-MFCC. The results for both current and voltage values are illustrated in Figures 6.11 and 6.12. As shown, linear pressure is disconnected at 117 ms and then reconnected at 134 ms, while nonlinear demand is disconnected at 100 ms and then reconnected at 45 ms. Motor load torque drops at 170 ms by 50% and continues for a duration of 45 ms, after which it rises by 50% at 250 ms seconds for a duration of 45 ms.

6.12 Power Systems Harmonics Analysis

One useful metric for estimating the harmonics in voltage or current waveforms is the total harmonic distortion. The harmonics effect of the voltage and current load bus are discussed in this section. The voltage and current THD of the load bus without FACTS-MFCC-SFC as a function of time are seen in Figures 6.13 (A) and 6.14 (A), respectively. The rate of THD has increased for constant series compensation because the nonlinear loads are used on power systems; however, the THD of the line current terminal voltage in the load bus is improved, as shown in Figures 6.13 (B) and 6.14 (B), by employing the FACTS-MFCC-SFC [183].

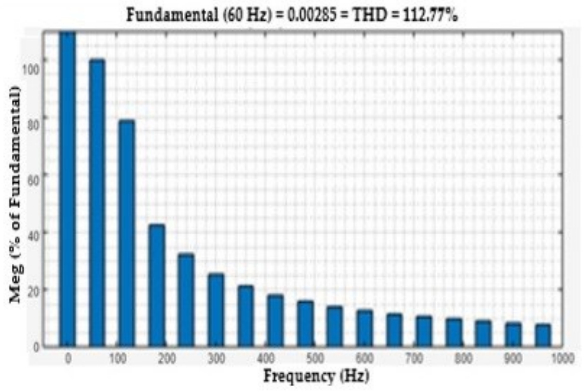

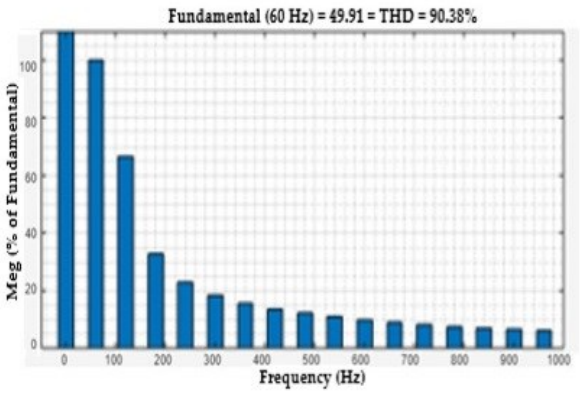

A B

Figure 6.13 (A) FFT Analysis of Voltage at Load Bus without FACTS-MFCC for Load-Changing Operation
(B) FFT Analysis of Voltage at Load Bus with FACTS-MFCC for Load-Changing Operation

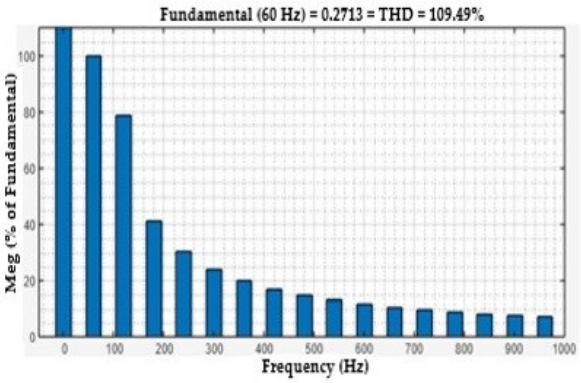

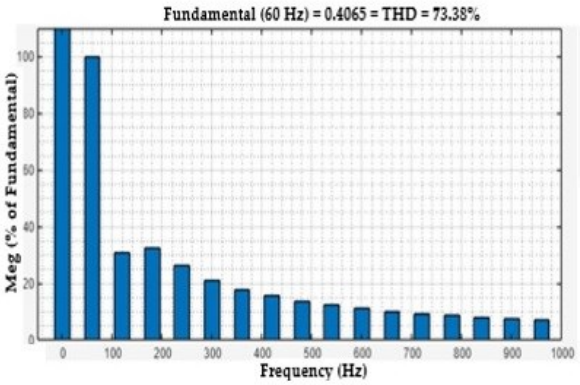

A B

Figure 6.14 (A) FFT Analysis of Current at Load Bus without FACTS-MFCC for Load-Changing Operation
(B) FFT Analysis of Current at Load Bus with FACTS-MFCC for Load-Changing Operation

6.13 Discussion of Digital Simulation Results

There are numerous reasons to propose a new device. First and foremost, there is a need for a low-cost structure with a dual-mode modulated filter and dual tuned arm filter plus capacitive compensation for dynamic inrush nonlinear loads. The function of the modulated pulse width duty cycle switching scheme is to dynamically cater to the nonlinear loads and inrush current variations and reactive compensation tasks in order to stabilize the AC voltages at key load buses with FACTS-MFCC-SFC, as presented in Table 6.1 and 6.2.

6.14 Conclusion and Extended Work

This chapter validated the concept of an AC plug switched filter modulated action using pulse-width modulation based on a multi-loop, self-adjusted, modified weighted PID structure controller and FLC. The modulated filter AC green plug ensures enhanced efficiency in operation, better power quality, reduced harmonics, and improved power factor operation at nonlinear type motorized inrush and rectifier nonlinear loads. For strong interfacing to the smart AC grid, the same filter structure MFCC-SFC device with different control techniques is currently being extended for hybrid renewable wind and micro-hydro green energy systems and applications, such as using virtual inertia static synchronous machines and energy storage DC-AC utility grid systems.

The digital simulation results validate the quick flexibility and efficiency of the proposed FACTS-MFCC-SFC scheme in improving voltage regulation, reducing inrush current conditions, and boosting the power factor. The AC green plug filter is also validated as an effective voltage stabilization and power factor improvement tool in case of slow dynamic nonlinear and inrush type loads. The PWM switching-modulation index is dynamically modified to modulate the tuned arm filter apparent admittance and capacitive VAR compensation level using the multi-loop, multi regulation, fuzzy logic fast dynamic controller. This controller was validated as an effective tool in voltage stabilization, power factor improvement, and power quality enhancement.

Chapter 7: Thesis Conclusion and Future Work

7.1 Thesis Conclusion

The study assessed and validated several flexible FACTS-based topologies and innovative control schemes. These include modified filter capacitor compensation-switched filter compensators (MFCC-SFC), switched filter compensators (SFC), DC-side green power filter compensators (GPFC), and hybrid switched filter compensators (HSFC). The proposed systems were demonstrated to stabilize AC and DC bus voltages, leading to reductions in load excursions, transient voltages under hybrid source changes, and inrush current conditions.

Chapter 1 investigated using a flexible AC transmission system (FACTS) and novel switched filter AC and DC side compensation for electric vehicle locomotion. The AC and DC motor drives were extended into robust low-impact V2H and V2G battery charging schemes that were either interfaced with smart grid utility or employed renewable energy systems, such as fuel cells, Lithium-ion batteries, photovoltaics, or hybrid DC sources.

Chapter 2 proposed a FACTS-based green plug-switched filter compensation (SFC-GP) approach that was controlled using a dynamic multi-loop error-driven fuzzy logic controller. A MATLAB/Simulink software environment and fast-acting dynamic fuzzy logic controller were used to validate the SFC-GP device, showing robust enhancement of voltage stabilization, power quality, and efficiency. Furthermore, the SFC-GP FACTS-based device with a PWM-switched filter compensator scheme was shown to be suitable for nonlinear inrush, dynamic, cyclical, and motorized loads and could be appropriately modified using fixed topologies or optimized structures of soft-computing ANN/NFIS/GA/PSO regulators with optimal gain scheduling and weightings. The proposed scheme was also extended to 3-phase nonlinear loads and applied to voltage dynamic stabilization by utilizing hybrid smart grid-renewable energy interface schemes.

Chapter 3 presented a novel switched modulated capacitive filter compensation scheme for distribution/resident systems in nonlinear inrush loads. The SFC-PWM switched filter employed a complementary switching in two IGBT/MOSFET to alter the capacitive compensation, and the SPWM pulse modulation was controlled online by a fuzzy logic multi-regulation loop based on aggregate weighted loop error weighted summation and configuration changes from capacitive compensation duty. The approach aimed to improve power quality in voltage and current transients.

Overall, the proposed SFC/MFCC filter was found to be effective in enhancing energy use and lowering harmonic contents in voltages and current at source and load buses while also boosting the power factor at source. Further, the SFC/MFCC filter could be extended to other power quality applications in AC-DC micro grids, motor drives, renewable energy, and battery-charging schemes.

Chapter 4 presented a novel modulated green plug AC-side filter compensation scheme for V2H stations. The proposed scheme was controlled with a type-2 fuzzy logic optimized controller and tested under a variety of operating conditions, such as state of the charge (SOC) 50% for hybrid weighted battery charging modes as well as open and short circuits. The tests showed that the modulated/switched filter-capacitor compensation and tuned arm filter were efficient and low-impact. This scheme is a novel reworking of micro AC-DC utilization grids and energy storage schemes, such as virtual energy and static transformer-less voltage stabilization systems. In using PV-fuel cell and Lithium-ion battery storage systems, the approach was proven to be effective in handling various operating conditions by enhancing overall system quality and performance. Specifically, the AC green plug switched filter compensation scheme improved AC power quality, mitigated AC side harmonics and AC-DC decoupling, and lowered inrush currents and transient voltage excursions on DC and AC interface buses.

Chapter 5 investigated a new approach to dual action multi-loop regulators that provides effective control at the tuning/compensation level in slow varying/motorized/nonlinear reactive loads. The low-cost parallel shunt switched modulated filter was found to be significantly improved by using the fast-acting multi-loop regulation scheme. This same scheme was then extended to AC-DC energy storage as well as to V2G battery-charging smart grid systems, such as Virtual Inertia Systems (VIS) and static synchronous dynamic voltage stabilization battery-based schemes for use in smart grids.

Chapter 6 validated the AC plug switched filter modulated action. Pulse-width modulation was used based on a multi-loop, self-adjusted, modified weighted PID structure controller and FLC. The modulated filter AC green plug was shown not only to improve operation efficiency, but also to enhance power quality, mitigate harmonics, and boost the power factor operation at nonlinear type motorized inrush and rectifier nonlinear loads. The proposed FACTS-MFCC-SFC scheme presented in this thesis can be extended to hybrid renewable wind and micro-hydro green energy

systems and applications, e.g., energy storage systems, AC-DC utility grid systems, and virtual inertia static synchronous machines.

Chapter 7 provided a summary of the research conclusions and proposed research extensions. In the summary, the DTC properties were characterized as follows:

- Flux and torque were changed quickly through reference changes.
- High efficiency and low losses/switching losses were minimized by switching transistors only when needed to maintain torque and flux within their hysteresis bands.
- This response had no overshot.
- Coordinate transforms were not required, as all calculations were performed in a stationary coordinate system.
- A separate modulator was also not required, as the hysteresis control directly defined the switch control signals.

Importantly, this thesis validated the concept of pulse-width modulated filters and capacitive compensation schemes as tools for improving voltage stability, boosting power quality, and reducing harmonics. These tools were successfully demonstrated to enhance the SC source power factor and minimize inrush currents and transient over-voltages in SC systems feeding nonlinear type loads as well as AC-DC interfaced battery-charging systems.

The difference between switched filter and modulated type filter.
Switched filter is control by PMW to change the apparent impedance of the system to improve power quality at gain AC bus. Modulated filter is complex switch filter controlled by a global error signal to improve power quality, power factor and enhance electric energy utilization.
Electrical power filter is classified as fixed, switch, modulated and active power filters, APF. There are many types of filters used them power system include tuned arm filters, C-type filter, waited tuned filter and other complex topologies. Switch modulated filers are fixed filters that are controlled by PWM to modify the apparent impedance at a gain AC bus system to reduce power harmonic, improve power quality, improve power factor and enhance energy utilization. Active Power Filters are complex topologies using sold state inverter interface with DC capacitor to inject harmonic compensating current at given AC bus.

PID or FLC controller tuned, and adjustment of parameters can be done by:

A. Trial and error technique.
B. Minimization of an objective criteria based on the error or error squares.

7.2 Future Work

Future work and extensions of the present study include the use of soft computing, random search, and optimization techniques in robust dynamic self-adjusting online gain-scheduling flexible control schemes to extend the family of switched filters/capacitor compensators, green filters, and variable architecture active power filters. This includes the use of particle swarm optimization, harmony search, Ant search, neuro fuzzy inference system, and weed invasion algorithm in developing new online gain-adjusting and efficient energy utilization/management strategies. The modulated switched filters and DC green plugs can be used as power quality enhancement tools and capacitive VAR switched compensators in a number of emerging smart AC grid applications, including:

- Energy storage Lithium-ion and fuel cell smart grid energy storage systems.
- VIS synchronous machine stability enhancement systems.
- Micro grid interfacing using wind, PV, and tidal-wave renewable energy schemes.
- New locomotion and EV drive systems using multi-source FC, battery, and super-capacitor storage systems.
- Battery-charging V2G stations using AC grid and PV solar systems.
- Hydrogen production green and energy production facilities.
- Efficient energy management and energy sharing strategies for hybrid renewable energy smart grid applications.
- Emerging large industrial and electric drives using PV and fuel cell stations.

References

[1] A. F. Attia and A. M. Sharaf "A robust FACTS based fuzzy control scheme for dynamic stabilization of generator station." *Ain Shams Eng. J.,* vol. 11, p. 629-641, 2020.

[2] F. M. Alhaddad, H. H. Aly and M. E. El-Hawary "An overview of wind-solar system output power." *in IEEE Canadian Conference of Electrical and Computer Engineering (CCECE)*, 2019.

[3] F. Alhaddad, H. H. Aly and M. El-Hawary "An overview of active power filters for harmonics mitigation of renewable energies resources." *in IEEE 10th Annual Information Technology, Electronics and Mobile Communication Conference (IEMCON)*, 2019.

[4] I. H. Altas and A. M. Sharaf "A generalized direct approach for designing fuzzy logic controllers in matlab/simulink GUI environment", International Journal of Information Technology and Intelligent Computing." *IJITIC,* vol. 1, 2007.

[5] E. Elbakush and A. M. Sharaf "Cakmak `'A Novel Fuzzy Logic Control Scheme for FACS-Based Switched Filter Compensation." *International Journal of Engineering Innovation and Research,* vol. 3, 2014.

[6] A. M. Sharaf, H. Huang and L. Chang "Power quality and nonlinear load voltage stabilization using error-driven switched passive power filter." *in Proceedings of the IEEE International Symposium on Industrial Electronics*, 2002.

[7] F. A. El-Sheikhi, Y. M. Saad, S. O. Osman and K. M. El-Arroudi "Voltage stability assessment using modal analysis of power systems including flexible AC transmission system (FACTS)." in *Large Engineering Systems Conference on Power Engineering,* 2003.

[8] A. M. Sharaf and W. Wang "A low-cost voltage stabilization and power quality enhancement scheme for a small renewable wind energy scheme." *in IEEE International Symposium on Industrial Electronics*, 2006.

[9] A. Sharaf and G. Wang "Wind energy system voltage and energy enhancement using low cost dynamic capacitor compensation scheme." *in Proc. IEEE International Conference on Electrical*, p. 804–807, 2004.

[10] I. A. Erinmez, and A. M. Foss. "Static synchronous compensator (STATCOM)." *Working group*. Vol. 14. 1999.

[11] H. F. Wang "Applications of damping torque analysis to STATCOM control." International Journal of Electrical Power & Energy Systems 22.3, 197-204, 2000.

[12] T. Masood, N. Al-Emadi, S. A. Qureshi, Y.Y. Almulla, A. J. Khan, S. K. Shah "FACTS Control Devices (Statcom, SSSC and UPFC) Re-Configuration Techniques By PSIM/MATLAB." *in International Conference on Electrical Engineering*, 2007.

[13] N. G. Hingorani and L. Gyugyi "FACTS concept and general system considerations." *IEEE International Conference on Electrical*, P. 1-35, 2000.

[14] D. Jiang "A nonlinear TCSC control strategy for power system stability enhancement." in *APSCOM - 5th International Conference on Advances in Power System Control, Operation and Management*, 2000.

[15] T. T. Nguyen and S. R. Wagh "Model predictive control of facts devices for power system transient stability." *in Transmission & Distribution Conference & Exposition: Asia and Pacific*, 2009.

[16] A. Kazemi, V. Vahidinasab and A. Mosallanejad "Study of STATCOM and UPFC controllers for voltage stability evaluated by saddle-node bifurcation analysis." *in IEEE International Power and Energy Conference*, 2006.

[17] J. Machowski, J. Bialek and J. Bumby " Power system dynamics." stability and control." , book, John Wiley and Sons, 2011.

[18] K. R. Padiyar "FACTS controllers in power transmission and distribution." New Delhi: New Age International, eBook, ISBN 9788122425413 (electronic version), P. 549, 2007.

[19] X.-P. Zhang, B. Pal and C. Rehtanz "Flexible AC transmission systems: Modeling and control. Berlin Heidelberg: Springer Verlag.", 2006.

[20] E. Acha "Power Electronic Control in Electrical Systems." , Book, Elsevier, 2001.

[21] S. Han, S. Han and K. Sezaki "Development of an optimal vehicle-to-grid aggregator for frequency regulation." *IEEE Trans. Smart Grid,* vol. 1, p. 65-72, 2010.

[22] A. M. Sharaf, E. Elbakush and I. H. Altas "Novel control strategies for photovoltaic powered PMDC motor drives." *in IEEE Canada Electrical Power Conference*, 2007.

[23] C. Zhou, K. Qian, M. Allan and W. Zhou "Modeling of the cost of EV battery wear due to V2G application in power systems." *IEEE Trans. Energy Convers.,* Vol. 26, P. 1041–1050, 2011.

[24] A. A. Abdelsalam and H. A. Gabbar and A.M. Sharaf "Performance enhancement of hybrid AC/DC microgrid based D-FACTS." *International Journal of Electrical Power & Energy Systems,* Vol. 63, P. 382-393, 2014.

[25] F. H. Gandoman, A. Ahmadi, A. M. Sharaf, P. Siano, J. Pou, B. Hredzak and V.G. Agelidis "Review of FACTS technologies and applications for power quality in smart grids with renewable energy systems." *International journal of Renewable and Sustainable Energy Review,* Vol. 82, P. 502-514, 2018.

[26] E. Elbakush, A. M. Sharaf and R. Cakmak "A Novel Fuzzy Logic Control Scheme for FACS-Based Switched Filter Compensation." *Compensation International Journal of Engineering Innovation & Research B,* Vol. 3, 2014.

[27] A. Abdelsalam and M. E. Eajal "El-Hawary," Optimal Capacitor Placement and Sizing in Unbalanced Distribution Systems with Harmonics Consideration Using Particle Swarm Optimization." *IEEE Transactions on Power Delivery,* Vol. 25, P. 1734-1741, 2010.

[28] P. A. Desale, V. J. Dhawale and R. M. Bandgar "Brief review paper on the custom power devices for power quality improvement." *International Journal of Electronic and Electrical Engineering,* Vol. 7, 2014.

[29] M. Rastogi, N. Mohan and A. A. Edris "Hybrid-active filtering of harmonic currents in power systems." *IEEE Transactions on Power Delivery ,* vol. 10, p. 1994–2000, 1995.

[30] A. A. Abdelsalam, M. E. Desouki and A. M. Sharaf "Power quality improvement using FACTS power filter compensation scheme." *J. Electrical Systems,* Vol. 9, P. 86-96, 2013.

[31] A. M. Sharaf and B. Khaki "A novel FACTS hybrid modulated filter/capacitor compensator." 2012 International Conference on Smart Grid (SGE). IEEE, 2012.

[32] A. M. Sharaf and F. H. Gandoman "A switched hybrid filter - DVS/green plug for smart grid nonlinear loads." *in IEEE International Conference on Smart Energy Grid Engineering (SEGE)*, 2015.

[33] A. M. Sharaf and F. H. Gandoman "A Flexible Facts Based Scheme for Smart Grid-PV-Battery Storage Systems." *International Journal of Distributed Energy Resources,* vol. 10, 2014.

[34] S. V. Korpade and J. R. Sawant " A case Study of Hybrid Solar-Wind Grid Connected System at Sanmati College of Engineering, Washim." *International Journal of Engineering of Science and Computing,* 2017.

[35] A. M. Sharaf, C. Guo and H. Huang "Distribution/Utilization system voltage stabilization and power quality enhancement using intelligent smart filter." *in UPEC'95*, 1995.

[36] M. Aredes, K. Heumann and E. Watanabe "An universal active power line conditioner," Power Delivery." *IEEE Transactions on,* Vol. 13, P. 545-551, 1998.

[37] A. Sharaf and R. Chetri "A novel dynamic capacitor compensator/green plug scheme for 3phase-4 wire utilization loads Proc." *IEEE Canadian Conference on Electrical and Computer Engineering,* P. 454-459, 2006.

[38] I. Vervenne, K. Van Reuse and R. Belmans "Electric arc furnace modelling from a power quality point of view Proc IEEE." p. 1-6, 2007.

[39] A. M. Sharaf, H. Huang and L. Chang "Power quality and nonlinear load voltage stabilization using error driven switched passive power filter." in *IEEE Proc. on International Symposium on Industrial Electronics*, P. 616-621, 1995.

[40] P. Ferracci and J. M. Lupin "Power quality: monitoring and innovation in PFC and harmonic filtering." *16th International Conference and Exhibition on Electricity Distribution, CIRED.(IEE Conf. Publ No. 482)*. Vol. 2. IET, 2001.

[41] H. Fujitaand and H. Akagi "A practical approach to harmonic compensation in power systems-series connection of passive and active filters." Industry Applications," *IEEE Transactions on,* vol. 27, p. 1020-1025, 1991.

[42] D. Sabin and A. Sundaram "Quality enhances reliability [power supplies]." IEEE spectrum Vol. 33.2, P. 34-41, 1996.

[43] G. Walid and M. E. Morsi "New Fuzzy-Based Representative Quality Power Factor for Nonsinusoidal Situations." IEEE Transcations on Power Delivery B 23 L 2, 2008.

[44] A. N. Azliza "Fuzzy Logic Controller for Controlling DC Motor Speed using MATLABApplications." (Doctoral dissertation, UMP), Power System, 2008.

[45] H. Fujita, T. Yamasaki and H. Akagi "A hybrid active filter for damping of harmonic resonance in industrial power systems." Power Electronics," *IEEE Transactions on,* vol. 15, P. 215-222, 2000.

[46] P. S. Sanjan, N. Gowtham, M. S. Bhaskar, U. Subramaniam, D.J. Almakhles, S. Padmanaban and N. G.Yamini " Enhancement of power quality in domestic loads using harmonic filters." *IEEE Access*, *8*, 197730-197744, 2020.

[47] A. M. Sharaf "A facts based dynamic capacitor scheme for voltage compensation and power quality enhancement." in Industrial Electronics," in *IEEE International Symposium on*, Vol. 2, IEEE, P. 1200-1205, 2006.

[48] I. Altas and A. Sharaf "A generalized direct approach for designing fuzzy logic controllers in matlab/Simulink gui environment." *International Journal of Information Technology and Intelligent Computing,* 1(4), P.1-7*,* 2007.

[49] G. Walid and M. E. Morsi " new fuzzy-based representative quality power factor for no sinusoidal situations." IEEE Transactions on Power Delivery," Vol. 23, P. 930-936, 2008.

[50] A. M. Sharaf and R. Chhetri "A novel dynamic capacitor compensator/green plug scheme for 3Phase-4Wire Utilization Loads." in *IEEE Canadian Conference on Electrical and Computer Engineering (CCECE'06)*, P. 454-459, 2006.

[51] A. A. Abdelsalam and M. E. Eajal " Optimal Capacitor Placement and Sizing in Unbalanced Distribution Systems With Harmonics Consideration Using Particle Swarm Optimization" IEEE Transactions On Power Delivery B 25 L3, 2010.

[52] A. A. Abdelsalam, M. E. Desouki and A. M. Sharaf "Power quality improvement using FACTS power filter compensation scheme." *International Journal. Electrical Systems Pages,* P. 73-83, 2013.

[53] A. A. Abdelsalam, A. M. Sharaf and A. A. Eldesouk "Power quality enhancement in wind-grid interface based on dynamic filter Compensator." *International Journal of Distributed Energy Resources and Smart Grids,* Vol. 9, P. 367 - 381, 2013.

[54] A. M. Sharaf and A. A. Abdelsalam "A novel switched filter compensation scheme for power quality enhancement and loss reduction." INSPEC Accession Number: 12116224," in *IEEE International Symposium on Innovations in Intelligent Systems and Applications*, P. 398-403, IEEE, 2011.

[55] A. M. Bloul, A. Sharaf and M. El-Hawary "An energy saving green plug device for nonlinear loads." IOP Conference Series: Earth and Environmental Science. Vol. 127. No. 1. IOP Publishing, 2018.

[56] A. M. Nurul "Md Fokhrul Islam, Ashik Ahmed ``Power quality improvement of a proposed grid-connected hybrid system by load flow analysis using static VAR compensator." *Heliyon journal,* Vol. 9, no 7, 2023.

[57] A. A. Ghadimi, M. Gholami and M. R. Mive "Review of FACTS technologie s and applications for accelerating penetration of wind energies in the powersystem." *Energy Science & Engineering,* Vol. 11, P. 1819–2234, 2023.

[58] A. A. Dutta, M. Sabley, B. S. Sudama and A. N. Kadu "Harmonic Compensation in Power system using active power filters." *International Journal of Multidisciplinary and Current Research,* P. 188-192, 2013.

[59] K. Y. W. Hong, H. S. H. Chung, Y. Xiang and A. W. L. Lo "Experimental assessment of a tiny AI-empowered output filter parameter extraction framework for digital power." *IEEE Access,* Vol. 11, P. 14728-14741, 2023.

[60] S. Pujitha, D. Eps and Gowtami "Enhancement of power quality by using modified power filter and compensator in grid network K." *International Journal of Scientific & Technology Research,* Vol. 3, No 8. 2014.

[61] H. H. Aly "A hybrid optimized model of Adaptive Neuro-Fuzzy Inference System, Recurrent Kalman Filter and Neuro-Wavelet for Wind Power Forecasting Driven by DFIG." *International Journal of Energy* 239: 122367, 2022.

[62] R. Betala "An innovative fuzzy fractional order controller for electric vehicle system for power factor improvement." in *International Conference on Emerging Trends in Engineering & Technology- Signal and Information Processing*, P. 1-6, 2023.

[63] R. Raja, L.J. Nirmal, P. K. Mani, and M. Kavitha "Power quality enhancement using dynamic voltage restorer in distributed networks." *8th International Conference on Communication and Electronics Systems (ICCES)*. P. 210-215, IEEE, 2023.

[64] H. H. Aly and M. El-Hawary "Small signal stability analysis of tidal in-stream turbine using DDPMSG with and without controller." 5th," *IEEE Annual Electrical Power and Energy Conference,* P.239-243,IEEE*,* 2011.

[65] Y. Xu, B. Zhou, W. Wei, L. Jiang, X. Sun and T. Zheng "Evaluation method of energy storage control strategy for AC/DC hybrid system based on DC power transfer influence factor." in *6th International Conference on Energy, Electrical and Power Engineering (CEEPE)*, P.1109-1114, 2023.

[66] S. Benisha, J. Roseline, K. Murugesan, D. Lakshmi, G. Ezhilarasi and P. Muthukumar "Enrichment in power quality using Power Factor Correction Cuk converter fed BLDC Motor Drive." *in 9th International Conference on Electrical Energy Systems (ICEES),* P. 590-598, 2023.

[67] A. Busacca, A. O. Di Tommaso, R. Miceli, C. Nevoloso, G. Schettino, G. Scaglione, F. Viola and I. Colak "Switching frequency effects on the efficiency and harmonic distortion in a three-phase five-level CHBMI prototype with multicarrier PWM schemes: Experimental analysis." *Energies,* Vol. 15, P. 586, 2022.

[68] W. Miao and H. Bo "Research on fast power flow calculation method for multiple faults based on double line outage distribution factors." in *4th International Conference on Power and Energy Technology (ICPET)*, IEEE, P. 493-497, 2022.

[69] K. Vinodhini, A. Sobiya, M. Gengaraj, M. Nanthini, M. Subashini and L. Kalaivani "Fuzzy logic controller based power factor correction converter for industrial applications." in *Second International Conference on Artificial Intelligence and Smart Energy (ICAIS)*, 2022.

[70] R. Patil "Comparative study of single-phase power factor correction topologies for electric vehicle battery charger based on boost converter." in *IEEE Conference on Interdisciplinary Approaches in Technology and Management for Social Innovation (IATMSI)*, 2022.

[71] K. S. Vadivu, A. Anbazhagan, P. Abirami and R. H. Laitha "Analysis of different control techniques for improved power factor and reduced THD on three level full bridge AC-DC Converter." 2022.

[72] L. Sarker, M. Nazir and M. A. Razzak "Harmonics reduction and power factor correction for electric vehicle charging system." *in Innovations in Power and Advanced Computing Technologies (i-PACT)*, 2021.

[73] M. Boutoubat, S. Marmouh and A. Hadjaissa "Grid connected WECS control for power production and power factor correction." *in 1st International Conference on Communications, Control Systems and Signal Processing (CCSSP)*, 2020.

[74] I. S. Mohamed, S. Rovetta, T. D. Do, T. Dragicevic and A. A. Z. Diab "A neural-network-based model predictive control of three-phase inverter with an output LC filter." *IEEE Access,* pp. IEEE Access 7 : P.124737-124749, 2019.

[75] A. Y. Solanki and S. R. Vyas "A review on power quality enhancement using custom power devices." *International Research Journal of Engineering and Technology,* Vol. 8, P. 287-290, 2021.

[76] F. Nejabatkhah, Y. W. Li and H. Tian "Power quality control of smart hybrid AC/DC microgrids: An overview." *IEEE Access,* Vol. 7, P. 52295-52318, 2019.

[77] A. M. Bloul, A. M. Sharaf, H. M. Mosbah and M. E. El-Hawary "A robust fuzzy logic controller for a Green Plug-switched filter for nonlinear loads." *in IEEE 28th Canadian Conference on Electrical and Computer Engineering (CCECE)*, P.1409-1413, 2015.

[78] A. M. Sharaf and F. H. Gandoman "A Flexible Facts Based Scheme for Smart Grid-PV-Battery Storage Systems." *International Journal of Distributed Energy Resources,* Vol. 10, P. 261-271, 2014.

[79] S. D. Nuran, Y. Ismail, H. Atlas and A. M. Sharaf "A Novel FACTS based on modulated power filter compensator for wind-grid energy systems." in *IEEE 5th International Symposium on Power Electronics for Distributed Generation Systems (PEDG)*, P. 1-7, 2014.

[80] S. Arulselvi and U. Govindarajan "Real-time implementation of modified fuzzy logic controller for a non-linear quasi-resonant DC-DC converter." *IETE Journal of Research* 53.5, P. 401-416, 2007.

[81] P. Frgal "Average current mode interleaved PFC control." Application Note (2016): AN5257.

[82] W. N. Nomihla and E. D. Innocent , "Power Planning for a Smart Integrated African Super-Grid", 2022 30th Southern African Universities Power Engineering Conference (SAUPEC), P.1-6, 2022.

[83] A. M. Sharaf "A facts based dynamic capacitor scheme for voltage compensation and power quality enhancement." in Industrial Electronics," IEEE International Symposium on, Vol. 2, 2006.

[84] F. H. Gandoman, A. Ahmadi, A. M. Sharaf, P. Siano, J. Pou, B. Hredzak and V. G. Agelidis "Review of FACTS technologies and applications for power quality in smart grids with renewable energy systems." *Renew. Sustain. Energy Rev.,* Vol. 82, P. 502-514, 2018.

[85] M. Narimani and G. Moschopoulos "A three level integrated AC-DC converter." *IEEE Trans. On Power Electron,* Vol. 29, P. 1813-1820, 2014.

[86] H. H. Aly "Intelligent optimized deep learning hybrid models of neuro wavelet, Fourier Series and Recurrent Kalman Filter for tidal currents constitutions forecasting." *Ocean Eng.,* Vol. 218, P. 108254, 2020.

[87] M. Kiasari, M. Ghaffari, and H. H. Aly. "A Comprehensive Review of the Current Status of Smart Grid Technologies for Renewable Energies Integration and Future Trends: The Role of Machine Learning and Energy Storage Systems." Energies 17.16: 4128, 2024.

[88] H. H. Aly "A novel approach for harmonic tidal currents constitutions forecasting using hybrid intelligent models based on clustering methodologies." *Renew. Energy,* vol. 147, P. 1554-1564, 2020.

[89] H. H. Aly "A novel deep learning intelligent clustered hybrid models for wind speed and power forecasting." *Energy (Oxf.),* Vol. 213, P. 118773, 2020.

[90] H. H. Aly "Dynamic modeling and control of the tidal current turbine using DFIG and DDPMSG for power system stability analysis." *Int. J. Electr. Power Energy Syst.,* Vol. 83, P. 525-540, 2016.

[91] J. Rocabert, A. Luna, F. Blaabjerg and P. Rodríguez "Control of power converters in AC microgrids." *IEEE Trans. Power Electron.,* Vol. 27, P. 4734-4749, 2012.

[92] M. M. EI-Arini, M. T. Youssef and H. H. Aly "Voltage sag analysis and its reduction to improve power system performance." *2006 Eleventh International Middle East Power Systems Conference*. Vol.1, IEEE, 2006.

[93] A. M. Sharaf and G. Wang "Wind energy system voltage and energy enhancement using low cost dynamic capacitor compensatio scheme." in *International Conference on Electrical, Electronic and Computer Engineering, ICEEC '04*, P. 804-807 IEEE,2004.

[94] I. Altas and A. M. Sharaf "A generalized direct approach for designing fuzzy logic controllers in matlab/Simulink gui environment." *International Journal of Information Technology and Intelligent Computing,* Vol. 1, no 4, P. 1-27, 2007.

[95] A. A. Ghadimi, M. Gholami and M. R. Miveh "Review of FACTS technologies and applications for accelerating penetration of wind energies in the power system." *Energy Sci. Eng.,* P. 2218-2234., 2023.

[96] A. G. Zidan "Design and control of V2G", Smart Energy Grid Engineering." Elsevier Inc, mart energy grid engineering, P.187-205, 2017.

[97] F. H. Gandoman, A. M. Sharaf, S. H. AbdulAleem and F. Jurado "Distributed-FACTS stabilization scheme for efficient utilization of distributed. wind energy systems." *Ltd. Int Trans Electrical Energy System,* Vol. 27, no 11, P. 2391, 2017.

[98] V. Rishishwar and Raghuwanshi "Single phase Bi-directional Electric vehicle battery charger with G2V." in *V2G & V2L Technologies" IEEE Renewable Energy and Sustainable E-Mobility Conference (RESEM)*, P. 1-6, 2023.

[99] F. M. Shakeel and O. P. Malik "Vehicle-to-grid technology in a micro-grid using DC fast charging architecture." *in IEEE Canadian Conference of Electrical and Computer Engineering (CCECE)*, 2019.

[100] A. G. Olabi and M. A. Abdelkareem "Renewable Energy and Climate Change." Renewable and Sustainable Energy Reviews 158: 112111, 2022.

[101] M. Brenna, F. Foiadelli, M. Longo and D. Zaninelli "Power quality improvement in primary distribution grids through vehicle-to-grid technologies." *in IEEE International Electric Vehicle Conference (IEVC)*, IEVC, 2014.

[102] S. Mishra, L. K. Sahu, A. K. Tiwari and A. H. Chander "Modelling of electric vehicle direct current fast charging station." *in Asian Conference on Innovation in Technology (ASIANCON)*, 2021.

[103] K. R. Naik, B. Rajpathak, A. Mitra and M. Kolhe "Renewable Energy Integrated DC Microgrid for EV Charging Station." in *IEEE Transportation Electrification Conference (ITEC-India*, P. 1-6, 2021

[104] A. M. Sharaf and P. Kreidi "Power quality enhancement using a unified switched capacitor compensator." *Cat. No. 03CH37436,*Vol. 1, P. 331-333, IEEE, 2003.

[105] A. M. Bloul, M. Abuhamdah, A. M. Sharaf, H.H. Aly and J. Gu "An Efficient Shunt Modulated AC Green Plug–Switched Filter Compensation Scheme for Nonlinear Loads." *MDPI, Energies,,* Vol. 17, no. 10, 2024.

[106] S. G. Selvakumar "Electric and Hybrid Vehicles - A Comprehensive Overview," in *2nd International Conference on Electrical Power and Energy Systems (ICEPES)*, IEEE, P. 1-6, 2021.

[107] D. Sha, D. Zhang and J. Zhang "A single-stage dual-active-bridge AC-DC converter employing mode transition based on real-time calculation." *IEEE Trans. Power Electron.,* vol. 36, P. 10081-10088, 2021.

[108] H. Dong and J. Xi "Model predictive longitudinal motion control for the unmanned ground vehicle with a trajectory tracking model." *IEEE Trans. Veh. Technol.,* vol. 71, P. 1397–1410, 2022.

[109] A. M. Sharaf and M. A. H. El-Sayed "Dynamic control of fuel cell powered water pumping station." *Renew. Energy Power Qual. J.,* vol. 1, P. 203-209, 2009.

[110] S. Kumar, T. Upadhyay and O. H. Gupta "Power quality improvement and signal conditioning of PV array and grid interfaced off-board charger for electric vehicles with V2G and G2V capabilities." *Chinese Journal of Electrical Engineering,* 2023.

[111] R. Thamizharasan, V. Anbarasan, R. Priya and T. L. Joshua, "Solar PV Array Based Multi-Functional Smart EV Charger." *in 9th International Conference on Advanced Computing and Communication Systems (ICACCS)*, Coimbatore, Vol. 1, P.1731-1737, 2023.

[112] S. Vendoti, A. C. Shekhar, S. V. V. G. Bapuji and G. L. Reddy, "Controlling of Electrical Vehicle Charging Conditions using PV based Multi-Mode Converter," *in International Conference on Intelligent and Innovative Technologies in Computing, Electrical and Electronics (IITCEE)*, P. 146-149, IEEE.2023.

[113] A. Yamamoto, H. Omori, M. Tsuno, T. Morizane and N. Kimura "A novel type of single-ended wireless V2H system with a supply voltage control and a capacitor selector scheme." *in IEEE PES Asia-Pacific Power and Energy Engineering Conference (APPEEC)*, P.1-5, 2019.

[114] Y. Fu, Y. Li, Y. Huang, X. Lu, K. Zou, C. Chen and H. Bai "Imbalanced load regulation based on virtual resistance of A three-phase four-wire inverter for EV vehicle-to-home applications." *IEEE Trans. Transp. Electrif.,* vol. 5, p. 162–173, 2019.

[115] T. Takahashi, H. Omori, M. Tsuno, T. Morizane and H. Matayoshi "A new type of wireless V2H system with a single-ended converter controlled by resonant selector and voltage changer." vol. 158, P.1-7, 2020.

[116] C. K. Gowda, V. G. Khedekar, N. Anandh, L. R. S. Paragond and P. Kulkarni "Bidirectional on-board EV battery charger with V2H application." in *Innovations in Power and Advanced Computing Technologies (i-PACT)*, Vol.1, 2019.

[117] R. Bose and P. G. Latha "Modified EV charging/discharging control for hybrid DC fast charging stations." *in IEEE IAS Global Conference on Renewable Energy and Hydrogen Technologies (GlobConHT)*, P. 1-6, IEEE, 2023.

[118] M. Kwon, S. Jung and S. Choi "A high efficiency bi-directional EV charger with seamless mode transfer for V2G and V2H application." *in IEEE Energy Conversion Congress and Exposition (ECCE)*, P. 5394-5399, 2015.

[119] K. Sudarshan, M. Valluru, A. Singh, M. Goel, D. Kaur, K. Dobhal, A. Kartikeya and A. Verma "Design of Multi-Loop L-PID and NL-PID Controllers: An Experimental Validation." *IEEE International Conference on Power Electronics, Intelligent Control and Energy Systems (ICPEICES),* P. 1228-1231, 2018.

[120] A. Saxena, R. Shankar and S. K. Parida "Vehicle-to-grid technology with virtual inertia control for enhanced frequency regulation in smart grid." *in IEEE Global Conference on Computing, Power and Communication Technologies (GlobConPT)*, P. 1- 6, 2022.

[121] A. Dendouga, A. Dendouga and N. Essounbouli "Performance Enhancement of Wind Turbine Systems using Type-2 Fuzzy Logic Control: comparative study." 19th International Multi-Conference on Systems in *Signals & Devices (SSD'22)*, P. 946-951, 2022.

[122] A. H. Qutaiba, A. Kiftaro, M. Alsheikh and M. A. Jaradat "An Intelligent Controller for an Assisted Electric Wheelchair based on Interval Type-2 Fuzzy Logic." *Advances in Science and Engineering Technology International Conferences (ASET)*, IEEE, P. 1- 6, 2023.

[123] J. Zhang, L. Zhang, F. Sun and Z. Wang "An Overview on Thermal Safety Issues of Lithium-ion Batteries for Electric Vehicle Application." IEEE Special Section on Battery Energy Storage and Management Systems." vol. 6, P. 23848-23863, 2018.

[124] B. S. Aravind, E. Raju, S. Hari, J. Vincent, P. K. Prathibha and C. A. Sam "CCCV controlled solar integrated on-board charger for vehicle-to-home operation using bridgeless bi-directional flyback converter." *in 2nd International Conference on Power Electronics & IoT Applications in Renewable Energy and its Control (PARC)*, P. 1- 6, IEEE, 2022.

[125] P. K., A.M. Sharaf, "Nonlinear Speed Control of Large Industrial DC Motor Drives with an Energy Efficiency Enhancement Loop." Waterloo, ON, Canada, 1998.

[126] A. M. Bloul, A. M. Sharaf, H.H. Aly and J. Gu "An Energy Efficient Green Plug Filter Compensation Scheme for Hybrid Nonlinear Loads." *International Journal of Engineering Innovation & Research,* vol. 12, P. 2277 – 5668, 2023.

[127] H. H.Aly "An intelligent hybrid model of neuro Wavelet, time series and Recurrent Kalman Filter for wind speed forecasting." *Sustain. Energy Technol. Assessments,* Vol. 41, P. 100802, 2020.

[128] A. M. Sharaf and F. H. Gandoman "A Switched Hybrid Filter - DVS/Green Plug for Smart Grid Nonlinear Loads." in *IEEE International Conference on Smart Energy Grid Engineering (SEGE)*, P. 1-6, 2015.

[129] Aniket Nitin Pal and Gaurav Karlekar "Vehicle-To-Grid Technology in a Micro-grid Using DC Fast Charging Architecture." *International Journal for Multidisciplinary Research (IJFMR),* vol. 5, P. 1- 4, 2023.

[130] Y.C. Hsu, S.C. Kao, C.Y. Ho, P.H. Jhou, M.Z. Lu and C.M. Liaw "On an electric scooter with G2V/V2H/V2G and energy harvesting functions." *IEEE Trans. Power Electron.,* vol. 33, P. 6910-6925, 2018.

[131] A. M. Sharaf "Harmonic interference from distribution systems." *IEEE Trans. Power Appar. Syst.,* Vol. PAS-101, P. 2975-2981, 1982.

[132] K. V. Sastry, S. Shashank Holla, E. Tater, D. G. Gustafson and M. J. Taylor "Design and Demonstration of a Smart Charging System for Plug-in Electric Vehicles." in *2023 IEEE Transportation Electrification Conference & Expo (ITEC)*, IEEE, P. 1-6, 2023.

[133] O. Castro-Heredia, J. Linares-Flores, C. Garcia-Rodriguez, J. Salazar-Oropeza, O.-D. Ramirez-Cardenas and R. Heredia-Barba "Electronic differential based on active disturbance rejection control for a four in-wheel drive electric-vehicle (go-kart)." *in IEEE International Power and Renewable Energy Conference (IPRECON)*, P. 1-6, 2021.

[134] Y. Zhang, S. Lu, Y. Yang and Q. Guo "Internet-distributed vehicle-in-the-loop simulation for HEVs." *IEEE Trans. Veh. Technol.,* Vol. 67, P. 3729-3739, 2018.

[135] W. Wang, Y. Li, J. Shi and C. Lin "Vibration Control Method for an Electric City Bus Driven by a Dual Motor Coaxial Series Drive System Based on Model Predictive Control." Vol. 6, P. 41188-41200, 2018.

[136] K. Miao Tan, V. K. Ramach and J. Y. Ramamurthy "Integration of electric vehicles in smart grid: A review on vehicle to grid technologies and optimization techniques." *in Renewable and Sustainable Energy Reviews,* vol. 53, P. 720-732, 2016.

[137] Y. Song, P. Li, Y. Zhao and S. Lu "Design and Integration of the Bidirectional Electric Vehicle Charger into the Microgrid as Emergency Power Supply." *in International Power Electronics Conference*, Niigata, P. 3698-3704, 2018.

[138] J. Pahasa and I. Ngamroo "PHEVs bidirectional charging/discharging and SoC control for microgrid frequency stabilization using multiple MPC." *IEEE Trans. Smart Grid,* vol. 6, P. 526-533, 2015.

[139] M. Marinelli, S. Martinenas, K. Knezović and P. B. Andersen "Validating a centralized approach to primary frequency control with series-produced electric vehicles." *J. Energy Storage,* Vol. 7, P. 63-73, 2016.

[140] D. Sha, D. Zhang and J. Zhang "A single-stage dual-active-bridge AC–DC converter employing mode transition based on real-time calculation." *IEEE Transactions on Power Electronics ,* Vol. 36, P. 10081-10088, 2021.

[141] V. Rishishwar and Raghuwanshi "Single phase Bi-directional Electric vehicle battery charger with G2V, V2G & V2L Technologies." *IEEE Renewable Energy and Sustainable E-Mobility Conference,* P. 1-6, 2023.

[142] M. R. Khalid, M. S. Alam, A. Sarwar and M. S. Jamil Asghar "A Comprehensive review on electric vehicles charging infrastructures and their impacts on power-quality of the utility grid." *eTransportation,* Vol. 1, P. 100006, 2019.

[143] S. Chakraborty, H.N. Vu, M. M. Hasan, D.D. Tran, M. E. Baghdadi and O. Hegazy "DC-DC converter topologies for electric vehicles, Plug-in Hybrid Electric Vehicles and Fast Charging Stations: State of the art and future trends." Energies Vol. 12, no 8, P. 1569, 2019.

[144] M. S. Mastoi, S. Zhuang, H. M. Munir, M. Haris, M. Hassan, M. Usman, S. S. H. Bukhari and J.S. Ro "An in-depth analysis of electric vehicle charging station infrastructure, policy implications, and future trends." *Energy Rep.,* Vol. 8, P. 11504-11529, 2022.

[145] S. Hemavathi and A. Shinisha "A study on trends and developments in electric vehicle charging technologies." *J. Energy Storage,* Vol. 52, P. 105013, 2022.

[146] M. A. Hannan, M. S. Mollik, A. Q. Al-Shetwi, S. A. Rahman, M. Mansor, R. A. Begum, K. M. Muttaqi and Z. Y. Dong "Vehicle to grid connected technologies and charging strategies: Operation, control, issues and recommendations." *J. Clean. Prod.,* Vol. 339, P. 130587, 2022.

[147] R. Thamizharasan, V. Anbarasan, R. L. Priya and T. L. Joshua "Solar PV Array Based Multi-Functional Smart EV Charger." *IEEE, International Conference on Advanced Computing and Communication Systems (ICACCS),,*Vol. 1, P. 1731-1737, 2023.

[148] F. Mohammadi, G.A. Nazri and M. Saif "A bidirectional power charging control strategy for plug-in Hybrid Electric Vehicles." *Sustainability,* Vol. 11, P. 4317, 2019.

[149] H. Yu, S. Niu, Y. Shang, Z. Shao, Y. Jia and L. Jian "Electric vehicles integration and vehicle-to-grid operation in active distribution grids: A comprehensive review on power architectures, grid connection standards and typical applications." *Renew. Sustain. Energy Reviews.,* Vol. 168, P. 112812, 2022.

[150] Vadi, Bayindir, Colak and Hossain "A review on communication standards and charging topologies of V2G and V2H operation strategies." *Energies,* Vol. 12, P. 3748, 2019.

[151] S. Cundeva and A. Dimovski "Vehicle-to-grid system used to regulate the frequency of a microgrid." in *IEEE EUROCON -17th International Conference on Smart Technologies*, P. 456-460, 2017.

[152] Y. Teng, H. Li and F. Wu "Design of distributed fractional order PID type dynamic matrix controller for large-scale process systems." *IEEE Access,* Vol. 8, P. 179754–179771, 2020.

[153] A. F. Zobaa and H. E. Shady "Power quality in future electrical power systems." *Energy Engineering, IET Digital Library,* P. 200–230, 2017.

[154] A. A. Abdelsalam and A. M. Gabbar "Performance enhancement of hybrid AC/DC microgrid based D-FACTS." *International Journal of Electrical Power & Energy Systems,* Vol. 63, P. 382–393, 2014.

[155] L. V. Raviteja and G. Gurrala "A Review of Lithium-ion Battery Physics-based Models." *IEEE Power & Energy Society General Meeting.* P. 1-5, 2023.

[156] E. Elbakush and A. M. Sharaf "A FACTS Based Hybrid Filter Compensator (HFC) for H2V Battery Charging Schemes." *International Journal of Renewable Energy Research,* Vol. 3, P. 289-300, 2013.

[157] A. M. Sharaf and P. Kreidi "Power Quality Enhancement Using a Unified Compensator and Switched Filter-Capacitor Compensator." *RE&PQJ,* Vol. 1, no 1, 2003.

[158] A. M. Sharaf and P. M. S. KREID, "Electric power quality, harmonic reduction and power/energy saving using modulated power filters and capacitor compensators." IEEE, fredericton, NB, 1819-1819,2004.

[159] E. Kazemi-Robati, H. Hafezi, M. S. Sepasian and B. Silva "Probabilistic planning of virtually-hybrid harmonic filters inmodern distribution systems." *in International Conference on Smart Energy Systems and Technologies (SEST)*, P. 1-6, 2023.

[160] S. D. Biswas, S. Chowdhury, C. Nandi and B. Das "Power quality improvement with hybrid shunt active power filter." *in IEEE International Conference on Power Electronics, Smart Grid, and Renewable Energy (PESGRE)*, P. 1- 6, 2023.

[161] A. M. Sharaf and B. Khaki "A novel FACTS hybrid modulated filter/capacitor compensator." *in International Conference on Smart Grid (SGE)*, P. 1-6, 2012.

[162] R. S. Yallamilli and M. K. Mishra "Instantaneous symmetrical component theory based parallel grid side converter control strategy for microgrid power management." *IEEE Trans. Sustain. Energy,* Vol. 10, P. 682-692, 2019.

[163] M. E. Şahin and A. M. Sharaf "A robust decoupled microgrid charging scheme using a DC green plug-switched filter compensator." in *Fast Charging and Resilient Transportation Infrastructures in Smart Cities*, Cham, Springer International Publishing, P. 89-116, 2022.

[164] A. M. Sharaf "A novel filter compensation scheme for hybrid (photovoltaic-fuel cell)-dc utilization systems." *International Journal of Advanced Renewable Energy Research,* Vol. 1, P. 283-291, 2012.

[165] Y. Xie, Q. Ma, J. Gu and G. Zhou "Event-triggered fixed-time practical tracking control for flexible-joint robot." *IEEE Transactions on Fuzzy Systems ,* Vol. 1, P. 67-76, 2022.

[166] M. Alghassab "Performance Enhancement of Stand-Alone Photovoltaic Systems with household loads." *in 2nd International Conference on Computer Applications & Information Security (ICCAIS)*, P.1-6, IEEE, 2019.

[167] S. Fry, M. Irtiza, A. Hoffman and Y. Sardahi "Fuzzy Logic Control for Flexible Joint Manipulator: An Experimental Implementation." *International Journal of Mechanical and Mechatronics Engineering,* Vol. 18, P. 16-20, 2024.

[168] W. Chao, L. Dai, J. Huang and M. Chen "Research on hybrid active power filter and its control and protection system for LCC-HVDC." *in IEEE 11th Joint International Information Technology and Artificial Intelligence Conference (ITAIC)*, Vol. 11, P.139-142, 2023.

[169] L. Wang, W. Sun, H. Xu, J. Dong, C. Li and W. Li "A three-phase-module-parallel Si & SiC hybrid inverter with smaller filter size and low cost." *in IEEE Transportation Electrification Conference and Expo, Asia-Pacific (ITEC Asia-Pacific)*, P.1-6, 2022.

[170] E. O. H. Catata, P. J. Dos Santos Neto, M. V. De Paula, J. P. Carvalho Silveira, T. A. D. S. Barros and E. Ruppert Filho "In-loop adaptive filters to improve the power quality of switched reluctance generator in WECS." *IEEE Access,*Vol. 10, P. 2941-2951, 2022.

[171] V. Singh, S. J. Iqbal, S. Gupta and A. Yadav "Performance evaluation of A shunt active power filter for current harmonic elimination." *in IEEE Region 10 Symposium (TENSYMP)*, P.1- 6, 2021.

[172] V. L. Lima and T. J. M. Dezuo "Robust switching rule design for single-phase shunt active power filter." *in Brazilian Power Electronics Conference (COBEP)*, P.1- 4, 2021.

[173] H. Lin, L. Wu, X. Guo and G. Chen "Shunt active power filter using SiC-MOSFET with high accuracy compensation." *in IEEE 9th International Power Electronics and Motion Control Conference (IPEMC-ECCE Asia)*, P. 2872-2876, 2020.

[174] D. Daftary and M. T. Shah "Design and analysis of hybrid active power filter for current harmonics mitigation." *in IEEE 16th India Council International Conference (INDICON)*, P.1- 4, 2019.

[175] D. H. S. Nolasco, D. K. Alves, F. B. Costa, E. S. Palmeira, R. L. A. Ribeiro and E. A. F. Nunes "Application of fuzzy systems in power quality: Diagnosis of total harmonic distortions." in *2018 IEEE International Conference on Fuzzy Systems (FUZZ-IEEE)*,P.1-6, IEEE, 2018.

[176] F. Nejabatkhah and Y. Li "Power quality control of smart hybrid AC/DC Microgrids: An Overview." in *IEEE conference. Translations and content mining*, P. 2169-3536, 2019.

[177] A. H. Qutaiba, A. Al-Bashayreh, M. Kiftaro and M. A. Alsheikh "An Intelligent Controller for an Assisted Electric Wheelchair based on Interval Type-2 Fuzzy Logic." in *Science and Engineering Technology International Conferences (ASET), IEEE,* P.1-6, 2023.

[178] J. Zhang, L. Zhang, F. Sun and Z. Wang "An overview on thermal safety issues of lithium-ion batteries for electric vehicle application." *IEEE Access,* Vol. 6, P. 23848-23863, 2018.

[179] S. Agrawal, D. Sharma, V. K. Gupta & R. K.Somani "Performance Evaluation of 3-Phase 4-Wire SAPF based on Synchronizing EPLL with Fuzzy Logic Controller." in *IEEE International Conference on Power Electronics, Intelligent Control*, P. 483-487,2018.

[180] H. Hagras "A Hierarchical type-2 Fuzzy Logic Control Architecture for Autonomous Mobile Robots." *IEEE Transactions on Fuzzy Systems,* Vol. 12, P. 524-539, 2004.

[181] H. H. Aly "A Proposed Hybrid Machine Learning Model Based on Feature Selection Technique for Tidal Power Forecasting and Its Integration." *Electronics* 13.11: 2155, 2024.

[182] J. Mendel, H. Hagras, W.W. Tan, W. W. Melek and H. Ying "Introduction to Type-2 Fuzzy Logic Control: Theory and Applications." Hoboken, New: John Wiley & Sons, Inc, P.32-79, 2014.

[183] A. M. Sharaf and P. Kreidi "Power quality enhancement using a unified switched capacitor compensator." *in CCECE Canadian Conference on Electrical and Computer Engineering. Toward a Caring and Humane Technology (Cat. No.03CH37436)*, P. 331-333, 2004.

[184] P. Kreidi " Electric power quilty, harmonic reduction and power/energy saving using modulated power filters and capacitor compensators." Thesis, New Brunswick - Canada, 2003.

APENDIX A

Published Papers from This Work

Journal Papers:

1. **Bloul, Albe M**., Adel M. Sharaf, Hamed H. Aly, and Jason Gu. 2024. "A Low Impact V2H Battery Charging Station Using an AC Green Plug Switched Filter Scheme." ***IEEE*** *Access: Practical Innovations, Open Solutions 12*: 81410–27. https://doi.org/10.1109/access.2024.3411408.
2. **Bloul, Albe M.,** Mohamad Abuhamdah, Adel M. Sharaf, Hamed H. Aly, and Jason Gu. "An Efficient Shunt Modulated AC Green Plug–Switched Filter Compensation Scheme for Nonlinear Loads." MDPI, Energies 17, no. 10 (2024): 2426.
3. **Bloul**, **Albe M.,** Adel M. Sharaf, Hamed H. Aly and Jason Gu, "An Energy Efficient Green Plug Filter Compensation Scheme for Hybrid Nonlinear Loads", International Journal of Engineering Innovation & Research Volume 12, Issue 5, ISSN: 2277 – 5668, (2023).
4. **Bloul**, **Albe M.,** Adel M. Sharaf, Hamed H. Aly and Jason Gu, "A Novel AC Green Plug Switched Filter Scheme for Low Impact Efficient V2G Battery Charging Stations", *International Transactions on Electrical Energy Systems, Wiley,* (2024).

Conference Papers:

5. **Bloul, A. M.,** A. M. Sharaf, H. M. Mosbah, and Mohamed E. El-Hawary. "A robust fuzzy logic controller for a Green Plug-switched filter for nonlinear loads." In 2015 IEEE 28th Canadian Conference on Electrical and Computer Engineering (CCECE), pp. 1409-1413. IEEE, 2015.
6. **Bloul, A. M.,** Adel Sharaf, and Mohamed El-Hawary. "An Energy Saving Green Plug Device for Nonlinear Loads." In IOP Conference Series: Earth and Environmental Science, Volume 127, 2017 International Conference on Renewable Energy and Environment (ICREE) 1-3 November 2017, Toronto, Canada.

APENDIX B: 3.1

Device	Value
FACTS-GP Controller	γ_p= 10, γ_Q = 0.75
Frequency	f_S=3700 Hz
Gains	K1 = K2 = 0.35

APENDIX C: 3.2

Utility Grid	**3 phases, 2 poles**	
	11KV LL X/R ratio 10 MVA Short Circuit 75-100 MVA	
Transmission Line	500 KV (L-L), 8 km	
	R1/km=0.01273 Ω, R0/km = 0.3864 Ω L1/km=0.9337mH, L0/km = 4.1264 mH C1/km=12.74e µF, C00/km = 7.751 µF	
Base Power VS Bus Base Power VL Bus	100 MVA 200 MVA	
Transformer	11 kv/600v at 300-500 KVA	
Frequency	3700 Hz	
MFCC	C_a=275µF, C_b = 275µF, C_c = 275µF	
	R_f=0.15Ω, L_f =3mH	
Hybrid AC Load	Induction Motor	30 MVA, 4 poles
		Rs=0.01965 pu Ls=0.0397 pu
		Rr=0.01909 pu Lr=0.0397 pu
		Lm=1.354 pu.
	Linear Load	P=3000 KW, Q=4 MVAr
	Nonlinear Load	20 MVA, PF=0.85

APENDIX D: 4.1

Parmeter	Value
Source Voltage	240 v
Frequency	60 Hz
R_{AC} Side and R_{DC} Side	0.05Ω, 0.05Ω
L_{AC} Side and L_{DC} Side	3mH, 3mH
C_s, C_r	275 μF, 275 μF
C_d, C_B	225 μF, 225 μF
MFCC	C_f=225μF, C_{fl}=225μF, C_r=300μF
	Rf=0.05 Ω, Lf =3mH
Battery _ Lithium-lon	650Ah, 300v, SOC 50%

APPENDIX E: 5.1

Lithium-ion Battery Parameters	
Parameters	Value
Nominal Voltage	240V DC
Internal R, Initial SOC	2.4 mΩ, 50%
Rated Capacity, Max Capacity	650 Ah, 650 Ah
Fully Charged, Nor. Discharge Current	349.2 V DC, 543.5 A
Capacity at Nor. Voltage.	1130.4 V
Expon.volt. zone.	324.116 V
Buck-Boost Converter Parameters	
Ro, Lo	50 mΩ,5 mH

APPENDIX F: 5.2

AC and DC Side Parameters	
$R_{AC\ Side}, R_{DC\ Side}$	0.05 Ω
$L_{AC\ Side}, L_{DC\ Side}$	3 mH
$\{C_s, C_r\}, \{C_d, C_B\}$	275 µF, 2750 µF
V_S, S. C. Level, S. C. Level	11 kV, 50 MVA
MFCC-HFC Parameters	
C_F, C_{F1}, C_r	225 µF, 225 µF, 300 µF
R_F, L_F	0.05 Ω,3 mH
WMPID Controller Parameters	
Kp, K_i, K_d, γ_e, γ_R	0.1, 0.05, 0.05, 0.5, 0.1
γV_R, γI_R, γV_d, γI_d , γV_B, γI_B	1, 0.5, 1, 0.5, 1, 0.5

APPENDIX G: 6.1

Parameters	Value
AC Utility Grid Parameters	
Nominal Voltage	138 KV (L-L), 100 MW
Ratio X/R	10
Base Power Vs Bus	100 MVA
Base Power VL Bus	200 MVA
Frequency	1.750 KHz
FACTS-MFCC Parameters	
C_F	275µF
R_D, R_F,L_F	1Ω, 0.15Ω, 3mH
Width Modulation Proportional Integral Derivative (WMPID) Controller Parameters	
Ke, Kp, K_i, K_d, γ_e, γ_R	0.7, 5, 1.5, 0.5, 0.5, 0.1
Transmission Line	
Feeder	25 kv(L-L),10 km
R/km, L/km	0.4Ω, 0.45Ω

APPENDIX H: 6.2

Parameters	Value
Transformer Parameters	
Power Transformer 1	138 KV to 25kv, 5 MW
Power Transformer 2	25 KV to 4.16kv, 5 MW
Hybrid AC Load Parameters	
Induction Motor	2.5 MVA, 4 poles
	Rr = 0.01807p.u., Lr = 0.0497 pu.
	Lm =1.354 pu.
Linear Load	P = 2500 KW, Q = 2 MVAr
Nonlinear Load	P = 1250 KW, Q = 2 MVAr

Appendix I

NON-EXCLUSIVE DISTRIBUTION LICENSE

I, Albe M. Bloul, grant Dalhousie University the non-exclusive right to reproduce and distribute your submission worldwide in any medium.
I agree that Dalhousie University may, without changing the content, reformat the submission for the purpose of preservation.

I also agree that Dalhousie University may keep more than one copy of this submission for purposes of security, back-up, and preservation.

I agree that the submission is your original work, and that I have the right to grant the rights contained in this license. I also agree that my submission does not, to the best of my knowledge, infringe upon anyone's copyright.

I agree that I have obtained the unrestricted permission of the copyright owner to grant Dalhousie University the rights required by this license, and that such third-party owned material is clearly identified and acknowledged within the text and content of the submission.

Appendix J
TUNED-ARM FILTER MODULATION SCHEME

Tuned-Arm Filter Model

According to [184], The tuned-arm filter scheme is shown in Figure Q. 1 where VF is the voltage across the filter. A semiconductor switch such as GTO, MOSFET, Triac, and IGBT plus Bridge can perform the switching function. The modulated/switching circuit is operated with pulse width modulation (PWM) and controlled by an on-line dynamic tracking controller as shown in Figures A. 1 to A.8 (Appendix A: Dynamic Controller Schemes). The dynamic tracking controller can be a single loop, dual, or tri-loops circuit. The switched/modulated filter can be adjusted by the duty cycle ratio CD=ton/Ts/w to represent an equivalent shunt impedance, hence adjusting the current flowing in the filter so as to compensate for any feeder inrush or on/off current fluctuations or waveform distortions, such as flickering and quasi-static harmonic content.

The modulated tuned-arm filter TAF scheme can be derived as follows: Assume that the voltage across the filter has a sinusoidal waveform with the expression of $V_F=V_m\sin(wt+\varphi)$, where, w is the fundamental frequency, (P is the initial phase angle with respect to a common voltage reference

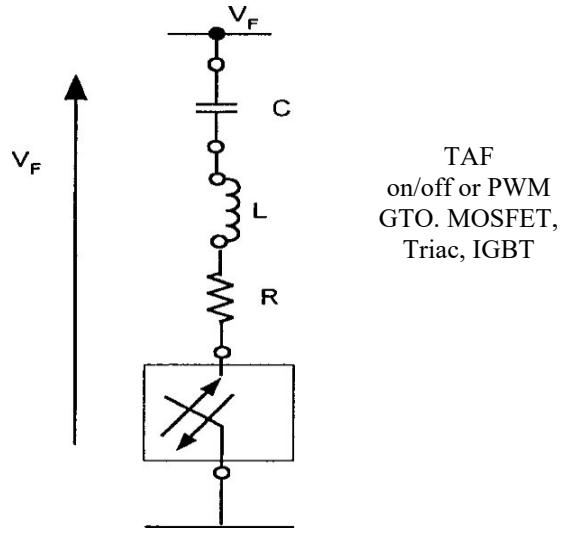

Figure Q. 1: Tuned-Arm Filter Layout

Considering the filter circuit, when the filter is turned on, the voltage across the filter can also be obtained as:

$$V_F = \frac{1}{C}\int i_F dt + L\frac{di_F}{dt} + Ri_F \quad \text{(Q.1)}$$

The impedance of the filter can be written in the Laplace Transform function as:

$$Z_F(s) = \frac{1}{sC} + sL + R = \frac{1+s^2LC+sRC}{sC} = \frac{s^2LC+sRC+1}{sC} \quad \text{(Q.2)}$$

Therefore, during the "on" duration period of the filter (ton), the voltage can be expressed:

$$V_F = Vm \sin(\omega t + \varphi) \bullet [u(t) - u(t-t_0)] \quad \text{(Q.3)}$$

Where, u (t) is a step function that has unit value from t=0 to t= t_0 and zero value for all other time as shown in figure Q.2. This function is described as a pulse of unit magnitude and duration to and represents the turning on/off. Also t_0 is the turning on time of the filter; therefore, the filter current IF can also be expressed in the Laplace transform function.

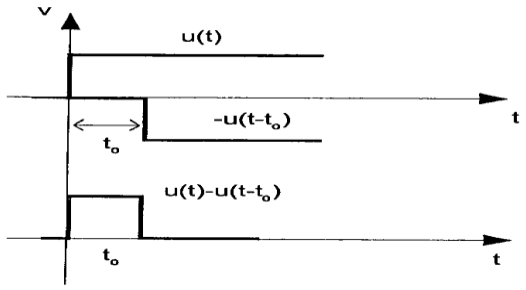

Figure Q.2: The Linear Combination of two Unit Step Functions to describe a Pulse of Amplitude 1 and duration t_0

When using Laplace transform of equation (Q.3) becomes:

$$\mathscr{L}V_F = \mathscr{L}V_m \sin(\omega t + \varphi) \bullet [u(t) - u(t-t_0)] \quad \text{(Q.4)}$$

The Laplace Transform of V_F can be written as and expression (Q.4) becomes:

$$Z_F(s) \bullet I_F(s) = V_m \sin(\omega t + \varphi) \bullet [u(t) - u(t-t_0)] \quad \text{(Q.5)}$$

The filter current I_F can be written as:

$$I_F(s) = Y_F(s) \bullet V_m \left\{ \frac{(\sin\varphi s + \cos\varphi\omega) - \sin[(\omega t_0 + \varphi)s + \cos(\omega t_0 + \varphi)\omega] e^{-st_0}}{s^2 + \omega^2} \right\} \quad \text{(Q.6)}$$

Where $Y_F(s)$ is the filter admittance and equal the inverse of the impedance:

$$Y_F(s) = \frac{1}{Z_F(s)} = \frac{Cs}{LCs^2 + RCs + 1} \quad \text{(Q.7)}$$

Therefore, the current IF expression becomes:

$$I_F(s) = \frac{Cs}{LCs^2 + RCs + 1} \bullet \left\{ \frac{(\sin\varphi s + \cos\varphi\omega) - [\sin(\omega t_0 + \varphi)s + \cos(\omega t_0 + \varphi)\omega] e^{-st_0}}{s^2 + \omega^2} \right\} \quad \text{(Q.8)}$$

Where $t_0 = \alpha * T_{s/w}$, $T_{s/w}$ is the selected switching period of the switching function, and $f_{s/w}=1/T_{s/w}$ is the switching signal frequency from 100-1200Hz, and α is the duty cycle ratio of the control pulse varying from 0-1.0.

Q.2 Tuned-Arm Filter Model Characteristics with Varying Conditions

The frequency response of the TAF power filter model is shown in Figures Q.3 (a) &(b) and Q.4 (a) & (b). Figure Q.3 (a) illustrates the current amplitude frequency response when varying the values of the filter parameters (R, L, C) and keeping the duty cycle ratio 01 constant. It shows that when the filter parameters (R, L, C) change, the central frequency of the filter will change consequently, and the smaller the (R, L, C) values, higher the current frequency response. This can be used to select and optimize the filter parameter depending on the dominant harmonic frequency. Figure Q.4 (b) shows the phase angle frequency response with the changing (R, L, C) and constant. Figure Q.4 (a) depicts the effect of the duty cycle ratio 01 varying from 0 to 1.0, and the values of the filter parameters are constant. The larger the duty cycle ratio a, the higher the filter current IF frequency response, or the lower the equivalent impedance (Z_F) and the higher the current flowing into the filter. The duty cycle ratio u can be modulated by different dynamic control strategies using different feedback control signals. Figure Q.4 (b) shows the phase angle frequency response while varying the duty cycle ratio u and keeping the filter parameters constant. Figure Q.5 (a) & (b) depicts the modulated admittance as function of filter parameters.

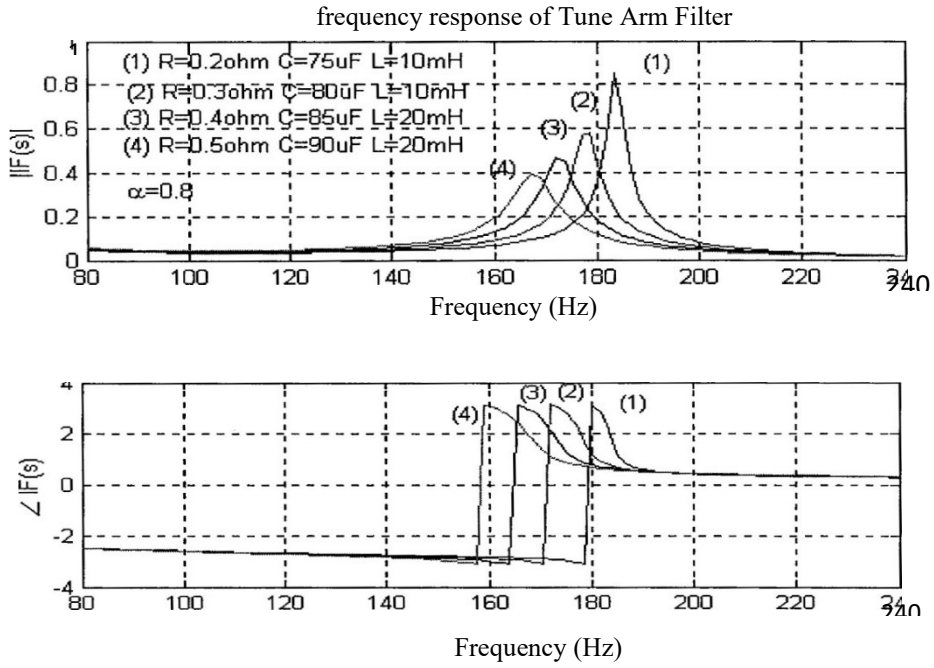

Figure Q.3: Frequency Response of the Tuned-Arm Filter with Varying Filter parameters R, L, C and Fixed Duty Cycle CD—ton/Ts/w

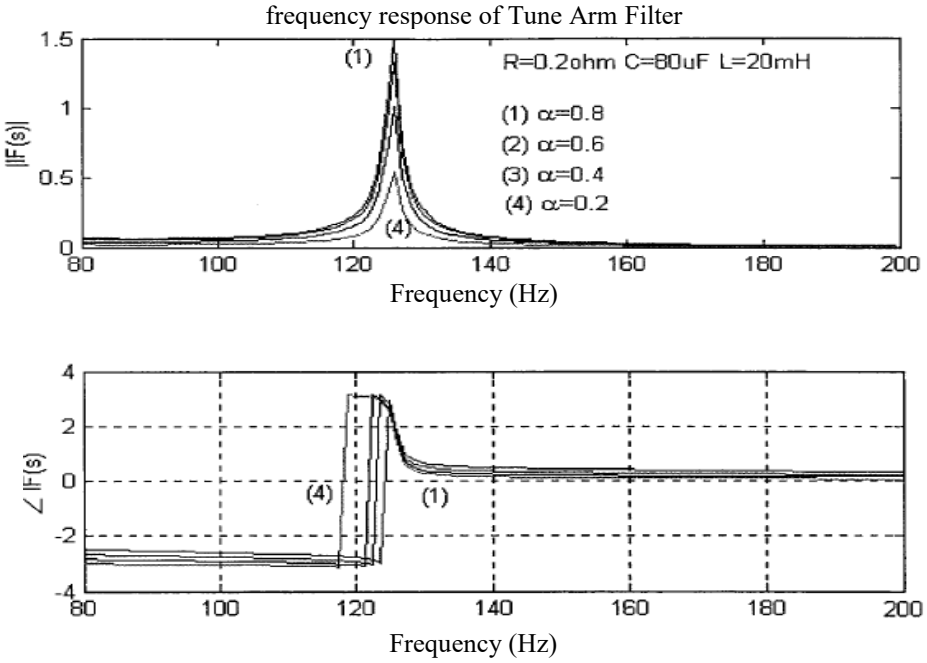

Figure Q.4: Frequency Response of the Tuned-Ann Filter with Fixed Filter parameters R, L, C and Varying Duty Cycle α_D

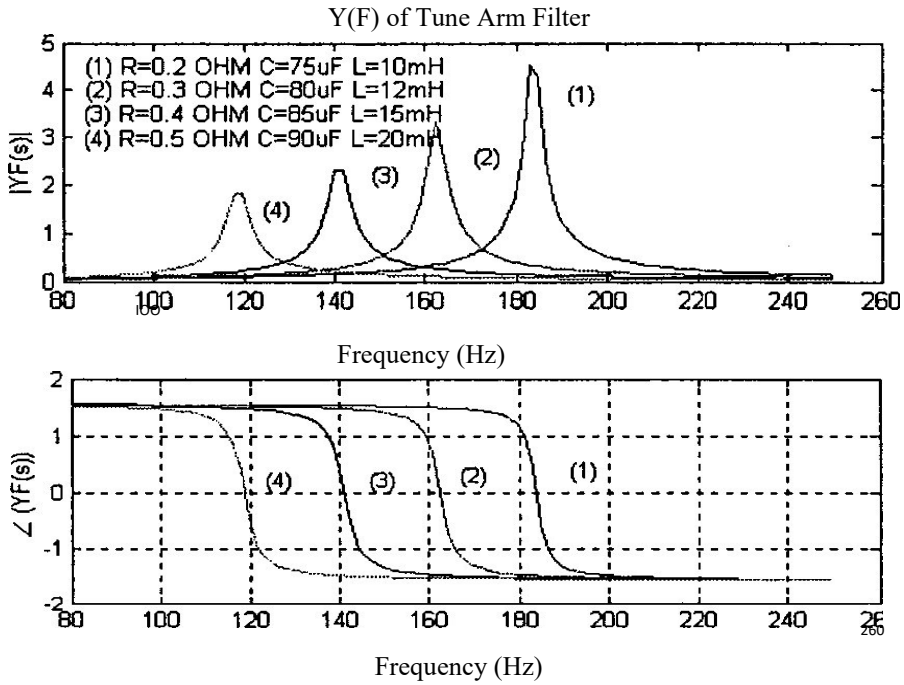

Figure Q.5: Frequency Response of Y(F) (Tuned-Arm Filter) with Varying Filter parameters R, L, C.

Appendix K

C-TYPE FILTER MODULATION SCHEME

R.1 C-Type Power Filter Model

According to [184], The C-type power filter scheme is shown in Figure R.I where VF is the terminal voltage across the filter. A semiconductor solid-state switch such as SSR, GTO, MOSFET, Triac, and IGBT plus bridge can perform the switching function. The modulated filter and switching circuit is operated with a pulse-width modulation (PWM) strategy and controlled by on-line dynamic tracking controllers as shown in Figures A. I to A.8 (Appendix A: Dynamic Controller Schemes). The dynamic tracking controller can be a single loop, dual, or tri-loop control schemes. The C-type filter can be modulated via PWM-switching to provide an adjustable equivalent shunt impedance, hence adjusting the current flowing in the filter so as to compensate for feeder dynamic or on/off current fluctuations and distortions, flickering and harmonic contents.

The C-type filter scheme can be derived as follows: Assume that the voltage across the filter has a sinusoidal waveform with the expression of $V_F = V_m \sin(\omega t + \varphi)$ where, w is the fundamental frequency, φ is the initial phase angle for a specified reference voltage.

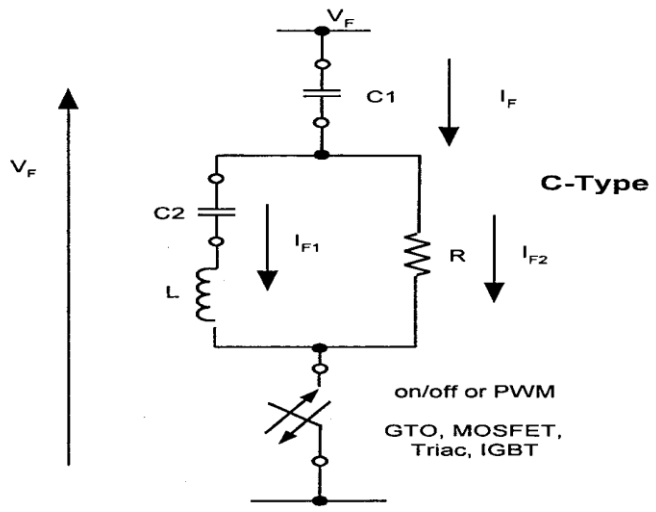

Figure R. 1: C-Type Low Q Filter Layout

Considering the filter circuit, when the filter is turned on, the voltage across the filter can also be obtained as:

$$V_F = \frac{1}{C_1}\int i_F dt + \left[\frac{\left(\frac{1}{C_2}\int i_{F1}dt + \frac{Ldi_{F1}}{dt}\right)}{Ri_{F2}}\right] \quad \text{(R.1)}$$

The impedance of the filter can be written in the Laplace Transform function as:

$$Z_F(s) = \frac{s^3RLC_1C_2 + s^2LC_2 + sR(C_1+C_2)+1}{s^3LC_1C_2 + s^2RC_1C_2 + sC_1} \quad \text{(R.2)}$$

Therefore, during the tuning "on" period of the filter (ton), the voltage can be expressed:

$$V_F = V_m \sin(\omega t + \varphi) \bullet [u(t) - u(t - t_0)] \quad \text{(R.3)}$$

Where, u (t) is a function that has unit value from t=0 to t=t_0 and zero value for all other time as shown in Figure Q.2 (Appendix Q). This function is described in detail in Appendix Q

When using Laplace transform, expression (R.3) becomes:

$$\mathscr{L}(V_F) = \mathscr{L}(V_m \sin(\omega t + \varphi) \bullet [u(t) - u(t - t_0)]) \quad (R.4)$$

The Laplace Transform of VF can be written as and expression (R.4) becomes:

$$Z_F(s) \bullet I_F(s) = \mathscr{L}(V_m \sin(\omega t + \varphi) \bullet [u(t) - u(t - t_0)]) \quad (R.5)$$

The filter current IF can be written as:

$$I_F(s) = Y_F(s) \bullet V_m \left\{\frac{(\sin\varphi s + \cos\varphi\omega) - \sin[(\omega t_0 + \varphi)s + \cos(\omega t_0 + \varphi)\omega]e^{-st_0}}{s^2 + \omega^2}\right\} \quad (R.6)$$

Where YF(s) is the filter admittance and equal the inverse of the impedance:

$$Y_F(s) = \frac{1}{Z_F(s)} = \frac{s^3 LC_1C_2 + s^2 RC_1C_2 + sC_1}{s^3 RLC_1C_2 + s^2 LC_2 + sR(C_{1+C_2}) + 1} \quad (R.7)$$

Therefore, the current IF expression becomes:

$$I_F(s) = \frac{s^3 LC_1C_2 + s^2 RC_1C_2 + sC_1}{s^3 RLC_1C_2 + s^2 LC_2 + sR(C_{1+C_2}) + 1} \bullet \left\{\frac{(\sin\varphi s + \cos\varphi\omega) - \sin[(\omega t_0 + \varphi)s + \cos(\omega t_0 + \varphi)\omega]e^{-st_0}}{s^2 + \omega^2}\right\} \quad (R.8)$$

Where $t_0 = \alpha_D * T_{s/w}$, Ts/w is the selected switching period of the switching function, and fs/w=1/Ts/w is the switching signal frequency from 100-1200Hz, and α is the duty cycle ratio of the control pulse varying from 0-1.0.

R.2 C-Type Power Filter Model Characteristics for Varying Parameters and Duty Cycle α_D

The frequency response of the C-type filter model is shown in Figures R.3 (a) &(b) and R.4 (a) & (b). Figure R.3 (a) illustrates the amplitude frequency response when varying the values of the filter parameters (R, L, Cl, C2) and keeping the duty cycle ratio αconstant. It shows that when the filter parameters (R, L, Cl, C2) change, the central frequency of the filter will change consequently, and the higher the (R, L, Cl, C2) values, higher the current frequency response. This can be used to select and optimize the filter parameter depending on the dominant harmonic frequency. Figure R.4 (b) shows the phase angle frequency response with the changing (R, L, Cl, 02) and oc constant. Figure R.4 (a) depicts the effect of the duty cycle ratio varying from 0 to 1.0, and the values of the filter parameters are constant. The larger the duty cycle ratio a, the higher the filter current IF frequency response, or the lower the equivalent impedance (Z_F) and the higher the current flowing into the filter. The duty cycle ratio a can be modulated by different dynamic control strategies using different feedback control signals. Figure R.4 (b) shows the phase angle frequency response while varying the duty cycle ratio and keeping the filter parameters constant. Figure R.5 (a) & (b) depicts the modulated admittance as function of C-type filter varying parameters.

frequency response of Tune Arm Filter

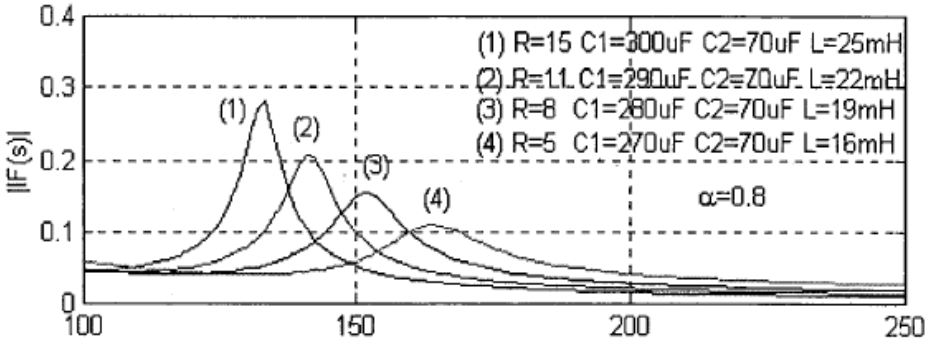

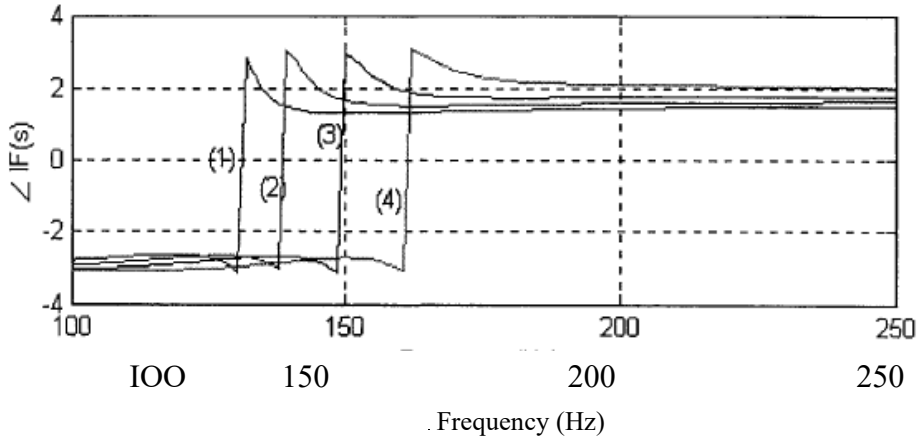

IOO 150 200 250

Frequency (Hz)

Figure R.2: Frequency Response Magnitude & phase vs Frequency of the C-type Filter with Varying Filter parameters R, L, C 1, C2 and Fixed Duty Cycleα_D

frequency response of Tune Arm Filter

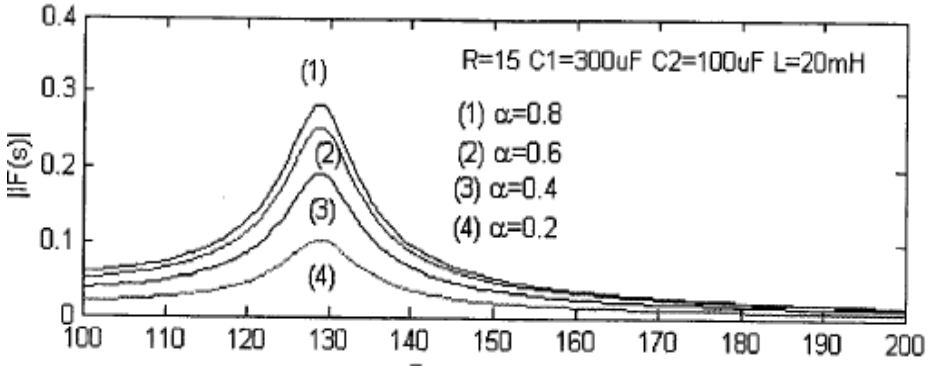

Frequency (Hz)

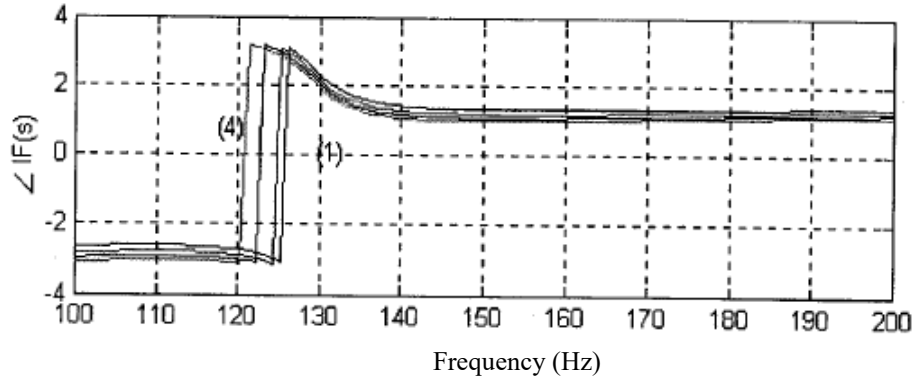

Frequency (Hz)

Figure R.3: Filter Current Frequency Response Magnitude & phase vs Frequency of the C-type Filter with Fixed Filter parameters R, L, C 1, C2 and Varying Duty Cycle

Y(F) of c-Type Filter

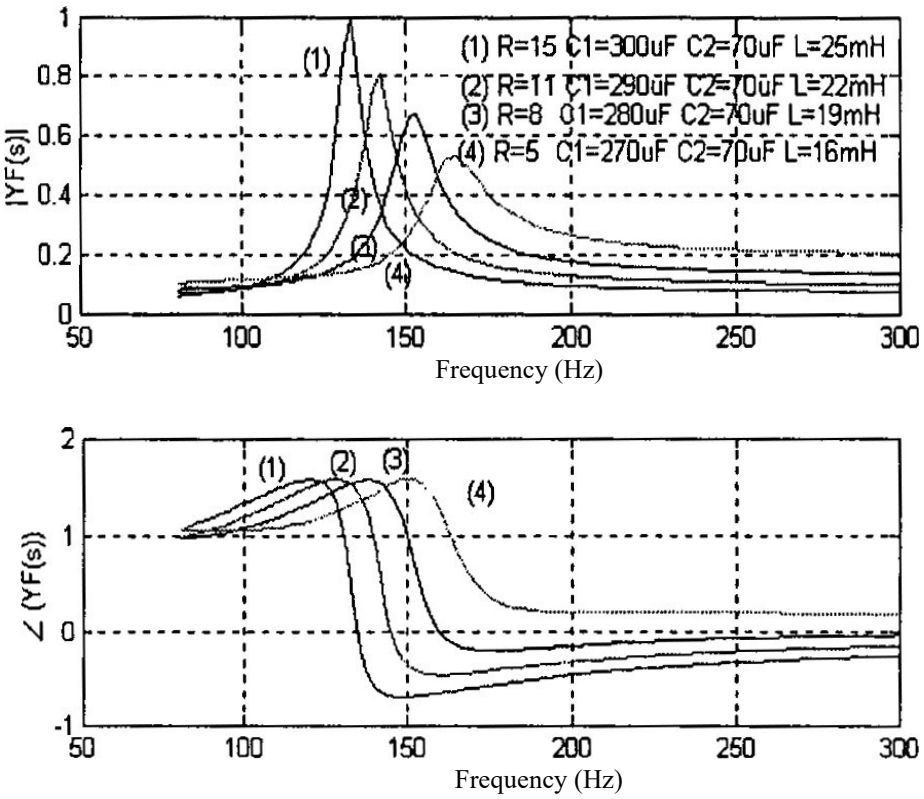

Figure R.4: Frequency Response of Y(F) (C-Type Filter) with Varying Filter parameters R, L, C 1, C2.

Appendix L

TESTING: SWITCH-MODE-POWER-SUPPLY AND TEMPORAL TYPE NONLINEAR LOADS WITH TAF

s.1 Switch Mode Power Supply With TAF

According to [184], Some results from laboratory testing are presented and discussed in this Appendix. The test set-up is shown in Figure S. 1. The AC supply voltage is 120VAC supply. The power filter used is a switched/modulated tuned-arm type filter.

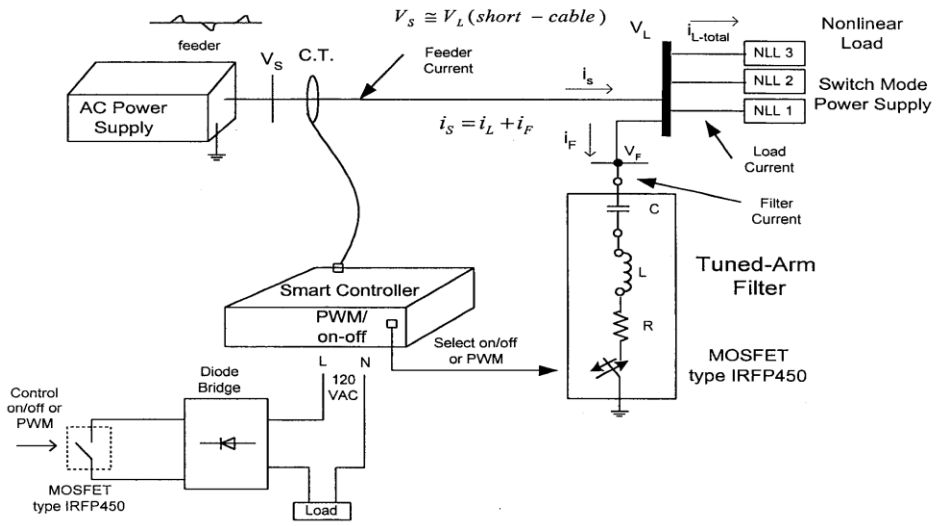

Figure S. 1: Test Set-Up for the witched/Modulated Power Filter

The test instruments used are the Fluke 43 - (Power Quality Analyzer) and the Fluke 97 -(Scope-meter). A nonlinear Switch Mode Power Supply load is used. This nonlinear load is the most common consumer nonlinear device causing a great deal of power quality PQ problems due to their massive use and proliferation around the world. The dynamic controller used is a simple dynamic current tracking controller type.

Figures S.2 to S. 17 show sample test results for the voltage and current dynamic response without and with the tuned-arm filter using the simple PWM-switching strategy.

Figures S2 (a) & (b) & S3 (a) and (b) show Fast Fourier transform (FFT) spectrum of the feeder current (Is) with the total harmonic distortion (THI)i. The FFT has been applied to the sampling feeder current (i_s) without and with the modulated tuned arm-filter. Comparing Figure S2 (a) and (b), or S3 (a) and (b), it is observed that the harmonic ripple contents have been reduced significantly especially for the high order harmonics (from 68.9% to 15.0% or from 68.9% to 31.1%, depending on the values of filter parameters).

Figures S4 (a) & (b) depict The Fast Fourier transform (FFT) of the feeder load bus Voltage (VL) with the total harmonic distortion (THD)v. The FFT has been applied to the sampling Feeder Voltage (VL) without and with the filter. Comparing figure S4 (a) and (b), it is observed that the harmonic contents have been slightly reduced.

Figure S5 (a) and (b) depicts the Feeder current (i_s), load voltage V_L, without and with the modulated PWM-tuned-arm power filter. It is observed that Feeder current waveform distortion has been reduced and power quality is greatly enhanced.

Figure S6 (a) and (b) depicts the Feeder powers (Ps, ss) current waveforms and power factor PF of the feeder without and with the modulated tuned-arm power filter. It is observed that the power factor has been improved from PF=0.71 to PF=0.94, which is highly desirable.

Figure S.7 shows the Load current (i_L) and load voltage V_L, with the PWM-modulated tuned-arm power filter. Figure S.8 depicts the tuned-arm filter voltage and current (V_F, I_F). Figures S.9, S.11 & S.12 show the PWM-MOSFET switching signal and Figures S. 10 & S. 17 show the MOSFET/Bridge current. Figures S. 13 to S. 16 show the signal through the controller. The modulated tuned-arm filter parameters are C=80 μF, L=80 mH and R=40 Ω or R = 5 Ω.

It is evident that the power quality (PQ) is enhanced, and source current waveform distortion is greatly reduced. (THD)i is reduced by over 55% from 68.9% to 31.1% (or from 68.9% to 15.1% when R=5Ω). The propose modulated filter with the simple current tracking control scheme can be utilized to enhance both power quality, reduce harmonics and improve the power factor at the expense of a noticeable increase in the source current needed for pulsed waveform fill-in factor.

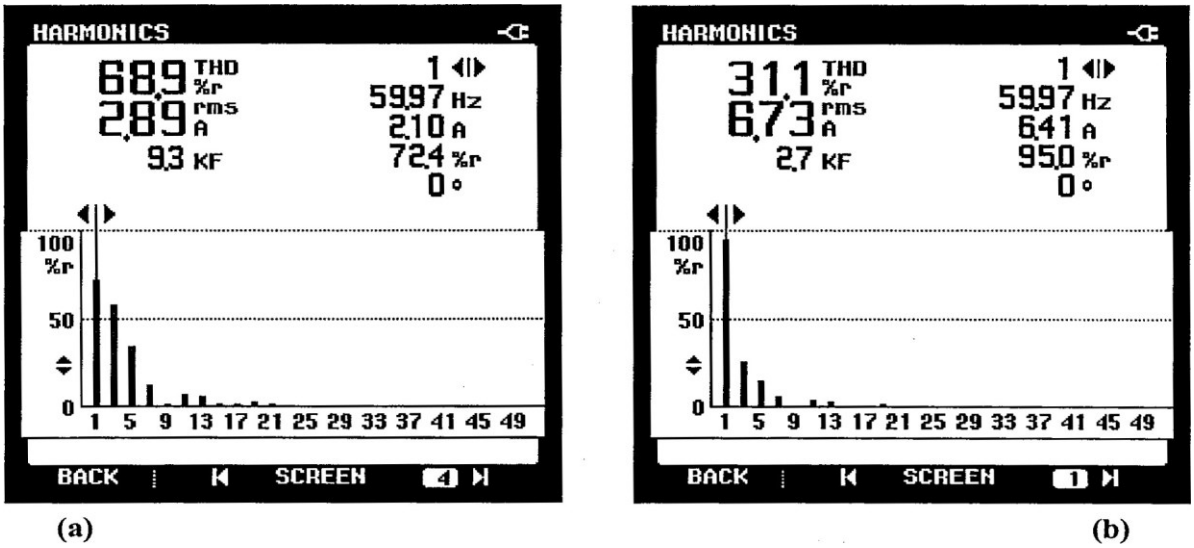

Figure S .2 Frequency-Spectra of Feeder Current (i_s)
(a) Without the TAF and (b) With the TAF (THD)i
Dropped from 68.9% to 31.1%.

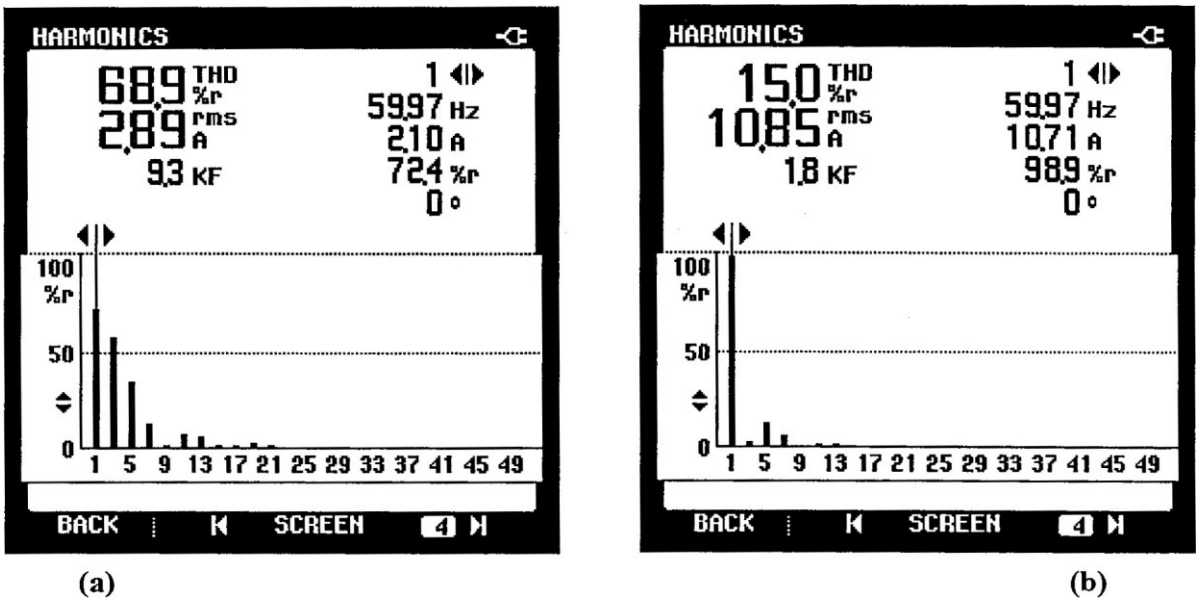

Figure S.3 Frequency-Spectra of Feeder Current (*is*)
(a) Without the TAF and (b) With the TAF
(THD)i Dropped from 68.9% to 15.0%

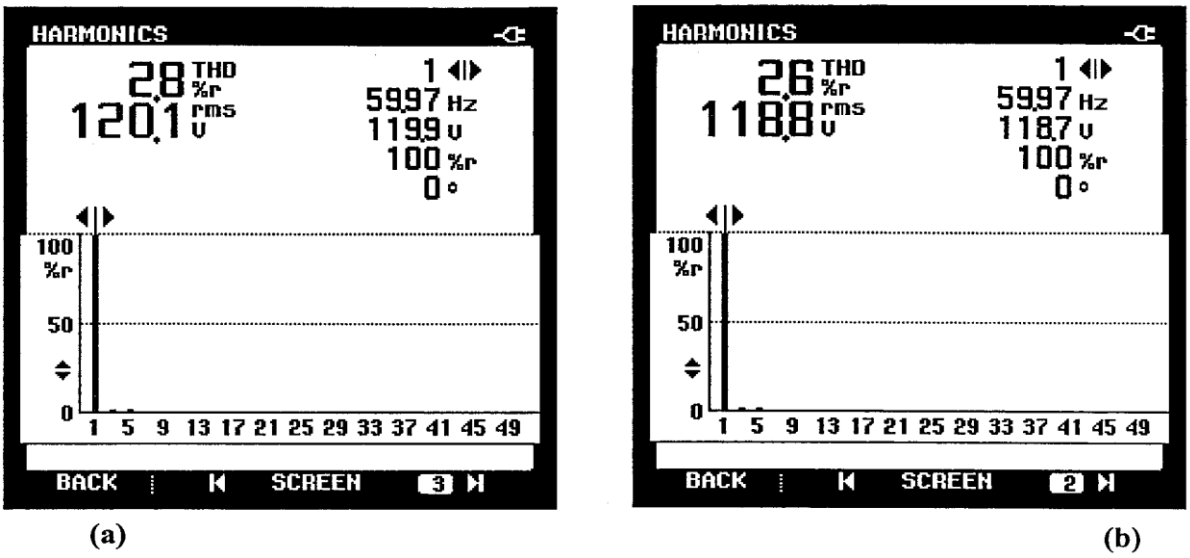

Figure S.4 Frequency-Spectra of feeder Voltage VL
(a) Without the TAF and (b) With the TAF

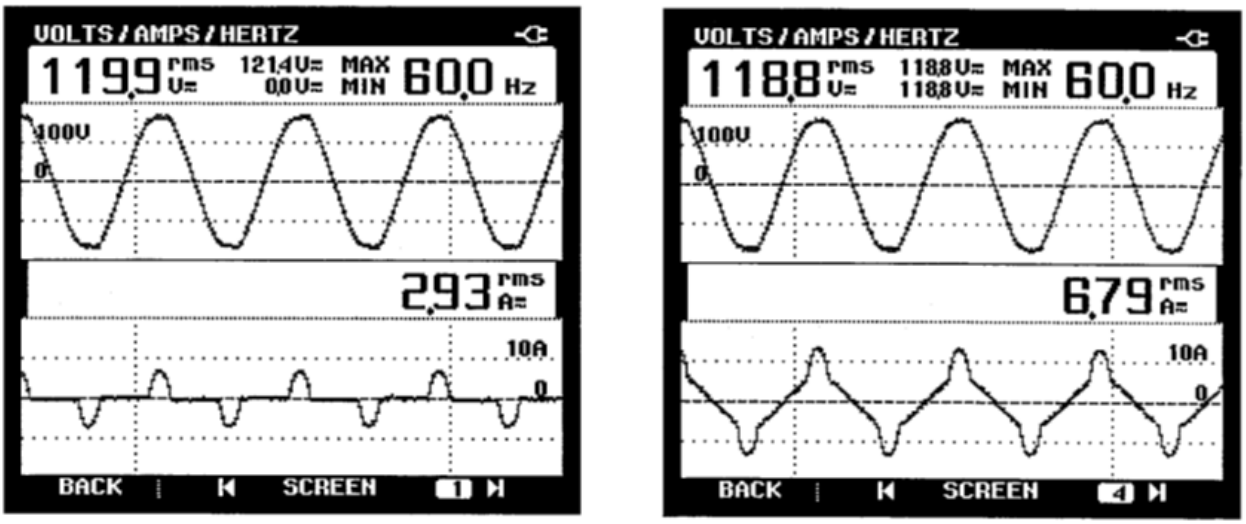

(a) (b)

Figure S.5 Feeder Voltage and Pulsed Current Waveforms
(a) Without the TAF and (b) With the TAF(a)

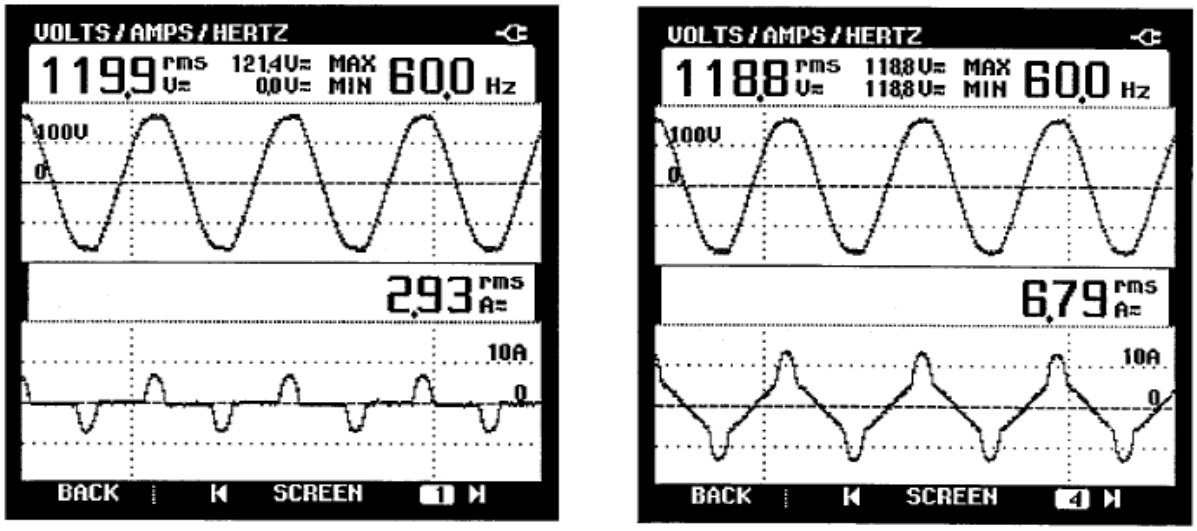

(a) (b)

Figure S.6 Feeder Power Ps, Current is Waveforms and Power
Factor PF (a) Without the TAF and (b) With The TAF

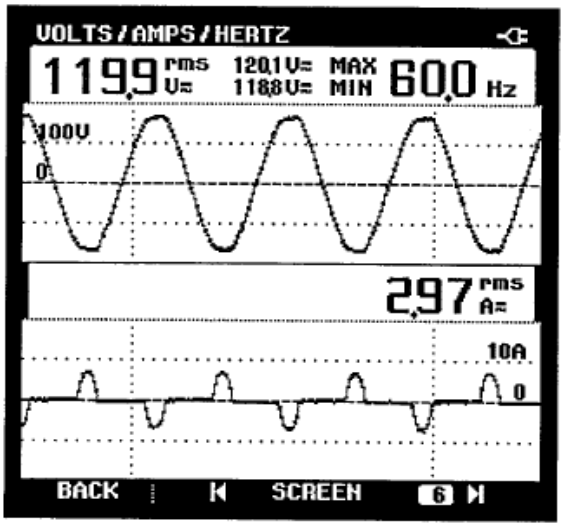

Figure S.7 Load Current and Voltage Waveforms With the TAF

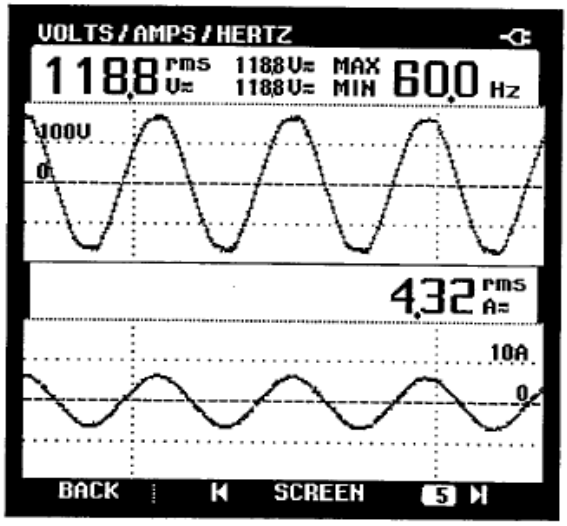

Figure S.8 TAF Filter Current and Voltage Waveforms

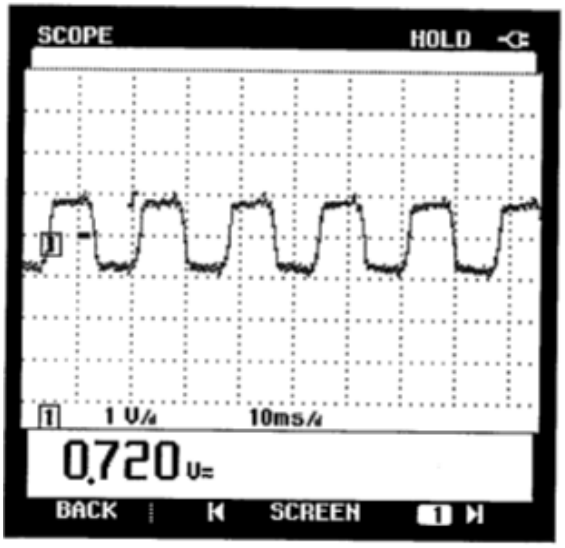

Figure S.9 PWM-MOSFET Switching Function without Load

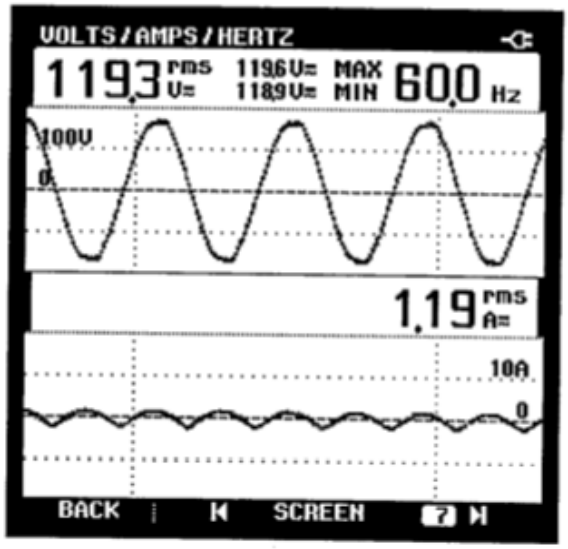

Figure S.10 PWM-MOSFET/Bridge Current (Positive side) and Feeder Voltage [reference figure 8.2]

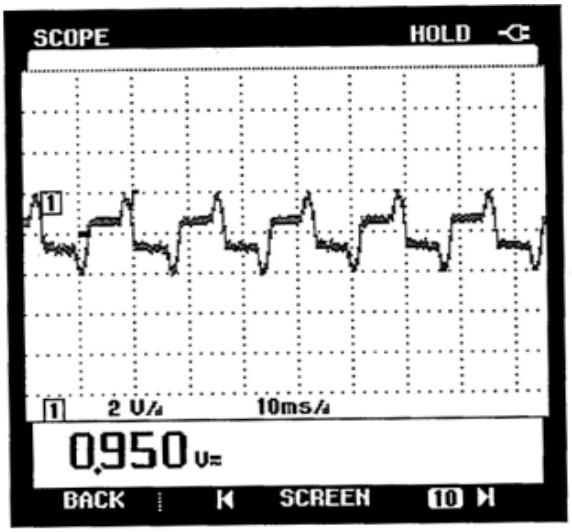

Figure S. 1 1 PWM-MOSFET Switching Function with Load

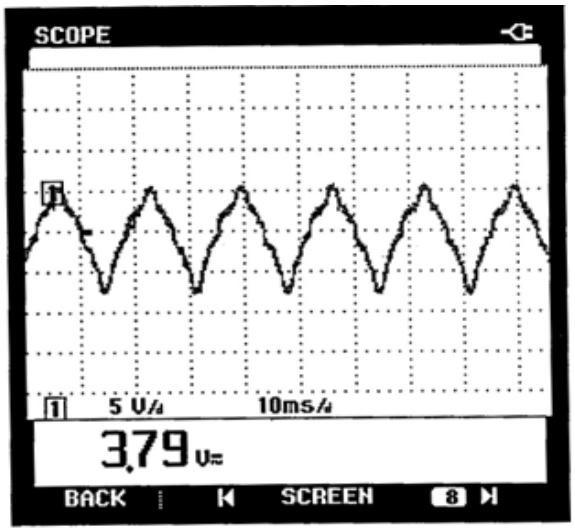

Figure S. 12 PWM-MOSFET Switching Function with Load & Filter

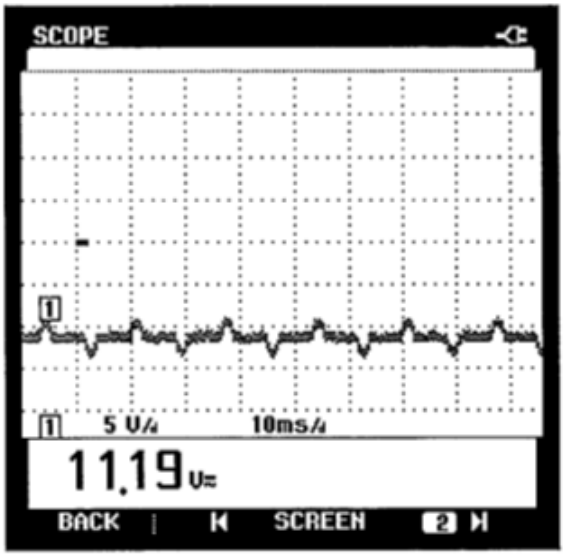

Figure S. 13 Voltage Output of PI Controller (P) [reference figure] [8.8]

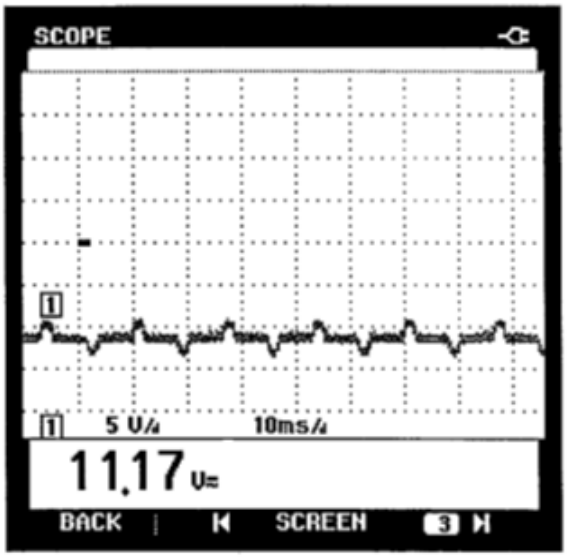

Figure S. 14 Voltage Output of PI Controller (I) [reference figure [8.8]

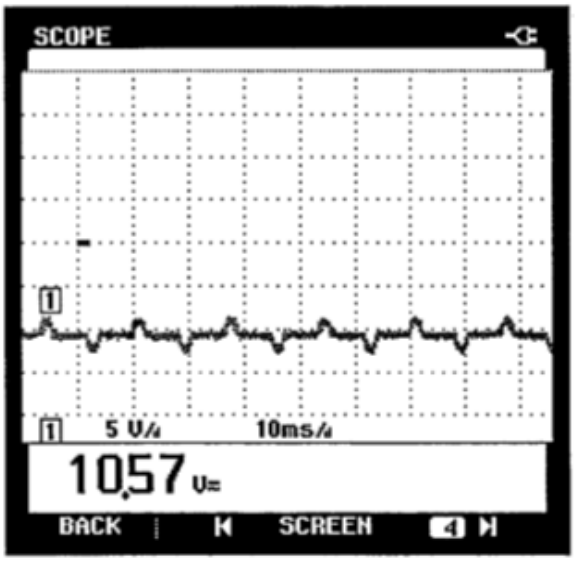

Figure S. 15 Voltage Input into PI Controller (PI) [reference figure] [8.8]

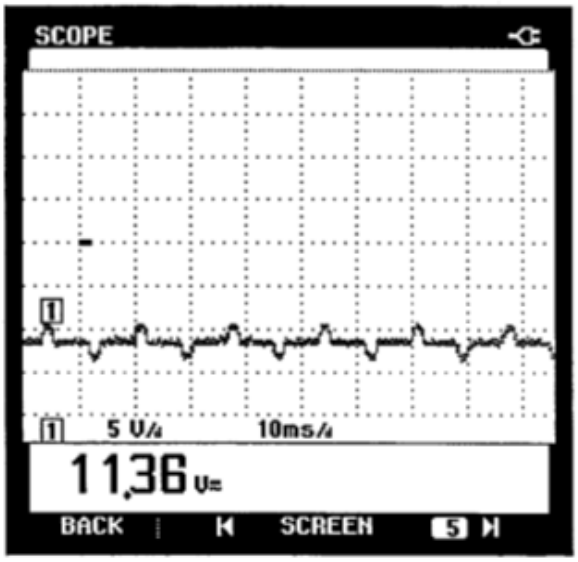

Figure S. 16 Voltage Vc input to PWM Chip [reference figure] [8.10]

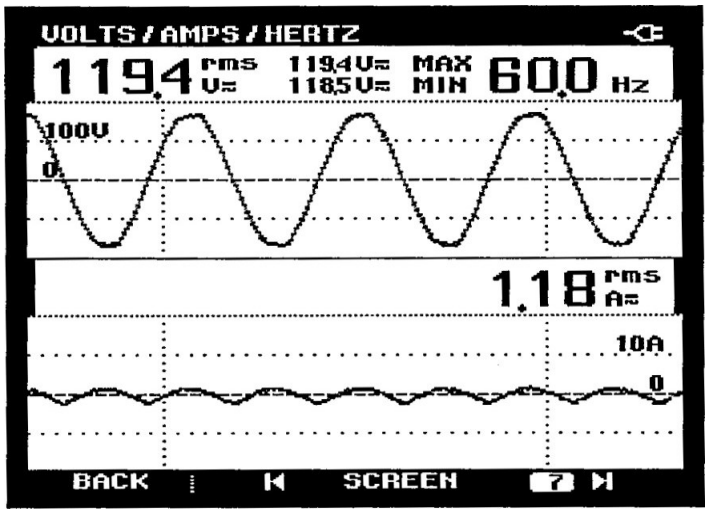

Figure S.17 MOSFET/Bridge Current (negative side) and Feeder Voltage [reference figure 8.2]

Table S. 1: Data for Laboratory Testing for Case (2) SMPS Type Load

	Without the Switched/ Modulated Power Filter	With the Switched / Modulated Power Filter
THD (current)	68.9%	31.1% & 15.0%
THD (voltage)		o
Power Factor (PF) **	0.71	0.94
Displacement Power Factor (DPF)	1.00	1.00
Frequency	60.0	60.0

(**) PF enhancement is assured for frequent on-off, inrush, temporal type or cyclical type loads.

S.2 Temporal NLL With TAF

The continuation of the results of the temporal nonlinear load is presented in this section.

The full unified system and results of this temporal nonlinear load are covered in Chapter 8.

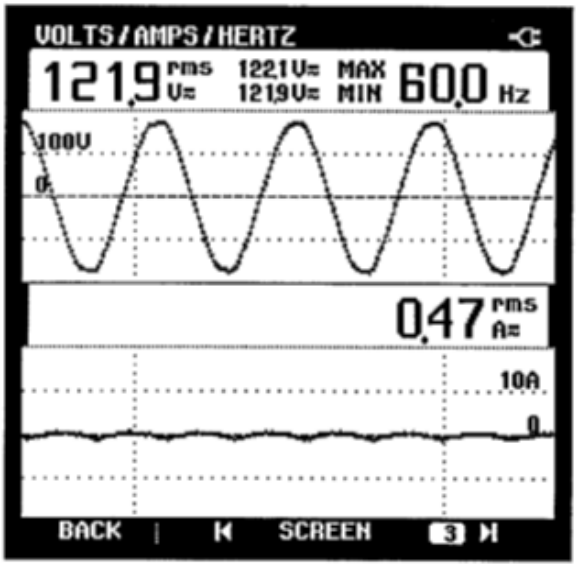

Figure S. 18 MOSFET/Bridge Current (negative side) and Feeder Voltage [reference figure] [8.2]

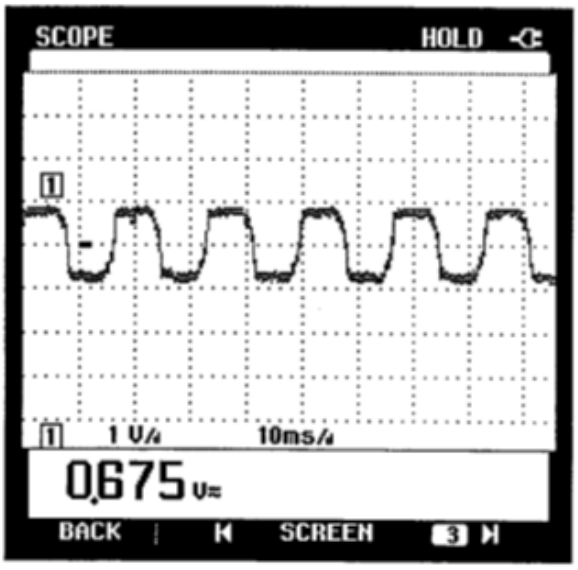

Figure S. 19 PWM-MOSFET Switching Function without Load

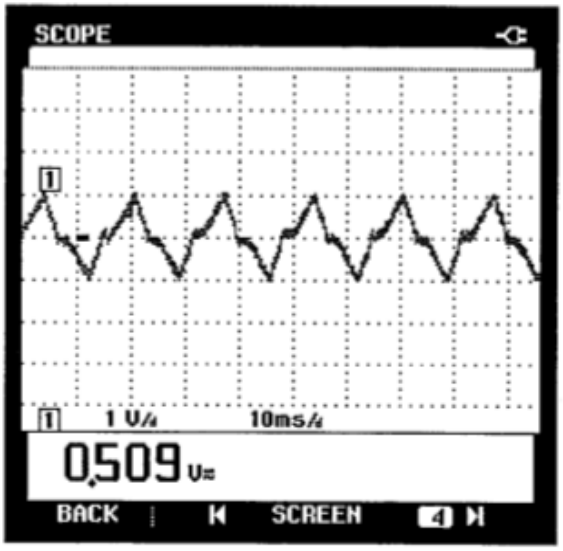

Figure S.20 PWM-MOSFET Switching Function with Load

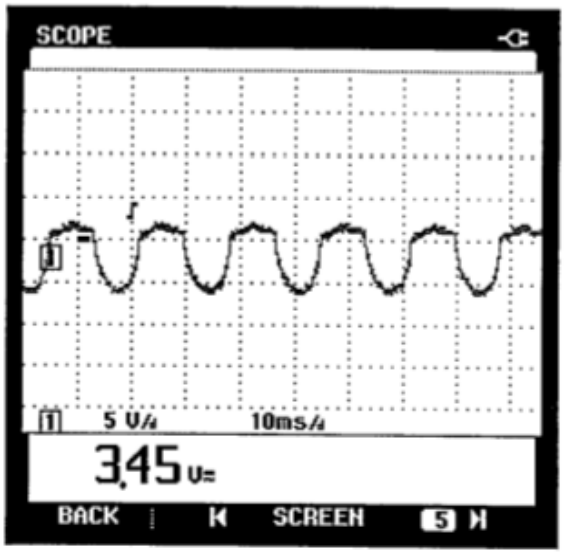

Figure S.21 PWM-MOSFET Switching Function with Load & Filter

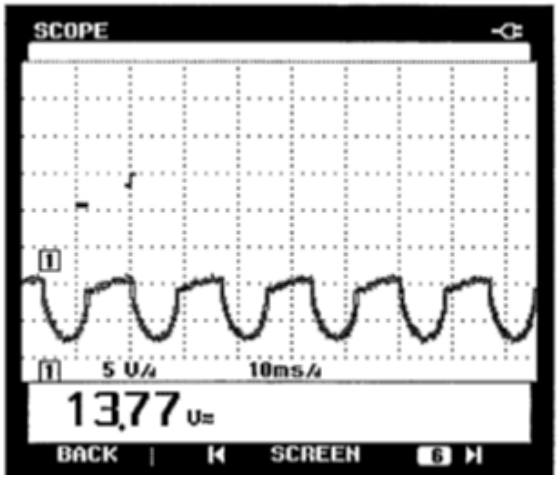

Figure S. 22 Voltage Onput of PI Controller (P) [reference figure] [8.8]

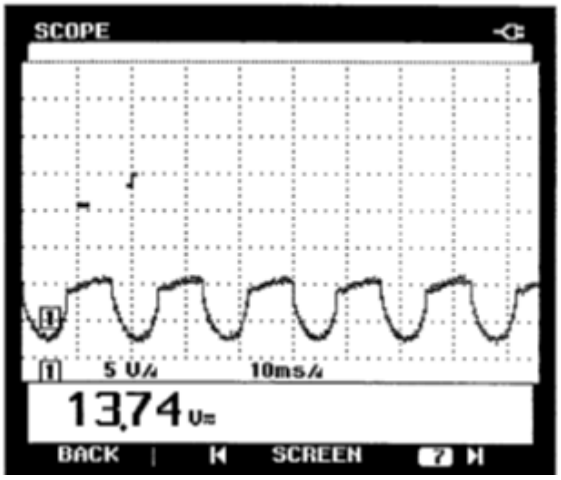

Figure S. 23 Voltage Onput of PI Controller (I) [reference figure] [8.8]

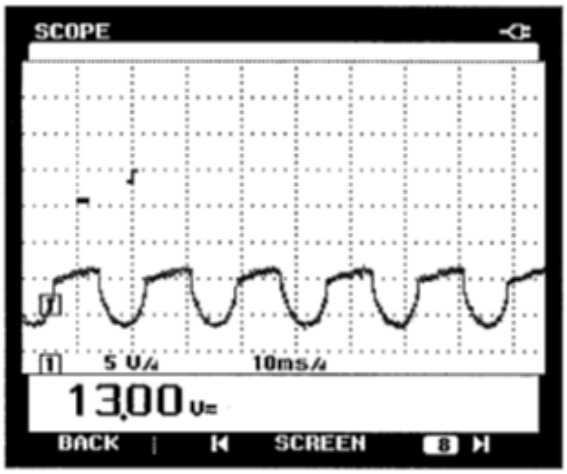

Figure S. 24 Voltage input into PI Controller (PI) [reference figure] [8.8]

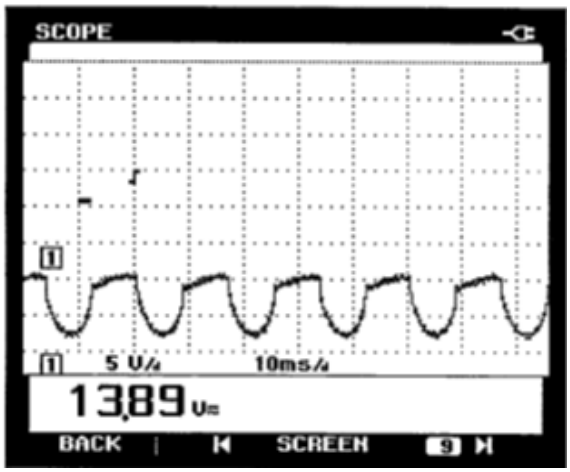

Figure S. 25 Voltage Vc input to PWM Chip [reference figure] [8.10]

Appendix M

OTHER EXTENDED SWITCHED /MODULATED POWER FILTER TOPOLOGIES

T .1 Modulated Power Filter/Static Capacitor Compensator

According to [184], Figure T. 1 shows the single line diagram of the electric distribution/utilization system comprising the AC supply feeder, an arc-type nonlinear load and the extended dynamic power filter and switched capacitor compensator (MPF/SCC).

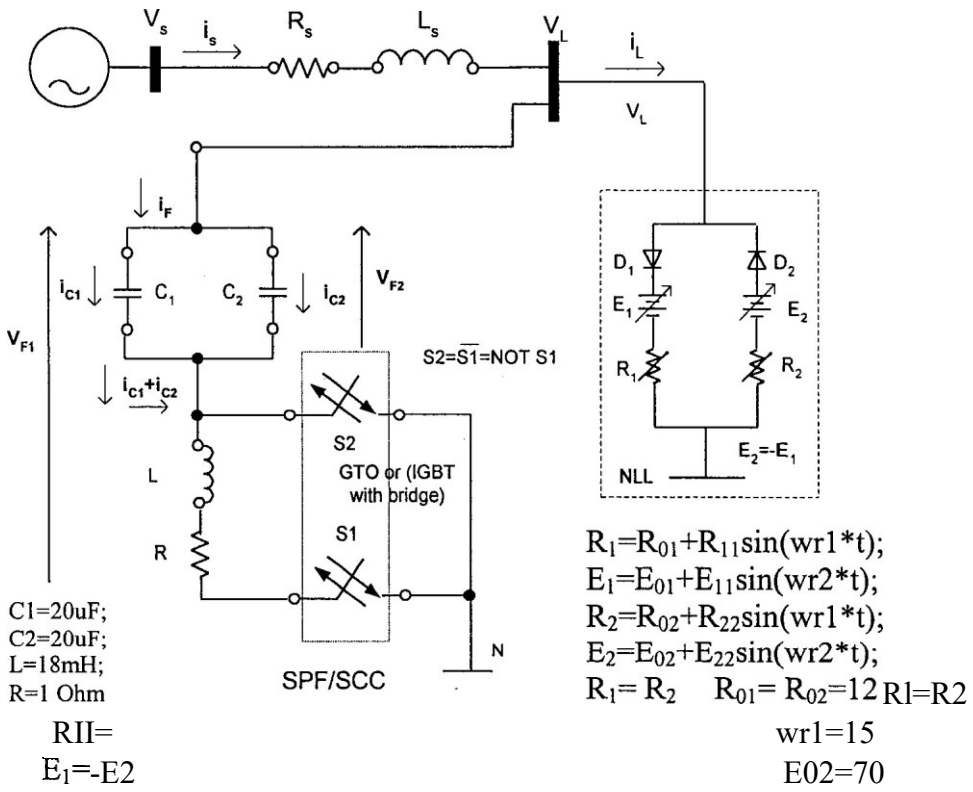

Figure T. 1: Single Line Diagram of System and Modulated / PWM Power Filter

Figures T.2 to T.6 show the MATLAB/SIMULINK digital simulation of the unified AC system and the signals dynamic response without and with the proposed PWN - modulated power filter/ static capacitor compensator scheme. These waveforms illustrate the resultant power quality enhancement and appreciable reduction in (THD) values of both supply current and load voltage. Figures T .2 and T .3 depict The Fast Fourier transform (FFT) (the magnitude of harmonics in percentage % of fundamental RMS and the total harmonic distortion (THD) of source current. The FFT has been applied to the feeder current (i_s)without and with the novel MPF/SCC filter. Comparing Figure T .2 and Figure T.3, it is observed that the harmonic spectra have been significantly reduced in magnitude.

Figures T .4 and T .5 depict The Fast Fourier transform (FFT) (the magnitude of harmonics in percentage % of fundamental) RMS of the load voltage (V_L) and the total harmonic distortion

(THD). The FFT was calculated for the load voltage (V_L) without and with the combined novel MPF/SCC filter. Comparing Figure T .4 and Figure T.5, it is observed that the voltage total harmonic contents have be en reduced to an acceptable level.

Figure T .6 depicts the modulated power filter current and voltage through the switched capacitor section and the other modulated power filter section. The novel dynamic controller used in this case is the dual loop version using dynamic minimum power tracking (reference Figure A.3) and the dynamic minimum RMS current tracking (A.5).

The switching frequency of the PWM-block was selected at 900Hz. The modulated power filter parameters were selected using the guided Trial and Error method described in full detail in Appendix 'W' (Cl=20pF, C2=20μF, L=18 mH and R=IQ). All filters utilize a highly permeable ferromagnetic material (pr=3000-5000) core to minimize cost, size and weight of the filter assembly.

It is evident that the supply power quality (PQ) is enhanced, and source current waveform distortion is greatly reduced. (THD)i from 40% to 11% as well as the load voltage waveform distortion is reduced from 16% to 7%. The proposed modulated and filter capacitor compensator with the dual loop dynamic control scheme can be utilized to enhance power quality and reduce harmonic content for an effective double mitigative action that also provide for enhanced power factor and efficient utilization.

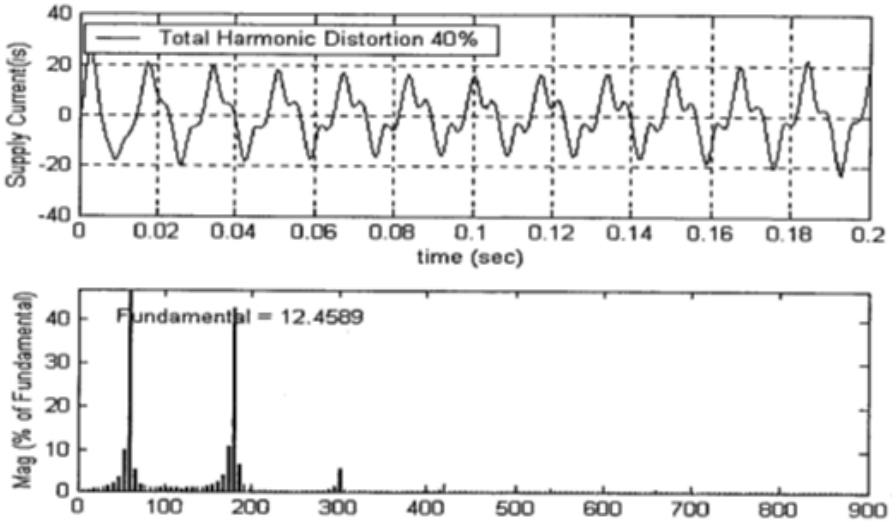

Figure T.2: Frequency – Spectra of Supply Current (i_s) and Supply Current (i_s) Waveform without the Modulated Power Filter

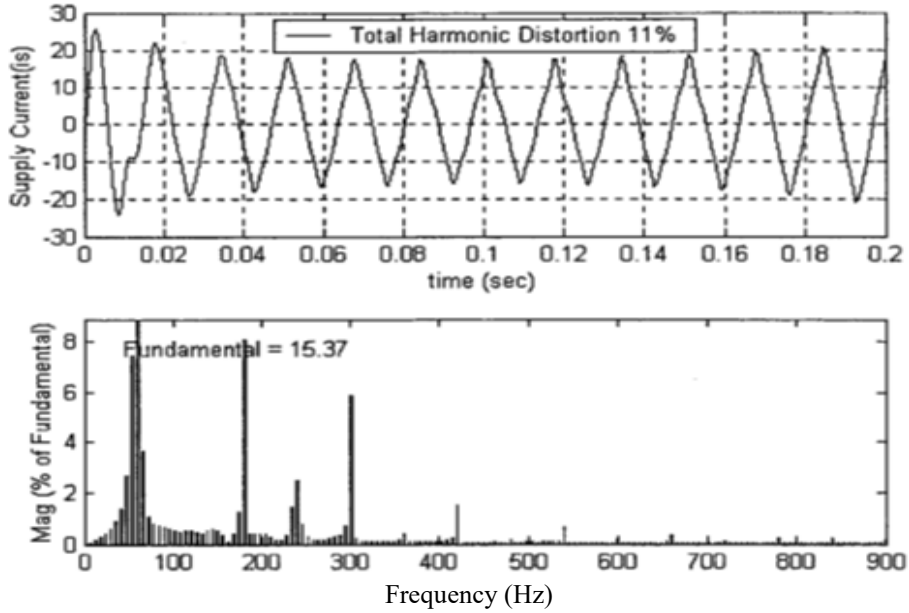

Figure T.3: Frequency – Spectra of Supply Current (i_s) and supply current (i_s) waveform with the Modulated Power Filter

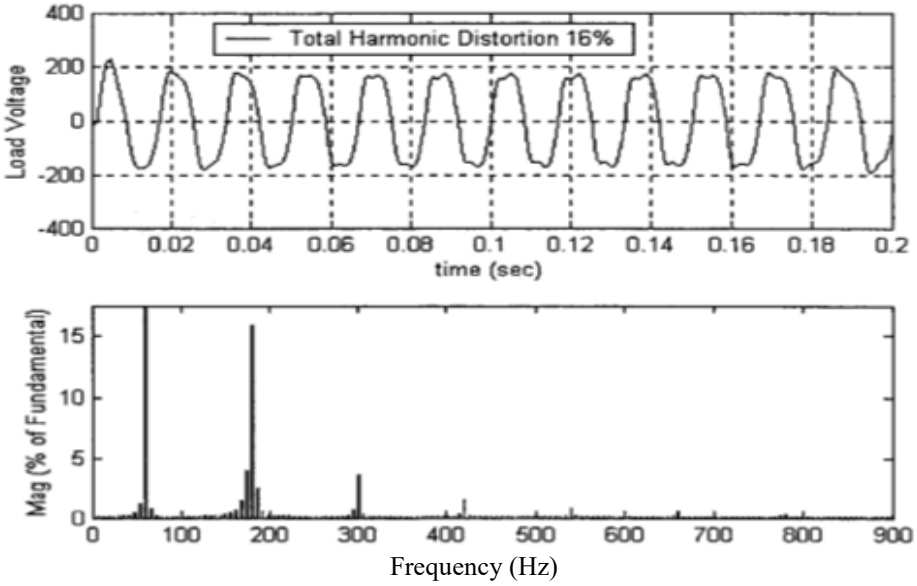

Figure T.4: Frequency – Spectra of Load Voltage (V_L) and Load Voltage (V_L) Waveform without the Modulated Power Filter

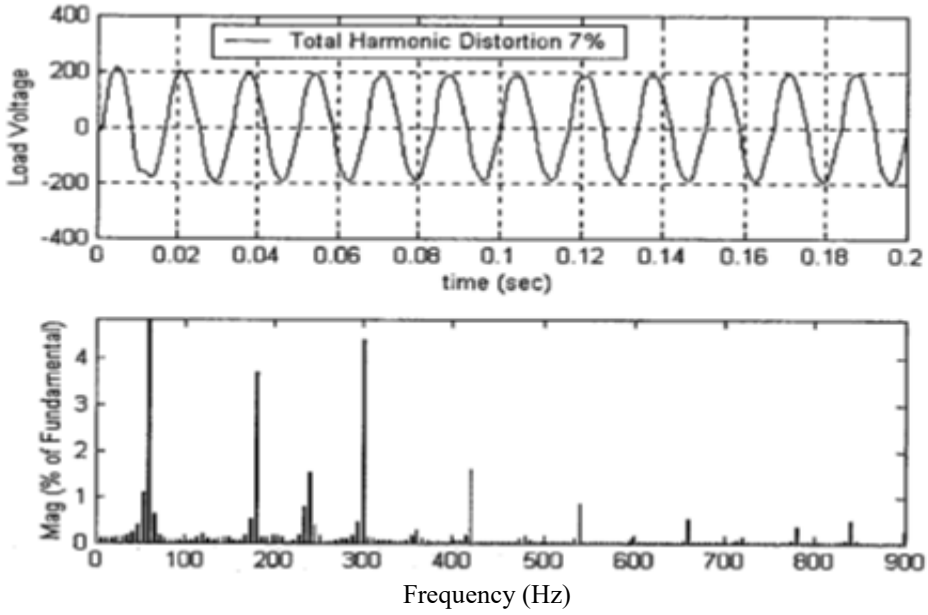

Figure T.5: Frequency – Spectra of Load Voltage (VL) and Load Voltage (VL) Waveform with the Modulated Power Filter

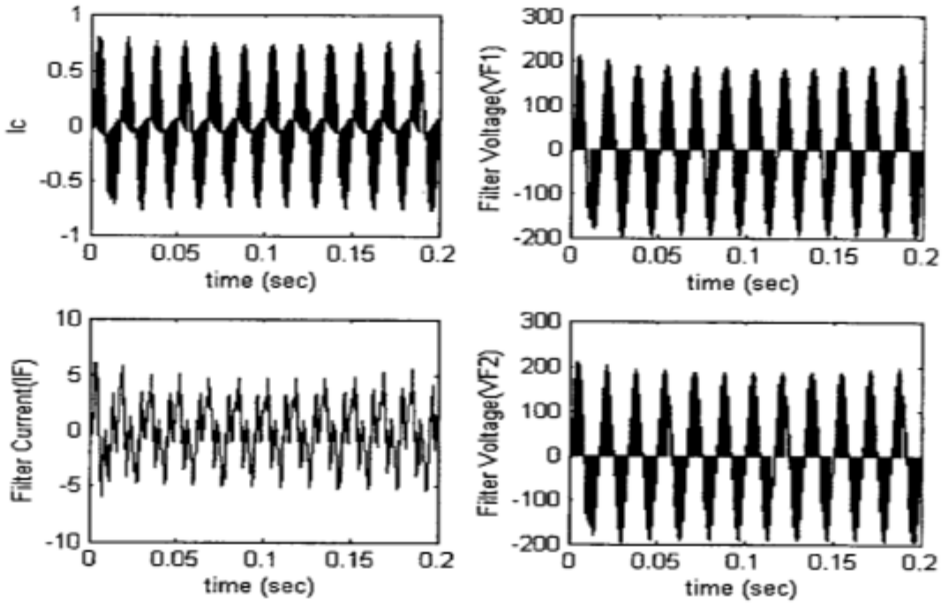

Figure T.6: Time Domain Dynamic Simulation Results of Filter Voltage and Current Waveforms with the Modulated Power Filter

T .2 Dual (Double) Tuned-Arm Switched/Modulated Power Filter (DTAF/MPF)

Figure T. 7 shows the single line diagram of the distribution/utilization electric system with the AC supply, feeder, a symmetrical arc-type nonlinear load and the dynamic dual tuned-arm filter. This particular arc type load produces a third harmonic of (>35% of fundamental) and fifth order harmonic (> 20% of fundamental).

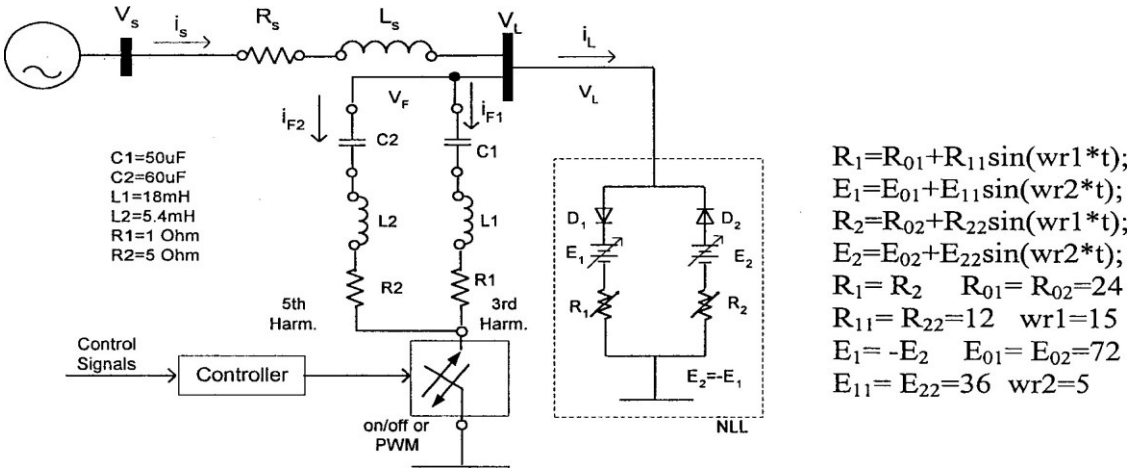

Figure T. 7: Single Line Diagram of System and Modulated / PWM Dual Tuned-Arm Power Filter

Figures T.8 to T.11 show the MATLAB/SIMULINK digital simulation of the unified AC system with the DTAF/MPF dynamic response without and with the proposed PWM modulated dual arm power filter. The dynamic waveforms illustrate both power quality enhancement and the reduction in the total harmonic distortion values for both supply current and load voltage.

Figures T .8 and T.9 show The Fast Fourier transform (FFT) (the magnitude of harmonics in percentage % of RMS fundamental component) and the feeder current (i_s) total harmonic distortion (THD). The FFT has been applied to the source current (i_s) without and with the double tuned-arm filter/MPF. Comparing Figure T .2 and Figure T.3, it is observed that the source current harmonic content have been significantly reduced from 45% to 9%.

Figures T. 10 and T. 11 show The Fast Fourier transform (FFT) (the magnitude of harmonics in percentage % of RMS fundamental) and the load voltage (V_L) and the total harmonic

distortion (THD). The FFT has been applied to the load voltage (V_L) without and with the DTAF/MPF filter. Comparing Figure T .4 and Figure T.5, it is observed that the total harmonic contents have been reduced to an acceptable level from 12% to 6.5%.

The novel dynamic dual-loop controller circuit used both the dynamic minimum-effective power tracking (reference Figure A.4) and the minimum harmonic ripple content (A. 7). The switching frequency of the PWM-block is selected to be 1000Hz. The modulated power filter parameters were selected by the same Trial and Error method (Cl=50uF, C2=60gF, Ll=18 mH, L2=5.4mH, RI-I Q and R2=5Q) presented in Appendix 'W'.

It is evident that the power quality (PQ) is effectively enhanced, and source current waveform distortion is greatly reduced. (THD)i from 45% to 9% as well as the load voltage waveform distortion is also reduced from 12% to 6.5%. The propose DTAF/MPF filter scheme with the novel dual-loop dynamic control scheme can be utilized to enhance both power quality, reduce harmonics content and eliminate excessive waveform distortion due to low order dominant harmonics ($3^{rd,}$ 7^{th}, 9 1 1^{th},13^{th}).

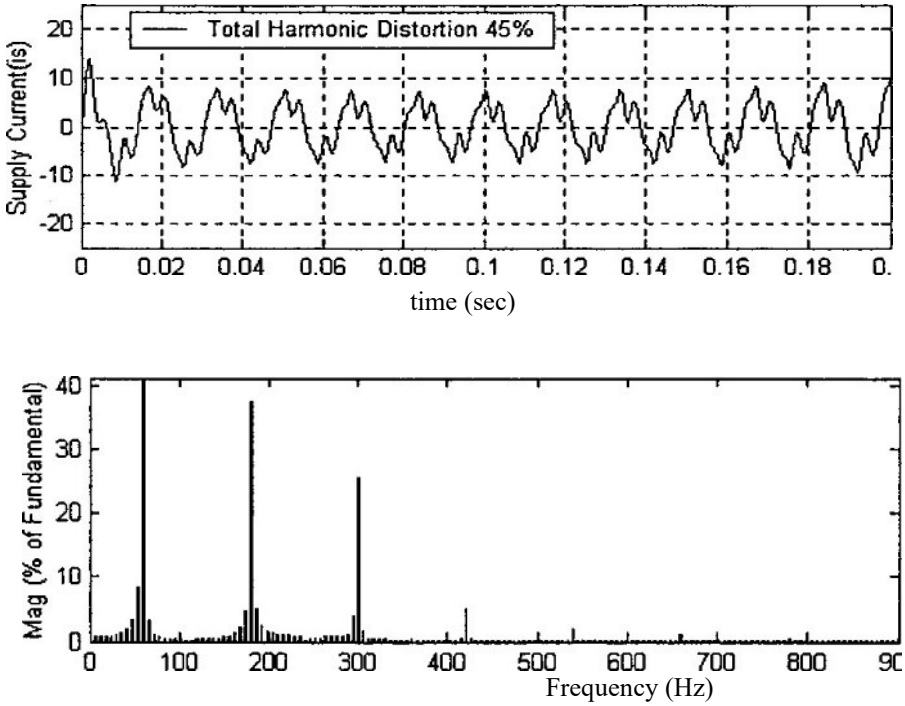

Figure T.8: Frequency-Spectra of Supply Current (Is) and Supply Current (i_s) Waveform Without the Modulated Power Filter

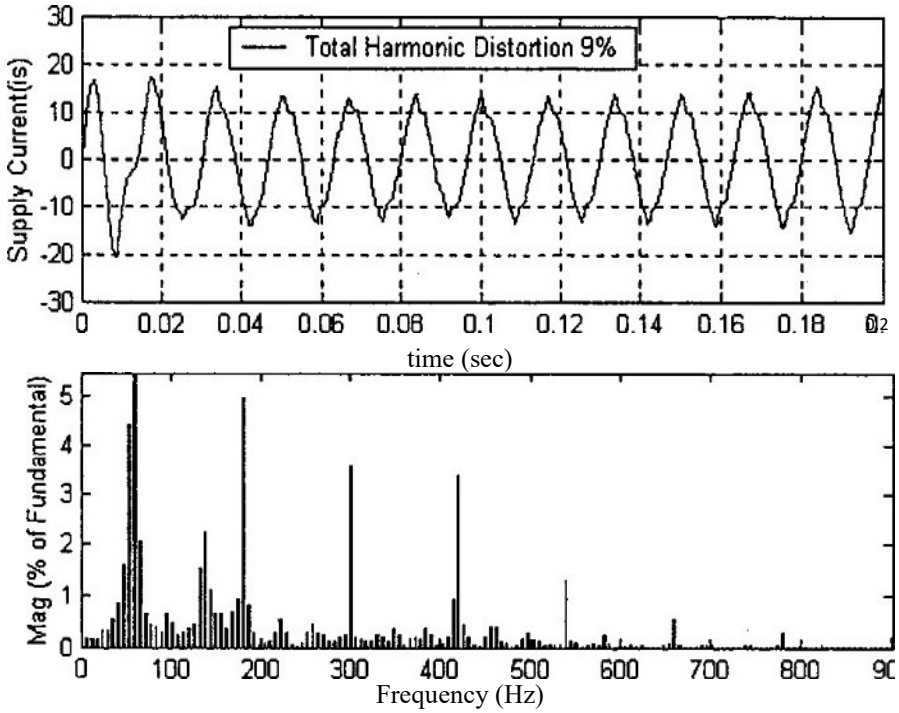

Figure T.9: Frequency-Spectra of Supply Current (Is) and Supply Current (Is) waveform With the Modulated Power Filter

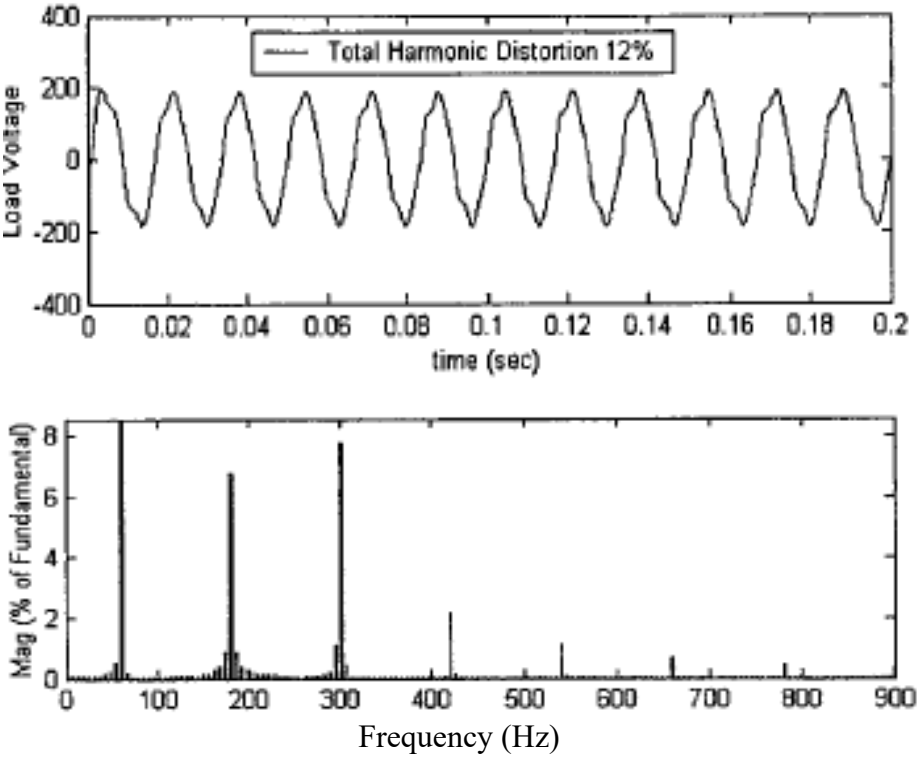

Figure T. 10: Frequency-Spectra of Load voltage (V_L) and Load Voltage (VL) waveform Without the Modulated Power Filter

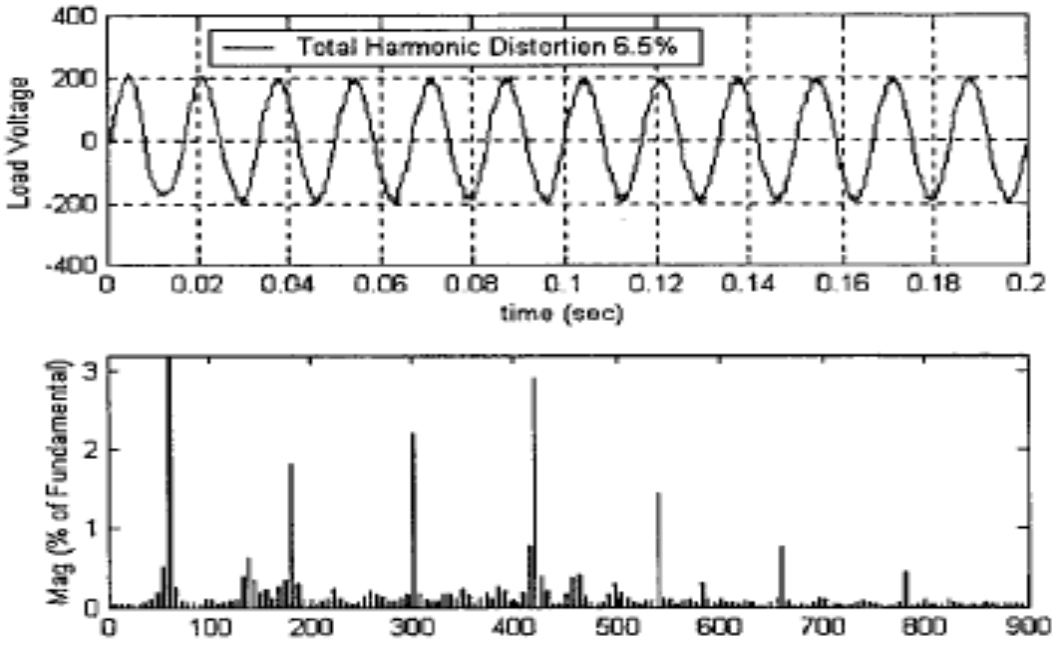

Figure T. 1 1: Frequency-Spectra of Load voltage (VL) and Load Voltage (VL) Waveform with the Modulated Power Filter